Modelling Fluorescence Quenching in Systems with Restricted Diffusion: Applications to Oligonucleotides and Polypeptides

INAUGURALDISSERTATION

zur

Erlangung der Würde eines Doktors der Philosophie

vorgelegt der

Philosophisch-Naturwissenschaftlichen Fakultät

der

UNIVERSITÄT BASEL

von

XIAOJUAN WANG

aus Shandong, China

Basel, 2004

Genehmigt von der Philosophisch-Naturwissenschaftlichen Fakultät

auf Antrag von

Prof. Dr. J. Wirz und Prof. Dr. H. Huber

Basel, den 30.03.2004

Prof. Dr. M. Tanner

Dekan

To my baby coming in September:

For the excitement you bring,

For your brilliant smile in my dream.

Acknowledgements

The thesis is a record of my growth in both the interest and ability to carry out scientific research work. I owe special thanks to my supervisor Prof. Werner Nau for the opportunity of working in his group and for his support, encouragement, and guidance, which enabled me to persist with the projects and focus on the really interesting points.

I thank Prof. Jakob Wirz and Prof. Hanspeter Huber in their function as co-referees and Prof. Wolfgang P. Meier for his function as chairman.

I am indebted to the group members of Prof. Werner Nau and Prof. Jakob Wirz for their scientific support and stimulating discussions.

I am also grateful to Prof. Evgeny N. Bodunov (St. Petersburg, Russia) for the fruitful collaboration in the simulation project and Prof. Elisha Haas (Ramat-Gan, Israel) for his help on the data analysis in the FRET project.

A special acknowledgement goes to my parents and friends. Their kind support and help warmed me up in the most difficult period.

Lastly, I would like to give a lot of thanks to Fang, my constant source of pride and inspiration, for providing patient and unfaltering encouragement during the past years.

Contents

1. Abstract and Scope

The objectives of the present thesis are 1) to systematically develop a series of models and theoretical expressions for the diffusion-controlled reaction, which can be used to analyze the time-resolved fluorescence data in systems where the diffusion is restricted, and 2) to investigate the structural and dynamic properties of oligonucleotides and polypeptides by applying fluorescence-based methods and theoretical models.

Firstly, the diffusion-controlled reaction in one- to three-dimensional systems was analyzed with the Smoluchowski approach. The analytical expressions containing diffusion coefficient in different systems were summarized for time-resolved fluorescence data fitting. Some of these expressions were drawn from literature sources and presented here in a unified form and new expressions have also been derived to fill some gaps found in the literature. This work is very useful not only for my own project but also for the global research framework in our group. ("*Biomolecular and Supramolecular Kinetics in the Submicrosecond Time Range: The Fluorazophore Approach*", W. M. Nau and X. Wang, *ChemPhysChem*, **2002**, *3*, 393-398 (Appendix II)).

The diffusion-controlled intrachain fluorescence quenching was also analyzed. With the help of Prof. E. N. Bodunov, equilibrium conformational distributions of short polymer chains were simulated with Monte Carlo techniques. The kinetics of intramolecular end-to-end collisions of short biopolymer chains that are labelled with a probe and a quencher at opposite ends was numerically simulated and the survival probability of the excited end-attached probe, which reacts with the quencher at the other end upon contact, has been calculated. The results were compared with the experimental work on polypeptides carried out by other group members, suggesting that the reduced mobility of the ends of shorter chains was attributed to an increased steric hindrance, which results in an “internal friction” during intrachain motion. ("*Fluorescence Quenching Kinetics in Short Polymer Chains: Dependence on Chain Length*". X. Wang, E. N. Bodunov, and W. M. Nau *Opt. Spectrosc.* **2003,** *95*, 560-570 (Appendix IV)).

Furthermore, two novel FRET energy donor/acceptor pairs with small critical radius, Trp/DBO and Nal/DBO, were employed to experimentally recover the end-to-end distance

distribution and the intramolecular diffusion coefficient in Gly-Ser peptides. This work offered an independent approach to verify the theoretical analysis and compare it with the previous study based on collision-induced quenching systems. ("*Application of FRET donor/acceptor pairs with small critical radius to recover the structural and dynamic properties in short flexible peptides*", F. Huang, X. Wang, E. Haas, and W. M. Nau, **2004**, *in preparation* (Appendix VII)).

At the same time, some experimental projects were also carried out to investigate the structural and dynamic properties in DNA, RNA and 2′-*O*-methyl RNA single-stranded oligonucleotides. A phosphoramidite DBO derivative was synthesized, which can be directly applied in the automated solid-phase synthesis to obtain 5'-DBO-labeled oligonucleotides. The desirable properties of DBO, such as long lifetime, good solubility in water as well as efficient quenching by guanine upon direct contact, make it possible to extract the kinetics of molecular fluctuations from the intrachain fluorescence quenching. The end-to-end collision rates in short single-stranded oligodeoxyribonucleotides were successfully measured for the first time, which provided a strong support for the configurational diffusion model of hairpin formation. ("*Kinetics of End-to-End Collision in Short Single-Stranded Nucleic Acids*". X. Wang and W. M. Nau, *J. Am. Chem. Soc.* **2004,** *126*, 808-813 (Appendix VI)). The investigation on RNA and 2′-*O*-methyl RNA oligomers showed that the 2′ substitutions could result in different sugar puckering and fluctuational freedom in these analogues. Consequently, the conformational and dynamic properties of different oligonucleotides can be predicted, which will be useful for the research efforts in the area of antisense agents.

Additionally, a kinetic hopping model for one- and two-directional charge migration in a one-dimensional system was developed and applied to the analysis of charge transfer processes in DNA strands. ("*Kinetics of one- and two-directional charge hopping in one-dimensional system: application to DNA*". X. Wang and W. M. Nau, *ChemPhysChem* **2001,** *2*, 761-766 (Appendix I))

The mathematic methods obtained from these projects were also applied in the data analysis of cyclodextrin host-guest complexation and diffusion-controlled fluorescence quenching in biopolymer chains. ("*A Joint Structural, Kinetic, and Thermodynamic Investigation of Substituent Effects on Host-Guest Complexation of Bicyclic Azoalkanes by β-*

Cyclodextrin", X. Zhang, G. Gramlich, X. Wang, and W. M. Nau, *J. Am. Chem. Soc*. **2002**, *124*, 254-263 (Appendix III) and "*Exploiting Long-Lived Molecular Fluorescence*" W. M. Nau, F. Huang, X. Wang, H. Bakirci, G. Gramlich, and C. Marquez, *Chimia* **2003**, *57*, 161-167 (Appendix V)).

2. Introduction

Fluorescence spectroscopy is a powerful technique to investigate the structural and dynamic properties of biological macromolecules. The excited states of fluorophores are very sensitive to the changes in their environment, which can result in a shift of the absorption or emission wavelength, or an intensity variation. Alternatively, when time-resolved measurements are performed, the different decay rates of fluorescence intensity or the polarization anisotropy can be recorded. The former stems from the fact that many dynamic events can deactivate the excited state and hence influence the lifetime, while the latter reflects the temporal reorientation of the emission dipole. Since time-resolved measurements can provide much more molecular information than steady-state data, they have been intensively employed to monitor the segmental or over-all motions of biomolecules, such as the conformational fluctuations of proteins and nucleic acids, the interaction between proteins and substrates, as well as the lateral diffusion in membrane systems.[1] Those features are extremely useful for our understanding of the fundamental processes in life science at the molecular level.

The studies presented in this thesis focused on the time-resolved fluorescence intensity decay. In this method, the fluorophores are excited by a sudden pulse of light, which results in an initial population of excited states. Then this population decays through two channels: 1) random deactivation through fluorescence emission and nonradiative processes, 2) quenching due to excited-state reactions, energy transfer, as well as collision with quencher molecules. Among them, the collision-induced quenching is also considered as dynamic quenching since it requires the excited fluorophores and quenchers to diffuse into a close proximity during the lifetime, which is the main point of interest in this thesis.

Experimentally, what one can record is the fluorescence intensity, which is proportional to the excited state population. At present, the most frequently used technique is time-correlated single-photon counting, which records the histogram of photon arrival times in relation to the excitation pulse.

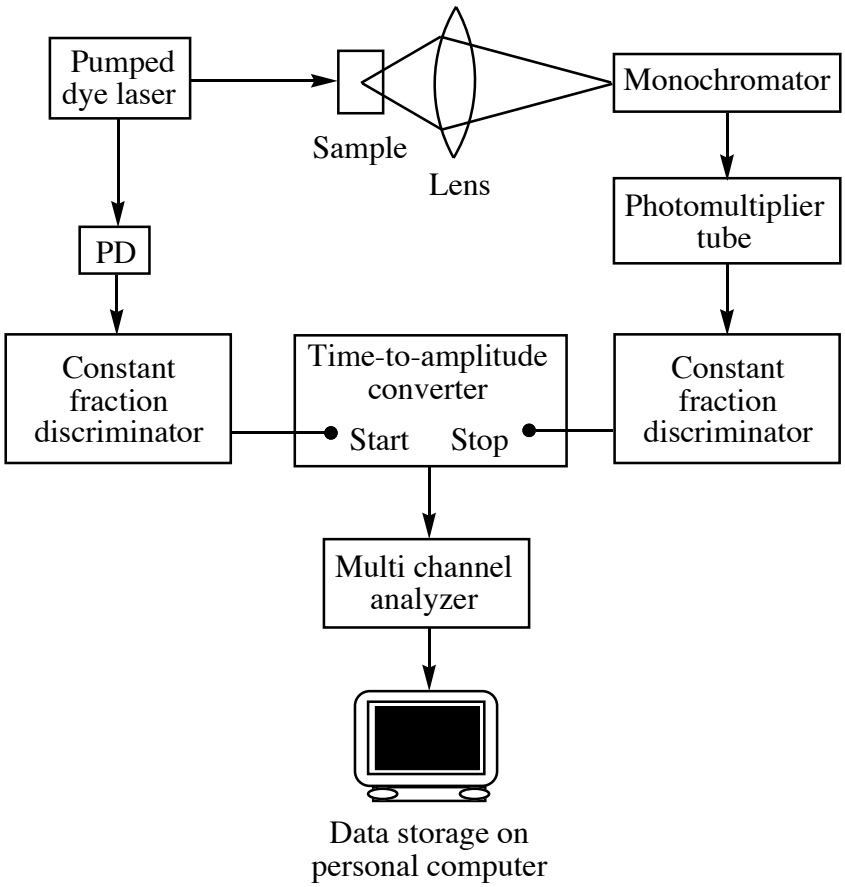

Scheme 2.1. Schematic diagram for time-correlated single-photon counting

Very recently, the advances in ultrafast laser devices, which emit pulses on the picosecond to femtosecond scale, as well as the development of novel detection systems, have extended time-resolved fluorescence measurements into the subnanosecond region.[2] The streak cameras technique can even provide time resolution of several picoseconds.[3]

In view of the advancement of technology towards fast time scales, it is important to recall that due to the typically high molecular weight and the strong geometric effects, it is the time scale of nanosecond to microsecond that is relevant to diffusion-controlled reactions and diffusive motions in solution like those occurring in biomolecular and supramolecular systems, e.g., the association of supramolecular components,[4] the binding of substrates to enzymes or catalysts, biopolymer or polymer chain folding,[5,6] as well as intermolecular chemical processes in constrained low-dimensional systems such as membranes[7] and unidirectional zeolites.[8] However, the lifetimes of excited states of fluorescence probes are

normally very short, ranging from picoseconds to a few nanoseconds, which defines a limitation to the application of time-resolved spectroscopic techniques since the excited states decay only reports on the events, which occur at comparable rates. Therefore, the search for novel fluorescent probes with long lifetimes and high environmental sensitivity is crucial in the field of biomolecular dynamics.

Additionally, since the dynamics of biomolecules are normally complex, the mathematical analysis of the fluorescence decay is also a challenge to the experimentalists. Theories of diffusion-controlled reactions are usually formulated in terms of a concentration which evolves according to Fick's law. However, major difficulties in interpretation may arise for the systems where the diffusion is restricted, such as in low dimensions and within biopolymer chains.[9]

In the present thesis, the general objective is to extract dynamic properties of biomolecular and supermolecular systems from fluorescence data by applying a suitable model. Firstly, the diffusion-controlled reaction in one- to three-dimensional systems was systematically analyzed with the Smoluchowski approach. The analytical expressions were summarized for time-resolved fluorescence data fitting to obtain diffusion coefficients in different systems. Additionally, the kinetics of intramolecular end-to-end collision-induced fluorescence quenching in short biopolymer chains was numerically simulated to understand the experimental observations. On the other hand, a long-lived fluorescence probe, 2,3-diazabicyclo[2,2,2]-oct-2-ene (DBO), was employed to measure the structural and dynamic properties in single-stranded nucleic acids, including DNA, RNA and 2′-*O*-methyl RNA, as well as in polypeptides.

The results of the present studies contribute to a better understanding of the theoretical models related to diffusion-controlled fluorescence quenching. Additionally, the successful applications of the long-lived fluorophore and relevant models in the dynamic studies in oligonuleotides and polypeptides are invaluable for the research on folding problems in polymers and biopolymers.

References

(1) Millar, D. P., *Curr. Opin. Struct. Bio.* **1996,** *6*, 637-642.

(2) Holzwarth, A. R., *Methods Enzymol.* **1995,** *246*, 334-362.

(3) Lakowicz, J. R. *Principles of Fluorescence Spectroscopy*, 2nd ed.; Kluwer Academic/Plenum Publishers: New York, 1999.

(4) Zhang, X.; Gramlich, G.; Wang, X.; Nau, W. M., *J. Am. Chem. Soc.* **2002,** *124*, 254-263.

(5) Hudgins, R. R.; Huang, F.; Gramlich, G.; Nau, W. M., *J. Am. Chem. Soc.* **2002,** *124*, 556-564.

(6) Wang, X.; Nau, W. M., *J. Am. Chem. Soc.* **2004,** *126*, 808-813.

(7) Gramlich, G.; Zhang, J.; Nau, W. M., *J. Am. Chem. Soc.* **2002,** *124*, 11252-11253.

(8) Pischel, U.; Galletero, M. S.; Garcia, H.; Miranda, M. A.; Nau, W. M., *Chem. Phys. Lett.* **2002,** *359*, 289-294.

(9) Nau, W. M.; Wang, X., *ChemPhysChem* **2002,** *3*, 393-398.

3. Diffusion-Controlled Fluorescence Quenching in One- to Three-Dimensional Systems

Theories of diffusion-controlled reactions in one- to three-dimensional systems are usually formulated in terms of a concentration which evolves according to a diffusion equation. This theory is based on the isotropic model proposed by Smoluchowski,[1] which assumes that around one of the reacting particles (***B***) a concentration gradient for the other species (***A***) is set up, and that the rate of flow of particles along this concentration gradient is governed by Fick's law. The fundamental differential equation is

$$\frac{\partial c}{\partial t} = D\nabla^2 c \tag{3.1}$$

where c represents the concentration of flowing particles, D is the diffusion coefficient, and ∇^2 is the Laplacian operator. Strictly speaking, at higher levels of theory, D is a function of c. For small concentrations D is found to be nearly constant. This approximation is also adopted in the following treatment.

Solutions of this equation for different dimensions are quite different. Moreover, the form of the solution even for the same number of dimensions will vary for different systems of coordinates.

3.1. Diffusion-Controlled Reaction in Three-Dimensional Systems (3D)

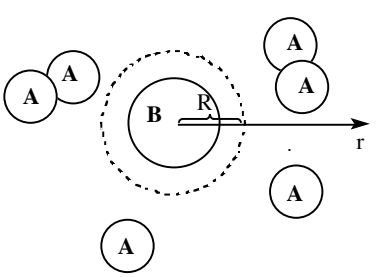

Scheme 3.1. Schematic representation for three-dimensional diffusion in spherical coordinates

The model for diffusion in a three-dimensional solution is illustrated in Scheme 3.1, where the molecule ***B*** is placed at the origin of the coordinate system and is surrounded by a

population of ***A***. Expressing Eq. (3.1) in polar (spherical) coordinates yields the following differential equation for $c(r, t)$ of ***A*** molecules:

$$\frac{\partial c}{\partial t} = D\left(\frac{\partial^2 c}{\partial r^2} + \frac{2}{r}\frac{\partial c}{\partial r}\right) \tag{3.2}$$

the concentration is subject to the so-called Smoluchowski boundary conditions:

$$c(r,0) = c_0, \qquad r > R \tag{3.3}$$

$$c(\infty,t) = c_0, \qquad r >> R \tag{3.4}$$

$$c(R,t) = 0, \qquad t \geq 0 \tag{3.5}$$

Here the radius R represents the distance of the closest approach of two particles and D is equal to the sum of the diffusion coefficients of the two species. Eqs. (3.3) and (3.4) specify that the initial distribution of ***A*** molecules is uniform and remains constant at very great distances from the boundary sphere. Eq. (3.5) arises from the assumption that every collision between particles is effective, e.g., leads to a chemical reaction and the deactivation of molecule ***B***.

The solution of Eq. (3.2) with the boundary conditions (3.3) – (3.5) is

$$c(r,t) = c_0\left[1 - \frac{R}{r}erfc\left(\frac{r-R}{\sqrt{4Dt}}\right)\right] \tag{3.6}$$

where $erfc(x) = \frac{2}{\sqrt{\pi}}\int_x^\infty e^{-\xi^2} d\xi$.

The flux across the boundary sphere at $r = R$ is

$$J = 4\pi R^2 D\left(\frac{\partial c}{\partial r}\right)_{r=R} = 4\pi RDc_0\left(1 + \frac{R}{\sqrt{\pi Dt}}\right) \tag{3.7}$$

As the reaction proceeds with a rate determined by the formation of encounters, one can get the decay rate of molecules ***B*** as

$$-\frac{d\rho}{dt} = \frac{dc_{enc}}{dt} = \left[4\pi RDc_0\left(1 + \frac{R}{\sqrt{\pi Dt}}\right)\right]\rho \tag{3.8}$$

which can be integrated to yield the final time-resolved decay of ***B*** molecules according to the 3D diffusion model

$$\frac{\rho(t)}{\rho_0} = \exp\left[-\int 4\pi RDc_0(1+\frac{R}{\sqrt{\pi Dt}})dt\right] = \exp\left(-4\pi RDc_0 t - 8\sqrt{\pi D}R^2 c_0\sqrt{t}\right) \tag{3.9}$$

3.2. Diffusion-Controlled Reaction in Two-Dimensional Systems (2D)

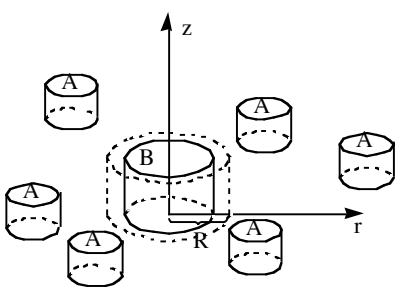

Scheme 3.2. Schematic representation for two-dimensional diffusion in cylindrical coordinates

The diffusion model in two-dimensional systems is based on an ideal system where all molecules are located with their centres in a plane and their paths of diffusion occur also in this plane (Scheme 3.2). An experimental approximation for this situation would be lateral diffusion in monolayers, phospholipid bilayers or biological membranes.[2-5] Expressing Eq. (3.1) in cylindrical coordinates yields the following differential equation,

$$\frac{\partial c}{\partial t} = D\left(\frac{\partial^2 c}{\partial r^2} + \frac{1}{r}\frac{\partial c}{\partial r}\right) \tag{3.10}$$

The solution of this equation subject to the boundary conditions (3.3)-(3.5) is shown in Eq. (3.11),[2]

$$c(r,t) = -\left(\frac{2}{\pi}\right)c_0 \times \int_0^\infty e^{-u^2 Dt}\,\frac{J_0(ur)Y_0(uR) - Y_0(ur)J_0(uR)}{J_0^{\,2}(uR) + Y_0^{\,2}(uR)}\,\frac{du}{u} \tag{3.11}$$

where $J_0(x)$ and $Y_0(x)$ refer to the zero-order Bessel functions of the first and second kinds respectively. Here, the concentration $c(r, t)$ is still characterized by the usual volume

concentration in molecules·cm^{-3}. If Z is defined as the membrane thickness in cm, the concentration can then be expressed as molecules per cm^2 as cZ.

This solution for $c(r, t)$ can be related to the reaction process in the same manner as in 3D to derive the final result for the time-resolved decay of molecule ***B*** in two-dimension as:

$$\begin{aligned}\frac{\rho(t)}{\rho_0} &= \exp\left(-\int 2\pi RZD\left(\frac{\partial c}{\partial r}\right)_{r=R} dt\right) \\ &= \exp\left(-8Zc_0\frac{R^2}{\pi}\int_0^\infty \frac{1-e^{-x^2tD/R^2}}{x^3\left[J_0{}^2(x)+Y_0{}^2(x)\right]}dx\right)\end{aligned} \tag{3.12}$$

Since Eq. (3.12) is not readily integratable, a semiempirical approximation has been suggested by Owen[6] as

$$\frac{\rho(t)}{\rho_0} = \exp\left(-1.585Zc_0Dt - 7.09Zc_0R\sqrt{Dt}\right) \tag{3.13}$$

which was proposed to provide a good fit over the range $0 \le t \le 10R^2/D$.

In the past thirty years the discussion about the most suitable approximations has continued. Approximate expressions with different values were reported by several groups.[3,7] We proposed a new approximation in the form:

$$\frac{\rho(t)}{\rho_0} = \exp\left(-\frac{\pi}{2}c_0Dt - 4\sqrt{\pi D}c_0R\sqrt{t}\right) \tag{3.14}$$

with c_0 as the concentration in 2D. Though this equation might not provide a better approximation to the integral in Eq. (3.12) than others, it can be analytically compared with the solutions in one- and three-dimensions.

3.3. Diffusion-Controlled Reaction in One-Dimensional Systems (1D)

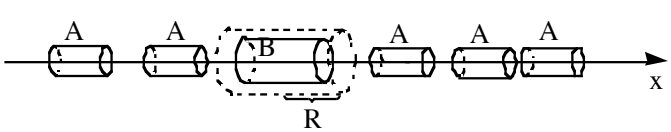

Scheme 3.3. Schematic representation for one-dimensional diffusion in a linear filament

Supposing that a flow of particles ***A*** along concentration gradient is in a linear filament like a unidirectional zeolite which is placed along the *x*-axis with molecule ***B*** at the origin (Scheme 3.3), Eq. (3.1) in rectangular coordinates yields the following equation for one-dimensional model:

$$\frac{\partial c}{\partial t} = D\frac{\partial^2 c}{\partial x^2} \tag{3.15}$$

The solution of this equation subject to the boundary conditions (3.3)-(3.5) ($|x| = r$) is

$$c(|x|,t) = c_0\left(1 - erfc\left(\frac{R-|x|}{2\sqrt{Dt}}\right)\right) \tag{3.16}$$

where $erfc(x) = \frac{2}{\sqrt{\pi}}\int_x^\infty e^{-\xi^2} d\xi$ and concentration c_0 is characterized by molecules per cm.

Treated in the same manner as in two and three dimensions, the final result for the time-resolved decay of molecule ***B*** in one dimension can then be obtained as

$$\frac{\rho(t)}{\rho_0} = \exp\left(-2c_0\sqrt{\frac{Dt}{\pi}}\right) \tag{3.17}$$

3.4. Time-Resolved Fluorescence Decays

The above analysis can be applied to the cases of fluorescence quenching, where the reacting molecule ***B*** represents the excited fluorescence probe and ***A*** takes over the role of the quencher. In this case, the fluorescence intensity is proportional to the survival of excited fluorophores. Additionally, an independent spontaneous decay term must be considered.[8] in the limiting condition that every collision between two species is followed by rapid deactivation of the excited fluorophore before the encounter dissociates (Eq. 3.5), the bimolecular quenching rates will equal to the formation rates of the encounters. Therefore, according to the above analysis on the kinetics of encounters formation and the time-resolved decay of molecule ***B*** in different dimensions, the time-dependent bimolecular quenching rate constants and fluorescence decays are then summarized in Table 3.1.

Table 3.1. Kinetics of diffusion-controlled fluorescence quenching in one to three dimensions

dimension	time-dependent bimolecular quenching rate constant[a]	decay of the fluorescence intensity[a,b]
1D	$k(t') = \sqrt{\frac{D}{\pi t'}}$	$I(t) = I_0 \exp\left(-\frac{t}{\tau} - 2c_0\sqrt{\frac{Dt}{\pi}}\right)$
2D	$k(t') \approx 2\pi D\left(\frac{1}{4} + \frac{R}{\sqrt{\pi Dt'}}\right)$	$I(t) \approx I_0 \exp\left(-\frac{t}{\tau} - \frac{\pi}{2}c_0 Dt - 4c_0 R\sqrt{\pi Dt}\right)$
3D	$k(t') = 4R\pi D\left(1 + \frac{R}{\sqrt{\pi Dt'}}\right)$	$I(t) = I_0 \exp\left(-\frac{t}{\tau} - 4c_0 R\pi Dt - 8c_0 R^2\sqrt{\pi Dt}\right)$

[a] R represents the distance of the closest approach of two reactants. D is equal to the sum of the diffusion coefficients of the two species.

[b] $\frac{I(t)}{I_0} = \frac{\rho(t)}{\rho_0} = \exp\left(-\frac{t}{\tau} - c_0\int_0^t k(t')dt'\right)$, ρ_0 and $\rho(t)$ are the populations of excited states at time 0 and t, respectively. τ is the intrinsic fluorescence lifetime of the excited states. c_0 is the concentration of quencher.

Comparing the equations of 2D and 3D models, it is found that both of them include a long-time term, i.e., the t term and a short-time term, i.e., the $\sqrt{t}$ term. For the solution in 1D, there is only a short-time term. The corresponding bimolecular quenching rate constants are all time-dependent in 1D, 2D and 3D. However, the relative weight of the long-time term in 2D is much smaller than that in 3D, which can partly explain that at long time, the solution in 3D can be reduced to an equation which only contains the long-time term, i.e., the $\sqrt{t}$ term can often be neglected,[9] but in the solutions for 2D and 1D it is indispensable. It means that in 3D, following an initial transient period in which the fluorescence decays rapidly, a diffusional steady state is established. By contrast, in 2D and 1D, the decay rate continues to decrease with time and a steady state is never established.[2,3]

References

(1) von Smoluchowski, M., *Z. Phys. Chem* **1917,** *92*, 129-168.

(2) Razi Naqvi, K., *Chem. Phys. Lett.* **1974,** *28*, 280-284.

(3) Caruso, F.; Grieser, F.; Murphy, A.; Thistlethwaite, P.; Urquhart, R.; Almgren, M.; Wistus, E., *J. Am. Chem. Soc.* **1991,** *113*, 4838-4843.

(4) Gramlich, G.; Nau, W. M., *Org. Lett.* **1999,** *1*, 603-605.

(5) Gramlich, G.; Zhang, J.; Nau, W. M., *J. Am. Chem. Soc.* **2002,** *124*, 11252-11253.

(6) Owen, C. S., *J. Chem. Phys.* **1974,** *62*, 3204-3207.

(7) Razi Naqvi, K.; Martins, J.; Melo, E., *J. Phys. Chem. B* **2000,** *104*, 12035-12038.

(8) Nau, W. M.; Wang, X., *ChemPhysChem* **2002,** *3*, 393-398.

(9) Miller, D. D.; Evans, D. F., *J. Phys. Chem.* **1989,** *93*, 323-333.

4. Intrachain Fluorescence Quenching: Application to Polypeptides

As mentioned in the introduction, time-resolved fluorescence spectroscopy is a powerful technique to monitor the segmental or over-all motions of biomolecules. Recently the time scale and mechanism of intramolecular contact formation in biopolymer chains, especially in polypeptides, have been extensively studied by the probe-quencher methodology with fluorescence as well as other techniques.[1-8]

In the representative experiments on polypeptide dynamics carried out in our group,[6,7] a long-lived fluorescent probe, 2,3-diazabicyclo[2.2.2]oct-2-ene (DBO), is attached to one end of the peptides and the efficient contact quencher of the excited probe, tryptophan (Trp), is attached to the other end. The quenching of the excited DBO reflects the kinetics of end-to-end collision (Scheme 4.1).

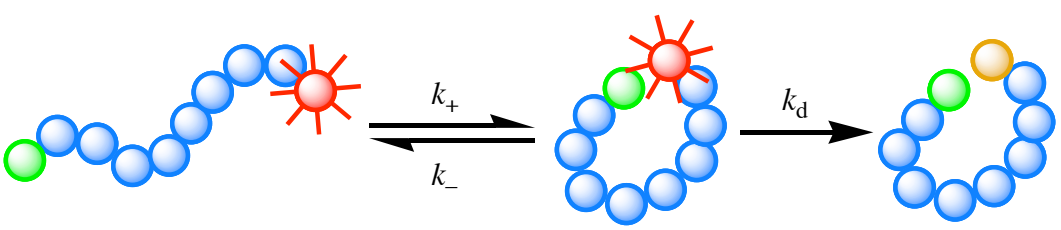

Scheme 4.1. Schematic representation for collision-induced intrachain fluorescence quenching

However, the experimental data for short Gly-Ser peptides as well as the results reported by other groups,[3,6,9] have revealed several contrasts to the theoretical models, which refer to long chains and are based on a Gaussian distribution function of end-to-end distances (Gaussian chain model), e.g., double-logarithmic plots of the rate constants for end-to-end collision (k_+) *versus* the chain length of peptides (N) displayed relatively small slopes, which fall significantly below the theoretical value –1.50.[10,11] The deviations between experiment and theory may be due to the theoretical idealization of the (bio)polymer chain, which neglects "chemical" effects of steric hindrance between the residues and potential barriers of bond rotation,[9,12] or, alternatively, due to the theoretical approximations employed to obtain the equilibrium distribution functions (Gaussian chain model), which may be inappropriate at short chain lengths.[3,5,13,14] In order to find the underlying reasons, to recover the intrachain

diffusion coefficients, as well as to investigate the structural and dynamic properties of Gly-Ser peptides in detail, two independent projects were performed, 1) numerical simulation of the end-to-end collision induced fluorescence decay in short polymer chains and 2) measurements on intrachain fluorescence resonance energy transfer in peptides.

4.1. Modelling Collision-Induced Fluorescence Quenching in Non-Gaussian Short Molecular Chains

The Monte Carlo (MC) technique was employed to simulate the equilibrium chain conformations in order to evaluate variances in the distribution function and possible consequences for the intramolecular quenching kinetics. In order to study the impact of different approximations on the shape of the distribution functions and the kinetics of fluorescence quenching, simple chain models of the rigid segment type were employed.

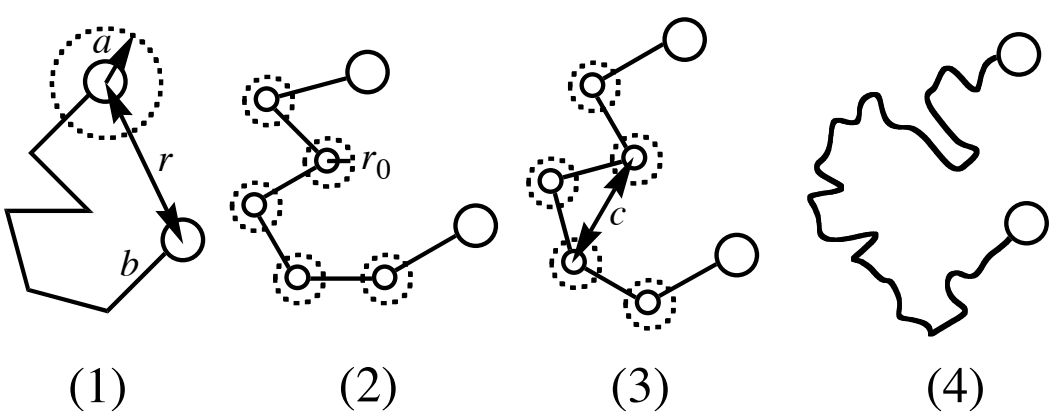

Scheme 4.2. Molecular chain models applied in the simulations

The modelled (bio)polymer chains are labelled with a fluorophore and a quencher at opposite ends. As shown in Scheme 4.2, three different chain models, the ideal short chain model (IC, 1), the self-avoiding chain model (SAC, 2), and the self-avoiding chain model with limited angular flexibility (SALF, 3) were applied to describe a real short polymer system (4).

For each chain model and for each chain length (2, 4, 6, 10, 14, and 22 segments) 10^6 conformations were sampled with the MC technique to obtain the equilibrium distribution

function, $g_N(r)$. In order to compare with the experimentally observed fluorescence decay, it is assumed that the initial distance distribution between the excited probe and quencher, $g_N^*(r)$, coincides with the equilibrium end-to-end ground-state distribution, i.e.,

$$g_N^*(r,t)\Big|_{t=0} = g_N(r) \tag{4.1}$$

Then the population of excited probe was described by the radial diffusion equation according to the theory by Szabo, Schulten, and Schulten (SSS),[10,12,15-17] which is based on a modified Smoluchowski equation:

$$\frac{\partial}{\partial t} g_N^*(r,t) = -\frac{1}{\tau_0} g_N^*(r,t) + D\frac{1}{r^2}\frac{\partial}{\partial r} r^2 \frac{\partial}{\partial r} g_N^*(r,t) + D\frac{1}{r^2}\frac{\partial}{\partial r}\left(r^2 g_N^*(r,t)\frac{\partial}{\partial r}\beta U(r)\right) \tag{4.2}$$

Eq. 4.2 can be used to calculate the survival probability density of an excited state at distance *r* subject to the initial distribution and the absorbing boundary conditions. Therefore, the total fluorescence intensity at time *t* can be deduced since it is proportional to the survival probability of the excited states at that moment.

$$I(t) = I_0 \int_0^{Nb} 4\pi r^2 g_N^*(r,t) dr \tag{4.3}$$

It was found from our simulation that for a very short chain, such as N = 4–6, regardless whether volume interaction is considered or not, the end-to-end distance distribution is substantially different from Gaussian. However, for longer chains the coefficients in the IC distribution functions approach more and more the Gaussian ones with increasing N while those obtained from simulations according to the SALF model deviate significantly also at large N values. Obviously, Gaussian distributions are inapplicable for short chains.

Then the fluorescence decay kinetics was numerically simulated by using the previously determined MC distribution functions, Eq. 4.2, and a constant end-to-end diffusion coefficient. The fluorescence decays for all chains with 4-22 segments are reproduced to be monoexponential over the entire time range except in a very short initial time interval; this applies to all models investigated (IC, SALF, and Gaussian chain), which is consistent with the experimental observation. By fitting the numerically simulated decay traces to monoexponential functions, the end-to-end collision rate constants, k_+, were obtained for the Gaussian chain model, IC model, as well as SALF model and then plotted in log(k_+)-log(N)

format. It was found that for the Gaussian and IC models, the slopes are very close to the theoretical values. On the other hand, the plot produced by the SALF model is not linear any more. However, the negative curvature is still much less pronounced than the negative curvature observed in experimental studies (Figure 4.1, see detailed results and discussion in Appendix IV).

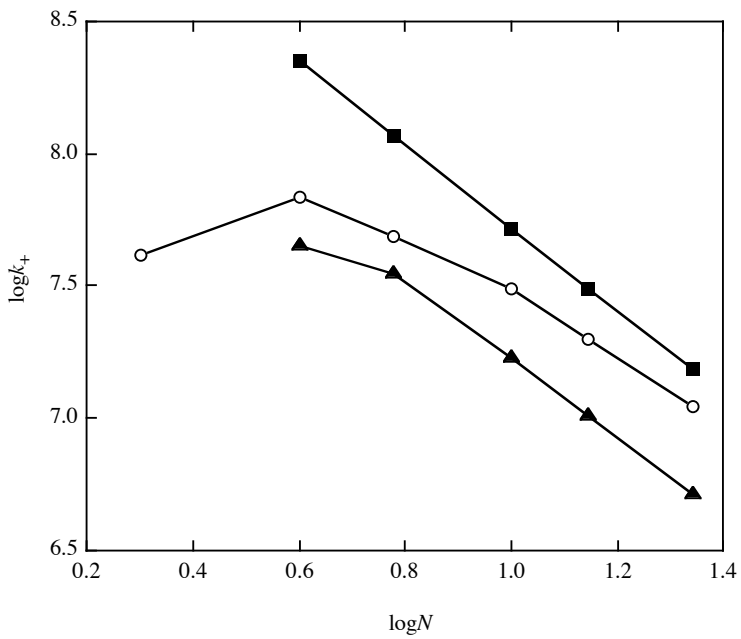

Figure 4.1. Double-logarithmic plot of the end-to-end collision rate constant k_+ of Trp-(Gly-Ser)-DBO vs the peptide length, taken as the number of intervening peptide units (N). The experimental value is taken from Ref. 6 (open circle). The simulation results are taken from Ref. 20, where the IC model (solid square, with slope of –1.57) and SALF model (solid triangle) were applied and a constant intrachain diffusion coefficient D of 9×10^{-7} cm^2/s and reaction radius a of 5 Å were assumed.

Deviations of the conformational distribution of short chains from the ideal Gaussian one are therefore unlikely to be responsible for the disagreement of the length dependence plots with theoretical predictions. The deviations could be related to the shortcomings of the presently employed chain models. Alternatively, the assumption of a constant diffusion coefficient for chains of different lengths may be inappropriate.

Then, by varying the end-to-end diffusion coefficient D in the modified diffusion equation (Eq. 4.2) and fitting the numerically calculated traces to the experimental ones for the DBO/Trp pair in polypeptides,[6] the intramolecular diffusion constants in polypeptides with different chain lengths were obtained. A decrease of the diffusion constants for smaller values of N was observed. This trend is presumably the underlying reason for the negative curvature observed experimentally.[3,6,9,12] It appears that shorter chains limit the flexibility and hinder end-to-end collisions more than longer ones do, i.e., shorter chains may exhibit a larger "internal friction".[12] Consequently, end-to-end collision becomes increasingly difficult for shorter chains. These results lead to the proposal that steric hindrance of the (bio)polymer side chains and the potential barriers of bond rotation lead to the peculiarities of the experimental length dependence, i.e., the deviation of the slope as well as the negative curvature in the $\log(k_+)$-$\log(N)$ plots.

4.2. Intrachain FRET in Peptides to Recover the End-to-End Distance Distribution and Diffusion Coefficient

Fluorescence resonance energy transfer (FRET) is also a widely used method to investigate the structural and dynamic properties in biomolecular systems. Since the energy transfer rates are strongly dependent on the donor/acceptor distance, the fluorescent dyes labelled in the biomolecules can serve as spectroscopic ruler.[15] In this project, with the help of global data analysis offered by Prof. Haas and his co-workers, this independent approach is employed to experimentally recover the end-to-end distance distribution and the intramolecular diffusion coefficient in short flexible Gly-Ser peptides, where the end-to-end collision rates have been measured with DBO/Trp, a fluorescent probe/quencher pair based on collision-induced quenching mechanism.[6]

Experimentally, the difficulties come from the short end-to-end distance of those peptides (< 20 Å) and the relatively large critical radius of conventional energy donor/acceptor pairs (20 – 100 Å), which reduce the sensitivity of the energy transfer efficiency on the dynamic process of the peptide backbone. To extend the distance range accessible to the FRET measurements towards the short limit, two energy donor/acceptor pairs with small critical

radius, Trp/DBO and Nal/DBO, were introduced. The small R_0 value of these two pairs, 9.9 Å and 9.8 Å respectively, lie at the lower limit but are exactly suitable for the short Gly-Ser peptides.

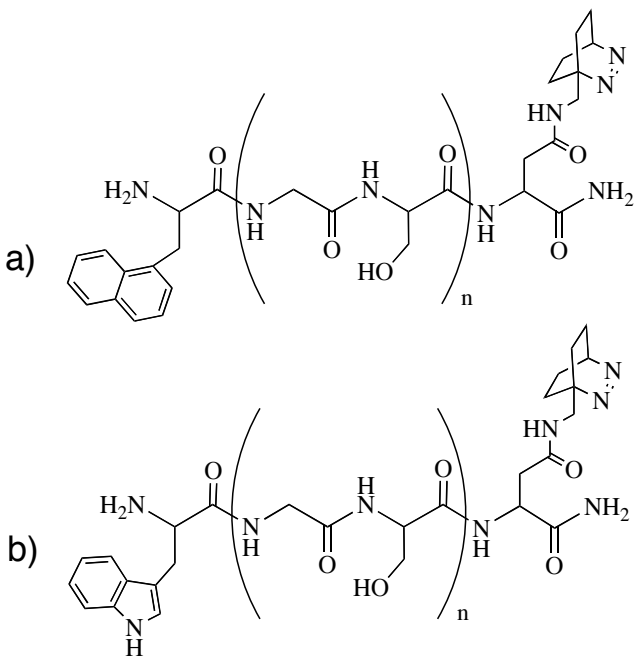

Scheme 4.3. Structure of doubly labelled Gly-Ser peptides: a) Nal/DBO labelled peptides, Nal-(Gly-Ser)$_n$-DBO and b) Trp/DBO labelled peptides, Trp-(Gly-Ser)$_n$-DBO

The energy donor and acceptor were attached at the opposite ends of the peptides (Scheme 4.3). In principle, the decay of the excited donor residue, which is dependent on the end-to-end distance distribution at each moment and the intrachain diffusion, can be described by the following equation:[12,16-18]

$$\frac{\partial}{\partial t} g_{\mathrm{N}}^{*}(r,t) = -\frac{1}{\tau_0}\left(1+\left(\frac{R_0}{r}\right)^6\right) g_{\mathrm{N}}^{*}(r,t) + D\frac{1}{r^2}\frac{\partial}{\partial r} r^2 \frac{\partial}{\partial r} g_{\mathrm{N}}^{*}(r,t) + D\frac{1}{r^2}\frac{\partial}{\partial r}\left(r^2 g_{\mathrm{N}}^{*}(r,t)\frac{\partial}{\partial r}\beta U(r)\right) \quad (4.4)$$

However, since the key parameters (the distribution function and the diffusion coefficient) are tightly correlated, the fluorescence of acceptor residue was also recorded to improve the analysis accuracy. Therefore, for each peptide, time-resolved fluorescence decay traces of

donor and acceptor residue in the presence and absence of FRET were recorded under the same condition and then applied to a global analysis.

For the series of naphthalene/DBO labelled peptides, the equilibrium end-to-end distance distribution and the intrachain diffusion coefficient were successfully recovered (Table 4.1). The results showed that the average end-to-end distances of those peptides are substantially shorter than their contour length. The recovered intramolecular diffusion coefficients are all in the order of 10^{-7}cm^2/s and increase with peptide length. These value verified our earlier assumption that the intrachain diffusion coefficient in peptides is at least one order of magnitude slower than the free amino acids and corroborated also the conclusions made in the simulation work,[19] namely that the slower diffusion coefficient for shorter peptides instead of the difference of end-to-end distance distribution from ideal chain model (Gaussian chain) is the key reason for the deviation of length dependent end-to-end collision rates from theoretical predictions (see detailed results and discussion in Appendix VII).

Table 4.1. Distance distribution and diffusion coefficient recovered from direct global analysis for Nal-(Gly-Ser)$_n$-DBO peptides.

peptide	N	L (Å)[a]	R_{mean} (Å)[b]	D (10^{-7}cm^2/s)	χ^2
Nal-DBO	2	7.6	6.14	2.67	1.12
Nal-G-S-DBO	4	15.2	6.26	2.76	1.09
Nal-(G-S)$_2$-DBO	6	22.8	7.96	4.03	1.13
Nal-(G-S)$_4$-DBO	10	38.0	10.39	5.66	1.11
Nal-(G-S)$_6$-DBO	14	53.2	10.91	4.91	1.08
Nal-(G-S)$_{10}$-DBO	22	83.6	[c]	[c]	[c]

[a] Contour length, L, equals the number of intervening peptide units, N, times 3.8Å.

[b] Average end-to-end distance obtained by FRET measurements and direct global analysis.

[c] Data analysis has not been finished.

The Trp/DBO doubly labelled peptides are of specific interest for us. In our previous work, the intrachain collision rates in various peptides have been successfully measured, where DBO serves as the fluorescence probe and Trp as an efficient collision-induced quencher. In this project, the structural properties of those peptides were investigated with an independent FRET approach, where the role of Trp was changed to an energy donor and DBO to the energy acceptor. The energy transfer efficiency in each peptide was measured based on the change of steady-state fluorescence intensity of the Trp residue and the corresponding effective average end-to-end distance was calculated. Since the lifetime of Trp is very short and the movement of the excited Trp donor can consequently be neglected, the effective average distances are very close to the equilibrium ones. The experimental results provided powerful evidence for the detailed structural properties for a specific group of peptides. For instance, in the case of peptides derived from the β-hairpin of ubiquitin,[8] the energy transfer efficiencies in different segments are quite close, indicating similar end-to-end distance. Therefore, the significant different end-to-end collision rates of those peptides can be attributed to the specific flexibility corresponding to the sequence.

References

(1) Hagen, S. J.; Hofrichter, J.; Szabo, A.; Eaton, W. A., *Proc. Natl. Acad. Sci. USA* **1996,** *93*, 11615-11617.

(2) Wallace, M. I.; Ying, L.; Balasubramanian, S.; Klenerman, D., *Proc. Natl. Acad. Sci. USA* **2001,** *98*, 5584-5589.

(3) Lapidus, L. J.; Eaton, W. A.; Hofrichter, J., *Proc. Natl. Acad. Sci. USA* **2000,** *97*, 7220-7225.

(4) McGimpsey, W. G.; Chen, L.; Carraway, R.; Samaniego, W. N., *J. Phys. Chem. A* **1999,** *103*, 6082-6090.

(5) Bieri, O.; Wirz, J.; Hellrung, B.; Schutkowski, M.; Drewello, M.; Kiefhaber, T., *Proc. Natl. Acad. Sci. USA* **1999,** *96*, 9597-9601.

(6) Hudgins, R. R.; Huang, F.; Gramlich, G.; Nau, W. M., *J. Am. Chem. Soc.* **2002,** *124*, 556-564.

(7) Huang, F.; Nau, W. M., *Angew. Chem. Int. Ed. Engl.* **2003,** *42*, 2269-2272.

(8) Huang, F.; Hudgins, R. R.; Nau, W. M., **2004,** *submitted for publication.*

(9) Zachariasse, K. A.; Macanita, A. L.; Kühnle, W., *J. Phys. Chem. B* **1999,** *103*, 9356-9365.

(10) Szabo, A.; Schulten, K.; Schulten, Z., *J. Chem. Phys.* **1980,** *72*, 4350-4357.

(11) Winnik, M. A., *Acc. Chem. Res.* **1985,** *18*, 73-79.

(12) Haas, E.; Katchalski-Katzir, E.; Steinberg, I. Z., *Biopolymers* **1978,** *17*, 11-31.

(13) Grosberg, A. Y.; Khokhlov, A. R. *Statistical Physics of Macromolecules*; American Institute of Physics: New York, 1994.

(14) Flory, P. J. *Statistical Mechanics of Chain Molecules*; John Wiley & Sons, Inc.: New York, 1969.

(15) Liu, G.; Guillet, J. E., *Macromolecules* **1990,** *23*, 2969-2973.

(16) Bodunov, E. N.; Berberan-Santos, M. N.; Martinho, J. M. G., *J. Lumin.* **2002,** *96*, 269-278.

(17) Bodunov, E. N.; Berberan-Santos, M. N.; Martinho, J. M. G., *High Energy Chem.* **2002,** *36*, 245-250.

(18) Lakowicz, J. R.; Kusba, J.; Wiczk, W.; Gryczynski, I.; Szmacinski, H.; Johnson, M. L., *Biophys. Chem.* **1991,** *39*, 79-84.

(19) Wang, X.; Bodunov, E. N.; Nau, W. M., *Opt. Spectrosc.* **2003,** *95*, 560-570.

5. Experimental Measurement of Structural and Dynamic Properties of Single-Stranded Oligonucleotides

Intramolecular contact formation is the elementary step in the folding of proteins and nucleic acids to form native three-dimensional structures. The rate constants for intrachain collision and the intrinsic flexibility of single-stranded nucleic acids are fundamental parameters in biophysical models and in addition they provide benchmark values for computational methods.[1] While the kinetics of end-to-end contact formation has been experimentally measured for polypeptides,[2-5] the characteristic time scale for intrachain collision in single-stranded nucleic acids has remained elusive.

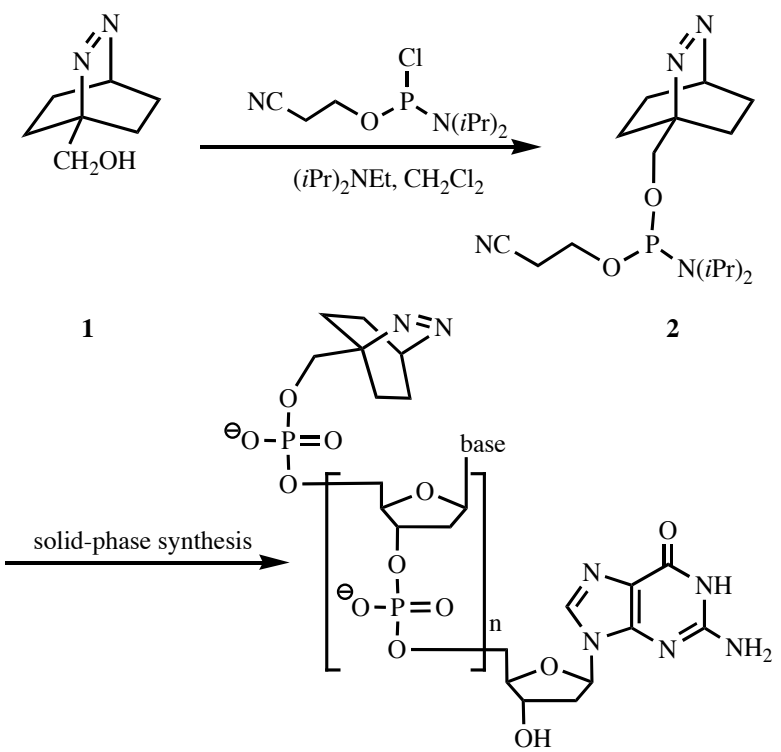

Scheme 5.1. Synthetic route for DBO-labelled oligonucleotides

In this project, the end-to-end collision rates and the fluctuation of the base parts were experimentally measured with a method based on intramolecular fluorescence quenching of the long-lived fluorescent probe DBO. Our previous work showed that DBO can be

selectively quenched by guanine though other bases also work as weak quenchers and all these quenching reactions require a direct probe-quencher contact.[6] A new phosphoramidite DBO derivative was synthesized and directly applied in the automated solid-phase synthesis to obtain DBO-labelled oligonucleotides (Scheme 5.1). The fluorescence lifetimes of the target oligonucleotides (τ_{obs}), where guanine was attached at the opposite ends, as well as those of reference strands with identical sequence but without the 3' terminal quencher (τ_0) were measured. The quenching rate constants related to quenching by guanine (k_q) can then be obtained according to Eq. 5.1, which corresponds, subject to the assumption of nearly-quantitative quenching upon contact ($k_d >> k_-$), to the rate of end-to-end collision (k_+ in Eq. 5.2).

$$k_q = \frac{1}{\tau_{obs}} - \frac{1}{\tau_0} \tag{5.1}$$

$$k_q = \frac{k_+ \cdot k_d}{k_d + k_-} \approx k_+, \text{ for } k_d >> k_- \tag{5.2}$$

5.1. End-to-End Collision in Short Single-Stranded Oligodeoxyribonucleotides

Several groups have already studied the coil-to-hairpin transition in short single-stranded DNA by absorption or FRET methods.[7-12] However, even for this simple system, the inconsistent experimental results point to an important question, namely whether or not the two-state model of an all-or-none transition between open and closed states is appropriate. Ansari and co-workers later suggested a configurational diffusion model, in which the ssDNA can be transiently trapped in misfolded states prior to the nucleation step.[12] The test of this model requires experimental rate constants for the collision between the two ends of a DNA strand, which was not available before.

Herein, the end-to-end collision rates have been reported for the first time in short single-stranded oliodeoxyribonucleotides, which correspond in their size to the loop segment of an entire hairpin.[13] The intramolecular quenching rate constants for oligonucleotides composed of a backbone of different length and type of nucleotide were determined in a temperature range between 25 to 40°C (some results are shown in Table 5.1. See detailed experimental procedure, results and discussion in Appendix VI).

Table 5.1. Rate constants and activation energies for end-to-end collision in single-stranded oligonucleotides

base sequence	oligonucleotide	τ_{obs} (ns)	τ_0 (ns)[a]	k_+ (10^6 s^{-1})[b]	E_a (kJ/mol)[c]
5'-DBO-AAAAG	DNA	247	255	0.12	33
	RNA	111	125	1.0	36
	2'-OMe RNA	152	170	0.70	38
5'-DBO-TTTTG	DNA	72	87	2.4	14
5'-DBO-CCCCG	DNA	96	115	1.8	16
	RNA	71	83	2.0	24
	2'-OMe RNA	*d*	*d*	*d*	*d*
5'-DBO-UUUUG	DNA	83	118	3.6	10
	RNA	58	73	3.7	11
	2'-OMe RNA	82	101	2.3	13

[a] τ_0 is the lifetime of the reference strands with identical sequence but without the 3' terminal dG as quencher, 5'-DBO-$(X)_4$.

[b] At 25°C, error in data is 10%.

[c] Temperature range 25 – 40°C; error in data is ±3 kJ/mol.

[d] Results are not available due to the problem in 2'-OMe RNA synthesis.

It was found that the collision rates are strongly dependent on the type of nucleotide in the backbone. The rates in pyrimidine-derived oligonucleotides are all in the order of 10^{-6} s^{-1}, which are one order of magnitude slower than the collision rates in flexible peptides with same number of units. On the other hand, oligoadenylates displayed much slower collision rates and significantly higher activation energies, which point to a higher intrinsic "rigidity". This rigidity is presumably due to two reasons. On one hand, purine bases are larger than pyrimidines, which decreases the intrachain diffusion coefficient and imposes higher steric

restrictions towards bond rotation. On the other hand, adjacent purine bases undergo sizeable base-stacking interactions,[14,15] which impose a barrier towards free bond rotation.

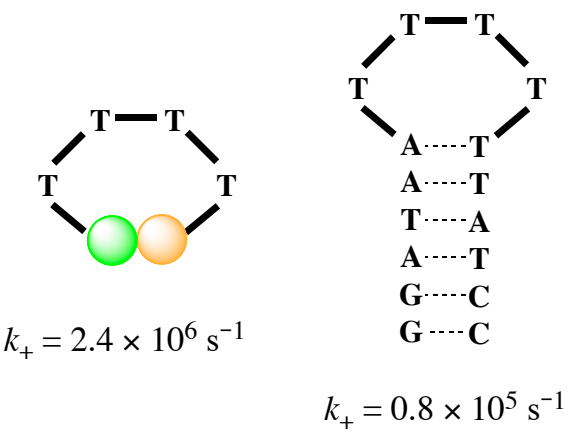

Scheme 5.2. End-to-end collision in DBO-$(dT)_4$-dG and kinetics of DNA hairpin closing with $(dT)_4$ as the loop

As mentioned above, end-to-end collision rates are important to understand the mechanism of hairpin formation. While the closing rate for a DNA hairpin with 4 dT in the loop was reported as ca. $0.8 \times 10^5\ s^{-1}$ (25°C),[12] our experiments afforded an end-to-end collision rate of $2.4 \times 10^6\ s^{-1}$ for 5'-DBO-$(dT)_4$-dG (Scheme 5.2), which is much faster and suggests that the time for hairpin formation is "longer" than expected from the time of forming a loop. This result is consistent with the idea that not all end-to-end or other intrachain contacts induce hairpin formation, i.e., there are mismatches and inefficient contacts, which require the ssDNA to explore several local minima conformations until the "correct" nucleating loop is reached. The absolute rate constants for end-to-end collision in oligonucleotides provide therefore strong support for the configurational diffusion model by Ansari and co-workers.

5.2. Intrachain Fluorescence Quenching in Short RNA and 2'-OMe RNA Single Strands: Comparison of Conformations and Dynamics with DNA Analogues

The potential use of short oligonucleotides as antisense agents inhibiting gene expression has attracted intensive interests on the structure and dynamic properties of DNA and RNA

oligomers and their analogues.[16-18] In this project, the selective quenching of DBO by guanine was employed to measure the fluorescence decay in DNA, RNA and a representative antisense oligonucleotide, 2′-*O*-methyl RNA. The effect of 2′-hydroxyl and 2′-*O*-methyl sugar substitutions on the structure and dynamics of short oligomers is discussed.

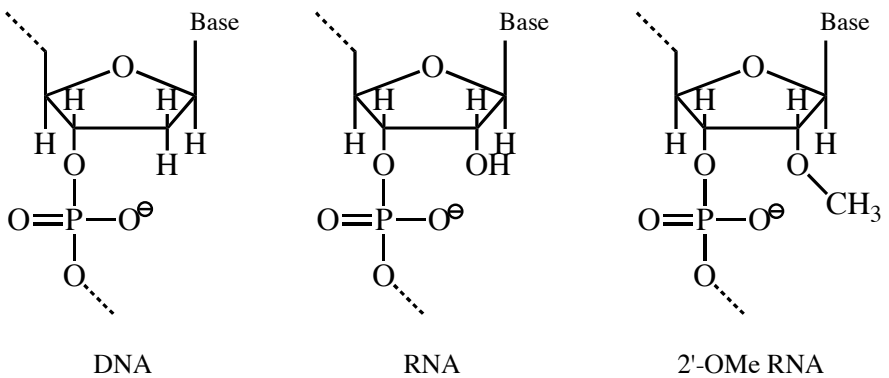

Scheme 5.3. Structural variation between DNA, RNA, and 2'-OMe RNA

Sequences of single-stranded oligonucleotides were designed as 5'-DBO-$(X)_4$-G, where X = C, U or A. Reference strands, which have the identical sequences but lack the 3' terminal quencher (5'-DBO-$(X)_4$) were also measured (Results are shown in Table 5.1).

It was interesting to find that the fluorescence lifetimes of the reference strands, where no guanine was attached at the 3' end, showed a significant variation between DNA, RNA and 2′-*O*-methyl RNA analogues in the same base sequence with the order: DNA > 2′-*O*-methyl RNA > RNA. Measurements in D_2O showed that the quenching in RNA strands had relatively weak isotopic effects for all three kinds of strands with different types of base (1.2 – 1.3), which are much smaller than the isotopic effect expected from quenching of DBO by an OH group.[19,20] The small ratio herein can exclude the contribution of 2′ hydroxyl groups. This is also supported by the finding that the ribonucleotide and deoxyribonucleotide monomers containing the same base performed the same quenching ability to excited DBO.[6] Considering that the viscosity of D_2O is ca. 25% higher than that of H_2O, the difference of quenching effect of the backbone in H_2O and D_2O can be assigned to the higher external friction with the solvent in D_2O. Detailed structural research have shown that in DNA oligomers, the

preferable C2'-endo sugar pucker results in a more fixed *syn* conformation, where the bulky part of the base is located over the sugar, giving rise to closer interatomic contacts and higher steric barrier to the rotation of the base part. On the contrary, the dominating C3'-pucker in RNA oligomers prefers an *anti* conformation, which gives more movement freedom of the bases.[15] Therefore, we suggest that the quenching of the backbone is mainly due to the collision between the end-attached probe and its nearest-neighbour base. This process is controlled by the mutual intrachain fluctuation of the probe and the base, which is dependent on the structural property of the backbone, such as sugar pucker conformation, and the external friction with the solvent medium.

We encountered some troubles in the measurements of end-to-end collision rates in 2′-*O*-methyl RNA due to the solid-phase synthesis difficulties. For RNA strands, the end-to-end collision rates are strongly dependent on the type of nucleotide with the same order as in DNA: U > C > A. The strand composed of adenine displayed significantly higher activation energy (36 kJ/mol) than others, which suggests that the base stacking interactions together with the steric effect corresponding to the larger size of adenine also contribute to the rigidity of RNA analogue. At the same time, the activation energy of end-to-end collision in the cytosine strand is 24 kJ/mol, which is also a little higher than 16 kJ/mol, the activation energy for solvent viscous flow in H_2O, indicating some additional energy barrier than the solvent friction. The end-to-end collision in uracil strand displayed very similar rate constant and activation energy as its DNA analogue, which suggests that the uracil strand is the most flexible one and the process is only limited by solvent friction.

It should be noted that although the collision rates of cytosine and uracil RNA strands are very close to their DNA analogues, in case of the adenine strand, the collision in RNA strand is one order of magnitude faster than its DNA analogue. Such a significant difference indicated that it is either structure-related, e.g., to a different end-to-end distance due to the sugar pucker conformation, or dynamics-related, e.g., to a the different global flexibility between these two analogues. Recent computer simulation work suggested that RNA strands are more flexible than the DNA analogue based on the simulated root-mean-squared-deviations of the end-to-end distance in two DNA and RNA strands with same sequence.[21]

However, before the final conclusion is drawn, more well-designed experiments should be done.

References:

(1) Yeh, I.-C.; Hummer, G., *J. Am. Chem. Soc.* **2002,** *124*, 6563-6568.

(2) Lapidus, L. J.; Eaton, W. A.; Hofrichter, J., *Proc. Natl. Acad. Sci. USA* **2000,** *97*, 7220-7225.

(3) Hudgins, R. R.; Huang, F.; Gramlich, G.; Nau, W. M., *J. Am. Chem. Soc.* **2002,** *124*, 556-564.

(4) Bieri, O.; Wirz, J.; Hellrung, B.; Schutkowski, M.; Drewello, M.; Kiefhaber, T., *Proc. Natl. Acad. Sci. USA* **1999,** *96*, 9597-9601.

(5) Huang, F.; Nau, W. M., *Angew. Chem. Int. Ed. Engl.* **2003,** *42*, 2269-2272.

(6) Marquez, C.; Pischel, U.; Nau, W. M., *Org. Lett.* **2003,** *5*, 3911-3914.

(7) Bonnet, G.; Krichevsky, O.; Libchaber, A., *Proc. Natl. Acad. Sci. USA* **1998,** *95*, 8602-8606.

(8) Goddard, N. L.; Bonnet, G.; Krichevsky, O.; Libchaber, A., *Phys. Rev. Lett.* **2000,** *85*, 2400-2403.

(9) Ying, L.; Wallace, M. I.; Klenerman, D., *Chem. Phys. Lett.* **2001,** *334*, 145-150.

(10) Wallace, M. I.; Ying, L.; Balasubramanian, S.; Klenerman, D., *Proc. Natl. Acad. Sci. USA* **2001,** *98*, 5584-5589.

(11) Shen, Y.; Kuznetsov, S. V.; Ansari, A., *J. Phys. Chem. B* **2001,** *105*, 12202-12211.

(12) Ansari, A.; Kuznetsov, S. V.; Shen, Y., *Proc. Natl. Acad. Sci. USA* **2001,** *98*, 7771-7776.

(13) Wang, X.; Nau, W. M., *J. Am. Chem. Soc.* **2004,** *126*, 808-813.

(14) Mills, J. B.; Vacano, E.; Hagerman, P. J., *J. Mol. Biol.* **1999,** *285*, 245-257.

(15) Saenger, W. *Pinciples of nucleic acid structure*; Springer-Verlag: New York, 1984.

(16) Braasch, D. A.; Corey, D. R., *Biochemistry* **2002,** *41*, 4503-4510.

(17) Kurreck, J., *Eur. J. Biochem.* **2003,** *270*, 1628-1644.

(18) Zamaratski, E.; Pradeepkumar, P. I.; Chattopadhyaya, J., *J. Biochem. Biophys. Methods* **2001,** *48*, 189-208.

(19) Nau, W. M.; Greiner, G.; Rau, H.; Olivucci, M.; Robb, M. A., *Ber. Bunsenges. Phys. Chem.* **1998,** *102*, 486-492.

(20) Nau, W. M.; Greiner, G.; Rau, H.; Wall, J.; Olivucci, M.; Scaiano, J. C., *J. Phys. Chem. A* **1999,** *103*, 1579-1584.

(21) Sen, S.; Nilsson, L., *J. Am. Chem. Soc.* **2001,** *123*, 7414-7422.

6. Additional Project: Charge Hopping in DNA Strands

This project was motivated by the discussions on the mechanism of charge migration in DNA.[1-6] Since more and more experimental results have provided evidence for charge hopping between individual bases, a weaker distance dependence (Eq. 6.1) for charge migration was proposed,[7-9]

$$k_{CT} \approx k_{HOP} N^{-\eta} \tag{6.1}$$

where N, the number of hopping sites, is a measure of the distance and η is the parameter for the bias towards charge migration in the direction of the trap, which ranges between 1 (irreversible hopping) and 2 (unbiased hopping).

However, our analysis showed that this equation only applied for very long one-directional systems, which have not been studied experimentally. Additionally, since under natural conditions the charge migration would generally proceed in two directions, we suggested that hopping towards traps on opposite ends should be considered. Therefore, in this project, the kinetics of charge migration in DNA strands was analysed on the basis of a one- and two-directional hopping model, where the long-range charge migration occurs through a sequence of several superexchange charge transfer steps between nearest guanine bases.[10]

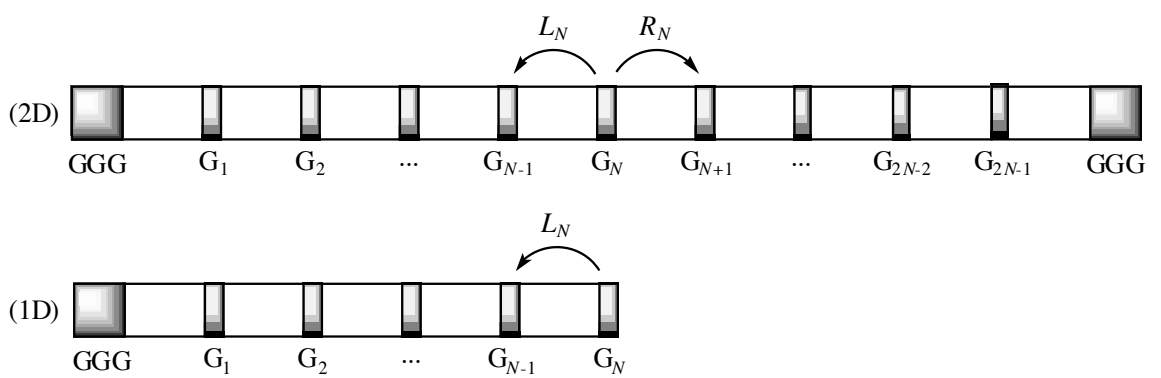

Scheme 6.1. One- and two-directional hopping in one-dimensional systems

A finite one-dimensional system is considered, where the charge has been generated at one end and there is a perfect trap at the other end (Scheme 6.1, 1D case), or, the charge has been generated at the central site and there are two perfect traps at the opposite ends (Scheme 6.1, 2D case). The charge undergoes a random walk which involves only hopping to the nearest-

neighbour sites until trapped at the terminal traps. In DNA strands hopping of a positive charge has been assumed to take place between guanine bases (G), which are separated by a given set of adenine, thymine, and cytosine bases.[6-9,11-15] The latter have less favourable oxidation potentials and generally do not serve as charge carriers,[16,17] but the nature and number of these intervening bases determine how fast hopping occurs. Trapping of the charge may occur at a guanine cluster (GGG), which is particularly prone to oxidation.[17] The hopping sites therefore are designated as G and the traps as GGG.

The lifetime of charge migration between generation and irreversible trapping was calculated, which showed a weak distance dependence both for the one- and two-directional cases (see detailed procedure, results and discussion in Appendix I):

$$\tau(2D) = \frac{(2N-1)}{2k_t} + \frac{(N-1)^2}{2k} \tag{6.2}$$

$$\tau(1D) = \frac{N}{k_t} + \frac{N(N-1)}{2k} \tag{6.3}$$

where the number of hopping sites is N for the 1D case and $2N–1$ for the 2D case. k is the hopping rate constant between neighbouring sites, except for hopping to the trap, for which a different rate constant k_t is presumed. These rate constants correspond to the respective rate constants for coherent superexchange charge transfer between two nearest-neighbour hopping sites, i.e., guanine bases. Eqs (6.2) and (6.3) can be further simplified for the unbiased hopping ($k_t = k$) to

$$\tau(2D) = \frac{N^2}{2k}, \quad k_t = k \tag{6.4}$$

$$\tau(1D) = \frac{N(N+1)}{2k}, \quad k_t = k \tag{6.5}$$

It is noted that for the one-directional case Bar-Haim and Klafter[18,19] have provided the same result for the lifetime of the random walker before trapping. In particular, for "a finite but large system" and $k_t = k$, they developed an approximate expression for the lifetime as $\tau \approx N^2/(2k)$ for unbiased hopping and a related equation for hopping with systematic bias in direction of the trap. The latter was modified[7-9] to provide the more general approximate

relationship $\tau \propto N^{\eta}$, which has recently been adopted to analyze charge migration in DNA as the distance dependence test for the charge hopping mechanism,[3,4,7-9,11-13,20,21] η is the parameter for the bias towards charge migration in the direction of the trap, which ranges between 1 (irreversible hopping) and 2 (unbiased hopping). However, in most experimental studies only small N values are accessible (N = 1-5). In these cases, Eqs (6.2)-(6.5) apply.

Furthermore, the *approximate* relationship suggested[7-9] for unbiased (η = 2) *one-directional* charge migration (N^2 dependence) is identical to the *exact* relationship obtained in the present work for unbiased *two-directional* charge migration with two equidistant traps. Such two-directional charge migration in DNA has not yet been subject to experimental tests, although it is most relevant for the corresponding natural processes.

We recommend a plot of the increase in lifetime upon increasing N to N+1, $\Delta\tau$, against N:

$$\Delta\tau(\mathrm{2D}) = \frac{1}{k_t} - \frac{1}{2k} + \frac{N}{k}, \text{ which simplifies to } \Delta\tau(\mathrm{2D}) = \frac{1}{2k} + \frac{N}{k} \text{ for } k_t = k \qquad (6.6)$$

$$\Delta\tau(\mathrm{1D}) = \frac{1}{k_t} + \frac{N}{k}, \text{ which simplifies to } \Delta\tau(\mathrm{1D}) = \frac{1}{k} + \frac{N}{k} \text{ for } k_t = k \qquad (6.7)$$

In this manner, one obtains a linear dependence on N for both the one- and two-directional hopping process. In the one-directional case a linear dependence can be alternatively obtained by plotting τ/N (rather than τ) against N according to Eq. (6.8).

$$\frac{\tau(\mathrm{1D})}{N} = \left(\frac{1}{k_t} - \frac{1}{2k}\right) + \frac{1}{2k}N \qquad (6.8)$$

We suggest that the linearity of the corresponding plots provides evidence for hopping. In case experimental methods for the direct determination of the absolute lifetimes become available, such plots may be useful to extract the rate constant for hopping between G bases from the slope of such plots ($1/k$).

References:

(1) Ly, D.; Kan, Y.; Armitage, B.; Schuster, G. B., *J. Am. Chem. Soc.* **1996,** *118*, 8747-8748.

(2) Murphy, C. J.; Arkin, M. R.; Jenkins, Y.; Ghatlia, N. D.; Bossman, S. H.; Turro, N. J.; Barton, J. K., *Science* **1993,** *262*, 1025-1029.

(3) Kelley, S. O.; Barton, J., *Science* **1999,** *283*, 375-381.

(4) Henderson, P. T.; Jones, D.; Hampikian, G.; Kan, Y.; Schuster, G. B., *Proc. Natl. Acad. Sci. USA* **1999,** *96*, 8353-8358.

(5) Giese, B.; Amaudrut, J.; Köhler, A.; Spormann, M.; Wessely, S., *Nature* **2001,** *412*, 318-320.

(6) Giese, B.; Wessely, S.; Spormann, M.; Lindemann, U.; Meggers, E.; Michel-Beyerle, M. E., *Angew. Chem. Int. Ed. Engl.* **1999,** *38*, 996-998.

(7) Jortner, J.; Bixon, M.; Langenbacher, T.; Michel-Beyerle, M. E., *Proc. Natl. Acad. Sci. USA* **1998,** *95*, 12759-12765.

(8) Bixon, M.; Giese, B.; Wessely, S.; Langenbacher, T.; Michel-Beyerle, M. E.; Jortner, J., *Proc. Natl. Acad. Sci. USA* **1999,** *96*, 11713-11716.

(9) Bixon, M.; Jortner, J., *J. Phys. Chem. B* **2000,** *104*, 3906-3913.

(10) Wang, X.; Nau, W. M., *ChemPhysChem* **2001,** *2*, 761-766.

(11) Nunez, M. E.; Hall, D. B.; Barton, J. K., *Chem. Biol.* **1999,** *6*, 85-97.

(12) Meggers, E.; Michel-Beyerle, M. E.; Giese, B., *J. Am. Chem. Soc.* **1998,** *120*, 12950-12955.

(13) Giese, B., *Acc. Chem. Res.* **2000,** *33*, 631-636.

(14) Giese, B.; Spichty, M., *ChemPhysChem* **2000,** *1*, 195-198.

(15) Davis, W. B.; Naydenova, I.; Haselsberger, R.; Ogrodnik, A.; Giese, B.; Michel-Beyerle, M. E., *Angew. Chem. Int. Ed. Engl.* **2000,** *39*, 3649-3652.

(16) Steenken, S.; Jovanovic, S. V., *J. Am. Chem. Soc.* **1997,** *119*, 617-618.

(17) Sugiyama, H.; Saito, I., *J. Am. Chem. Soc.* **1996,** *118*, 7063-7068.

(18) Bar-Haim, A.; Klafter, J., *J. Chem. Phys.* **1998,** *109*, 5187- 5193.

(19) Bar-Haim, A.; Klafter, J., *J. Phys. Chem. B* **1998,** *102*, 1662-1664.

(20) Ratner, M., *Nature* **1999,** *397*, 480-481.

(21) Schuster, G. B., *Acc. Chem. Res.* **2000,** *33*, 253-260.

7. Summary and Outlook

In this thesis, the diffusion-controlled fluorescence quenching in different dimensions as well as in molecular chains was theoretically analyzed. A series of mathematical expressions were derived. These results are helpful for understanding the reaction mechanism in various dimensions and consequently for choosing suitable models to fit the time-resolved fluorescence intensity data and extract the key dynamic parameters. On the other hand, the experimental projects were also carried out to investigate the structural and dynamic properties in oligonucleotides and polypeptides by employing fluorescence-based methods. The end-to-end collision rate constants in short ssDNA were measured for the first time and offered powerful support for the configurational diffusion model of hairpin formation. Structural properties, such as the base-stacking interactions and the sugar pucker conformations were also experimentally checked. These results are essential to predict the time scale and determine the mechanism of secondary structure formation and to evaluate the flexibility of biopolymers with different sequences. In addition, the experimental results provide benchmark values for the development of computational methods for biopolymer dynamics.

The ideas for future work focus on two directions: 1) Further application of the DBO/guanine fluorescent probe/quencher pair in the dynamics of oligonucleotides and nucleic acids. The efficient intramolecular quenching can be applied to investigate the structural and dynamic properties of various oligonuleotides, such as 2′-*O*-methyl RNA, phosphorothioate DNA, and PNA. Some initial work in this direction has already been done. 2) Exploring new fluorophore/quencher pairs to extend the research fields. In addition to the natural nucleotide monomer, there are more analogues reported with varying photochemical properties. It will be very useful to experimentally test the reaction mechanism of different fluorophore/quencher pairs and establish new methods based on various mechanisms, such as FRET or electron transfer, which could be applied to measure the end-to-end distance distribution or charge transfer kinetics in DNA strands.

8. Publications (Contained in Appendix)

I. Kinetics of one- and two-directional charge hopping in one-dimensional system: application to DNA.
Wang, X.; Nau, W. M., *ChemPhysChem* **2001,** *2*, 761-766.

II. Biomolecular and supramolecular kinetics in the submicrosecond time range: The fluorazophore approach.
Nau, W. M.; Wang, X., *ChemPhysChem* **2002,** *3*, 393-398.

III. A joint structural, kinetic, and thermodynamic investigation of substituent effects on host-guest complexation of bicyclic azoalkanes by β-cyclodextrin.
Zhang, X.; Gramlich, G.; Wang, X.; Nau, W. M., *J. Am. Chem. Soc.* **2002,** *124*, 254-263.

IV. Fluorescence quenching kinetics in short polymer chains: Dependence on chain length.
Wang, X.; Bodunov, E. N.; Nau, W. M., *Opt. Spectrosc.* **2003,** *95*, 560-570.

V. Exploiting Long-Lived Molecular Fluorescence.
Nau, W. M., Huang, F., Wang, X., Bakirci, H., Gramlich, G. Marquez, C. *Chimia* **2003,** *57*, 161-167.

VI. Kinetics of end-to-end collision in short single-stranded nucleic acids.
Wang, X.; Nau, W. M., *J. Am. Chem. Soc.* **2004,** *126*, 808-813.

VII. Application of FRET donor/acceptor pairs with small critical radius to recover the structural and dynamic properties in short flexible peptides.
Huang, F.; Wang, X.; Haas, E.; Nau, W. M., **2004**, *in preparation*

9. Presentations at Conferences

Oral Presentation:

1. Kinetics of End-to-End Collision in Short Single-Stranded Nucleic Acids
   X. Wang and W. M. Nau, the XXIth International Conference on Photochemistry, Nara, Japan, July 2003.

Posters:

1. Fluorescence Quenching in Low Dimensions
   X. Wang and W. M. Nau, Joint Meeting of the Italian, French, and Swiss Photochemistry Group, Lausanne, Switzerland, February 2001.
2. The Fluorazophore Approach: Applications in Supramolecular Chemistry and Biology
   H. Bakirci, U. Pischel, X. Wang, and W. M. Nau, NRP 47 "Supramolecular Functional Materials" 1st Progress Report Meeting, Bern, Switzerland, October 2001.
3. Kinetics of Biopolymer Folding: Flexibility Scales for Polypeptides and Oligonucleotides
   F. Huang, X. Wang, and W. M. Nau, International Conference on Reactive Intermediates and Reaction Mechanisms, Ascona, Switzerland, July 2002.
4. Dynamics of Diffusion-Controlled Intramolecular Reaction of Short Chains Based on Monte Carlo Simulation
   X. Wang and W. M. Nau, 38th Symposium for Theoretical Chemistry: Electron Transfer and Femtosecond Spectroscopy, Bremen, Germany, August 2002.
5. Kinetics of End-to-End Collision in Short Single-Stranded Nucleic Acids
   X. Wang and W. M. Nau, SGPP Graduate Student Symposium in Photochemistry, Photobiology and Photophysics, Fribourg, Switzerland, April 2003.
6. Chain Flexibility of Biopolymers: An Example of Supramolecular Mechanics
   F. Huang, X. Wang, G. Gramlich, and W. M. Nau, "Supramolecular Functional Materials" Meeting, Bern, Switzerland, July 2003.

10. Appendix

Kinetics of One- and Two-Directional Charge Hopping in One-Dimensional Systems: Application to DNA

Xiaojuan Wang and Werner M. Nau*[a]

KEYWORDS:

charge transfer · DNA oxidation · hopping · kinetics

Charge migration in DNA has attracted significant attention because of its importance for DNA damage and repair. Several experimental and theoretical studies have focused on the mechanism and distance dependence of charge migration in DNA. Ly et al. suggested[1, 2] that the migration of a positive charge in DNA occurs by hopping[3, 4] from one base to a neighboring base, while Barton and co-workers considered that charge transport in DNA occurs coherently, by a superexchange mechanism, through the π-stack of the DNA base pairs.[5, 6] The rate of charge transfer (k_{CT}) by superexchange should follow the distance (R) dependence in Equation (1). Experiments on diverse

$$k_{CT} \propto \exp(-\beta R) \quad (1)$$

donor-bridge-acceptor systems yielded a large scatter in the magnitude of the β values, implying large variances in the conductive properties.[6–14] Recent studies suggest a more complex interplay between both mechanisms.[15–22] In particular, Giese and co-workers have provided evidence for charge hopping between individual bases,[20–22] which is also in line with previous experimental observations by Barton and co-workers[11, 18] as well as Schuster and co-workers.[16] Jortner and co-workers have described a hopping mechanism, for which a weaker distance dependence for charge migration according to Equation (2) is expected,[23–25] where N,

$$k_{CT} \approx k_{hop} N^{-\eta} \quad (2)$$

the number of hopping sites, is a measure of the distance and η is the parameter for the bias towards charge migration in the direction of the trap, which ranges between 1 (irreversible hopping) and 2 (unbiased hopping).

Recent theoretical and experimental work on the kinetics of charge transfer in DNA strands has focused on one-directional charge transfer in DNA strands, where the charge migrates to a single trap.[20–25] However, under natural conditions where radiation and dissolved reagents react with the nucleotide bases or sugars in an essentially random manner, charge formation will generally occur in the middle of a DNA strand, such that charge migration *in two directions* towards one trap on either side requires attention. Such a situation has been examined by Schuster and co-workers.[2] Herein, we analyze the kinetics of charge migration on the basis of a one- and two-directional hopping model (1D, 2D), where the long-range charge migration occurs through a sequence of several superexchange charge-transfer steps between nearest guanine bases. The results are compared with the kinetic model for charge migration in a one-directional system with one trap, which has been proposed by Bar-Haim and Klafter[3, 4] for energy transfer in antenna systems and transferred to the DNA problem by Jortner and co-workers.[23–25]

Theory

We consider first a finite one-dimensional system composed of $2N-1$ hopping sites and two perfect traps at the opposite ends, in which a charge has been generated on the central site (Scheme 1, 2D case). The charge undergoes a random walk which involves only hopping to the nearest-neighbor sites. Hopping will occur until the charge is trapped at a terminal trapping site. In DNA strands, positive charge hopping has been assumed to take place between guanine bases (G) separated by

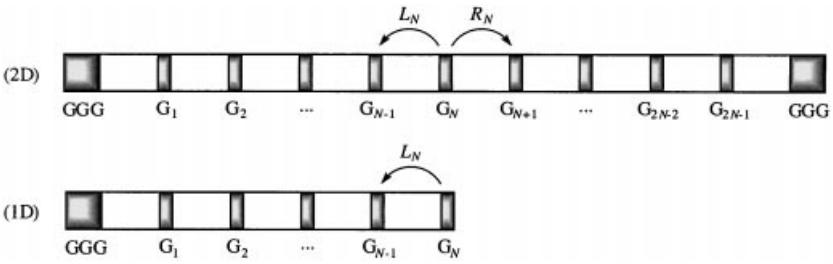

Scheme 1. *The basic format of the two- and one-directional charge-hopping models.*

a given set of adenine, thymine, and cytosine bases.[18–27] The latter have less favorable oxidation potentials and generally do not serve as charge carriers[28, 29] but the nature and number of these intervening bases determine how fast hopping occurs. Trapping of the charge may occur at a guanine cluster (GGG), which is particularly prone to oxidation.[29] We therefore designate the hopping sites as G and the traps as GGG, keeping in mind that the principle model is transferable to other bases in DNA as well as charge transfer in other natural or artificial one-dimensional systems like peptides.[30]

The probabilities that the randomly walking charge in the 2D case of Scheme 1 reaches the ith G after n steps, $p_i^{(n)}$, is given by Equation (3). The probabilities L_i and R_i represent the charge hops from G_i to its left- and right-nearest neighbor hopping site (G base), respectively, with $0 \leq L_i, R_i \leq 1$ and $L_i + R_i = 1$. Both L_i and R_i are functions of $k_{i,L}$ and $k_{i,R}$, the corresponding unistep charge transfer rate constants via coherent superexchange between two nearest neighbor G bases. These are determined by the specific base sequence between the guanine units.[21–23]

[a] *Prof. Dr. W. M. Nau, X. Wang*
Departement Chemie der Universität
Klingelbergstrasse 80, 4056 Basel (Switzerland)

$$\begin{array}{rcl} p_{GGG}^{(n)} &=& L_1 \cdot p_{G1}^{(n-1)} \\ p_{G1}^{(n)} &=& L_2 \cdot p_{G2}^{(n-1)} \\ p_{G2}^{(n)} &=& L_3 \cdot p_{G3}^{(n-1)} + R_1 \cdot p_{G1}^{(n-1)} \\ \cdots &=& \cdots + \cdots \\ p_{Gi}^{(n)} &=& L_{i+1} \cdot p_{Gi+1}^{(n-1)} + R_{i-1} \cdot p_{Gi-1}^{(n-1)} \\ \cdots &=& \cdots + \cdots \\ p_{G2N-1}^{(n)} &=& R_{2N-2} \cdot p_{G2N-2}^{(n-1)} \\ p_{GGG}^{(n)} &=& R_{2N-1} \cdot p_{G2N-1}^{(n-1)} \end{array} \quad \text{with} \begin{cases} L_i = \dfrac{k_{i,L}}{k_{i,L} + k_{i,R}} \\ R_i = \dfrac{k_{i,R}}{k_{i,L} + k_{i,R}} \end{cases} \tag{3}$$

Since all relevant parameters (hopping sites, step size, hopping probabilities) are fixed once the DNA strand is chosen, the survival probability distribution in the system on distinct G bases (hopping sites) can be solved as a Markov chain problem. The state vector of a Markov chain is defined as $\boldsymbol{P}(n) = [p_{G1}^{(n)}\ p_{G2}^{(n)} \cdots p_{GN}^{(n)} \cdots p_{G2N-1}^{(n)}]^T$, which can be calculated according to Equation (4), where $\boldsymbol{A}$ is the $(2N-1) \times (2N-1)$transition matrix and $\boldsymbol{P}(0)$ is the initial state vector. If the charge is generated on the Nth site, only the Nth element of $\boldsymbol{P}(0)$ is occupied, namely $\boldsymbol{P}(0) = [0 \cdots 1\ 0 \cdots 0]^T$.

$$\boldsymbol{P}(n) = \boldsymbol{A}^n \cdot \boldsymbol{P}(0) \quad \text{with } \boldsymbol{A} = \begin{vmatrix} 0 & L_2 & 0 & 0 & \cdots & 0 & 0 \\ R_1 & 0 & L_3 & 0 & \cdots & 0 & 0 \\ 0 & R_2 & 0 & L_4 & \cdots & 0 & 0 \\ 0 & 0 & R_3 & 0 & \cdots & 0 & 0 \\ \cdots & \cdots & \cdots & \cdots & \cdots & \cdots & \cdots \\ 0 & 0 & 0 & 0 & \cdots & 0 & L_{2N-1} \\ 0 & 0 & 0 & 0 & \cdots & R_{2N-2} & 0 \end{vmatrix} \tag{4}$$

The survival probability $F_s(n)$, which is the probability that the charge has not been trapped after n hops, can be obtained by adding up all the coordinates in the state vector $\boldsymbol{P}(n)$ as Equation (5), where $\boldsymbol{S} = [1\ 1 \cdots 1]$ is the matrix operation for

$$F_s(n) = \boldsymbol{S} \cdot \boldsymbol{P}(n) = \boldsymbol{S} \cdot \boldsymbol{A}^n \cdot \boldsymbol{P}(0) \tag{5}$$

obtaining the pertinent sum. On a long time-scale ($n \to \infty$) the coordinates in the state vector $\boldsymbol{P}(n)$ vanish, indicating that the charge is being completely trapped, that is, $F_s(n) \to 0$. For a charge generated on G_N, the average number of hopping steps before trapping is directly related to $F_s(n)$ by Equation (6a).

$$H(N) = \sum_{n=0}^{\infty} F_s(n) \tag{6a}$$

The average number of hopping steps, $H(N)$, can be dissected into the individual contribution of each G_i base, $H(i,N)$, which is the average number of steps the charge hops from G_i to its nearest neighbors before trapping. It describes the probability density of unit hopping steps from G_i. For the charge generated on G_N, it can be obtained as Equation (6b).

$$H(i,N) = \sum_{n=0}^{\infty} p_i^{(n)} = \sum_{n=0}^{\infty} \boldsymbol{Q} \cdot \boldsymbol{A}^n \cdot \boldsymbol{P}(0) \tag{6b}$$

The vector $\boldsymbol{Q}$ equals $[0 \cdots 1\ 0 \cdots 0]$, which means that only the ith element is occupied. From Equations (6a) and (6b) it follows that $H(N)$ is the sum of all $H(i,N)$, Equation (7).

$$H(N) = \sum_{i=1}^{2N-1} H(i,N) \tag{7}$$

Since the unit hopping time from G_i to its nearest neighbor, $\tau_{h(i)}$, is determined by the system, a mean residence time of the charge $\tau(i)$ can be defined for each distinct base G_i, such that the total lifetime of the charge τ is equal to the sum of all mean residence times, Equation (8). The lifetime of the charge is the average survival time of a charge between generation on G_N and trapping by GGG.

$$\tau = \sum_{i=1}^{2N-1} \tau(i) \quad \text{with } \tau(i) = H(i,N) \cdot \tau_{h(i)} \tag{8}$$

A general expression for the average hopping steps $H(N)$ and lifetime can be obtained by matrix algebraic operations. From the definitions of matrix $\boldsymbol{A}$ and vector $\boldsymbol{P}(0)$ in Equation (4) and the properties of the matrices, the sum in Equation (6b) equals Equation (9), where $\boldsymbol{I}$ is the $(2N-1) \times (2N-1)$ identity matrix, $\boldsymbol{B}$ is the $(2N-1) \times (2N-1)$ inverse matrix of $(\boldsymbol{I} - \boldsymbol{A})$, $H(i,N)$ is the (i,N) element of matrix $\boldsymbol{B}$, and $H(N)$ is the sum of all elements in the Nth column of matrix $\boldsymbol{B}$.

$$H(i,N) = \boldsymbol{Q} \cdot \boldsymbol{B} \cdot \boldsymbol{P}(0) \quad \text{with } \boldsymbol{B} = (\boldsymbol{I} - \boldsymbol{A})^{-1} \tag{9}$$

To this point the analysis is general, and if all L_i and R_i values between all hopping sites were known for a particular strand the dynamics of charge migration to the trap could be solved analytically. For a natural part of a DNA strand, the individual values of L_i and R_i, which are a function of the distance and bases sequence,[21–23] are not known accurately and further approximations are essential. Two assumptions appear reasonable and have been previously considered: a) The L_i and R_i values are the same or differ in a random manner (unbiased hopping); b) the L_i and R_i decrease or increase in a systematic manner towards the trap (biased hopping). We note here that a systematic long-range gradient towards charge hopping to the trap is unlikely to apply, since even the short-range gradient is small. For example, the GGG cluster in a single strand, which is a favorable trap, reacts with strong electron acceptors separated by one or two adenine bases less than a factor of two faster than a guanine base separated by the same intervening sequence.[27, 31] These reactions are both equivalent to "nearest neighbor" hops within the framework of Scheme 1. Moreover, any long-range gradient would be effectively prevented by the more pronounced dependence of the rate constants on the specific base sequence in a natural strand, which can be considered as random in terms of charge transfer. A gradient could be in principle created by the "polaron mechanism",[16] which allows also for conformational and environmental changes along the DNA strand. However, such changes should occur in a random fashion and they therefore cannot create a systematic gradient.

Consequently, while a systematic bias for charge hopping to the trap ($L_i/R_i = \text{const.} \neq 1$) may apply in certain dendrimer-type antenna systems,[3, 4] it appears unlikely to dominate in DNA. In the absence of experimental evidence for trap-direction biased charge hopping in DNA, it will not be considered further. Instead, we assume a constant hopping rate k between single guanine bases, which is thought to be a particularly suitable description for previously studied synthetic strands with equidistant hopping sites, for example with the same intervening DNA sequence

  1439-4235/01/02/12 $ 17.50+.50/0 CHEMPHYSCHEM **2001**, No. 12

(2D) $GGG \underset{k_t}{\rightleftharpoons} G_1 \underset{k}{\overset{k}{\rightleftharpoons}} \cdots\cdots G_{N-1} \underset{k}{\overset{k}{\rightleftharpoons}} G_N \underset{k}{\overset{k}{\rightleftharpoons}} G_{N+1} \cdots\cdots \underset{k}{\overset{k}{\rightleftharpoons}} G_{2N-1} \overset{k_t}{\rightleftharpoons} GGG$

(1D) $GGG \underset{k_t}{\rightleftharpoons} G_1 \underset{k}{\overset{k}{\rightleftharpoons}} \cdots\cdots G_{N-1} \underset{k}{\overset{k}{\rightleftharpoons}} G_N$

Scheme 2. *Description of the two- and one-directional charge-hopping kinetics between guanine bases in a strand terminated by guanine clusters.*

between guanine bases (Scheme 2, 2D case). This may also present a suitable description for hopping with random rates over large distances, since an average rate constant may then be defined.[16] However, in Scheme 2 we do take into account the experimental result that the final hopping step to the adjacent GGG trap (k_t) may differ slightly from the other rates (k).[27, 31] Note that this explicit consideration of different hopping rate constants should not be understood in terms of a bias according to the η value in Equation (2). The latter implies a systematically increasing hopping rate in the direction of the trap, namely a gradient.

In the limiting 2D case of Scheme 2 we have $L_i = R_i = 0.5$ ($i \neq 1$, $2N-1$), such that the transition matrix $\boldsymbol{A}$ of Equation (4) reduces to matrix $\boldsymbol{A}'$ of Equation (10).

$$\boldsymbol{A}' = \begin{bmatrix} 0 & 0.5 & 0 & 0 & \cdots & 0 & 0 \\ k/(k+k_t) & 0 & 0.5 & 0 & \cdots & 0 & 0 \\ 0 & 0.5 & 0 & 0.5 & \cdots & 0 & 0 \\ 0 & 0 & 0.5 & 0 & \cdots & 0 & 0 \\ \cdots & \cdots & \cdots & \cdots & \cdots & \cdots & \cdots \\ 0 & 0 & 0 & 0 & \cdots & 0 & k/(k+k_t) \\ 0 & 0 & 0 & 0 & \cdots & 0.5 & 0 \end{bmatrix} \quad (10)$$

According to Equation (9), the Nth column in matrix $\boldsymbol{B}'$, the inverse matrix of $\boldsymbol{A}'$, can be obtained as Equation (11).

$$\left[\frac{1}{2}\left(1+\frac{k}{k_t}\right) \quad 1+\frac{k}{k_t} \quad 2+\frac{k}{k_t} \quad \cdots \quad N-2+\frac{k}{k_t} \quad N-1+\frac{k}{k_t} \quad N-2+\frac{k}{k_t} \quad \cdots \quad \frac{1}{2}\left(1+\frac{k}{k_t}\right)\right]^T \quad (11)$$

The average hopping steps before trapping for the charge generated on G_N is the sum of all elements in this column, Equation (12).

$$H(2D) = (N-1)^2 + 1 + 2(N-1)\frac{k}{k_t} \quad (12)$$

In the 2D system of Scheme 2, the unit hopping times from a distinct guanine base to its nearest-neighbors are given by Equation (13).

$$\tau_{h(1)} = \tau_{h(2N-1)} = \frac{1}{k+k_t}; \quad \tau_{h(i)} = \frac{1}{2k} \text{ for } 2 \le i \le 2N-2 \quad (13)$$

From the definition of the lifetime in Equation (8), one obtains τ for the charge which is generated on G_N and migrates in two directions (2D) as Equation (14a), and which simplifies to Equation (14b).

$$\tau(2D) = \left(1+\frac{k}{k_t}\right)\frac{1}{k+k_t} + \left[\sum_{j=1}^{N-1}\left(j+\frac{k}{k_t}\right) + \sum_{j=1}^{N-2}\left(j+\frac{k}{k_t}\right)\right]\frac{1}{2k} = \frac{2N-1}{2k_t} + \frac{(N-1)^2}{2k} \quad (14a)$$

$$\tau(2D) = \frac{N^2}{2k} \quad \text{for } k_t = k \quad (14b)$$

The case of one-directional charge migration (1D in Schemes 1 and 2) is obtained by setting $k_{N,R} = 0$, that is, $L_N = 1$ and $R_N = 0$. The transition matrix $\boldsymbol{A}$ in Equation (4) reduces then to the $N \times N$ matrix $\boldsymbol{A}''$, Equation (15).

$$\boldsymbol{A}'' = \begin{bmatrix} 0 & 0.5 & 0 & \cdots & 0 & 0 \\ k/(k+k_t) & 0 & 0.5 & \cdots & 0 & 0 \\ 0 & 0.5 & 0 & \cdots & 0 & 0 \\ \cdots & \cdots & \cdots & \cdots & \cdots & \cdots \\ 0 & 0 & 0 & \cdots & 0 & 1 \\ 0 & 0 & 0 & \cdots & 0.5 & 0 \end{bmatrix} \quad (15)$$

According to Equation (9), the Nth column in the inverse matrix $\boldsymbol{B}''$ can be obtained as Equation (16).

$$\left[1+\frac{k}{k_t} \quad 2\left(1+\frac{k}{k_t}\right) \quad 2\left(2+\frac{k}{k_t}\right) \quad \cdots \quad 2\left(N-2+\frac{k}{k_t}\right) \quad N-1+\frac{k}{k_t}\right]^T \quad (16)$$

The value of $H(1D)$, the average hopping steps for the charge generated on G_N, is again the sum of all elements in this column as described in Equation (17) and this value equals $H(2D)$; compare Equation (12).

$$H(1D) = (N-1)^2 + 1 + 2(N-1)\frac{k}{k_t} = H(2D) \quad (17)$$

In the 1D case of Scheme 2, the unit hopping times from a distinct guanine unit to its nearest neighbor are given by Equation (18).

$$\tau_{h(1)} = \frac{1}{k+k_t}; \quad \tau_{h(i)} = \frac{1}{2k} \text{ for } 2 \le i \le N-1; \quad \tau_{h(N)} = \frac{1}{k} \quad (18)$$

Therefore, from the definition of lifetime, τ, the average survival time for the charge which is generated on G_N and migrates in one direction (1D), can be obtained as Equation (19a), which simplifies to Equation (19b).

$$\tau(1D) = \left(1+\frac{k}{k_t}\right)\frac{1}{k+k_t} + 2\left[\sum_{j=1}^{N-2}\left(j+\frac{k}{k_t}\right)\right]\frac{1}{2k} + \left(N-1+\frac{k}{k_t}\right)\frac{1}{k} = \frac{N}{k_t} + \frac{N(N-1)}{2k} \quad (19a)$$

$$\tau(1D) = \frac{N(N+1)}{2k} \quad \text{for } k_t = k \quad (19b)$$

Note that the values for the lifetimes are different for one- and two-directional one-dimensional hopping (compare Equations (19) and (14)), although the average hopping steps for a given value of N are identical (compare Equations (17) and (12)). This is due to the fact that the value of $\tau_{h(N)}$ differs (compare Equations (18) and (13)), since this position has only one neighbor in the 1D case.

The above analysis refers to a situation where the charge is generated on G_N, which is the most remote single guanine base from the GGG trap in the case of one-directional migration and the central single guanine base in the case of two-directional migration. For the more general case of Scheme 1 with charge generation on a general site G_s ($1 \le s \le N$ for one-directional migration and $1 \le s \le 2N-1$ for two-directional migration), only $\boldsymbol{P}(0)$, the initial state, will change according to Equation (4) and, since only the sth element of $\boldsymbol{P}(0)$ is occupied, the transition matrix $\boldsymbol{A}$ and the unit hopping time $\tau_{h(i)}$ remain the same as those defined above.

In a series of experiments pioneered by Giese and co-workers,[22] the radical cation $G_i^{\bullet+}$ can undergo several side reactions, for example deprotonation and a reaction with water. The yield of the side reaction product derived from a distinct guanine base is proportional to the probability density of the charge on this site and the chemical reaction rate, such that analytical expressions for the mean residence times are very useful for experimental analysis. According to Equations (8), (9), (13), and (18), the mean residence times on distinct guanine bases for a charge which is generated on any hopping site can be obtained by matrix algebraic operations.[4] In the limiting case where the DNA strands can be described by Scheme 2, the mean residence time on G_i between generation on G_s and trapping are summarized in Table 2.

For the case that the charge is generated on G_N, the mean residence time on a distinct guanine base is independent on N, which determines the size of the system (Scheme 1). This means that the mean residence time on a particular hopping site depends on the directionality but not on the length of the system. For one-directional charge migration the value of $\tau(i,N)$, the mean residence time on G_i, equals the shortest time it takes the charge to migrate from G_i to the cluster GGG, which is the sum of $i-1$ step times of superexchange charge transfer between nearby single G bases, $(i-1)/k$, and the charge-transfer step time from G_1 to the GGG cluster, $1/k_t$. For two-directional migration the mean residence times on G_i and G_{2N-i} are the same and equal one half of the shortest time it takes the charge to migrate from G_i or G_{2N-i} to the closer GGG cluster.

Since the lifetime is the sum of the mean residence times on distinct guanine bases in the system, the value of $\Delta\tau$, the increase in the lifetime upon increasing N to $N+1$, equals the residence time on the single additional hopping site (1D case) or the sum of the residence times on the two additional hopping sites (2D case). The $\Delta\tau$ values, which are contained in Table 1, increase linearly with N, both for one- as well as two-directional charge migration.

Table 1. *Lifetime of a charge between generation on G_N and trapping according to Scheme 2.*

two-directional migration (2D)	one-directional migration (1D)
$\tau(2D) = \frac{2N-1}{2k_t} + \frac{(N-1)^2}{2k}, k_t \neq k$	$\tau(1D) = \frac{N}{k_t} + \frac{N(N-1)}{2k}, k_t \neq k$
$\tau(2D) = \frac{N^2}{2k}, k_t = k$	$\tau(1D) = \frac{N(N+1)}{2k}, k_t = k$
$\Delta\tau(2D) = \frac{N}{k} + \frac{1}{k_t} - \frac{1}{2k}, k_t \neq k$	$\Delta\tau(1D) = \frac{N}{k} + \frac{1}{k_t}, k_t \neq k$
$\Delta\tau(2D) = \frac{N}{k} + \frac{1}{2k}, k_t = k$	$\Delta\tau(1D) = \frac{N}{k} + \frac{1}{k}, k_t = k$

Discussion

The accurate understanding of the formal kinetics of charge hopping in one-dimensional systems is essential for the interpretation of recent experimental results for DNA.[15–22, 26, 27, 31] Positive charge hopping along a DNA strand may occur between bases with favorable oxidation potentials (generally guanine) until a trap (often a guanine cluster) is reached, Scheme 1. We have now analyzed in detail the kinetics of charge migration in DNA for the limiting cases in Scheme 2, where a sequence of G bases and GGG traps is separated by one or more of the other bases with less favorable oxidation potentials, such as adenine. Since a systematic bias towards charge hopping between the G bases appears unlikely to apply, the rate constants for hopping between nearest-neighbor G bases (k) in Scheme 2 are assumed to be equal and only the rate of trapping by GGG (k_t) is considered to be different. This situation corresponds to unbiased charge hopping between equidistant G bases but allows for a somewhat faster charge transfer in the final step.

Of primary interest is the lifetime of the charge, the mean survival time between generation on G_N and trapping by GGG. The dependence of the lifetime on the size of the system (N) and the number of directions of migration are summarized in Table 1.

Table 2. *Mean residence time on a particular base G_i before trapping according to Scheme 2*

site of charge generation	two-directional (2D) charge migration	one-directional (1D) charge migration
G_N	$\tau(i,N) = \frac{1}{2}\left(\frac{1}{k_t} + \frac{i-1}{k}\right)$, for $i \le N$ $\tau(i,N) = \frac{1}{2}\left(\frac{1}{k_t} + \frac{2N-i-1}{k}\right)$, for $N < i$	$\tau(i,N) = \frac{1}{k_t} + \frac{i-1}{k}$
G_s	$\tau(i,s) = \frac{[(i-1)k_t + k][(2N-1-s)k_t + k]}{2k_t k[(N-1)k_t + k]}$, for $i \le s$ $\tau(i,s) = \frac{[(s-1)k_t + k][(2N-1-i)k_t + k]}{2k_t k[(N-1)k_t + k]}$, for $s < i$	$\tau(i,s) = \frac{1}{k_t} + \frac{i-1}{k}$, for $i \le s$ $\tau(i,s) = \frac{1}{k_t} + \frac{s-1}{k}$, for $s < i$

  1439-4235/01/02/12 $ 17.50+.50/0 CHEMPHYSCHEM **2001**, No. 12

The results confirm the previously noted weak distance dependence, which is much smaller than that expected for the superexchange mechanism described by Equation (1). For the one-directional case, Bar-Haim and Klafter[3, 4] have provided the same result for the lifetime of the random walker before trapping. In particular, for "a finite but large system" and $k_t = k$, they developed an approximate expression for the lifetime as $\tau = N^2/(2k)$ for unbiased hopping and a related equation for hopping with systematic bias in direction of the trap. The latter was modified[23–25] to provide the more general approximate relationship $\tau \propto N^{\eta}$ ($\eta = 1-2$), which has recently been adopted to analyze charge migration in DNA.[20–26] It must be re-emphasized in the present context that the original equations for one-directional migration derived by Bar-Haim and Klafter, which were later modified, apply only to $N \gg 1$. However, in most experimental studies only small N values are accessible ($N = 1-5$). In these cases, the equations in Table 1 apply.

Interestingly, the *approximate* relationship suggested[23–25] for unbiased ($\eta = 2$) *one-directional* charge migration (N^2 dependence) is identical to the *exact* relationship obtained in the present work for unbiased *two-directional* charge migration with two equidistant traps. The kinetics of such two-directional charge migration in DNA has not yet been subject to experimental tests, although it is most relevant for the corresponding natural processes.[2] The lifetimes expected for two- and one-directional charge migration differ significantly for small N values (Table 1) and they have a characteristic ratio, Equation (20a), which simplifies to Equation (20b).

$$\frac{\tau(2D)}{\tau(1D)} = 1 - \frac{k + k_t(N-1)}{2kN + k_t N(N-1)} \qquad (20a)$$

$$\frac{\tau(2D)}{\tau(1D)} = 1 - \frac{1}{N+1} \quad \text{for } k_t = k \qquad (20b)$$

For $N = 1$, which means that the charge is generated on the only bridge G base and undergoes unistep charge transfer to GGG, the lifetimes of two- and one-directional charge migration are $1/(2k_t)$ and $1/k_t$, respectively. The ratio is $^1/_2$, which is characteristic for an *elementary reaction* and, in this case, coherent superexchange charge transfer. As N increases, this ratio increases, which reflects the complexity of the reaction mechanism, which now involves intermediates, and differentiates it from an elementary reaction. Finally, when $N \gg 1$, the ratio equals approximately unity, and therefore the lifetimes of one- and two-directional charge migration are virtually the same. This surprising result can be rationalized, if one considers that the charge in the two-directional system has not only a twice as high probability to be trapped, but also a twice as high probability to survive, that is, to rest on guanine bases before being trapped. This feature can serve as the fingerprint for charge hopping in DNA. We suggest that for all one-dimensional systems according to Scheme 1, deviations from the expected ratio in Equation (20) must be ascribed to a competitive long-range superexchange charge transfer between remote bases.

The dependence of the lifetimes on a discrete number of hopping sites introduces essentially a "quantization" of the lifetime. In fact, the dependence of lifetime on N for one-directional hopping is reminiscent of the quantization of rotational energy $E = B \cdot J(J+1)$, where $\Delta E = 2B + 2BJ$. Accordingly, we recommend a plot of the increase in lifetime $\Delta\tau$ upon increasing N to $N+1$ against N (Table 1 and Figure 1). In this manner, one obtains a linear dependence on N for both one- and two-directional hopping process. In the one-directional case a linear dependence can be alternatively obtained by plotting τ/N (rather than τ) against N according to Equation (21).

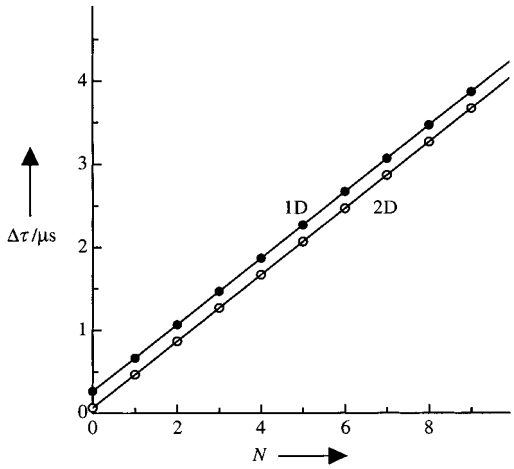

Figure 1. *Model calculations of the increase in lifetime ($\Delta\tau$) for one-directional (1D) and two-directional (2D) charge migration upon increasing the size of the system from* N *to* N + *1. The data were obtained from Equations (19a) and (14a) by using* $k = 2.5 \times 10^6\ s^{-1}$ *and* $k_t/k = 1.5$, *as derived in ref. [26].*

We suggest that the linearity of the corresponding plots provides evidence for hopping. In case experimental methods for the *direct* determination of the *absolute* lifetimes become available, such plots may be useful to extract the rate constant for hopping between guanine bases from the slope of such plots (proportional to $1/k$). This should provide the rate constant of superexchange charge transfer between two nearest G bases, which may be difficult to determine otherwise. The correctness of the results entered in Figure 1 and obtained from Equations (14) and (19) has been independently confirmed through numerical integration of the systems of coupled differential rate laws related to Scheme 2.

Plotting lifetimes or directly related quantities like derived product yields in an exponential fashion[20–26] is equivalent to approximating the pertinent equations in Table 1, where η serves as an extra free fitting parameter. Simulations reveal that an exponential fit to the lifetimes obtained from Equations (14) and (19) results in η values below two, implying a systematic direction-biased hopping where there is none. For example, the η value of 1.7 obtained by Giese et al.[20] is actually the one expected, when an exponential function is forced to the data for unbiased hopping (dashed line in Figure 2).[32] Vice versa, a plot of the reported experimental data according to the simplest Equation (21) *for unbiased hopping* provides excellent agree-

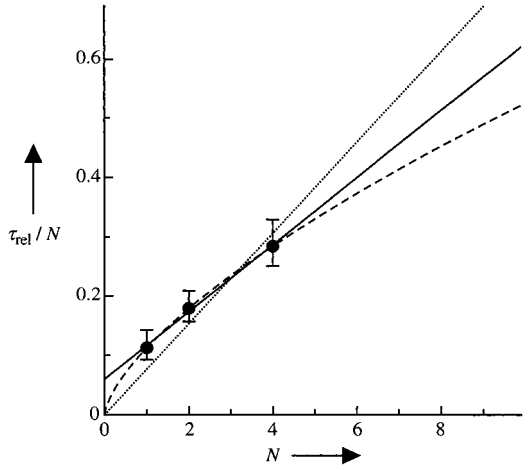

Figure 2. *Dependence of the relative lifetime for charge migration obtained from the product studies in ref. [20] ($\tau_{rel} = 1/k_{rel}$) on the size of the system (N; see Scheme 1).[32] The solid line is obtained from fitting according to Equation (21) which applies to the one-directional kinetics in Scheme 2. The dashed line is the fitting result from the rearranged Equation (2), that is, $(\tau_{rel}/N) \propto N^{(\eta-1)}$ with $k_{rel} \propto k_{CT}$, and affords $\eta = 1.67$ as the parameter for the bias towards charge migration in the direction of the trap. If η is set to two, the value proposed for unbiased hopping, the dotted line results as the best fit.*

ment and is in line with the kinetic model in Scheme 2 ($r = 0.998$, solid line). In contrast, Equation (2) cannot describe the data if unbiased hopping is assumed ($\eta = 2$, dotted line). Clearly, as can be seen from the large deviation between the projected behavior from Equations (2) and (21), access to additional accurate experimental data, preferably absolute rates, is vital for the deeper understanding of charge hopping in DNA.

$$\frac{\tau(1D)}{N} = \frac{1}{2k}N + \left(\frac{1}{k_t} - \frac{1}{2k}\right) \qquad (21)$$

In conclusion, the interpretation of the magnitude of the η value resulting from the analysis according to Equation (2) may be less productive than the discussion of the β value within the framework of Equation (1). A successful fit to Equation (2) should not be considered as demonstration of its validity.[33] In particular, deviations from the limiting η value of two may reflect the inherent approximations rather than true bias towards charge transfer, since Equation (2) applies only for very long one-directional systems, which have not been experimentally analyzed. In the absence of evidence for a systematic bias for charge migration in DNA as well as related systems, it may be preferable to employ the equations in Table 1 or Equation (21) for fitting and data analysis, both for one- and two-directional systems. They apply accurately to systems which comply with Scheme 2 and should hold for the experimentally accessible range of DNA strands, including short-range charge transfer, where Equation (2) does not apply.

This work was supported by the Swiss National Science Foundation (projects 620-58000.99 and 4047-057552) within the Swiss National Research Program "Supramolecular Functional Materials".

[1] D. Ly, Y. Kan, B. Armitage, G. B. Schuster, *J. Am. Chem. Soc.* **1996**, *118*, 8747 – 8748.
[2] B. Armitage, D. Ly, T. Koch, H. Frydenlund, H. Ørum, H. G. Batz, G. B. Schuster, *Proc. Natl. Acad. Sci. USA* **1997**, *94*, 12320 – 12325.
[3] A. Bar-Haim, J. Klafter, *J. Phys. Chem. B* **1998**, *102*, 1662 – 1664.
[4] A. Bar-Haim, J. Klafter, *J. Chem. Phys.* **1998**, *109*, 5187 – 5193.
[5] N. J. Turro, J. K. Barton, *J. Biol. Inorg. Chem.* **1998**, *3*, 201 – 209.
[6] C. J. Murphy, M. R. Arkin, Y. Jenkins, N. D. Ghatlia, S. H. Bossman, N. J. Turro, J. K. Barton, *Science* **1993**, *262*, 1025 – 1029.
[7] A. M. Brun, A. Harriman, *J. Am. Chem. Soc.* **1994**, *116*, 10383 – 10393.
[8] A. M. Brun, A. Harriman, *J. Am. Chem. Soc.* **1992**, *114*, 3656 – 3660.
[9] T. J. Meade, J. F. Kayyem, *Angew. Chem.* **1995**, *107*, 358 – 360; *Angew. Chem. Int. Ed. Engl.* **1995**, *34*, 352 – 354.
[10] S. J. Atherton, P. C. Beaumont, *J. Phys. Chem.* **1995**, *99*, 12025 – 12029.
[11] D. B. Hall, R. E. Holmlin, J. K. Barton, *Nature* **1996**, *382*, 731 – 735.
[12] S. O. Kelley, R. E. Holmlin, E. D. A. Stemp, J. K. Barton, *J. Am. Chem. Soc.* **1997**, *119*, 9861 – 9870.
[13] F. D. Lewis, T. Wu, Y. Zhang, R. L. Letsinger, S. R. Greenfield, M. R. Wasielewski, *Science* **1997**, *277*, 673 – 676.
[14] K. Fukui, K. Tanaka, *Angew. Chem.* **1998**, *110*, 167 – 170; *Angew. Chem. Int. Ed.* **1998**, *37*, 158 – 161.
[15] S. O. Kelley, J. Barton, *Science* **1999**, *283*, 375 – 381.
[16] P. T. Henderson, D. Jones, G. Hampikian, Y. Kan, G. B. Schuster, *Proc. Natl. Acad. Sci. USA* **1999**, *96*, 8353 – 8358.
[17] G. B. Schuster, *Acc. Chem. Res.* **2000**, *33*, 253 – 260.
[18] M. E. Nuñez, D. B. Hall, J. K. Barton, *Chem. Biol.* **1999**, *6*, 85 – 97.
[19] B. Giese, J. Amaudrut, A. Köhler, M. Spormann, S. Wessely, *Nature* **2001**, *412*, 318 – 320.
[20] B. Giese, S. Wessely, M. Spormann, U. Lindemann, E. Meggers, M. E. Michel-Beyerle, *Angew. Chem.* **1999**, *111*, 1050 – 1052; *Angew. Chem. Int. Ed.* **1999**, *38*, 996 – 998.
[21] E. Meggers, M. E. Michel-Beyerle, B. Giese, *J. Am. Chem. Soc.* **1998**, *120*, 12950 – 12955.
[22] B. Giese, *Acc. Chem. Res.* **2000**, *33*, 631 – 636.
[23] J. Jortner, M. Bixon, T. Langenbacher, M. E. Michel-Beyerle, *Proc. Natl. Acad. Sci. USA* **1998**, *95*, 12759 – 12765.
[24] M. Bixon, J. Jortner, *J. Phys. Chem. B* **2000**, *104*, 3906 – 3913.
[25] M. Bixon, B. Giese, S. Wessely, T. Langenbacher, M. E. Michel-Beyerle, J. Jortner, *Proc. Natl. Acad. Sci. USA* **1999**, *96*, 11713 – 11716.
[26] B. Giese, M. Spichty, *ChemPhysChem* **2000**, *1*, 195 – 198.
[27] W. B. Davis, I. Naydenova, R. Haselsberger, A. Ogrodnik, B. Giese, M. E. Michel-Beyerle, *Angew. Chem.* **2000**, *112*, 3795 – 3798; *Angew. Chem. Int. Ed.* **2000**, *39*, 3649 – 3652.
[28] S. Steenken, S. V. Jovanovic, *J. Am. Chem. Soc.* **1997**, *119*, 617 – 618.
[29] H. Sugiyama, I. Saito, *J. Am. Chem. Soc.* **1996**, *118*, 7063 – 7068.
[30] A. K. Mishra, R. Chandrasekar, M. Faraggi, M. H. Klapper, *J. Am. Chem. Soc.* **1994**, *116*, 1414 – 1422.
[31] F. D. Lewis, X. Liu, J. Liu, R. T. Hayes, M. R. Wasielewski, *J. Am. Chem. Soc.* **2000**, *122*, 12037 – 12038.
[32] A reviewer of this manuscript correctly pointed out that the experimental data used in Figure 2 rely on relative yields and not rate constants, such that the application of the kinetic expressions may lead to quantitative deviations, compare ref. [25]. Figure 2 is solely provided for comparison with the same data analysis used in earlier work (ref. [20]) and to reveal the significant deviations between the various kinetic expressions.
[33] M. N. Paddon-Row in *Stimulating Concepts in Chemistry* (Eds.: F. Vögtle, J. F. Stoddart, M. Shibasaki), VCH, Weinheim, **2000**, pp. 267 – 291.

Received: May 7, 2001 [Z225]

Biomolecular and Supramolecular Kinetics in the Submicrosecond Time Range: the Fluorazophore Approach

Werner M. Nau* and Xiaojuan Wang[a]

Fluorophores based on the azo chromophore 2,3-diazabicyclo[2.2.2]oct-2-ene, referred to as fluorazophores, display an exceedingly long fluorescence lifetime and undergo quenching upon contact with efficient hydrogen or electron donors. These photophysical and photochemical properties allow several uncommon applications to biomolecular and supramolecular kinetic studies in the submicrosecond time range. Examples for kinetics of host–guest complexation, end-to-end contact formation in polypeptides, and lateral diffusion in membrane models are described. Principal requirements for these types of kinetic measurements and the dependence of the kinetics of diffusion-controlled reactions on the dimensionality of the system are discussed.

KEYWORDS:

fluorescence · host–guest systems · kinetics · membranes · peptides

Introduction

The study of chemical kinetics is essential to identify the elementary processes of reaction mechanisms, to develop structure–reactivity relationships, and to control chemical reactions. This applies also to the field of supramolecular chemistry, where there is an intensive quest for "functional" supramolecular materials which could catalyze and thus alter the reactivity of their components or perform mechanical, electrical, or optical operations on the nanoscale level at a desired speed. The investigation of supramolecular kinetics is therefore essential and will present, in our opinion, an active and interdisciplinary area of future research. To the extent that supramolecular assemblies mimic biomolecular systems or, vice versa, that the understanding of biological activity serves as a design criterion for artificial chemical devices, supramolecular kinetics has strong ties with biomolecular kinetics.[1]

We have recently designed a series of fluorescent probes (see structures) based on the azo chromophore 2,3-diazabicyclo[2.2.2]oct-2-ene,[2] for which we have coined the name *fluorazophores* (fluorescent azo chromophores).[3–7] The use of these fluorescent probes has allowed us to design new methods for examining certain types of supramolecular and biomolecular reaction kinetics. Through this approach, we can obtain kinetic information in the submicrosecond time range, in which some of the most fundamental and fastest diffusion-related elementary processes like those depicted in Scheme 1 occur. These comprise (1) the association and self-assembly of supramolecular or biomolecular components and the binding of substrates to enzymes or catalysts, (2) biopolymer or polymer chain folding, as well as intermolecular chemical processes in constrained low-dimensional media like (3) reactions in membranes and (4) in unidirectional zeolites. These are examples of reactions in quasi-two-dimensional (2D) and one-dimensional (1D) systems, respectively.

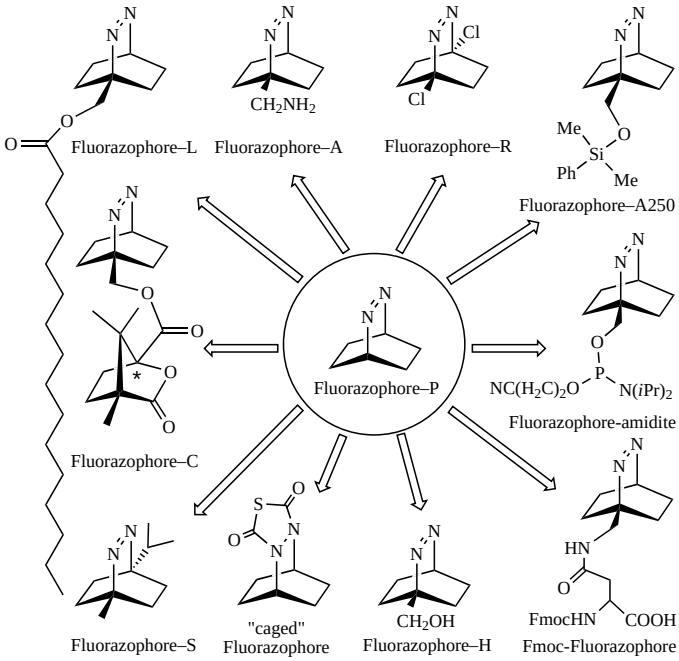

There has been a continuous search for kinetic methods suitable for measuring chemical processes which occur over a large range of time scales. Following the classification by Eigen,[8] the different methods and the time scales in which they are applicable can be depicted as in Figure 1. The methods can be roughly divided into three categories: relaxation methods

[a] *Prof. Dr. W. M. Nau, Dipl.-Chem. X. Wang*
Departement Chemie
Universität Basel
Klingelbergstrasse 80, 4056 Basel (Switzerland)
Fax: (+41) 61-267-3855
E-mail: Werner.Nau@unibas.ch

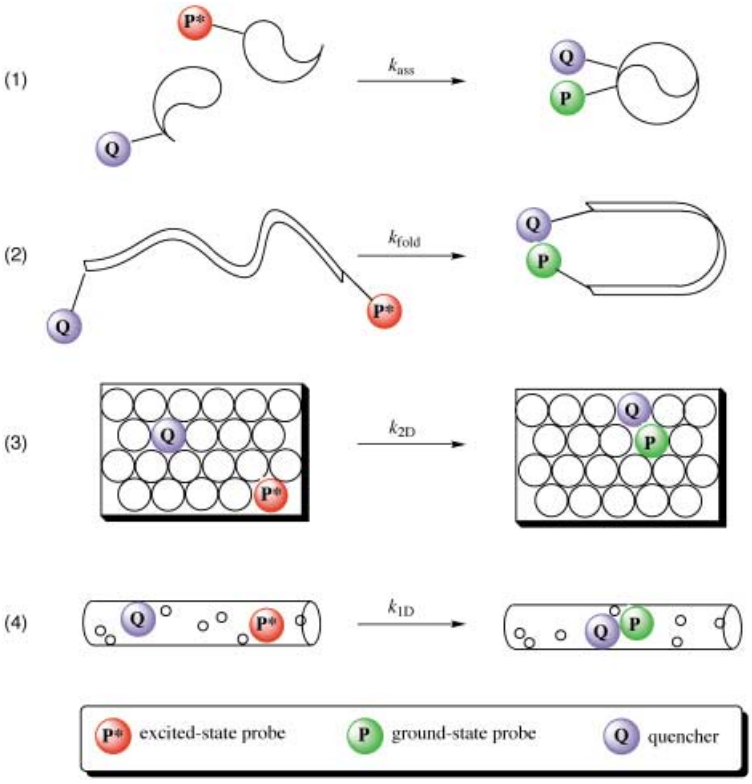

Scheme 1. *Processes accessible for study by the fluorazophore method. (1) Host–guest complexation and quenching by antioxidants in solution. (2) Chain folding in biopolymers. (3) Diffusion in two-dimensional systems (membrane models). (4) Diffusion in one-dimensional systems (unidirectional zeolites, for example).*

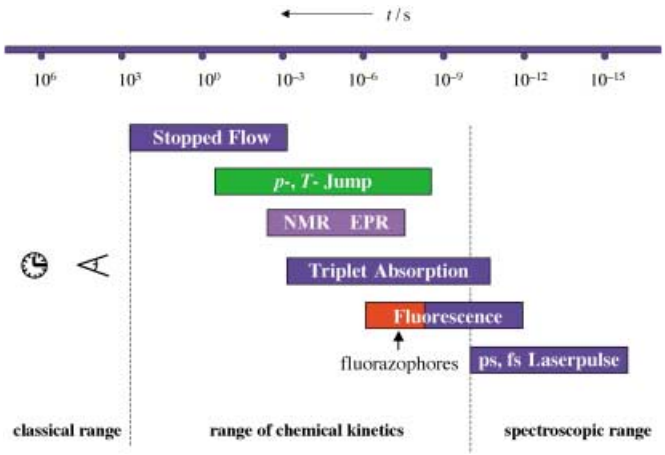

Figure 1. *Time scales of chemical reactions and their accessibility by different spectroscopic methods (adapted from Eigen, ref. [8]). The range accessible to the fluorazophore method is marked in red.*

(green), resonance methods (violet), and the direct monitoring of probe molecules by time-resolved spectroscopy (blue). With the fluorazophore approach (red), which allows direct monitoring of the reaction kinetics, we have now extended the time range accessible to fluorescence measurements of supramolecular and biomolecular chemical kinetics towards the slow end, into the microsecond region. This allows one to use this most sensitive time-resolved detection technique in the critical range, which is relevant for the processes in Scheme 1.

Direct kinetic measurements with time-resolved spectroscopic techniques commonly employ photophysical probes[9] which allow fast generation of an excited state, for example by a laser pulse. It is a prerequisite that the probe used in this method shows an "environmental" sensitivity which results from a change of the absorption or emission wavelength when the process occurs. Alternatively, a decrease of the fluorescence intensity or lifetime may result in a different environment. This case of simple fluorescence quenching forms the basis for all measurements according to Scheme 1. One reactant (in the case of intermolecular processes) or one chain end (in the case of intramolecular processes) is labeled with the fluorescent probe and the other one with a fluorescence quencher (left side of equations in Scheme 1). Upon contact (right side of equations in Scheme 1) an encounter complex or in limiting cases a genuine complex (such as a host–guest complex) is formed and efficient quenching of the excited-state probe occurs. This quenching can be directly related with the reaction kinetics to determine either an association rate constant (k_{ass}), a folding rate constant (k_{fold}), or rates of diffusion in 2D and 1D (k_{2D} and k_{1D}). As will be shown, each reaction type requires a different kinetic analysis of fluorescence quenching.

The drawbacks of photophysical probes are the finite lifetimes of excited states, which limit the accessible events to those which occur at comparable rates as the excited states's decay. In other words, for a photophysical probe to be useful for the described kinetic applications, its excited state decay should be slower than the kinetics of the process to be monitored. The fastest supramolecular and biomolecular reaction types according to Scheme 1 occur with observed rates in the nano- to microsecond time range. The main factors which limit the rates of supramolecular and biomolecular processes to this range are the high molecular weight and commonly employed low concentrations of biomolecules and supramolecules. On the other hand, fluorescence lifetimes are typically very short, ranging from picoseconds to a few nanoseconds, which renders most fluorophores unsuitable to follow the kinetics of the described supramolecular or biomolecular processes. This limitation motivates the search for long-lifetime probes with exceptionally long, yet environmentally sensitive, excited state lifetimes.

Fluorazophores display exceedingly long fluorescence lifetimes (up to 1 μs) and are ideal candidates for the desired types of kinetic measurements. These novel fluorescent probes are now turning out to have ample use in supramolecular and biomolecular kinetic studies. Those which we have in hand at present (see structures) are:

- Fluorazophore-P, the parent compound,[3, 10]
- Fluorazophore-S, a sterically elaborate, more selective probe,[11]
- Fluorazophore-R, a more reactive yet less oxygen-sensitive probe,[5]

- Fluorazophore-A250, which possesses an antenna functionality capable of light absorption around 250 nm,
- "caged" Fluorazophore, whose fluorescence can be photoactivated in a temporally and spatially resolved manner,[4]
- Fluorazophore-L, a lipophilic, membrane-bound antioxidant sensor,[7]
- Fluorazophore-C, for studying kinetic discrimination of chiral recognition,
- Fluorazophore-A, with a functional amino group for ease of derivatization,[12] and
- Fluorazophore-H, a highly water-soluble compound.

In addition, we have synthesized an Fmoc-protected asparagine derivative, Fmoc-Fluorazophore,[12] and a phosphoramidite, Fluorazophore-amidite. These two fluorescent modifiers can be attached to a polypeptide or an oligonucleotide by (commercial) automated solid-phase synthesis techniques to obtain fluorazophore-labeled biomolecules.

The photophysical properties of fluorazophores are not strongly dependent on the substitution pattern. All derivatives display a weak n,π* absorption in the near UV ($\lambda_{max} \approx 370$ nm, Table 1 and Figure 2),[13] whose oscillator strength depends on the solvent polarizability,[14] and they generally fluoresce with high quantum yield (≈20% in water) over a broad spectral range ($\lambda_{max} \approx 430$ nm, Figure 2).[15] The absorption and fluorescence spectra show only small solvatochromic shifts.[14] The fluorescence lifetimes and quantum yields are solvent dependent, however. This is a consequence of differential oxygen quenching as well as solvent-induced quenching in some solvents, in particular alcohols and alkanes.[15]

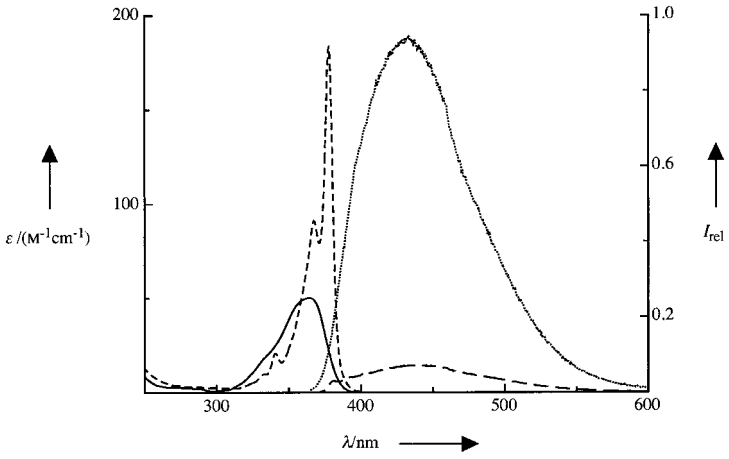

Figure 2. *Absorption spectra of Fluorazophore-P in D_2O (——) and in* n*-hexane (- - - -) and the corresponding fluorescence emission spectra ($\lambda_{exc} = 360$ nm) in D_2O (····) and in* n*-hexane (– – –).*

The small molecular size and spherical shape of fluorazophores as well as good solubility in water and organic solvents make them suitable to be used as guest molecules or linked to biomolecules. The fluorescence of fluorazophores is also environmentally sensitive, since it has been established through detailed mechanistic studies that efficient fluorescence quenching can be induced by making contact (< 3 Å distance) with good hydrogen donors, such as antioxidants (as well as certain solvents),[15, 16] or with electron donors, such as amines.[11] Contact quenching of fluorescent probes, while essential for direct kinetic measurements of the processes in Scheme 1, is quite unique from a photophysical point of view. Generally, quenching by energy or electron transfer dominates, which may occur over a large (for Förster resonance energy transfer) or moderate (5 – 8 Å, for electron transfer) distance through the solvent. Electron transfer may also be through-bond mediated, in particular for rigid and semi-rigid systems, such as structured biopolymers.[17] Moreover, the fluorescence quenching of fluorazophores is chemically unproductive due to mechanistic peculiarities, namely the occurrence of a conical intersection along the excited-state reaction path,[16] which assures good photochemical and thermal stability.

Most important, however, are the long fluorescence lifetimes of fluorazophores.[15] These are the prerequisite for the kinetic applications outlined above. In fact, fluorazophores have the longest fluorescence lifetimes known for organic chromophores in solution,[15] which allows one to probe a time range which is inaccessible for other organic fluorophores. In addition, oxygen is an inefficient quencher of the fluorescence of fluorazophores in aqueous solution (decrease from 420 to 325 ns for Fluorazophore-P), which allows measurements under air. In this context, it should be noted that some excited triplet ketones, which display long lifetimes in degassed solution, have also been used for kinetic studies in this time range.[9] In addition, there are also luminescent inorganic compounds, based on rare earth metal crypt- and or tris(bipyridyl)ruthenium complexes for example, which can be useful for certain applications. Finally, pyrene displays also a long fluorescence lifetime (120 ns for pyrene-1-butyrate in deaerated water) and its tendency to form excimers, in particular, has been exploited

Table 1. *Photophysical properties of fluorazophores.*[a]

	D_2O		*n*-hexane	
	λ_{max} [nm] (ε [M^{-1} cm^{-1}])	τ [ns] (deaerated)[b]	λ_{max} [nm] (ε [M^{-1} cm^{-1}])	τ [ns] (deaerated)[b]
Fluorazophore-P	364 (53)	505 (730)[c]	378 (177)	(340)
Fluorazophore-S	373 (54)	590 (810)	383 (200)	(770)
Fluorazophore-R	358 (40)	705 (750)	367 (190)	(30)
Fluorazophore-H	368 (54)	565 (840)	380 (140)	(335)
Fluorazophore-A	369 (43)	660 (880)	381 (120)	(420)
Fluorazophore-L	–[d]	–[d]	378 (160)	(325)

[a] From refs. [7, 13, 14]. [b] 5% error. [c] Values in degassed and deaerated H_2O are 325 and 420 ns. [d] Insoluble in water.

to study chain folding in polymers in organic solvents,[18] and self-diffusion in membrane models.[19]

Fluorazophores have numerous advantages over other long-lifetime probes which have been discussed elsewhere:[3, 12]

- Most importantly, fluorazophores are smaller than pyrene, which allows their inclusion into small host cavities;
- They are not as hydrophobic as pyrene, which improves the compatibility with biopolymers;[20]
- They do not form excimers like pyrene, which simplifies the kinetic analysis of bimolecular quenching;
- Their fluorescence is significantly longer-lived and less oxygen-sensitive than pyrene, which extends the dynamic range into the critical region and renders measurements in aerated water feasible.

Note also that substitution of pyrene inevitably shortens the fluorescence lifetime, while some substituted fluorazophores display even longer fluorescence lifetimes than the parent (Table 1). Consequently, the applications of fluorazophores are complementary to those of previously explored long-lifetime probes. Specific examples are highlighted in the following sections.

Bimolecular Reactions in Solution

Typical examples of bimolecular supramolecular and biomolecular reactions are host–guest complexation and DNA hybridization. If the intermolecular interactions are specific, for example in the case of enzyme–substrate interactions, molecular recognition occurs. The kinetics of these association processes are prominently relevant for the design of analytical tools, such as chemical sensors, as well as the design of catalysts.[9] In general, it may be desirable to achieve fast kinetics of association, to achieve a high turnover in catalysis for example, but in the case of supramolecular drug delivery the emphasis may lie on a slow and regulated release or uptake over periods of minutes to months.[21]

Fluorazophores have been used as guest molecules to study the kinetics of simple host–guest complexation processes, for example with cyclodextrins (CDs).[3, 13] The time-resolved fluorescence experiments with Fluorazophore-P, for example, show biexponential decays in the presence of β-CD. One time constant proved independent of the host concentration (static), while the second decay function was first-order in the CD concentration (dynamic). Scheme 2 can be used to analyze the kinetics for this supramolecular association process.[22] The static component corresponds to the quenching inside the cyclodextrin complex, while the dynamic component reflects the complexation by cyclodextrin within the excited state lifetime. The association rate constant can be simply extracted by plotting the dynamic component against the cyclodextrin concentration. The fast quenching inside the complex, which is induced by hydrogen abstraction from the inner glucose C–H bonds, assures that dissociation of the excited complex does not compete.[22] It is important to note that this application is made possible by the fact that the intrinsic fluorescence lifetimes of the uncomplexed and complexed fluorazophores differ significantly, in that they display an environmental sensitivity. This method is considered to be the first fluorescence-based method for the direct spectroscopic determination of the association rate constants with cyclodextrins. It can be extended to other host molecules as well as to the study of the effects of substituents[13] and guest chirality on the complexation kinetics.

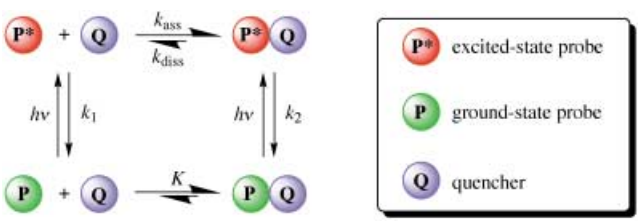

Scheme 2. *Kinetic scheme for the analysis of the kinetics of host–guest complexation involving a long-lived excited state (P*) as guest molecule.*

In another set of ongoing experiments, we are coupling Fluorazophore-amidite as a long-lived fluorescence label to the 5′-terminus of synthetic oligonucleotides at the last stage of automated DNA synthesis. The sensitivity of the fluorazophore to the environment offers a means to distinguish hybridized from unhybridized oligonucleotides in solution. The kinetics of fluorescence quenching can again be analyzed according to Scheme 2 and related to the hybridization rate of complementary oligonucleotides which contain guanine as a quencher.

If the deactivation of the excited-state complex (k_2 in Scheme 2) occurs virtually instantaneously, the net result is a simple bimolecular fluorescence quenching. The P–Q complex in Scheme 2 is now no longer a supramolecular associate, but a simple encounter complex. This situation arises when biological antioxidants are added to fluorazophore solutions. Antioxidants are good hydrogen donors and, thus, efficiently quench fluorescence with rate constants near the diffusion-controlled limit.[10] We have exploited this happenstance to establish Fluorazophore-P as a fluorescent probe for biologically relevant antioxidants, such as vitamin C, vitamin E, uric acid, and glutathione.[6, 10] Fluorazophores can thus be employed to measure the reactivity of antioxidants or, vice versa, if the quenching rate constant is known, to determine their concentration. This method itself presents a novel photochemical application of fluorescence quenching. Again, it needs to be emphasized that the long fluorescence lifetime is essential, since the biologically relevant concentrations of antioxidants (μM–mM) are too small to cause sizable quenching of shorter-lived fluorescent states.[10]

Intramolecular Contact Formation in Biopolymers

The folding events of short polypeptide fragments (to discuss only one important class of biopolymers) are the primary steps in protein folding and knowledge of the kinetics is indispensable for a complete understanding of this fascinating topic. In addition, domain motions in proteins are involved in receptor–substrate interactions, such that the study of the corresponding kinetics may also be important for the design of enzyme mimics as well as related supramolecular functional devices.[23] Stopped-flow techniques have been extensively used in the area of protein folding.[24] However, it is now accepted that the speed

limit for the elementary processes in polypeptide folding, namely intramolecular end-to-end contact formation, falls in the micro- to nanosecond range,[24] which is not accessible to stopped-flow studies. We have recently exploited the long lifetime of fluorazophores and their quenching mechanism, which requires a close probe – quencher contact, to introduce a fluorescence-based method for monitoring intramolecular contact formation in polypeptides.[16]

The main advantages of the fluorescence technique compared to the previously employed triplet absorption techniques[24] (see Figure 1) are: higher sensitivity, accuracy and precision, the use of a probe which is fully compatible with solid-phase peptide synthesis (use of Fmoc-Fluorazophore) and not prone to hydrophobic association, as well as the possibility to perform measurements in water under air with readily accessible spectroscopic equipment. Moreover, intermolecular fluorescence quenching by the 20 natural amino acids revealed that only Trp, Cys, Met, and Tyr act as efficient quenchers of fluorazophores. This means that experiments can be designed with labeled polypeptides, which employ the probe at one end, relatively inert amino acids to build the chain, and an intrinsic amino acid quencher, preferably Trp or Tyr, at the other end; see process (2) in Scheme 1. An exploratory study on the distance dependence of the rate of end-to-end contact formation in peptides with a $(Gly-Ser)_n$ backbone ($n = 0-10$) revealed the viability of this approach.[12] The data agreed in some respects with the predictions from theoretical kinetic models,[25, 26] including the Gaussian chain treatment by Flory,[27] but there were also contrasts to the results extrapolated from previous measurements.[24] For example, the kinetics measured by the fluorazophore method was slightly but consistently faster, which led us to the conclusion that end-to-end contact formation in the short flexible Gly – Ser polypeptides is as fast as 10 ns. This method should be transferable to other biopolymers like oligonucleotides and also polymers.

Low-Dimensional Systems: Diffusion-Controlled Reactions in Membrane Models

The architecture of biomolecular and supramolecular assemblies spans the whole range of one-dimensional, two-dimensional, and three-dimensional systems. For example, enzyme – substrate or host – guest complexations in aqueous solution can be considered as 3D reactions, reactions in the surfaces of biomembranes and lipid vesicles[19, 28] as idealized 2D examples, and the diffusion in carbon nanotubes and in the channels of unidirectional zeolites[29] as well as charge migration in oligonucleotides or proteins[30] as 1D models (Scheme 1). The dimensionality in which these reactions proceed has major consequences for the formal mathematical analytical treatment of the corresponding reaction kinetics. Theories of diffusion-controlled chemical reactions which are based on the isotropic model with Smoluchowski boundary conditions are usually formulated in terms of a concentration which evolves according to a diffusion equation. The bimolecular rate coefficient, $k(t')$, is obtained by assuming that the interaction radius between two reacting species is R, that one species initially has a random distribution, and that around each reactant the relative motion of the alternate species is governed by Fick's law of diffusion. The solutions for $k(t')$ in the case of free diffusion (3D), lateral diffusion (2D), and linear diffusion (1D) are compared in Table 2.[19, 28, 31] Note that the solution for 2D is only approximate; the precise expression contains complex Bessel functions.[19] As an alternative to the Smoluchowski approach, diffusion-controlled reactions, in particular for 1D systems, have been analyzed through a stochastic treatment which involves hopping of either the particle, the trap, or both.[32] The difference between the stochastic and the Smoluchowski treatment is most important for the 1D case.

The kinetic equations in Table 2 can be applied to the cases of fluorescence quenching in Scheme 1 with the condition that the exponent in the right column contains an additional term $(-k_0 t)$ to reflect the intrinsic fluorescence lifetime ($k_0 = 1/\tau_0$). In this case, molecule A, which undergoes transformation when the two reactants meet, is the excited fluorescent probe (P*), C corresponds to its ground state (P), and B takes over the role of the quencher (Q). The rate coefficient is in principle time-dependent in all dimensions. However, from the functional dependence in Table 2 it follows that a diffusional steady state can only be maintained in 3D, so that the bimolecular rate coefficient can reach a time-independent constant in 3D. This has the consequence that the short-time component, the $\sqrt{t}$ term, can generally be neglected in nonviscous 3D systems. Therefore 3D kinetics, such as for the association reactions discussed above, can be characterized in terms of a (time-independent) rate constant, the common kinetic measure of

Table 2. *Kinetics of diffusion-controlled bimolecular reactions of the type $A + B \rightarrow C + B$[a] in dependence on the dimensionality of the system.*

dimension	time-dependent bimolecular rate coefficient[b]	decay of the population of molecule A[b,c]
1D	$k(t') = \sqrt{\frac{D}{\pi t'}}$	$\frac{\rho(t)}{\rho_0} = \exp\left(-2c_0\sqrt{\frac{Dt}{\pi}}\right)$
2D	$k(t') \approx 2\pi D\left(\frac{1}{2} + \frac{R}{\sqrt{D\pi t'}}\right)$	$\frac{\rho(t)}{\rho_0} \approx \exp(-c_0\pi D t - 4c_0 R\sqrt{\pi D t})$[d]
3D	$k(t') = 4R\pi D\left(1 + \frac{R}{\sqrt{D\pi t'}}\right)$	$\frac{\rho(t)}{\rho_0} = \exp(-4c_0 R\pi D t - 8c_0 R^2\sqrt{\pi D t})$

[a] This reaction type is also referred to as a "coalescing" one. [b] R is the distance of the closest approach of two reactants. D is equal to the sum of the diffusion coefficients of the two species. [c] $\frac{\rho(t)}{\rho_0} = \exp\left(-c_0\int_0^t k(t')\mathrm{d}t'\right)$, ρ_0 and $\rho(t)$ are the populations of molecule A at time 0 and t, respectively, and c_0 is the concentration of molecule B. [d] Ref. [19].

bimolecular reactivity. For reactions in low-dimensional systems (1D and 2D) a diffusional steady state cannot be attained, such that the rate coefficient for diffusion-controlled reaction becomes measurably time-dependent at any time, which leaves the diffusion coefficient, *D*, of the active components as the preferable measure of chemical kinetics in 1D and 2D systems. Only for finite, small 2D systems, such as spherical micelles, does the bimolecular rate coefficient reach a time-independent value.[33–35]

We have employed the fluorescence quenching of fluorazophores in membrane models, which can be considered as self-assembling supramolecular aggregates, to obtain information on lateral diffusion in representative low-dimensional systems.[36] Due to the 2D structure of membrane models and the high viscosity of the constituent lipids, the mean displacement is relatively short,[28] such that the use of long-lifetime probes is again indispensable. We have synthesized a novel amphiphilic fluorescent probe, Fluorazophore-L, with a fluorazophore head group and a palmitoyl tail to study the diffusion-controlled kinetics in 2D systems such as POPC[*] air – water monolayers and solution bilayer systems. Fluorazophore-L was found to be sufficiently amphiphilic to form stable air – water monolayers and distribute homogeneously in the lipid.[7] The reactivity towards antioxidants as well as the advantageous photophysical properties of fluorazophores are retained when Fluorazophore-L is included in POPC lipid bilayer systems. In addition, the similarities between the location of UV absorption as well as fluorescence maxima in lipid and in nonhydroxylic organic solvents confirmed that the head group of Fluorazophore-L is located in the interface region.

Although the fluorescence lifetime of Fluorazophore-P (325 ns in aerated water) is shortened in aerated POPC vesicle solutions of Fluorazophore-L (125 ns), the resulting lifetimes are sufficiently long to allow the kinetic measurement of diffusion-controlled intermolecular reactions with biomolecules like lipid-soluble antioxidants dissolved in the membrane model. The equations for 2D diffusion-controlled bimolecular reactions (Table 2) can be applied to the experimental data. This has recently allowed us to determine the mutual lateral diffusion coefficient of this process and provided the first direct time-resolved measurement of a reaction of vitamin E (α-tocopherol) in a membrane. This is of utmost importance for the understanding of the antioxidant action of vitamin E in lipid peroxidation. In essence, we can employ Fluorazophore-L as a mimic for reactive alkoxyl or peroxyl radicals in membranes. The latter induce lipid peroxidation and are presumed, like Fluorazophore-L, to reside with their oxygen radical functionalities at the membrane interface.

Conclusion

Fluorazophores are a series of novel fluorescent probes which have a great potential to study the kinetics of supramolecular and biomolecular processes in the submicrosecond time scale. Their favorable properties such as sensitivity to the environment and long fluorescence lifetime allow one to obtain information on the kinetics of host – guest association, of end-to-end intrachain contact formation in polypeptides, and of diffusional processes in membrane models. These kinetic data are difficult to obtain by alternative methods. The present concept to exploit fluorazophores for monitoring the kinetics of supramolecular and biomolecular processes will be pursued in all directions.

This concept was developed within the Swiss National Research Program NFP 47 "Supramolecular Functional Materials".

[1] J. W. Steed, J. L. Atwood, *Supramolecular Chemistry*, John Wiley and Sons, Chichester, **2000**.
[2] P. S. Engel, C. Steel, *Acc. Chem. Res.* **1973**, *6*, 275 – 281.
[3] W. M. Nau, X. Zhang, *J. Am. Chem. Soc.* **1999**, *121*, 8022 – 8032.
[4] G. Gramlich, W. M. Nau, *Org. Lett.* **1999**, *1*, 603 – 605.
[5] W. M. Nau, *EPA Newsl.* **2000**, *70*, 6 – 29.
[6] X. Zhang, C. Erb, J. Flammer, W. M. Nau, *Photochem. Photobiol.* **2000**, *71*, 524 – 533.
[7] G. Gramlich, J. Zhang, M. Winterhalter, W. M. Nau, *Chem. Phys. Lipids* **2001**, *113*, 1 – 9.
[8] M. Eigen, *Pure Appl. Chem.* **1963**, *6*, 97 – 115.
[9] M. H. Kleinman, C. Bohne in *Organic Photochemistry* (Eds.: V. Ramamurthy, K. S. Schanze), Marcel Dekker, New York, NY, **1997**, pp. 391 – 466.
[10] W. M. Nau, *J. Am. Chem. Soc.* **1998**, *120*, 12614 – 12618.
[11] U. Pischel, X. Zhang, B. Hellrung, E. Haselbach, P.-A. Muller, W. M. Nau, *J. Am. Chem. Soc.* **2000**, *122*, 2027 – 2034.
[12] R. R. Hudgins, F. Huang, G. Gramlich, W. M. Nau, *J. Am. Chem. Soc.* **2002**, *124*, 556 – 564.
[13] X. Zhang, G. Gramlich, X. Wang, W. M. Nau, *J. Am. Chem. Soc.* **2002**, *124*, 254 – 263.
[14] C. Marquez, W. M. Nau, *Angew. Chem.* **2001**, *113*, 4515 – 4518; *Angew. Chem. Int. Ed.* **2001**, *40*, 4387 – 4390.
[15] W. M. Nau, G. Greiner, H. Rau, J. Wall, M. Olivucci, J. C. Scaiano, *J. Phys. Chem. A* **1999**, *103*, 1579 – 1584.
[16] W. M. Nau, G. Greiner, J. Wall, H. Rau, M. Olivucci, M. A. Robb, *Angew. Chem.* **1998**, *110*, 103 – 107; *Angew. Chem. Int. Ed.* **1998**, *37*, 98 – 101.
[17] A. K. Mishra, R. Chandrasekar, M. Faraggi, M. H. Klapper, *J. Am. Chem. Soc.* **1994**, *116*, 1414 – 1422.
[18] a) M. A. Winnik, *Acc. Chem. Res.* **1985**, *18*, 73 – 79; b) K. Zachariasse, A. L. Maçanita, W. Kühnle, *J. Phys. Chem. B* **1999**, *103*, 9356 – 9365.
[19] K. R. Naqvi, J. Martins, E. Melo, *J. Phys. Chem. B* **2000**, *104*, 12035 – 12038.
[20] D. L. Daugherty, S. H. Gellman, *J. Am. Chem. Soc.* **1999**, *121*, 4325 – 4333.
[21] C. Marquez, W. M. Nau, *Angew. Chem.* **2001**, *113*, 3248 – 3254; *Angew. Chem. Int. Ed.* **2001**, *40*, 3155 – 3160.
[22] M. Ameloot, N. Boens, R. Andriessen, V. Van den Bergh, F. C. De Schryver, *J. Phys. Chem.* **1991**, *95*, 2041 – 2047.
[23] V. Balzani, A. Credi, M. Venturi in *Stimulating Concepts in Chemistry* (Eds.: F. Vögtle, J. F. Stoddart, M. Shibasaki), Wiley-VCH, Weinheim, **2000**, pp. 255 – 266.
[24] W. A. Eaton, V. Munoz, S. J. Hagen, G. S. Jas, L. J. Lapidus, E. R. Henry, J. Hofrichter, *Annu. Rev. Biophys. Biomol. Struct.* **2000**, *29*, 327 – 359.
[25] G. Wilemski, M. Fixman, *J. Chem. Phys.* **1974**, *60*, 878 – 890.
[26] A. Szabo, K. Schulten, Z. Schulten, *J. Chem. Phys.* **1980**, *72*, 4350 – 4357.
[27] P. J. Flory, U. W. Suter, M. Mutter, *J. Am. Chem. Soc.* **1976**, *98*, 5733 – 5739.
[28] K. R. Naqvi, *Chem. Phys. Lett.* **1974**, *28*, 280 – 284.
[29] M. Pfenniger, G. Calzaferri, *ChemPhysChem* **2000**, *1*, 211 – 217.
[30] X. Wang, W. M. Nau, *ChemPhysChem* **2001**, *2*, 761 – 766.
[31] M. von Smoluchowski, *Z. Phys. Chem.* **1917**, *92*, 129 – 168.
[32] A. Szabo, R. Zwanzig, N. Agmon, *Phys. Rev. Lett.* **1988**, *61*, 2496 – 2499.
[33] P. P. Infelta, M. Graetzel, *J. Chem. Phys.* **1979**, *70*, 179 – 186.
[34] M. Van der Auweraer, J. C. Dederen, E. Geladé, F. C. De Schryver, *J. Chem. Phys.* **1981**, *74*, 1140 – 1147.
[35] M. Tachiya, *J. Chem. Phys.* **1982**, *76*, 340 – 348.
[36] Turro and co-workers have previously applied azo compounds in micellar systems but as quenchers rather than probes (M. Aikawa, A. Yejta, J.-M. Liu, N. J. Turro, *Photochem. Photobiol.* **1980**, *32*, 297 – 303).

[*] 1-palmitoyl-2-oleoyl-*sn*-glycero-3-phosphocholine.

Received: August 9, 2001 [C278]
Revised: January 28, 2002

J|A|C|S
ARTICLES
Published on Web 12/19/2001

A Joint Structural, Kinetic, and Thermodynamic Investigation of Substituent Effects on Host−Guest Complexation of Bicyclic Azoalkanes by β-Cyclodextrin

Xiangyang Zhang, Gabriela Gramlich, Xiaojuan Wang, and Werner M. Nau*

Contribution from the Department of Chemistry, University of Basel, Klingelbergstrasse 80, CH-4056 Basel, Switzerland

Received July 31, 2001

Abstract: Derivatives of the azoalkane 2,3-diazabicyclo[2,2,2]oct-2-ene (**1a**) with bridgehead 1,4-dialkyl (**1b**), 1,4-dichloro (**1c**), 1-hydroxymethyl (**1d**), 1-aminomethyl (**1e**), and 1-ammoniummethyl (**1f**) substituents form host−guest inclusion complexes with β-cyclodextrin. They were employed as probes to assess substituent effects on the kinetics and thermodynamics of this complexation by using time-resolved and steady-state fluorimetry, UV spectrophotometry, induced circular dichroism (ICD) measurements, and ^{1}H NMR spectroscopy. The kinetic analysis based on quenching of the long-lived fluorescence of the azoalkanes by addition of host provided excited-state association rate constants between 2.6×10^8 and 7.0×10^8 M^{-1} s^{-1}. The binding constants for **1a** (1100 M^{-1}), **1b** (900 M^{-1}), **1c** (1900 M^{-1}), **1d** (180 M^{-1}), **1e** (250 M^{-1}), and **1f** (ca. 20 M^{-1}) were obtained by UV, NMR, and ICD titrations. A positive ICD signal of the azo absorption around 370 nm was observed for the β-cyclodextrin complexes of **1a**, **1d**, and **1f** with the intensity order **1a** ≫ **1d** ≈ **1f**, and a negative signal was measured for those of **1b**, **1c**, and **1e** with the intensity order **1c** < **1b** ≈ **1e**. The ICD was employed for the assignment of the solution structures of the complexes, in particular the relative orientation of the guest in the host (co-conformation).

Introduction

Cyclodextrins (CDs) are naturally occurring water-soluble container-type host molecules.[1] Their host−guest complexes with organic guest molecules have application potential in catalysis,[2] photochemistry,[3] drug delivery,[4] and analytical chemistry.[5] In addition, they are attractive models for molecular recognition phenomena like enzyme−substrate or drug−target interactions.

Thermodynamic properties of CD complexes have been extensively studied.[6,7] In addition to thermodynamic data, knowledge of (1) the kinetics of host−guest complexation as well as (2) structural details is invaluable to assess the functionality of a particular host system and to develop structure−reactivity relationships in supramolecular chemistry in general. With respect to the latter aspect (2), crystallographic structures of several CD complexes have been obtained from X-ray and neutron diffraction data,[8] but relatively little is known about the solution structures of these complexes. NMR techniques have proven suitable to assess the depth of inclusion of the guest and to differentiate between inclusion and association complexes.[9] In addition, the induced circular dichroism (ICD) which arises from the interaction between an achiral chromophore with the chiral host molecules[6,7,10,11] has become a powerful tool for obtaining structural information on the relative orientation of the guest in the host, i.e., the so-called co-conformation.[12]

Relatively little is also known about aspect (1), i.e., the association and dissociation kinetics of guest molecules with CDs.[13] For exceptionally slow kinetics, the rate constants of CD complex formation can be assessed by stopped-flow methods[14,15] or NMR spectroscopy.[16,17] However, the inclusion of small guest molecules into CDs as well as other host structures with sufficiently large openings of the host cavity, e.g., calixarenes,[18] is typically a fast process with rate constants in the order of 10^7-10^8 M^{-1} s^{-1}. While such fast rate constants of supramolecular association may be desirable from certain application points of view, e.g., to allow high turnover rates in catalytic processes, their accurate determination presents an

(1) Szejtli, J. *Chem. Rev.* **1998**, *98*, 1743−1753.
(2) Takahashi, K. *Chem. Rev.* **1998**, *98*, 2013−2033.
(3) Bortolus, P.; Monti, S. *Adv. Photochem.* **1996**, *21*, 1−133.
(4) Uekama, K.; Hirayama, F.; Irie, T. *Chem. Rev.* **1998**, *98*, 2045−2076.
(5) Hedges, A. R. *Chem. Rev.* **1998**, *98*, 2035−2044.
(6) Connors, K. A. *Chem. Rev.* **1997**, *97*, 1325−1357.
(7) Rekharsky, M. V.; Inoue, Y. *Chem. Rev.* **1998**, *98*, 1875−1917.
(8) Harata, K. *Chem. Rev.* **1998**, *98*, 1803−1827.
(9) Schneider, H.-J.; Hacket, F.; Rüdiger, V.; Ikeda, H. *Chem. Rev.* **1998**, *98*, 1755−1785.
(10) Harata, K.; Uedaira, H. *Bull. Chem. Soc. Jpn.* **1975**, *48*, 375−378.
(11) Zhdanov, Y. A.; Alekseev, Y. E.; Kompantseva, E. V.; Vergeichik, E. N. *Russ. Chem. Rev. (Engl. Transl.)* **1992**, *61*, 563−575.
(12) Balzani, V.; Credi, A.; Raymo, F. M.; Stoddart, J. F. *Angew. Chem., Int. Ed.* **2000**, *39*, 3348−3391.
(13) Petrucci, S.; Eyring, E. M.; Konya, G. In *Comprehensive Supramolecular Chemistry*; Atwood, J. L., Ed.; Pergamon, New York, 1996; Vol. 8, pp 483−497.
(14) Yoshida, N. *J. Chem. Soc., Perkin Trans. 2* **1995**, 2249−2256.
(15) Abou-Hamdan, A.; Bugnon, P.; Saudan, C.; Lye, P. G.; Merbach, A. E. *J. Am. Chem. Soc.* **2000**, *122*, 592−602.
(16) Yim, C. T.; Zhu, X. X.; Brown, G. R. *J. Phys. Chem. B* **1999**, *103*, 597−602.
(17) Ghosh, M.; Zhang, R.; Lawler, R. G.; Seto, C. T. *J. Org. Chem.* **2000**, *65*, 735−741.
(18) Franchi, P.; Lucarini, M.; Pedulli, G. F.; Sciotto, D. *Angew. Chem., Int. Ed.* **2000**, *39*, 263−266.

10.1021/ja011866n CCC: $22.00

experimental challenge, since tailor-made probes (as guest molecules) and fast time-resolved techniques are required for their measurement. These include ultrasonic relaxation techniques,[19] temperature jump measurements,[20] and more frequently the absorption, emission, and quenching of triplet probes.[21,22] The latter has been recently reviewed.[23] Besides these direct spectroscopic methods, EPR line broadening was also exploited to examine the association kinetics for complexation of persistent nitroxide radicals with CDs.[24,25]

We have recently introduced a fluorescence-based method for assessing the kinetics of complexation by CDs.[26] In this photophysical method, 2,3-diazabicyclo[2.2.2]oct-2-ene (**1a**) is employed as a guest molecule, which serves also as a "dynamic" probe to monitor the kinetics of host−guest complexation by the fluorescence quenching inside the CD cavity. The exceedingly long-lived fluorescence of azoalkane **1a**, e.g., 730 ns in deaerated D_2O,[27,28] is the prerequisite for the direct measurement of absolute kinetic rate data by fluorescence, since the association process must occur within the lifetime of the excited state.[26] In addition to the kinetic measurements, azoalkane **1a** offered the possibility of thermodynamic measurements through several alternative methods, and it was also possible to assess the solution structure of the resulting CD complex by ICD.[29,30] The characteristic ICD of the n,π^* chromophore band around 370 nm depends sensitively on the alignment of this small chromophore within the CD complex, thus providing a unique tool for structure determination[29−32] in aqueous solution.

In this work, we employ bridgehead-substituted derivatives of the parent azoalkane **1a** as new probes to examine the effect of molecular structure of the guest molecule on the association rate constant and to compare it with the thermodynamics of association and the co-conformations of the host−guest complexes: 4-methyl-1-isopropyl-2,3-diazabicyclo[2.2.2]oct-2-ene (**1b**), 1,4-dichloro-2,3-diazabicyclo[2.2.2]oct-2-ene (**1c**), 1-hydroxymethyl-2,3-diazabicyclo[2.2.2]oct-2-ene (**1d**), and 1-aminomethyl-2,3-diazabicyclo[2.2.2]oct-2-ene in its neutral (**1e**) and protonated forms (**1f**) at pH 11 and pH 5, respectively. β-CD, which is composed of seven α-D-glucose units, was preferred over the smaller α-CD and the larger γ-CD forms, since it shows a 1−2 orders of magnitude stronger binding (e.g., for **1a**).[26,33,34]

Experimental Section

All commercial materials, including β-CD, were obtained from Fluka or Aldrich and were used as received. Column chromatography was performed on silica gel (60−200 μm). The azoalkane 2,3-diazabicyclo[2.2.2]oct-2-ene (**1a**)[35] and its derivatives **1b**,[29] **1c**,[36] **1d**,[37] and **1e**[38] were synthesized according to literature procedures. The detailed procedure and spectroscopic data for **1d**, which have not been previously reported, are given below. The azoalkanes were purified by sublimation at reduced pressure (not for **1d**) and subsequent 2-fold recrystallization from *n*-hexane (**1a**, **1b**, **1e**), methanol (**1c**), or diethyl ether (**1d**). D_2O (> 99.9%, Glaser AG, Basel, Switzerland) was used as solvent for all measurements.

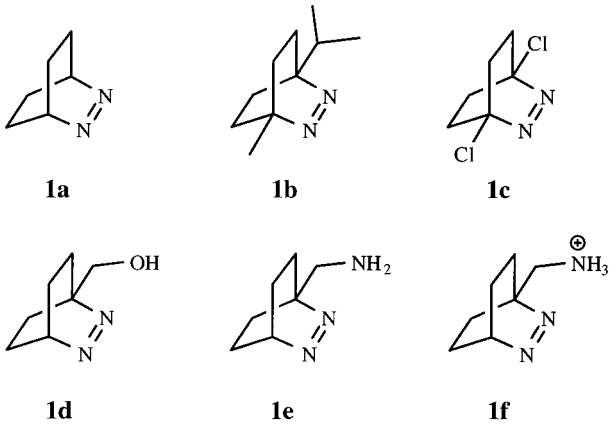

1a **1b** **1c** **1d** **1e** **1f**

1-(Hydroxymethyl)-2,3-diazabicyclo[2.2.2]oct-2-ene (1d). The starting material was the urazole 1-(hydroxymethyl)-4-methyl-2,4,6-triazatricyclo[5.2.2.0^{2,6}]undecane-3,5-dione, which was synthesized according to literature[37] from 2,3-dihydrobenzyl alcohol and 4-methylurazole and subsequent hydrogenation.[37] A 2.5 g (11.1 mmol) amount of the resulting urazole was dissolved in 50 mL of 2-propanol, and KOH pellets (4.8 g, 85.5 mmol) were added in small portions while stirring. After the solution was refluxed under argon for 15 h and cooled to room temperature, the solids were filtered off and washed with 2-propanol. Rotary evaporation of the filtrates gave a slurry which was suspended in CH_2Cl_2 and filtrated. After removal of solvent by rotary evaporation, the product was purified by silica gel chromatography (1.20 g, 8.55 mmol, 77%). Recrystallization from diethyl ether afforded colorless crystals of **1d** (mp 75−76 °C). UV (benzene): λ_{max} 380 nm, ϵ 220 cm^{-1} M^{-1}. ^{1}H NMR (400 MHz, $CDCl_3$): δ 1.33−1.79 (8 H, m, CH_2), 3.30 (1 H, s br, OH), 4.06 (2 H, s, CH_2OH), 5.25 (1 H, s br, CH). ^{13}C NMR (101 MHz, $CDCl_3$): δ 22.0 (2 C, CH_2), 23.3 (2 C, CH_2), 62.3 (CH), 67.3 (CH_2OH), 68.0 (C_q). Anal. Calcd for $C_7H_{12}N_2O$: C, 59.97; H, 8.63; N, 19.98; O, 11.41. Found: C, 60.14; H, 8.60; N, 20.04; O, 11.47.

Spectroscopic Measurements. All experiments were performed at ambient temperature in D_2O. For experiments with the amine form **1e** and the ammonium form **1f**, the pH values were adjusted to ca. 11 and 5 (by addition of NaOD or D_2SO_4) to bypass complications from the protonation equilibria, i.e., to work well below or above the pK_a value of the guest (pK_a = 9.2, see below), while avoiding deprotonation of the host, cf. pK_a(β-CD) = 12.34.[6] pH readings were taken from a 632 pH meter with a combined pH glass electrode (METROHM, Switzerland). Most spectroscopic experiments were performed in 4 mL cuvettes by using 3 mL of 4 mM stock solutions, except for **1c** (1.0 mM). Deaerated solutions, where required, were obtained by two *freeze−pump−thaw* degassing cycles using homemade quartz cells (4 × 1 × 1 cm) with high-vacuum Teflon stopcocks.

A XeF excimer laser pulse from a Lambda Physics COMPex 205 laser (351 nm, pulse width ca. 20 ns, pulse energy 40−175 mJ) or a

(19) Nishikawa, S.; Yokoo, N.; Kuramoto, N. *J. Phys. Chem. B* **1998**, *102*, 4830−4834.
(20) Cramer, F.; Saenger, W.; Spatz, H.-C. *J. Am. Chem. Soc.* **1967**, *89*, 14−20.
(21) Monti, S.; Flamigni, L.; Martelli, A.; Bortolus, P. *J. Phys. Chem.* **1988**, *92*, 4447−4451.
(22) Okano, L. T.; Barros, T. C.; Chou, D. T. H.; Bennet, A. J.; Bohne, C. *J. Phys. Chem. B* **2001**, *105*, 2122−2128.
(23) Bohne, C. *Spectrum* **2000**, *13* (3), 14−19.
(24) Kotake, Y.; Janzen, E. G. *J. Am. Chem. Soc.* **1992**, *114*, 2872−2874.
(25) Lucarini, M.; Luppi, B.; Pedulli, G. F.; Roberts, B. P. *Chem. Eur. J.* **1999**, *5*, 2048−2054.
(26) Nau, W. M.; Zhang, X. *J. Am. Chem. Soc.* **1999**, *121*, 8022−8032.
(27) Nau, W. M.; Greiner, G.; Rau, H.; Wall, J.; Olivucci, M.; Scaiano, J. C. *J. Phys. Chem. A* **1999**, *103*, 1579−1584.
(28) Nau, W. M. *J. Am. Chem. Soc.* **1998**, *120*, 12614−12618.
(29) Zhang, X.; Nau, W. M. *Angew. Chem., Int. Ed.* **2000**, *39*, 544−547.
(30) Mayer, B.; Zhang, X.; Nau, W. M.; Marconi, G. *J. Am. Chem. Soc.* **2001**, *123*, 5240−5248.
(31) Krois, D.; Brinker, U. H. *J. Am. Chem. Soc.* **1998**, *120*, 11627−11632.
(32) Bobek, M. M.; Krois, D.; Brinker, U. H. *Org. Lett.* **2000**, *2*, 1999−2002.
(33) Eftink, M. R.; Andy, M. L.; Bystrom, K.; Perlmutter, H. D.; Kristol, D. S. J. *J. Am. Chem. Soc.* **1989**, *111*, 6765−6772.
(34) Stoedeman, M.; Berg, U.; Svensson, A. *J. Chem. Soc., Faraday Trans.* **1998**, *94*, 1737−1741.
(35) Askani, R. *Chem. Ber.* **1965**, *98*, 2551−2555.
(36) Lüttke, W.; Schabacker, V. *Justus Liebigs Ann. Chem.* **1965**, *687*, 236−240.
(37) Engel, P. S.; Horsey, D. W.; Scholz, J. N.; Karatsu, T.; Kitamura, A. *J. Phys. Chem.* **1992**, *96*, 7524−7535.
(38) Hudgins, R. R.; Huang, F.; Gramlich, G.; Nau, W. M. *J. Am. Chem. Soc.*, in press.

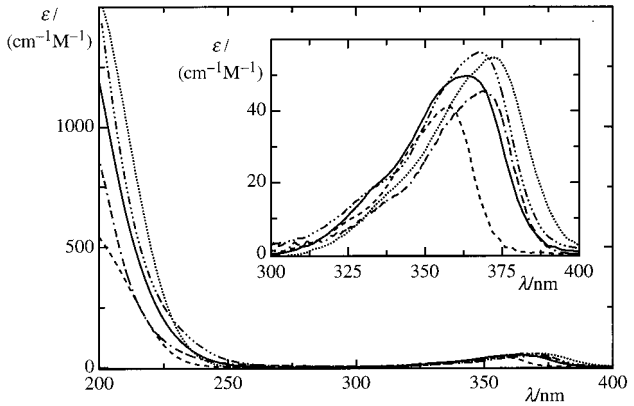

Figure 1. UV absorption spectra of azoalkane **1a** (—), **1b** (···), **1c** (- - -), **1d** (—···—), and **1e** (— —·— —), all in D_2O. The spectrum of **1f** is virtually superimposable with that of **1e** and is not shown for clarity. The inset shows the expanded spectra from 300 to 400 nm.

Table 1. Photophysical Properties of Azoalkanes **1** in D_2O, *n*-Hexane, and Their β-CD Complexes

	λ_{max}/nm [ϵ/(M^{-1} cm^{-1})]				τ/ns [deaerated][b]		
	D_2O	*n*-hexane	β-CD·**1**	λ_{iso}/ nm[a]	D_2O (τ_0)	*n*-hexane	β-CD·**1** (τ_{CD})[c]
1a	365 [48]	376 [200]	371	358	505 [730]	[340]	80
1b	373 [54]	383 [200]	379	376	590 [810]	[770]	430
1c	358 [40]	367 [190]	364	356	705 [750]	[30]	40
1d	368 [54]	380 [140]	370	371	565 [840]	[335]	95
1e	369 [43]	381 [120]	373	371	660 [880]	[420]	110
1f	370 [43]	*d*	370[e]	(370)[e]	670 [920]	*d*	75

[a] Isosbestic point in the UV titration by β-CD in D_2O. [b] Fluorescence lifetime in aerated [deaerated] solution; 5% error. [c] Fluorescence lifetime in the β-CD complex in aerated D_2O obtained by simultaneous fitting of the time-resolved and steady-state fluorescence data according to eqs 6 and 9; 10% error. [d] Insoluble in *n*-hexane. [e] No significant UV shift was observed upon addition of β-CD.

Continuum Minilite Nd:YAG laser (355 nm, pulse width 3−7 ns, 7 mJ) was used for excitation to obtain the time-resolved fluorescence decays. The decays were monitored with a monochromator−photomultiplier setup at 420−500 nm, depending on signal intensity. The kinetic traces were registered by means of a transient digitizer and analyzed by nonlinear least-squares fitting of monoexponential or biexponential decay functions, where appropriate. Steady-state fluorescence spectra were measured with a Spex Fluorolog fluorimeter or with an FLS900 setup from Edinburgh Instruments. Steady-state fluorescence quenching experiments with β-CD were performed with excitation at the isosbestic points (λ_{iso}) which were obtained from UV titrations. UV spectra were obtained with a Hewlett-Packard 8452 diode array spectrophotometer (2 nm resolution) or with a Perkin-Elmer Lambda 19 spectrophotometer (0.1 nm resolution). The NMR spectra were obtained with a Bruker DPX 400 MHz Avance NMR spectrometer. Induced circular dichroism spectra were recorded with a Jasco J-720 spectropolarimeter (0.2 nm resolution, 25 accumulations, 1 cm cell) or an AVIV circular dichroism spectrometer (model 62A DS, Lakewood, NJ).

Results

Photophysical Properties. The UV spectra of **1a**−**f** in D_2O are quite similar (Figure 1). The substituents have only a minor effect on the n,π* transition near 370 nm (Table 1), causing a slight bathochromic shift for electron-donating groups (**1b**) and a hypsochromic one for electron-withdrawing groups (**1c**). A substituent-dependent shift was also observed for the π,π* transition[30] below 220 nm (Figure 1).

Table 2. Binding Constants, ICD Ellipticities, and Association Rate Constants of the β-CD Complexes of Azoalkanes **1**

guest	K/M^{-1}[a]	θ/mdeg[b]	$\Delta\epsilon$/ (M^{-1} cm^{-1})[c]	k_{ass}/ 10^8 M^{-1} s^{-1}[d]	k_{diss}/ 10^5 s^{-1}
1a	1100 ± 200	19.3	+0.162	4.8 ± 0.5	(4.4)[e]
1b	900 ± 150	−4.0	−0.034	*f*	*f*
1c	1900 ± 300	−5.6	−0.119	7.0 ± 0.7	(3.7)[e]
1d	180 ± 20	5.6	+0.069	3.3 ± 0.4	(18)[e]
1e	250 ± 20	−1.9	−0.025	2.6 ± 0.6	(10)[e]
1f	20 ± 10[g]	1.1	+0.045	3 ± 1[h]	120 ± 50[h]

[a] Ground-state binding constants from UV and ^1H NMR. [b] ICD ellipticity at band maximum for 4 mM solutions of **1** (1.0 mM for **1c**) in the presence of β-CD (12.0 mM) in D_2O. [c] Molar ellipticity calculated as $\Delta\epsilon = \theta/(32982\ l\ c)$, cf. ref 76, with l = path length and c = actual concentration of complex in solution calculated by using the binding constants in this table. [d] Association rate constants in the excited state from the time-resolved and steady-state fluorescence quenching data by employing simultaneous fitting according to eqs 6 and 9. [e] Dissociation rate constant estimated as k_{ass}/K. [f] Quenching effect too small to analyze kinetics, cf. text. [g] Determined from ICD titration. [h] Obtained from global fitting to eqs 6 and 7, cf. text.

All azoalkanes **1a**−**f** display exceedingly long fluorescence lifetimes in deaerated D_2O between 730 and 920 ns (Table 1). Table 1 contains also the fluorescence lifetime in the corresponding β-CD·**1** complex (τ_{CD} values), which can be obtained from kinetic measurements in the presence of β-CD (see below). These reflect the reactivity of the excited azoalkane toward abstractable C−H hydrogens in the CD cavity. The method to determine the association rate constants (see below) relies on a fast quenching inside the CD cavity, i.e., small τ_{CD} values. Otherwise, exit from the cavity may compete with deactivation, which complicates the data analysis. The observed trend of the τ_{CD} values, i.e., **1c** ≪ **1a**, **1f** < **1d** < **1e** ≪ **1b**, corresponds to that observed for the solvent-induced quenching by *n*-hexane, cf. lifetimes in this solvent in Table 1: **1c** (30 ns) ≪ **1a** (340 ns) ≈ **1d** (335 ns) < **1e** (420 ns) ≪ **1b** (770 ns). This correlation is reasonable since the same quenching mechanism applies for both *n*-hexane and the interior of β-CD, namely an "aborted" hydrogen abstraction from C−H bonds.[27,39]

Shorter fluorescence lifetimes correspond to higher reactivity for hydrogen abstraction. Accordingly, the chlorinated derivative **1c** is the most reactive one, while the bis-alkylated derivative **1b** displays the lowest reactivity.[40] The hydroxymethyl- and aminomethyl-substituted azoalkanes fall in between. Hence, it appears that electron-withdrawing groups enhance the reactivity of these azoalkanes toward hydrogen donors, while electron-donating groups lower it.[40] This variation can be related to the changes in excitation energy, since the chlorinated derivative exhibits a significantly hypsochromically shifted absorption maximum (Figure 1), corresponding to a higher excitation energy. In addition to variations of the excitation energy, different contributions of charge transfer to the quenching mechanism may apply.[41,42]

Acid−Base Equilibrium of Azoalkanes 1e and 1f. The pK_a value of azoalkane **1e** can be readily determined through measurement of the ^1H NMR chemical shift of the α-CH_2 protons in D_2O ($\delta_{\mathbf{1e}}$ = 3.18 ppm and $\delta_{\mathbf{1f}}$ = 3.62 ppm) as a function of pH. A pK_a value of 9.2 in D_2O was obtained by

(39) Nau, W. M.; Greiner, G.; Wall, J.; Rau, H.; Olivucci, M.; Robb, M. A. *Angew. Chem., Int. Ed.* **1998**, *37*, 98−101.
(40) Zhang, X.; Nau, W. M. *J. Inf. Recording* **2000**, *25*, 323−330.
(41) Pischel, U.; Zhang, X.; Hellrung, B.; Haselbach, E.; Muller, P.-A.; Nau, W. M. *J. Am. Chem. Soc.* **2000**, *122*, 2027−2034.
(42) Sinicropi, A.; Pischel, U.; Basosi, R.; Nau, W. M.; Olivucci, M. *Angew. Chem., Int. Ed.* **2000**, *39*, 4582−4586.

Scheme 1

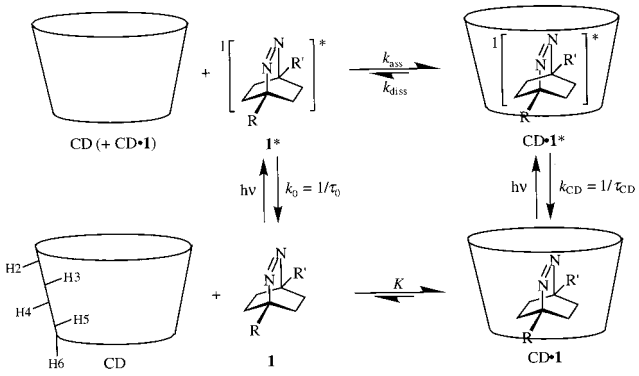

nonlinear least-squares fitting of the chemical shifts according to eq 1.[43] This value falls in the range of those for other amines

$$\delta_{obs} = \frac{\delta_{1e}K_a + \delta_{1f}[H^+]}{K_a + [H^+]} \quad (1)$$

with electron-withdrawing β substituents.[44] Note that the azo group in **1e** can be considered as such an electron-withdrawing β substituent (cf. Hammett σ value of 0.39 for *p*-N=NPh).[45]

Binding Constants. According to Scheme 1, a ground-state equilibrium exists between the free, uncomplexed form (**1**) and the complex (CD•**1**), which is characterized by the binding constant *K* (Table 2). The six differently substituted guest molecules show significant variations of the binding constants, which can be obtained by UV, NMR, ICD, and fluorescence titrations.[26] At least two independent techniques, generally UV and NMR, were employed for each guest, and the results were the same within error. The obtained data confirmed the formation of 1:1 complexes in all cases. For the protonated azoalkane **1f**, the UV and NMR spectral changes were too small to allow a reliable determination of the binding constant by these methods. Here, the more sensitive ICD measurement was employed to derive a much smaller binding constant (20 M^{-1}, see below) than for the amine **1e** (250 M^{-1}).

Induced Circular Dichroism. The analysis of the sign and intensity of the ICD effect arising from the n,π^* transition of azoalkanes has recently been recognized as a powerful tool for structure elucidation of their CD complexes in solution.[29−32] The ICD spectra of all β-CD complexes of azoalkanes **1a**−**f** were measured (Figure 2).[46] The molar ellipticities ($\Delta\epsilon$) were quantified through the respective concentrations and were corrected for the percentage of complexed guest by using the known binding constants (Table 2). For the determination of ICD effects of the amine form **1e** and the ammonium form **1f**, the pH values were again adjusted to 11 and 5. The parent compound **1a** gave a strong, positive ICD signal, and its monosubstituted derivatives **1d** and **1f** showed also a positive, but weaker signal, whereas the disubstituted derivatives **1b** and **1c**, as well the amino derivative **1e**, gave rise to negative ICD effects. Since the ICD signals report selectively on the population of the β-CD complexes, while the uncomplexed components

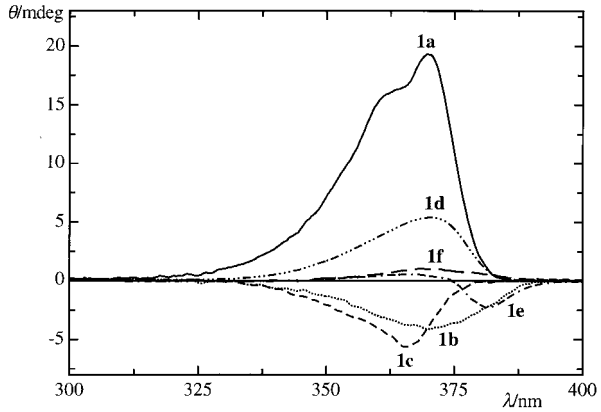

Figure 2. ICD spectra of 4.0 mM solutions (1.0 mM for **1c**) of azoalkane **1a** (—), **1b** (···), **1c** (- - -), **1d** (—···—), **1e** (— —·— —), and **1f** (— — —) in the presence of β-CD (12.0 mM) in D_2O.

Scheme 2

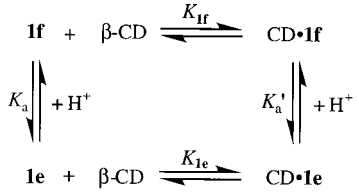

are ICD silent, this titration method may in some cases be more sensitive to determine the binding constants. For **1f**, ICD proved to be the method of choice to determine the binding constant since shifts in the UV and NMR spectra were too small to allow accurate titrations.

Addition of β-CD to a solution of **1e** results in a multiple acid−base equilibrium (Scheme 2),[33,47] and the variation of the ICD spectra with increasing pH reveals an interesting inversion in the sign of the ICD (Figure 3). This can be related to a structural change upon deprotonation (cf. Discussion).

From the thermodynamic cycle in Scheme 2, it is possible to determine the pK_a' value of the β-CD•**1e** complex from eq 2. One obtains a pK_a' value of 8.1, which reveals an apparently

$$K_a' = K_a K_{1e}/K_{1f} \quad (2)$$

lower basicity for the β-CD•**1e** complex compared to the free amine **1e** (pK_a = 9.2). This is synonymous with a higher preference of the ammonium compared to the amine form to remain in the aqueous phase. The known values for the two binding constants (Table 2) and the two pK_a values allow one also to fit the pH profile of the variation of the observed

(43) Arrowsmith, C. H.; Guo, H.; Kresge, A. J. *J. Am. Chem. Soc.* **1994**, *116*, 8890−8894.
(44) Jencks, W. P.; Regenstein, J. In *CRC Handbook of Biochemistry and Molecular Biology*, 2nd ed.; Sober, H. A., Ed.; CRC Press: Cleveland, OH, 1970; pp J187−J226.
(45) Hansch, C.; Leo, A.; Taft, R. W. *Chem. Rev.* **1991**, *91*, 165−195.

(46) ICD spectra were also obtained for azoalkanes **1** in the presence of α-CD and γ-CD as inducers. The experimental ICD intensities (θ/mdeg) at the band maximum of 4 mM solutions of azoalkanes **1** (1.0 mM for **1c**) in the presence of α-CD (12.0 mM) in D_2O were as follows: +14 for **1a**, +0.5 for **1b**, 0 for **1c**, and +0.5 for **1d**. In the presence of γ-CD (12.0 mM) the intensities were +1.5 for **1a**, +8.0 for **1b**, +2.1 for **1c**, and +2.5 for **1d**. As can be seen, the ICD signals were consistently positive, but for **1b**−**d** in the presence of α-CD, hardly any effect was noticed, which paralleled the absence of a significant effect on the UV spectra in these cases. The binding constants for α-CD and γ-CD are generally much lower than those for β-CD; e.g., for α-CD•**1a** ca. 50 M^{-1}, for β-CD•**1a** 1100 M^{-1}, for γ-CD•**1a** ca. 6 M^{-1} (ref 26); for α-CD•**1b** <3 M^{-1}, for β-CD•**1b** 900 M^{-1}, and for γ-CD•**1b** 150 M^{-1} (this work). More detailed investigations with the other cyclodextrins were not undertaken, since the weaker binding imposes experimental complications. Moreover, α-CD appears to be too small to form deep inclusion complexes with the guests, cf. absence of binding for **1b**−**d**, while γ-CD may be too large to cause a clear preference for a particular co-conformation.
(47) Yoshida, N.; Seiyama, A.; Fujimoto, M. *J. Phys. Chem.* **1990**, *94*, 4254−4259.

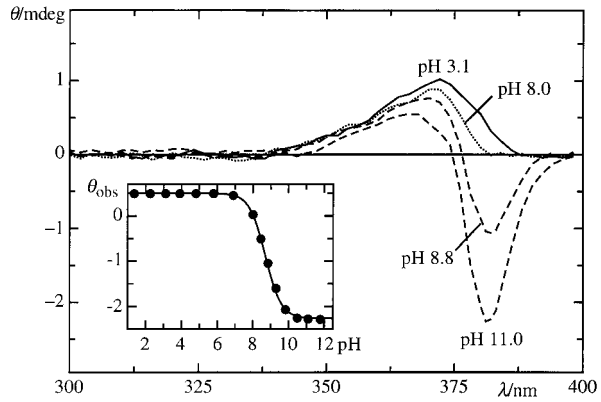

Figure 3. ICD spectra for azoalkane **1e** (4.0 mM) in the presence of β-CD (12.0 mM) in D_2O at varying pH values. The inset shows a plot of the ellipticity at 381 nm versus pH fitted according to eq 3.

ellipticity (θ_{obs}), e.g., in the region of maximum variation at 381 nm.[48] We have derived eq 3 to describe the pH dependence of the ellipticity (l = path length). The resulting fit[49] (inset in Figure 3) corroborates the applicability of Scheme 2. It should be noted that the analytical form of eq 3 should be generally applicable to describe related pH effects on ICD spectra.

$$\frac{\theta_{obs}}{32982\,l} = \Delta\epsilon_{\mathbf{1e}}[\mathrm{CD}\cdot\mathbf{1e}] + \Delta\epsilon_{\mathbf{1f}}[\mathrm{CD}\cdot\mathbf{1f}]$$

$$= \Delta\epsilon_{\mathbf{1e}}PK_a' + \Delta\epsilon_{\mathbf{1f}}P[H^+] \qquad (3)$$

$$\text{with} \quad P = \frac{[\mathbf{1e}]_0 + [\mathrm{CD}]_0}{2(K_a' + [H^+])} + \frac{K_a'([H^+] + K_a)}{2K_{\mathbf{1e}}K_a(K_a' + [H^+])^2} -$$

$$\{(K_{\mathbf{1e}}K_a([\mathbf{1e}]_0 + [\mathrm{CD}]_0)(K_a' + [H^+]) + K_a'([H^+] + K_a))^2 -$$
$$4[\mathbf{1e}]_0[\mathrm{CD}]_0K_{\mathbf{1e}}{}^2K_a{}^2(K_a' + H^+])^2\}^{1/2}/2K_{\mathbf{1e}}K_a(K_a' + [H^+])^2$$

The maxima of the ICD bands matched the UV absorption maxima for all β-CD·**1** complexes except for **1b** and **1e**. A hypsochromic shift from 379 nm (UV) to 370 nm (ICD) was registered for **1b** and a bathochromic shift from 373 nm (UV) to 382 nm (ICD) for **1e**. The ICD spectrum for **1e** exhibited also a distorted band shape, cf. pH 11 spectrum in Figure 2. These shifts may be indicative of a large co-conformational variability or nonuniformity (cf. Discussion).

Association Rate Constants. It should be noted in advance that our kinetic interpretations of the kinetic parameters are based on Scheme 1, which has been demonstrated to hold for the parent compound **1a**.[26] Excitation by UV light around 370 nm populates the fluorescent singlet-excited state of the free azoalkane (**1***) and the complex (CD·**1***). The environmental dependence of the fluorescence of **1** (quenching by abstractable C-H bonds) results in a shorter fluorescence lifetime within the complex (τ_{CD}) compared to the uncomplexed form (τ_0), see above. The kinetics can be analyzed through steady-state fluorescence measurements, which rely on the concomitant decrease of integrated fluorescence intensity upon addition of CD. These measurements require excitation at the isosbestic point (λ_{iso}, Table 1).[26] The intensity ratio in the absence (I_0)

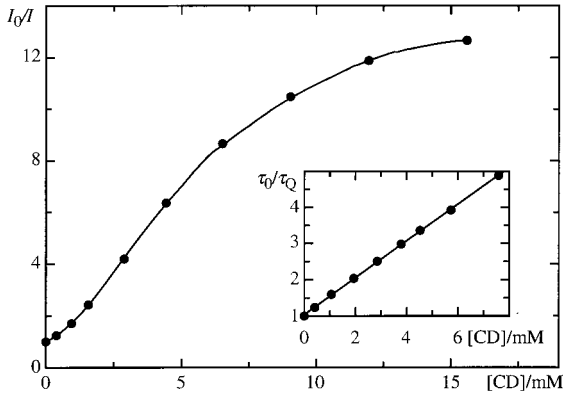

Figure 4. Steady-state and kinetic (inset) fluorescence quenching plots for **1c** (1.0 mM) by β-CD in D_2O and fits according to eqs 6 and 9 and the parameters in Table 2 (solid lines).

and in the presence of CD (I) is plotted against the total concentration of CD ($[CD]_0$) according to the previously introduced[26] eq 4, in which the concentration of uncomplexed azoalkane, [**1**], is defined by eq 5. Because the lifetime of the uncomplexed form (τ_0 in eq 4) and the binding constants (K in eq 5, Table 2) are known otherwise (Table 1), such plots (see Figure 4) are suitable to provide values for the association rate constant (k_{ass}), the dissociation rate constant (k_{diss}), and the fluorescence lifetime of the complex (τ_{CD}). τ_Q in eq 4 is the lifetime of the free excited guest, i.e., before it either deactivates or complexes with β-CD.

$$\frac{I}{I_0} = \frac{[\mathbf{1}]}{[\mathbf{1}]_0}\frac{\tau_Q}{\tau_0} + \frac{[\mathbf{1}]}{[\mathbf{1}]_0}QR\frac{\tau_{CD}}{\tau_0} + \left(1 - \frac{[\mathbf{1}]}{[\mathbf{1}]_0}\right)R\frac{\tau_{CD}}{\tau_0} \qquad (4)$$

$$\text{with} \quad Q = \frac{k_{ass}\tau_0[\mathrm{CD}]_0}{1 + k_{ass}\tau_0[\mathrm{CD}]_0},$$

$$R = \frac{1 + k_{ass}\tau_0[\mathrm{CD}]_0 + k_{diss}\tau_0}{1 + k_{ass}\tau_0[\mathrm{CD}]_0 + k_{diss}\tau_{CD}}, \text{ and } \tau_Q = \frac{1}{k_0 + k_{ass}[\mathrm{CD}]_0}$$

$$[\mathbf{1}] = (K[\mathbf{1}]_0 - K[\mathrm{CD}]_0 - 1 + \{(K[\mathbf{1}]_0 + K[\mathrm{CD}]_0 + 1)^2 -$$
$$4K^2[\mathbf{1}]_0[\mathrm{CD}]_0\}^{1/2})/2K \qquad (5)$$

The k_{diss} values recovered from fits according to eq 4 were very small for azoalkanes **1a**−**e**, and the errors were as large as the values themselves. This result confirmed that exit from the excited complex must be indeed insignificant for azoalkanes **1a**−**e**, as previously demonstrated for **1a**.[26] This was not the case for the ammonium derivative **1f**, for which the value of k_{diss}, within a large error, was only 1 order of magnitude below that of k_{ass}. This indicated the significance of exit in this case. If one assumes that the binding constants are similar in the ground and excited states (see Discussion), one may obtain estimates of the dissociation rate constants (k_{diss}, values in parentheses in Table 2). These values are much smaller than $k_{CD} = 1/\tau_{CD}$, the quenching rate constant inside the complex, *except for* **1f**. This supports the notion that k_{diss} cannot be neglected for **1f**, but it can be for the other derivatives **1a**−**e**, for which the simplified eq 6 can then be applied for fitting and extracting the values of k_{ass}.

$$\frac{I}{I_0} = \frac{\tau_{CD}}{\tau_0} + \frac{[\mathbf{1}]}{[\mathbf{1}]_0}\left(1 - \frac{\tau_{CD}}{\tau_0}\right)\left(\frac{1}{1 + k_{ass}\tau_0[\mathrm{CD}]_0}\right), \quad \text{for } k_{diss} \ll k_{CD} \qquad (6)$$

(48) Yi, Z.; Chen, H.; Huang, Z.; Huang, Q.; Yu, J. *J. Chem. Soc., Perkin Trans. 2* **2000**, 121−127.
(49) The computer program Pro Fit 5.5.0 (QuantumSoft, Zurich) was employed for individual fitting and global data analysis.

The time-resolved fluorescence decays were obtained by laser-flash photolysis. The resulting kinetics can be analyzed according to the formal kinetic scheme derived by Andriessen et al.[50] In our fluorescence measurement, both the free fluorophores and the complexes are simultaneously excited due to the very similar UV absorption spectra. Moreover, since the fluorescence spectra are virtually superimposable,[26,27] the sum of the fluorescence from both species is observed. If one further ensures equal absorption probabilities by excitation at the isosbestic point (λ_{iso}, Table 1) or corrects for differential absorption in cases where the excitation wavelength cannot be adjusted (e.g., for laser excitation), and in addition relies on the observation that the natural radiative lifetimes display no pronounced solvent dependence,[27] the emission intensities of each species are linearly related to its ground-state concentration. The time dependence of the observed fluorescence intensity, $I(t)$, normalized to unity at $t = 0$, is then given by eq 7, where [**1**] is defined by eq 5.

$$I(t) = \left(\frac{-[\mathbf{1}](k_0+\gamma_2) - [\mathrm{CD}\cdot\mathbf{1}](k_{CD}+\gamma_2)}{[\mathbf{1}]_0\sqrt{(k_0+k_{ass}[CD]_0-k_{CD}-k_{diss})^2+4k_{ass}k_{diss}[CD]_0}}\right)e^{\gamma_1 t} + \left(\frac{[\mathbf{1}](k_0+\gamma_1) + [\mathrm{CD}\cdot\mathbf{1}](k_{CD}+\gamma_1)}{[\mathbf{1}]_0\sqrt{(k_0+k_{ass}[CD]_0-k_{CD}-k_{diss})^2+4k_{ass}k_{diss}[CD]_0}}\right)e^{\gamma_2 t} \quad (7)$$

The time constants γ_1 and γ_2 in eq 7 are defined as follows:

$$\gamma_1 = -\frac{1}{2}\{k_0 + k_{ass}[CD]_0 + k_{CD} + k_{diss} - \sqrt{(k_0+k_{ass}[CD]_0-k_{CD}-k_{diss})^2+4k_{ass}k_{diss}[CD]_0}\}$$

$$\gamma_2 = -\frac{1}{2}\{k_0 + k_{ass}[CD]_0 + k_{CD} + k_{diss} + \sqrt{(k_0+k_{ass}[CD]_0-k_{CD}-k_{diss})^2+4k_{ass}k_{diss}[CD]_0}\}$$

When dissociation of the complex during its excited-state lifetime is negligible ($k_{diss} \ll k_{CD}$), eq 7 simplifies to the equation employed in our previous work (here rearranged):

$$I(t) = (1-S)\,e^{-(\tau_{CD})^{-1}t} + S\,e^{-(\tau_Q)^{-1}t}$$

$$\text{with} \quad S = \frac{[\mathbf{1}]}{[\mathbf{1}]_0}\left(1 + \frac{k_{ass}\tau_0[CD]_0}{\tau_0/\tau_{CD} - k_{ass}\tau_0[CD]_0 - 1}\right) \quad (8)$$

$$\text{and} \quad \tau_Q = \frac{1}{k_0 + k_{ass}[CD]_0}, \text{ for } k_{diss} \ll k_{CD}$$

An analysis of the preexponential factors in eqs 7 and 8, which are subject to a larger error,[26] was generally not attempted, but the two time constants (τ_{CD} and τ_Q) in the experimental decay traces were extracted by biexponential fitting. For azoalkanes **1a**−**e**, one component was found to be *constant* within error, i.e., independent of CD concentration. This suggested that eq 8 applied, in which exit is considered insignificant for **1a**−**e**, as already borne out by the steady-state analysis above. The meaning of the time constants in eq 8 can be readily rationalized. The first time constant corresponds to a *static* component (τ_{CD}), which is due to quenching inside the complex (Scheme 1) and therefore independent of CD concentration. The second, *dynamic* component (τ_Q) corresponds to the lifetime of the free form before complexation, which depends on the bimolecular association rate constant (k_{ass}) and the CD concentration. k_{ass} can then be extracted from the dependence of the τ_Q values on the total CD concentration (eq 9). Here, the analysis according to eq 8 rather than eq 7 has the advantage of a simple linearized data representation (eq 9) through a regression analysis of a kinetic quenching plot (inset in Figure 4).

$$\frac{\tau_0}{\tau_Q} = 1 + k_{ass}\tau_0[CD]_0 \quad (9)$$

In a final procedure, to obtain the best estimates of the association rate constants for azoalkanes **1a-e**, where exit is insignificant, the time-resolved and steady-state data were subjected to a *simultaneous* nonlinear fitting analysis according to eqs 6 and 9, putting arbitrarily an equal weight to both data sets.[49] The resulting values are entered in Table 2. For the ammonium derivative **1f**, the biexponential fitting of the excited-state lifetimes did not yield a static, i.e., constant, component at different CD concentrations. This, along with the indications from the steady-state experiments (see above), suggested that exit cannot be neglected and that eqs 6 and 9 no longer apply. This prevented also an analysis of the time-resolved data according to eq 9. A global analysis,[49] i.e., simultaneous fitting of the individual decay traces according to eq 7, is indicated in such cases,[50] which includes k_{diss} as a fitting parameter. Moreover, we have also included the steady-state treatment according to eq 4, which considers also k_{diss}, in the final analysis, putting again an equal weight to the steady-state and the combined time-resolved data. The resulting constants for **1f** are entered in Table 2. It should be mentioned that the binding constant obtained from the ratio of the recovered rate constants ($k_{ass}/k_{diss} = 25\ M^{-1}$) supports also the suggestion that the excited-state binding resembles that in the ground state (20 M^{-1}), which was obtained by ICD (see above).

For azoalkane **1b**, for which the fluorescence lifetime of the complex (τ_{CD}) was very long (430 ns) and too similar to that of the uncomplexed guest (590 ns, under air), a reliable differentiation of the static and dynamic components through biexponential fitting of the time-resolved decay traces could not be performed. In general, the differentiation of two exponential decay components becomes a formidable task when the lifetimes differ by less than a factor of 2.[51] The effects on the steady-state fluorescence intensity were also too small in relation to the error to allow a reliable fitting according to eq 6. As a consequence, no kinetic data for **1b** can be reported. The failure for **1b** reveals the limitations of our fluorescence-based method for determining association rate constants.

Discussion

The changes of the UV, ICD, and NMR spectra of azoalkanes **1** upon addition of β-cyclodextrin (β-CD) can be understood in terms of the formation of inclusion complexes, where the guest is positioned inside a hydrophobic cavity. This is confirmed,

(50) Andriessen, R.; Boens, N.; Ameloot, M.; De Schryver, F. C. *J. Phys. Chem.* **1991**, *95*, 2047−2058.

(51) Grinvald, A.; Steinberg, I. Z. *Anal. Biochem.* **1974**, *59*, 583−598.

for example, by the bathochromic shift of the near-UV azo absorption band (Table 1) and the chemically induced ^{1}H NMR shifts (CIS), which were observed for the inner H-3 and H-5, yet not for the outer H-2 and H-4 protons of β-CD (the approximate locations of these hydrogens are entered in Scheme 1, bottom left). The CIS values are significant not only for the upper H-3 (ca. 0.10 ppm) but also for the lower H-5 protons (ca. 0.08 ppm). This applies for all azoalkanes **1a**−**f** when the effects are extrapolated to quantitative binding. A small effect was also observed for the H-6 protons. The observed NMR shifts can be conclusively interpreted in terms of a *deep* inclusion for all complexes, as previously corroborated for azoalkanes **1a** and **1b**.[26,29] All data support the formation of complexes with 1:1 stoichiometry; e.g., the UV titrations show an isobestic point (Table 1) and the data from UV, NMR, fluorescence, and ICD titrations can be fitted with a 1:1 complexation model.

The Discussion is arranged such that we will first analyze the structure of the host−guest complexes in more detail, in particular with respect to the relative alignment of the guest to the host, i.e., the co-conformation of the complex.[12] In a second part, substituent effects on the thermodynamics of binding will be examined, keeping in mind a possible influence of structural variations. Finally, we will question to which degree the kinetics of host−guest complex formation can be understood in terms of the observed structural and thermodynamic trends.

Complex Structures by Induced Circular Dichroism and NMR. The induced circular dichroism (ICD) provides a unique analytical tool to investigate the structures of chiral host−guest (host−chromophore) inclusion complexes in solution.[6,7,11] Several rules for the assignment of the co-conformations and the depth of inclusion have been developed for cyclodextrins (CDs) as host systems.[10,52,53] In most studies, aromatic chromophores have been examined, whereas aliphatic ones have received comparably little attention. Aliphatic azoalkanes and diazirines have recently been employed in ICD measurements,[29−32] which has allowed several new insights into the inclusion geometries of aliphatic guests.

The ICD method was also applied in this work to the complexes between β-CD as chiral host and azoalkanes **1** as achiral chromophores.[46] In essence, the n,π* transition of the azo chromophore around 370 nm gives rise to a characteristic ICD signal when included in CD.[29−32] The magnitude and sign of the ICD effect are directly related to the orientation of the electric dipole transition moment relative to the axis of the CD. According to the rule of Harata,[10,29,30,53] which applies to chromophores immersed in the CD cavity, co-conformations with a parallel alignment produce a positive ICD signal, while those with an orthogonal alignment produce only a half as strong, negative ICD signal. In the case of azoalkanes, the electric dipole transition moment points along the azo π orbital and lies orthogonal to the plane defined by the C−N═N−C linkage.[29] Structural assignments of the β-CD complexes of the parent compound **1a** and the bis-alkylated derivative **1b** based on ICD effects have been communicated (Scheme 3, arrows indicate the direction of the electric dipole transition moment).[29] We refer to the respective co-conformations as lateral (**1a**) and frontal (**1b**).[29] These assignments have been recently confirmed

Scheme 3

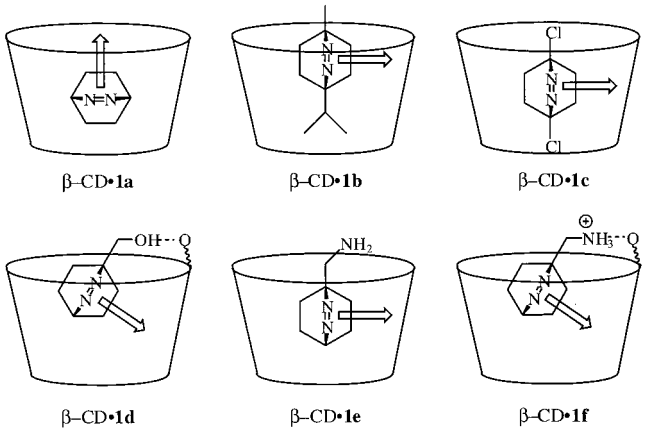

through force-field computed structures and energies as well as quantum-chemical calculations of ICD effects.[30]

The co-conformational assignments of the presently examined derivatives **1c**−**e** are made accordingly (Scheme 3), keeping in mind the NMR results (see above) which suggest the formation of deep inclusion complexes in all cases. Further, we adhere to the general notion that polar substituents reside near the secondary hydroxyl rim while more hydrophobic groups tend to protrude into the cavity.[6] For **1b**, in particular, the penetration of the isopropyl rather than the methyl group has been substantiated by force-field calculations.[30] The dichloro derivative **1c** resembles the bis-alkylated derivative **1b** in that it bears two bridgehead substituents. The van der Waals diameters along the bridgehead axis of **1c** (ca. 8 Å) and **1b** (ca. 9 Å) both exceed the diameter of the β-CD cavity (6.0−6.5 Å)[1] significantly, which promotes a frontal type of inclusion due to steric restraints.[29] The strong negative ICD for **1c** supports this structural assignment (Scheme 3).

The van der Waals diameter of the hydroxymethyl, aminomethyl, and ammoniummethyl derivatives **1d**−**f** (ca. 7 Å along bridgehead axis) lies between those for the parent **1a** (ca. 6 Å) and the disubstituted cases **1b** and **1c**. This reduces the preference for frontal inclusion, but a lateral or tilted lateral inclusion may still be viable. Indeed, the hydroxy and ammonium derivatives **1d** and **1f** display positive ICD effects, which suggest a more lateral co-conformation, as has been previously observed and analyzed for the parent compound **1a**. Note that among the four principal co-conformations (lateral, frontal, apical, basal), only the lateral one should give rise to a positive ICD.[29,30] Due to the angular dependence of the ICD effect in CD inclusion complexes, which predicts positive contributions to be twice as strong as negative ones for the same electronic transition,[10,29,30,53] a positive ICD signal is expected even for significant deviations from the ideal angle (Harata's rule, see above).[30]

Strikingly, the aminomethyl derivative produced a negative ICD effect, which resembles that observed for the bis-substituted derivatives **1b** and **1c**. This suggests that a frontal co-conformation is populated for **1e**. But why does the substitution of the hydroxy for the amino group (**1d** versus **1e**) or even the deprotonation of the ammonium group (**1f** versus **1e**) result in an inversion of the ICD sign from positive to negative, i.e., a pronounced change in the co-conformation of the host−guest complex? We propose that differences in host−guest hydrogen bonding are important. The intramolecular network of secondary

(52) Kajtár, M.; Horváth-Toró, C.; Kuthi, É.; Szejtli, J. *Acta Chim. Acad. Sci. Hung.* **1982**, *110*, 327−355.
(53) Kodaka, M. *J. Phys. Chem. A* **1998**, *102*, 8101−8103.

Scheme 4

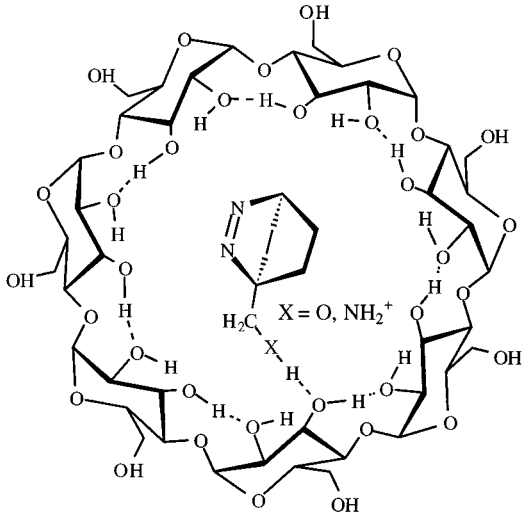

O2(n)···H···O3(n − 1) interglucose hydrogen bonds[9,54,55] stabilizes the macrocyclic host structures. These intramolecular hydrogen bonds at the upper rim are particularly strong for β-CD[56] compared to α-CD and γ-CD, which is also held responsible for the reduced solubility of β-CD.[57] It is conceivable that the intramolecular network prefers intermolecular interactions with hydrogen bond *donors* over those with hydrogen bond *acceptors* (Scheme 4). In fact, in most documented cases for hydrogen bonding, the guests, in particular phenols,[7,58−60] function as hydrogen bond donors.

The tendency for formation of hydrogen bonds in which the functional groups act as donors should approximately decrease with the group acidity, which follows the well-known order $R-NH_3^+ > R-OH \gg R-NH_2$. The hydroxyl and ammonium groups in **1d** and **1f** may thus form hydrogen bonds with the secondary hydroxyl rim (Scheme 4)[48,61] and, thus, adapt a tilted lateral co-conformation (Scheme 3). In contrast, the amino group as the poorest hydrogen bond donor may not form such hydrogen bonds. Steric effects (as those for **1b** and **1c**) may now prevail and induce a frontal co-conformation with the expected negative ICD. Hence, the variations in the signs of the experimental ICD effects may be due to a change of the co-conformations of azoalkanes **1d**−**f** as induced by hydrogen bonding with the secondary hydroxyl rim for the hydroxyl and ammonium but not for the amino group.

These tentative structural assignments are in line with literature findings. First, a lower tendency for hydrogen bonding of the amino compared to the hydroxyl group has been previously held responsible for a similar structural effect, namely a more axial co-conformation of anilines compared to phenols.[58] Second, according to crystal structures, the amino group in *p*-iodoaniline in its α-CD complex adapts a position very similar

Scheme 5

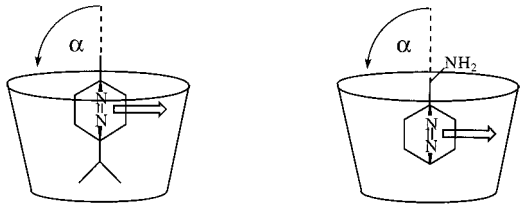

to that depicted in Scheme 3 for **1e** and does not engage in hydrogen bonding with the enclosing host, either.[62]

Based on the relative magnitude of the ^{1}H NMR shifts, H-3 > H-5 ≫ H-6, we propose for all azoalkanes **1a**−**f** a location with the center of mass somewhat displaced toward the upper rim, as previously found for **1b** by force-field calculations.[30] This location renders also hydrogen bonding of the functional groups in **1d** and **1f** with the lower rim O-6 protons unlikely, i.e., a 180° rotation of these guest molecules in Scheme 3. Such alternative hydrogen bonding with the primary hydroxyl rim has been occasionally invoked for very small guest molecules.[62] However, bonding with the upper secondary hydroxyl rim as depicted for **1d** and **1f** in Scheme 3 is more common.[48,60,61,63−66]

While we assume that the structure of the β-CD•**1e** complex in Scheme 3 gives rise to the negative ICD signal, scrutiny of the ICD spectra reveals that the complex of azoalkane **1e** differs from the other derivatives in that it gives rise to an ICD band, which is significantly distorted, cf. Figure 2, and shows also a bathochromic shift relative to the UV spectrum (cf. Results). A small shift of the band maximum of the UV and ICD spectrum was also observed for azoalkane **1b**, but not for the other four derivatives, for which the band shape and maximum were virtually the same. Moreover, the ICD of **1e** shows a small positive component at shorter wavelengths in addition to the stronger negative one. These irregularities suggest a large co-conformational variability, which has been previously corroborated for **1b**.[30] This means that complexes with different tilt angles (α in Scheme 5) may be present in solution. Note, in particular, that for **1e**, in contrast to **1d** and **1f**, the co-conformational space may not be restricted by hydrogen bonding with the upper rim. The co-conformers with different tilt angles may have quite different UV spectra (which reflect the depth of inclusion into the nonpolar environment) and ICD effects (which reflect the geometrical alignment with respect to the azo chromophore) and, thus, account for the observed shifts for **1b** and **1e**. For example, a tilted, less deeply immersed complex could be responsible for the small positive ICD contributions for **1e** at short wavelengths.

The possible involvement of more than one co-conformer and a large co-conformational variability constitute standing problems in the assignment of the solution structures of host−guest complexes. This is in contrast to crystal structures where one co-conformer may crystallize out preferentially, which does not

(54) Jacob, J.; Gessler, K.; Hoffmann, D.; Sanbe, H.; Koizumi, K.; Smith, S. M.; Takaha, T.; Saenger, W. *Angew. Chem., Int. Ed.* **1998**, *37*, 605−609.
(55) Harata, K. *Bull. Chem. Soc. Jpn.* **1982**, *55*, 2315−2320.
(56) Steiner, T.; Saenger, W. *Angew. Chem., Int. Ed.* **1998**, *37*, 3404−3407.
(57) Szejtli, J. *Cyclodextrin Technology*; Kluwer: Dordrecht, 1988.
(58) Kamiya, M.; Mitsuhashi, S.; Makino, M.; Yoshioka, H. *J. Phys. Chem.* **1992**, *96*, 95−99.
(59) Rekharsky, M. V.; Goldberg, R. N.; Schwarz, F. P.; Tewari, Y. B.; Ross, P. D.; Yamashoji, Y.; Inoue, Y. *J. Am. Chem. Soc.* **1995**, *117*, 8830−8840.
(60) Marconi, G.; Monti, S.; Mayer, B.; Köhler, G. *J. Phys. Chem.* **1995**, *99*, 3943−3950.
(61) Roberts, E. L.; Dey, J.; Warner, I. M. *J. Phys. Chem. A* **1997**, *101*, 5296−5301.
(62) Saenger, W.; Beyer, K.; Manor, P. C. *Acta Crystallogr.* **1976**, *B32*, 120−128.
(63) Wenz, G.; Hoefler, T.; Wehrle, S.; Schneider, M. *Polym. Prepr. (Am. Chem. Soc., Div. Polym. Chem.)* **1998**, *39*, 202−203.
(64) Kano, K.; Tatsumi, M.; Hashimoto, S. *J. Org. Chem.* **1991**, *56*, 6579−6585.
(65) Amato, M. E.; Djedaini-Pilard, F.; Perly, B.; Scarlata, G. *J. Chem. Soc., Perkin Trans. 2* **1992**, 2065−2069.
(66) Krishnamoorthy, G.; Dogra, S. K. *J. Phys. Chem. A* **2000**, *104*, 2542−2551.

necessarily provide evidence for the prevalence of this particular co-conformer in solution. The possibility of several populated co-conformers exposes also the limitations of ICD spectra for structural assignments, since ICD spectra reflect a Boltzmann-weighted average of all thermally accessible structures. In general, one must note that the proposed structural assignments based on NMR and ICD effects (Scheme 3) are tentative ones, since they rely, for example, on empirical rules for the interpretation of ICD effect. However, one must also recall that the determination of the solution structures of cyclodextrin complexes by NMR and ICD presents a great challenge since alternative experimental methods have not been established.

The *absolute* magnitude of the ICD effects can be compared on the basis of the molar ellipticity values ($\Delta\epsilon$, Table 2), which extrapolate the experimental θ values to quantitative complexation and, thus, present a comparable quantity for all complexes. The order observed for the positive ICD effects, i.e., **1a** > **1d** ≈ **1f**, is in agreement with the suggestion that **1d** and **1f** adapt a similar co-conformation, which, however, is somewhat less ideal than for azoalkane **1a**, i.e., the lateral co-conformation which gives rise to the positive ICD is somewhat tilted. The order observed for the negative ICD effects, i.e., **1c** < **1e** ≈ **1b**, suggests that the dichloro derivative **1c** adapts the "most perfect" frontal co-conformation, which may be caused by a particularly strong binding and deep penetration of this derivative into the cavity (see below). For comparison, **1b** may not protrude as deeply due to steric repulsion of the isopropyl group caused by the lower, tighter rim (note the conical shape of CD). This leaves the center of mass of **1b** more displaced toward the upper rim and may also be the reason for the large co-conformational variability, which is indicated for **1b**, yet not for **1c** (see above).[30]

Binding Constants. Relatively few thermodynamic studies of substituent effects have been devoted to aliphatic guest molecules[33,34] as opposed to aromatic guests.[6,7,67] The binding constants in Table 2 for azoalkanes **1** reflect the differential stabilization of the various guest molecules in the bulk water and the CD cavity. This results from a complex interplay between van der Waals and hydrophobic interactions, hydrogen bonding, release of high-energy water from the CD cavity, and relief of CD strain energy.[6,33,67] A quantitative analysis of the trends of the binding constants of azoalkanes **1** (Table 2) is not attempted, but some peculiarities and clear-cut rationalizations are addressed.

The parent compound **1a** serves as a reference with a binding constant of about 1000 M^{-1}. Based on the lower solubility of the dichloro derivative **1c** in water (1.0 mM) compared to the other azoalkanes (>10 mM) and well-known solubility trends (e.g., higher water solubility of alcohols compared to homologous amines), the hydrophobicity order of the examined guest molecules can be established as **1c** > **1b** > **1a** > **1e** > **1d** > **1f**. A higher hydrophobicity is expected to result in a larger binding constant, which is in an overall agreement with the experimental findings (1900 M^{-1} for **1c** > 1000 M^{-1} for **1a**,**1b** > 250 M^{-1} for **1e** > 180 M^{-1} for **1d** > 20 M^{-1} for **1f**). Interestingly, azoalkane **1b** does not show a higher binding affinity than **1a** despite its higher hydrophobicity. This can be rationalized in terms of the solution structures, which indicate that the lateral co-conformation, which is the energetically most favorable one for **1a**,[30] cannot be attained for **1b**. Instead, a frontal mode of inclusion must be adapted (Scheme 3). This co-conformation is energetically less favorable, which may offset the increased driving force due to its higher hydrophobicity and results in essentially the same binding constant as for **1a**.

Generally, the more hydrophilic guests **1d**−**f** show lower binding constants than **1a**−**c**. The ionic ammonium guest **1f** displays the weakest binding. The difference in binding constants between **1e** (250 M^{-1}) and **1f** (20 M^{-1}) is in line with the general observation that the ionization of the guest causes a destabilization of CD complexes in water.[33,68,69] We have shown above that hydrogen bonding is presumably an important structure-determining factor. However, the postulated hydrogen bonding of the hydroxyl and ammonium groups with the hydroxyl rim of the CD is not sufficiently large to result in an increased binding constant compared to that of **1a**. Moreover, the hydroxyl and ammonium derivatives **1d** and **1f**, for which hydrogen bonding is presumed, show actually a weaker binding than the amino derivative, for which hydrogen bonding to the CD may not play a role at all. The absence of a significant thermodynamic stabilization due to hydrogen bonding is in agreement with the results of other authors.[6,7] Consequently, the thermodynamics for binding of azoalkanes **1** is dominated by other factors. Namely, it can be adequately accounted for in terms of guest hydrophobicity and a change in the co-conformation due to the introduction of bridgehead substituents.

Complexation Kinetics. Knowledge of the association and dissociation rate constants of guest molecules with CDs is restricted to case studies,[19−23] and structural effects have only recently received attention.[70] Substituent effects have apparently not been examined for a common guest structure. This challenging aspect can now be studied by using the substituted azoalkanes **1** as dynamic fluorescent probes. As noted in the outset, the fluorescence quenching in the β-CD cavity allows one to obtain the association rate constants, while other techniques have proven particularly suitable for determining dissociation rate constants.[22,23] Strictly speaking, the association rate constants refer to the excited state, but it is presumed that these are comparable with those in the ground state, since the structure of these rigid bicyclic molecules and their dipole moments remain virtually unaffected by the electronic excitation (e.g., 3.5 D in the ground state vs 3.2 D in the singlet-excited state of **1a**).[71] This is in contrast to other guest molecules such as ketones, which undergo large dipole moment changes upon excitation.[22,23] Moreover, the very low pK_a values of the azo group in the ground state (0.5) and excited state (ca. −8) exclude the possibility of differential stabilization due to protonation.[72] In any case, the substituents hardly interact with the azo chromophore (cf. very similar UV spectra), such that the *relative* effects on the association rate constants, i.e., the substituent effects, should be meaningful even if small changes in the absolute thermodynamics due to excitation of the azo group apply.

As can be seen from Table 2, the overall variation in the association rate constants covers only a factor of 2−3, much

(67) Liu, L.; Guo, Q. *J. Phys. Chem. B* **1999**, *103*, 3461−3467.
(68) Matsuura, N.; Takenaka, S.; Tokura, N. *J. Chem. Soc., Perkin Trans. 2* **1977**, 1419−1421.
(69) Bergeron, R. J.; Channing, M. A.; McGovern, K. A. *J. Am. Chem. Soc.* **1978**, *100*, 2878−2883.
(70) Christoff, M.; Okano, L. T.; Bohne, C. *J. Photochem. Photobiol. A: Chem.* **2000**, *134*, 169−176.
(71) Nau, W. M.; Pischel, U. *Angew. Chem., Int. Ed.* **1999**, *38*, 2885−2888.
(72) Nau, W. M. *EPA Newsl.* **2000**, *70*, 6−29.

less than that for the binding constants. Efficient quenching upon complexation is a prerequisite for determining association rate constants by the fluorescence-based method. This is not met for azoalkane **1b**, such that this derivative could not be included in the kinetic analysis. Until recently, most reported association rate constants of small organic guest molecules with β-CD fell in the range of $(4-5) \times 10^8$ M^{-1} s^{-1} or below.[26] Recent measurements suggest that this does not constitute an upper limit and that rate constants may exceed this value.[22,70] The value measured for azoalkane **1c** (7.0×10^8 M^{-1} s^{-1}) is in line with this observation. Since the value for the dichloro derivative **1c** is the largest, a steric effect, which would predict a slower association rate, is clearly not observed. Moreover, the presence of hydrophilic substituents such as hydroxy, amino, and ammonium has no large effect on the kinetics. Consequently, guest desolvation does not dominate the complexation kinetics as in other cases, e.g., in the complexation of cations by crown ethers.[13] Rather, the observed order of the available association rate constants, namely, **1c** > **1a** > **1d**−**f**, follows roughly the order of the binding constants but does not allow definitive conclusions. However, it should be noted that a correlation between the kinetics of complexation and the binding constants is not a priori expected, and contrasting trends were observed in some cases.[73] This circumstance emphasizes the need for measurement of rate constants in addition to binding constants.

The dissociation rate constants (k_{diss}) define the lifetimes of the guests in the CD cavity ($\tau_{diss} = 1/k_{diss}$) and may be directly related to the efficiency of drug delivery and chemical protection of guests.[17,19] These values cannot be directly measured with our method, but they can be calculated from the experimental binding constants (K) and excited-state association rate constants (k_{ass}) subject to the above assumption that photochemical excitation does not significantly modify the affinity for binding. The calculated values for k_{diss} range from 10^5 to 10^7 s^{-1} and are included in Table 2. For **1a**−**e**, these values lie far below the rate constants for fluorescence in the CD cavity ($k_{CD} = 1/\tau_{CD} \approx 1 \times 10^7$ s^{-1}), but for **1f** exit occurs with a similar rate constant. This quantifies the previous notion (expressed for **1a**) that exit from the cavity does not compete significantly with deactivation for **1a**−**e**. Only for **1f** does exit become significant, such that the kinetics required a more evolved analysis in this case (cf. Results).

As previously emphasized, structural effects manifest themselves much more strongly in the exit than in the entry rate constants.[70] This notion is supported for the substituent effects on the dissociation rate constants for azoalkanes **1**, which display a much larger variation than the association rate constants: 1.2×10^7 s^{-1} (**1f**) > 1.8×10^6 s^{-1}(**1d**) > 1.0×10^6 s^{-1} (**1e**) > 4.4×10^5 s^{-1} (**1a**) > 3.7×10^5 s^{-1} (**1c**). Interestingly, this order is the reverse of that established for the hydrophobicity (cf. binding constants). This factor may be a common denominator of the dissociation rate constants.

Conclusions

Thermodynamic, kinetic, and structural aspects of complexation by cyclodextrins (CDs) play an essential role in the understanding of their functions and for the development of prospective applications. A fast kinetics, for example, is desirable for catalytic activity, and a regulated release of the guest is essential in drug delivery. On the other hand, a strong and selective binding may be of interest for analytical or environmental purposes. Finally, the solution structures are intimately related to molecular recognition, and the specific location of functional groups in the CD cavity, in particular in solution, may be the prerequisite for enzymatic specificity. A pertinent example is that of ester hydrolysis, where the secondary hydroxyl rim catalyzes the reaction at the acyl site.[74,75]

We have provided herein a comprehensive data set for substituent effects on the binding constants and association rate constants for complexation of azoalkanes **1** by β-CD and the solution structures of the resulting complexes (co-conformations). This joint study of structural, kinetic, and thermodynamic effects was made possible by the application of several independent spectroscopic techniques in aqueous solution. Azoalkanes **1** serve as molecular probes, which can be examined by UV, time-resolved and steady-state fluorescence, ICD, and NMR. We have shown that the structures of the CD complexes of azoalkanes **1**, which can be examined by ICD and NMR, are mainly governed by steric effects and hydrogen bonding. An unexpected structural variation, signaled by the inversion of the ICD sign, was observed for the hydroxyl, amino, and ammonium substituents. The complex stability appears to be dominated by an interplay between hydrophobic and specific structural effects, while the association rate constants, which can be determined by fluorescence decay, are relatively insensitive to substitution. The estimated dissociation rate constants show a larger variation and appear to be correlated with the hydrophobicity of the guest.

Acknowledgment. This work was supported by the Swiss National Science Foundation (projects 620-58000 and 4047-057552) within the Swiss National Research Program "Supramolecular Functional Materials" and MHV grant 2134-62567.00 for G.G.

JA011866N

(73) Liao, Y.; Bohne, C. *J. Phys. Chem.* **1996**, *100*, 734−743.

(74) VanEtten, R. L.; Sebastian, J. F.; Clowes, G. A.; Bender, M. L. *J. Am. Chem. Soc.* **1967**, *89*, 3242−3253.

(75) Tee, O. S.; Bozzi, M.; Hoeven, J. J.; Gadosy, T. A. *J. Am. Chem. Soc.* **1993**, *115*, 8990−8998.

(76) Rodger, A.; Nordén, B. *Circular Dichroism and Linear Dichroism*; Oxford University Press Inc.: New York, 1997.

Optics and Spectroscopy, Vol. 95, No. 4, 2003, pp. 560–570. From Optika i Spektroskopiya, Vol. 95, No. 4, 2003, pp. 603–613.

MOLECULAR SPECTROSCOPY

Fluorescence Quenching Kinetics in Short Polymer Chains: Dependence on Chain Length[1]

X. Wang*, E. N. Bodunov, and W. M. Nau*,*****

**Departement Chemie, Universität Basel, Klingelbergstrasse 80, CH-4056 Basel, Switzerland*

***Physics Department, Russian State Hydrometeorological University, St. Petersburg, 195196 Russia*

e-mail: bodunov@mail.admiral.ru

****School of Engineering and Science, International University Bremen, Campus Ring 1, D-28759 Bremen, Germany*

e-mail: Werner.Nau@unibas.ch

Received April 11, 2003

Abstract—Monte Carlo simulations of chain conformations and the diffusion equation were used to analyze the fluorescence kinetics of short polymer chains labeled with a probe and a quencher at opposite ends. In simulations, three chain models were considered: an ideal chain (without volume interactions); a self-avoiding chain taking into account the exclusive volume effect; and a self-avoiding chain with limited flexibility between nearest segments. For each model, end-to-end distance distribution functions were obtained, which were different from Gaussian ones. The distribution functions were used in a diffusion equation to simulate the fluorescence kinetics of the probe affected by intramolecular end-to-end collisions of short chains. The kinetics has been numerically calculated for a representative experimental system in a nonviscous solution. The simulated time-resolved fluorescence decays were monoexponential except at very short times (<2 ns). Diffusion coefficients were calculated for different chain models and different chain lengths. The experimental data could be reproduced by assuming systematically smaller end-to-end diffusion coefficients for the shorter chains. *© 2003 MAIK "Nauka/Interperiodica".*

INTRODUCTION

Recently, the time scale and mechanism of intramolecular contact formation in polymer chains have been extensively studied by optical spectroscopy using the probe–quencher methodology [1–9]. In the related experiments, a probe is attached to one end of the polymer and an efficient contact quencher of the excited probe is attached to the other end. The quenching of the excited probe, which can be monitored through its transient absorption in the case of triplet states [3] or through its emission for fluorescent probes [6], then reflects the kinetics of end-to-end collision (Scheme 1) and provides experimental information on the mutual diffusion of the chain ends.

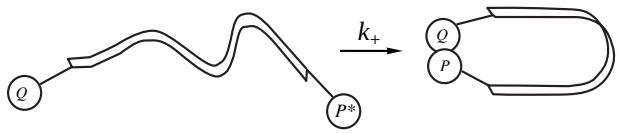

Scheme 1.

An important aspect in the choice of suitable probe–quencher pairs is the quenching mechanism, which should only involve quenching upon contact of the chain ends. Triplet energy transfer [5], electron transfer [10], hydrogen atom abstraction [6, 11], and exciplex formation [6, 11] have been proposed to satisfy this condition. Alternative experimental approaches to study of diffusion in polymers involve fluorescence resonance energy transfer (FRET) as the quenching mechanism [12–20] or, in the case of synthetic polymers, anthracene or pyrene excimer formation as the quenching mechanism [21].

Numerous treatments allow theoretical predictions of intramolecular diffusion processes in polymer chains [22–26]. Most treatments refer to long chains and are based on a Gaussian distribution function of end-to-end distances (Gaussian chain model). Recent experimental data for short polymer chains, in particular, those obtained from the collision-induced quenching of our fluorescent probe 2,3-diazabicyclo[2.2.2]oct-2-ene (DBO) by tryptophan (Trp) in peptides [6], as well as alternative probes employed by other groups [3, 21], have revealed several contrasts to the theoretical models: (1) Double-logarithmic plots of the rate constants for end-to-end collision (k_+) versus the chain length of peptides (N) were not linear as theoretically predicted [24–26], but displayed a negative curvature, in some sets of experiments with an inversion at very short chain lengths [6]. (2) The corresponding plots displayed relatively small slopes, e.g., -1.05 ± 0.06 for the DBO–Trp pair, which fall significantly below the theoretical value of –1.50 [24, 25]. The length dependence is therefore less pronounced than expected. (3) In experiments with end-attached contact quenching systems, simple monoexponential decay was observed.

[1] This article was submitted by the authors in English.

0030-400X/03/9504-0560$24.00 © 2003 MAIK "Nauka/Interperiodica"

This is in contrast to the Rouse–Zimm model, according to which quenching induced by end-to-end chain motion should be characterized by a series of relaxation times [25, 27–29].

The deviations between experiment and theory may be due to the theoretical idealization of the polymer chain, which neglects "chemical" effects of steric hindrance between the residues and potential barriers of bond rotation [15, 21], or, alternatively, due to the theoretical approximations employed to obtain the equilibrium distribution functions (Gaussian chain model), which may be inappropriate at short chain lengths [3, 5, 29, 30]. We have now employed Monte Carlo (MC) simulations for the equilibrium chain conformations in order to evaluate variances in the distribution function and possible consequences for the intramolecular quenching kinetics. In order to recognize the impact of different approximations on the shape of the distribution functions and the kinetics of fluorescence quenching, we have employed simple chain models of the rigid segment type.

It should be noted that, although the present investigations are mainly based on a comparison with biopolymer chains and, in particular, DBO–Trp polypeptides, they are transferable to other macromolecules. The DBO–Trp system was preferred for comparison with experiments, since it is the only one available that employs fluorescence rather than transient absorption for detection of biopolymer end-to-end collision. This offers the possibility of comparing direct time-resolved kinetic data with the indirect kinetic information extracted from steady-state fluorescence intensity measurements [6]. Both types of fluorescence data are theoretically predictable, which provides for an additional line of comparison with experimental data.

THEORETICAL MODELS AND COMPUTATIONAL DETAILS

The modeled (bio)polymer chains are labeled with a fluorophore and a quencher at opposite ends. As shown in Scheme 2, three different chain models (1–3) were applied to describe a real short polymer system (4).

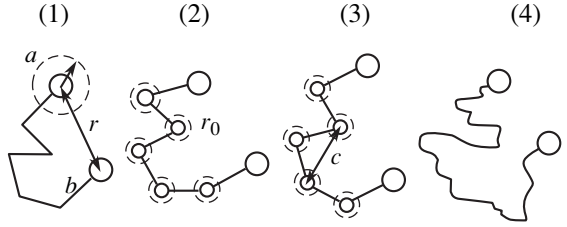

(1) Ideal short chain (IC) model. In this simple model, it is assumed that there is no interaction between the chain segments; accordingly, the segment movements are not correlated and the angle between segments may adopt, with equal probability, any value from 0 to 2π in a continuous three-dimensional space. Essentially, this is the assumption for an ideal chain with a Gaussian equilibrium end-to-end distance distribution, except that we limited the chain length to 22 segments, which is the experimental range typically accessible for monodisperse biopolymers and polymers [6, 21].

(2) Self-avoiding chain (SAC) model. This is a polymer chain model with volume interaction, for which we introduced a minimum distance (excluded volume) between any segment ends, r_0, into the simulation.

(3) Model of a self-avoiding chain with limited angular flexibility (SALF). This model introduces an additional limitation on the mutual orientation of nearest segments into the SAC model by restraining the angle between *connected* segments in addition to r_0. In essence, this limitation reflects in a simplistic way the chemical necessity that bonds connected to the same atom are subject to angular requirements otherwise accepted as hybridization. In the actual MC simulations, this additional restraint was introduced through the smallest available distance, c, between the two unconnected ends of two connected segments.

For each chain model and for each chain length (2, 4, 6, 10, 14, and 22 segments), 10^6 conformations were sampled with the MC technique. The end-to-end distance of each conformation, r, was recorded and then plotted in the equilibrium distribution function, $g_N(r)$, which is expressed as the probability of finding one end of the polymer chain within a unit volume with distance r to the other end. N denotes the number of segments in the chain. Because a probe and a quencher are attached at the two ends of the polymer chain, r is also the idealized distance between the probe and the quencher. For a sufficiently long ideal chain, the distribution is Gaussian, which is

$$g_N(r) = \left(\frac{3}{2\pi\langle r^2\rangle}\right)^{3/2} \exp\left(-\frac{3r^2}{2\langle r^2\rangle}\right), \qquad (1a)$$

where $\langle r^2\rangle$, the mean square end-to-end distance, depends on b, the length of each segment, and on N:

$$\langle r^2\rangle = Nb^2. \qquad (1b)$$

In the case of short chains with 2–22 segments, the distribution is more complex and differs substantially from Gaussian. The approximate equations

$$g_N(r/b) = A_0 \exp[-A_1(r/b) - A_2(r/b)^2 - A_3(r/b)^4], \qquad (2a)$$

$$g_N(r/b) = B_0 \exp[-B_1(r/b)^2 - B_2(r/b)^4] \qquad (2b)$$

were applied to describe the distribution functions obtained from simulations according to the IC model and the SALF model, respectively. Note that the end-to-end distance is here expressed as a relative distance that is the ratio of r and b. The constants A_0 and B_0 preceding

the exponential term normalize the distribution functions, such that

$$\int_0^N g_N(r/b)4\pi(r/b)^2 d(r/b) = 1. \quad (3)$$

It should be noted that a chain with two segments is distinct because the relative motion of one polymer end to the other is confined to the surface of a sphere with radius b and its center at the point where the two segments are connected. End-to-end diffusion is then reduced to a two-dimensional motion, to which Eq. (5) cannot apply. The $N = 2$ case must therefore be treated separately. For example, the analytical solution for the end-to-end distribution according to the IC model is $g_2(r/b) = b/(8\pi r)$. This is accurately reproduced by our MC simulations. Evidently, this function also differs strongly from Gaussian.

Experimentally, end-to-end collision is probed via the intramolecular quenching of the excited probe (attached to one chain end) by the quencher (attached to the other end). In the actual measurements, quenching is monitored through a sudden excitation with a laser pulse and subsequent observation of the time-resolved fluorescence decay of the probe. The decay rate depends on the intrinsic fluorescence decay rate and on the intramolecular quenching of the excited probe. If the quenching process is efficient (collision-controlled) the latter decay channel represents directly the end-to-end collision rate. To model the fate of the excited probe, it is suitable to assume that quenching occurs immediately upon contact between the excited probe and the quencher and that the end-attached probe molecule is instantaneously excited such that the initial distance distribution between the excited probe and the quencher, $g_N^*(r)$, coincides with the equilibrium end-to-end ground-state distribution obtained by the MC simulation, i.e.,

$$g_N^*(r, t)|_{t=0} = g_N(r). \quad (4)$$

Those probe molecules that are already in contact with the quencher when excitation occurs are immediately quenched (static quenching). The surviving excited states must undergo conformational changes to bring the chain ends together and therefore allow quenching. This mutual diffusion of the chain ends is caused by conformational fluctuation of the individual chain segments (Brownian motion). This motion can be described in the radial diffusion equation according to the theory of Szabo, Schulten, and Schulten [15, 24, 31–33], which is based on a modified Smoluchowski equation:

$$\frac{\partial}{\partial t}g_N^*(r, t) = -\frac{1}{\tau_0}g_N^*(r, t) + D\frac{1}{r^2}\frac{\partial}{\partial r}r^2\frac{\partial}{\partial r}g_N^*(r, t) + D\frac{1}{r^2}\frac{\partial}{\partial r}\left(r^2 g_N^*(r, t)\frac{\partial}{\partial r}\beta U(r)\right). \quad (5)$$

The first term on the right side of Eq. (5) represents the spontaneous decay in the absence of a quencher. D is the mutual intramolecular end-to-end diffusion constant, which is the sum of the diffusion coefficients of the individual ends. β^{-1} the product of the Boltzmann constant and the temperature ($\beta = 1/k_B T$), and $U(r)$ is the potential energy of the chain possessing an end-to-end distance r. If the equilibrium distribution $g_N(r)$ is known, the potential energy can be obtained according to equation [15, 24, 31, 32]

$$\beta U(r) = -\ln g_N(r). \quad (6)$$

Equation (5) can be used to calculate the survival probability density of an excited state at distance r subject to the initial distribution [Eq. (4)] and the absorbing boundary conditions

$$g_N^*(r, t)|_{r=a} = 0, \quad (7)$$

$$\frac{\partial}{\partial r}g_N^*(r, t) + g_N^*(r, t)\frac{\partial}{\partial r}\beta U(r)\Big|_{r=Nb} = 0. \quad (8)$$

The first boundary condition assumes that any excited probe (one end) approaching the quencher (the other end) to within a distance a will be quenched instantaneously. The second condition indicates the reflecting boundary at the maximum length of the chain, which is Nb.

The total fluorescence intensity detected in probe–quencher experiments is proportional to the survival probability of the excited states at time t,

$$I(t) = I_0\int_0^{Nb} 4\pi r^2 g_N^*(r, t)dr. \quad (9)$$

I_0 in Eq. (9) denotes a constant characteristic of the probe and the experimental set up. At time $t = 0$ $I(t)|_{t=0} = I_0$ due to Eq. (4).

When the diffusion equation (5) is solved, the kinetics of end-to-end collision, which is the quenching channel of the excited state, will be obtained. Unfortunately, analytical solutions are not available. In this work, we have numerically calculated the survival probability of the excited probe after different time intervals for a given MC simulated distribution function of polymer chains with 4–22 segments and have then plotted the time-resolved fluorescence decay.

RESULTS AND DISCUSSION

Our approach to modeling the dynamics of short polymer chains and then comparing it with experimental results is as follows: In the first stage, distribution functions are obtained by Monte Carlo simulations for different chain models; these are compared with a Gaussian function. In the second stage, the distribution functions are employed to model the kinetics of end-to-end collision in polymer chains by using appropriate diffusion equations. The resulting kinetics is then compared with experimental findings for biopolymer chains labeled with a fluorescent probe (DBO) at one chain end and a fluorescence quencher (Trp) at the other; both the time-resolved decay of emission and the (integrated) steady-state fluorescence intensity are analyzed. Finally, the theoretically expected dependence of the end-to-end collision kinetics on the chain length is compared with that obtained for the experimental biopolymer system to expose differences of the various chain models.

End-to-end distance distribution. The IC, SAC, and SALF models were applied for conformational simulations. The resulting end-to-end distance distributions for a chain with 4 segments ($N = 4$) are plotted in Fig. 1 as an example. Compared to a Gaussian distribution, the IC model, where no interaction is considered, gives rise to a lower distribution at the contact volume (very small r). When an excluded volume is introduced (SAC model with $r_0/b = 0.3$), i.e., the segment ends of the polymer chain cannot come infinitely close, this trend becomes more pronounced. When the folding of nearest segments is limited (SALF model with $r_0/b = 0.1$ and $c/b = 1.15$ corresponding to a minimum angle between connected segments of 70°), the distribution becomes completely different: the two ends have a much higher probability of staying apart as a result of a low tendency to approach each other.

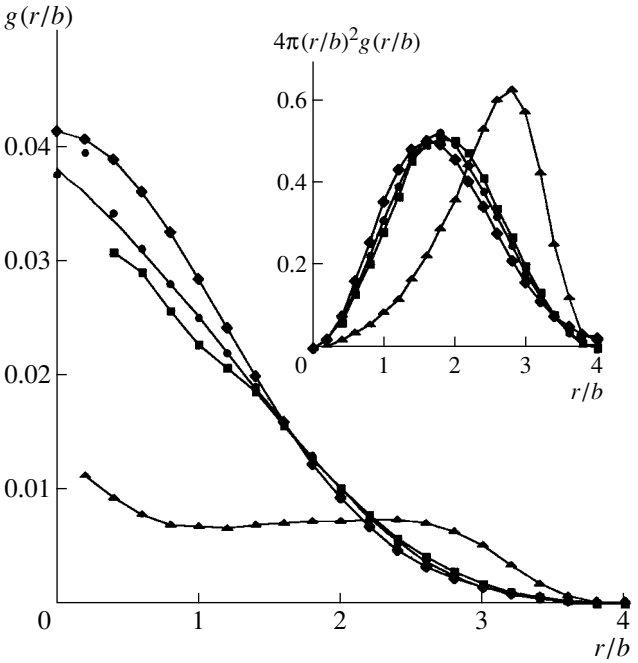

Fig. 1. Equilibrium end-to-end distribution of a chain with 4 segments ($N = 4$) simulated according to IC model (●), SAC model (■, $r_0/b = 0.3$), SALF model (▲, $r_0/b = 0.1$, $c/b = 1.15$), and according to the Gaussian chain model (◆).

Table 1. Parameters of end-to-end distance distribution functions obtained by fitting the MC simulation results to Eqs. (2a) and (2b)[a]

N	IC model				SALF model[b]		
	$A_0 \times 10^2$	$A_1 \times 10$	$A_2 \times 10^2$	$A_3 \times 10^3$	$B_0 \times 10^3$	$B_1 \times 10^2$	$B_2 \times 10^4$
4	3.80 [4.12]	2.55 [0]	14.7 [37.5]	14.2 [0]	*c*	*c*	*c*
6	2.17 [2.24]	2.00 [0]	11.2 [25.0]	6.04 [0]	*c*	*c*	*c*
10	1.06 [1.04]	1.30 [0]	8.47 [15.0]	1.71 [0]	3.18 [1.04]	5.69 [15.0]	3.30 [0]
14	0.630 [0.630]	0.850 [0]	6.99 [10.7]	0.729 [0]	1.98 [0.630]	4.19 [10.7]	1.68 [0]
22	0.320 [0.320]	0.500 [0]	5.09 [6.82]	0.212 [0]	1.04 [0.320]	2.80 [6.82]	0.603 [0]

[a] Values in brackets are parameters calculated according to the Gaussian distribution function. [b] Values of $r_0/b = 0.1$ and $c/b = 1.15$ were applied in the simulation. [c] End-to-end distance distribution functions for chains with 4 and 6 segments simulated with the SALF model can be approximated as follows:

$$g_4(r/b)\begin{cases} = 0.0067 + 0.0057(1.1 - r/b)^{2.3}, \text{ for } 0.1 \le r/b \le 1.1 \\ = 0.0067 + 0.00060(r/b - 1.1), \text{ for } 1.1 < r/b \le 2.2 \\ = 0.0074 + 0.0090(r/b - 2.2)^{4.3}, \text{ for } 2.2 < r/b \le 2.8 \\ = 0.0064\exp[-3.1(r/b - 2.8)^{1.626}], \text{ for } 2.8 < r/b \le 4, \end{cases}$$

$$g_6(r/b)\begin{cases} = 0.0067(1 - 0.19r/b), \text{ for } 0.1 \le r/b \le 3.8 \\ = 0.0020\exp[-1.41(r/b - 3.8)^{1.2} - 0.29(r/b - 3.8)^4], \text{ for } 3.8 < r/b \le 6. \end{cases}$$

The distributions according to the IC and SALF models for polymers with 4–22 segments were fitted to Eqs. (2a) and (2b) to obtain approximate distribution functions. The normalized parameters are summarized in Table 1. It follows that, for a very short chain, such as $N = 4–6$, regardless of whether volume interaction is considered or not, the end-to-end distance distribution is substantially different from Gaussian. However, for longer chains, the coefficients in the IC distribution functions approach more closely and more the Gaussian ones with increasing N, while the coefficients obtained from simulations according to the SALF model also deviate significantly at large values of N. Obviously, Gaussian distributions are inapplicable for short chains. Deviations from Gaussian distributions for short chains have also been deduced from FRET (fluorescence resonance energy transfer) experiments [15].

Chain dynamics. To evaluate the impact of varying distributions on the kinetics of end-to-end collision, it is essential to employ suitable dynamic models. The bead–spring models of Rouse and Zimm have been widely used in this context [27, 28]. In the full diffusion equation of the Rouse model, every change of the end vector can be thought of as originating in the cooperative motions of a large number of variables. Many computer simulations are based on this equation [34–36], but the general functions to be solved require various approximations.

The theories of Wilemski and Fixman [22, 23] and Szabo, Schulten, and Schulten [24] provide simple solutions for the chain motion. Both treatments predict that the end-to-end collision rate is a function of the diffusion coefficient, number of segments, segment length, and reaction radius. For a Gaussian chain and in the limit of a small reaction radius a, the mean first end-to-end passage time was derived as $\tau_m \propto b^3/(aDN^{-3/2})$ [24].

Recently, Pastor *et al.* performed a Brownian dynamics simulation on the mean first passage time of the two ends of a Rouse chain with the reaction radius as the absorbing boundary condition and compared the results with the WF and SSS theories [34]. A satisfactory agreement between simulation and theory was only obtained when the local equilibrium approximation was satisfied, i.e., when the memory effect could be neglected from in Langevin equation [37, 38]. This means that both the Wilemski-Fixman (WF) and Szabo-Schulten-Schulten (SSS) theories can only be applied for polymer chains in which the conformational fluctuations are sufficiently fast. The local equilibrium approximation holds, for example, in systems with a very small reaction distance [34]. The importance of the local equilibrium condition for application of the WF or SSS theories has subsequently been emphasized by others [35–37]. It is important to note that the local equilibrium condition can be experimentally corroborated through the observation of the monoexponential decay kinetics [3, 5, 21, 39].

Local equilibrium can be realized by different conditions in experimental systems, which include a small reaction radius ($\ll Nb$), fast diffusion (e.g., in nonviscous solvents), and a long lifetime of the excited state to extend the observation time. In our opinion, for the DBO-Trp, fluorescence-based contact quenching system the conditions of a local equilibrium are fulfilled: The reaction radius is small because the size of both probe and quencher is small and because the quenching process requires van der Waals contact and does not occur through space [6, 11, 40, 41]. The solvent is water, which is nonviscous in comparison to the mixtures with glycerol that are otherwise employed [12, 15], and the chain was designed to be flexible [5, 6], thereby facilitating fast diffusion. The fluorescence lifetime of the DBO probe (1 μs in the gas phase; 505 ns in aerated D_2O) is the longest among organic chromophores in solution. All of these properties render DBO an ideal candidate for the kinetic measurement of intrachain collision, a conjecture which has received support from a recent computational study [39]. In fact, the monoexponential decay kinetics of DBO–Trp-labeled polypeptides [6] suggests that the condition of local equilibrium is satisfied in this particular system.

Time-resolved fluorescence decays. In the theoretical simulations of the kinetics of fluorescence quenching induced by end-to-end collision, we employed parameters characteristic for the DBO–Trp probe–quencher system. Since local equilibrium is expected to apply for this system (see the previous section), the SSS diffusion equation (5) can be applied to numerically simulate the fluorescence decay kinetics by using the previously determined MC distribution functions. The fluorescence decays for all chains with 4–22 segments are reproduced as monoexponential over the entire time range (Fig. 2) except in a very short initial time interval; this applies to all models investigated (IC, SALF, and Gaussian chain).

The fast decay component at very short times (Fig. 2, inset) is presumably due to the fact that some excited probes with a very small end-to-end distance to the quencher require only minute Brownian motion to undergo quenching. Once this fast decay has occurred, equilibrium is established and the decay becomes monoexponential. This interpretation is supported by the evolution of the distribution function with time, which is depicted for the IC model in Fig. 3. (The evolution for the SALF model is qualitatively similar, but is not shown since the salient features are less readily apparent graphically.) Upon excitation, the original distribution function is cut off at the critical distance of static quenching. The sudden perturbation results in a nonsteady distribution function which is immediately restored on a very short time scale (<2 ns). During this initial time, which corresponds to the nonmonoexpo-

nential decay kinetics in the fluorescence decay, the shape of the distribution function (cf. the maximum in Fig. 3) undergoes a substantial shift. At longer time the shape of the distribution remains unchanged, corresponding to the region of monoexponential fluorescence decay. This scenario is reminiscent of bimolecular fluorescence quenching in a solution, where diffusional equilibrium (monoexponential decay) is only reached after a fast initial period with a faster decay component (transient effect) [42, 43].

The expected minute deviations from monoexponential decay kinetics are very unlikely to be experimentally detectable on a nanosecond scale. Monoexponential functions are therefore sufficient to describe the excited state decay within experimental error, and it is consequently proper to assign a single intrinsic "fluorescence lifetime" to each DBO–Trp peptide, which greatly simplifies data analysis. The time-resolved fluorescence decay traces can therefore be fitted to the equation

$$I(t) = I_0 \exp(-(1/\tau_0 + k_+)t). \qquad (10)$$

Here, $1/\tau_0$ is the decay rate in the absence of a quencher and k_+ is the quenching rate upon contact, which equals the end-to-end collision rate [6].

Steady-state fluorescence intensity. From the numerically calculated fluorescence decay in the inset of Fig. 2, it can be seen that the initial ($t = 0$) fluorescence intensity for each peptide falls somewhat below the expected maximum fluorescence intensity (I_0). This indicates that some conformations with end-to-end distance within the reaction radius undergo immediate quenching upon excitation (static quenching) [5]. Let ρ_N be the probability of finding both ends in the quenching sphere within the reaction radius, which corresponds to the fraction of encounters undergoing static quenching. From the equilibrium distribution function, ρ_N can be calculated according to the equation

$$\rho_N = \int_{r_0/b}^{a/b} g_N(r/b) 4\pi (r/b)^2 d(r/b), \qquad (11)$$

where r_0 is the distance limit between any two ends of different segments and a is the reaction radius, which cannot be smaller than r_0. (If ρ_N could be accurately experimentally determined, one could obtain information on the distribution function and the relevant parameters a and b. For example, when the IC model is applied, the initial contact probability could be approximately calculated as $\rho_N \approx A_0(N)(4\pi/3)(a/b)^3$.)

The actual fractions of static quenching are listed in Table 2. Expectedly, the fraction of static quenching is larger for the shorter chains, but it does not exceed values of 1% for the SALF model. The values for the simpler IC model are slightly larger (by up to 3%), which is directly related to the neglect of excluded volume ($r_0 = 0$). Deviations of the initial fluorescence intensity

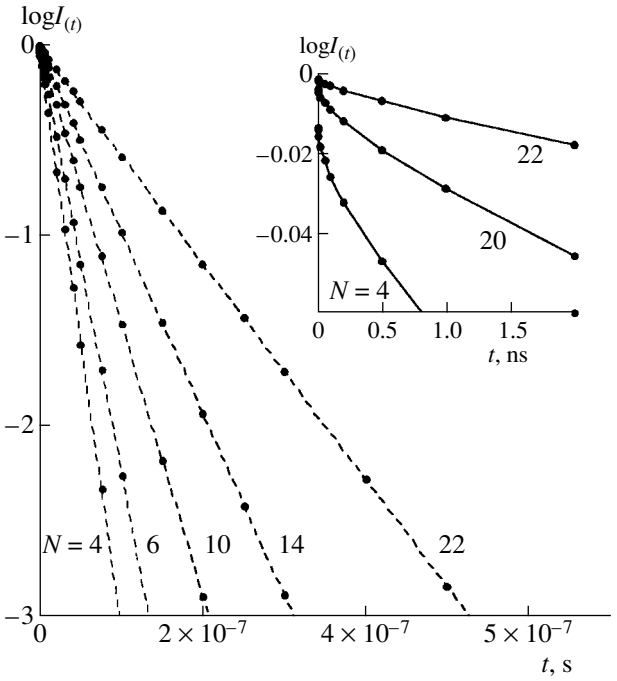

Fig. 2. Time-resolved fluorescence decays based on numerical calculations according to the IC model (•) and exponential approximation (dashed line) for polymer chains with 4–22 segments on a long time scale. The decay on a very short initial time scale is shown in the inset. The diffusion coefficients were taken from Table 3.

on the order of 1% are virtually impossible to detect in time-resolved experiments, and so the effect of static quenching can be neglected. However, when the steady-state fluorescence intensity is calculated for the numerically computed fluorescence decay traces in Fig. 2 (S_N values in Table 2), one finds nevertheless that the relative steady-state fluorescence intensities drop by up to 3% (10% in the IC model) below the values expected from the fluorescence lifetimes, i.e., from the monoexponential fit to the numerically calculated fluorescence decay traces in Fig. 2. This reduced steady-state fluorescence intensity can only in part be due to the static quenching, which can account only for about one-third of the total loss in the steady-state fluorescence intensity. The major fraction is due to the positive curvature of the fluorescence decay traces at very short times (Fig. 2, inset). In other words, the fluorescence decay has a very fast component at very short times, which is most pronounced for the shortest chains.

As a consequence of the static quenching and the initial fast decay component, the relative steady-state fluorescence intensity should be somewhat less than expected on the basis of the fluorescence lifetimes, but the effect may well fall within the rather large experimental error of steady-state fluorescence measurements, which are very sensitive to, among other factors, fluorescent or absorbing impurities. (A close inspection of the only available experimental comparison of time-

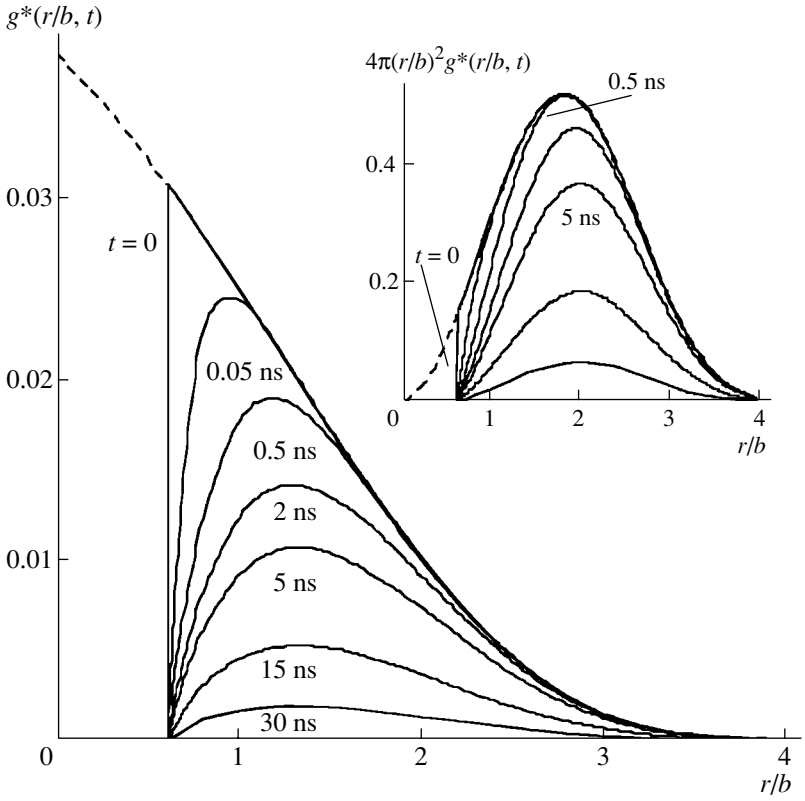

Fig. 3. Representative evolution of the distance distribution between excited probe and quencher with time (IC model, $N = 4$, $a/b = 0.6$, $D = 5.4 \times 10^{-7}$ cm^2 s^{-1}) obtained by using Eqs. (4)–(8). The dashed line corresponds to the ground-state equilibrium distribution. The computed data points are not shown for clarity. Note the displacement of the maximum at short times.

resolved and steady-state fluorescence data (for the DBO–Trp system in [6]) suggests indeed that the relative fluorescence intensities of short chains are somewhat "too small" in comparison to the fluorescence lifetimes. This trend may still be within error, but points in the theoretically expected direction.) The steady-state fluorescence intensity (S_N) is therefore in a good approximation proportional to the fluorescence lifetime,

$$S_N = \int_0^\infty I_N(t)dt \approx \int_0^\infty C(1-\rho_N)\exp(-t/\tau_N)dt = C(1-\rho_N)\tau_N \approx C\tau_N \quad (12)$$

(C is a constant), such that the kinetics of end-to-end collision can be alternatively quite reliably extracted from the relative steady-state fluorescence intensities, as was demonstrated in a preceding experimental study [6].

The first approximation takes into account that the decay of the fluorescence intensity (I_N) can be adequately fitted by a monoexponential decay function with a time constant τ_N, and the second approximation considers that the absolute values of ρ_N are very small.

Length dependence of end-to-end collision rates. In order to calculate the end-to-end collision rate for each chain and to investigate the functional form of the length dependence, we assumed a segment length b of 5 Å, which resembles the length of a peptide linkage (–CHR–CO–NH–), and a typical intrachain diffusion coefficient D of 9×10^{-7} cm^2/s. We then solved Eqs. (5)–(9) numerically and varied the reaction radius a from 0.5–5 Å; the lower limit of 0.5 Å is actually unreasonably small, but was included to better demonstrate the effect of varying reaction radius.

By fitting the calculated decay traces to monoexponential functions, the end-to-end collision rate constants k_+ were first obtained for the Gaussian chain model. The rates decrease with increasing chain length and can be linearly correlated according to $\log k_+ = \alpha \log N$ where α is equal to –1.51, to –1.53, and –1.60 for a/b = 0.1, 0.5, and 1, respectively. These slopes show a good agreement with the theoretical prediction. Note that a small reaction radius is essential to precisely reproduce the expectation value for a Gaussian chain (–1.5) [24, 25]. The length dependences of the collision rates were similarly obtained for the IC model and plotted in $\log(k_+) - \log(N)$ format (Fig. 4a). Increasing the radius of quenching from a/b = 0.1, 0.6 to 1 resulted in

Table 2. Experimental fluorescence lifetimes (τ_N) of DBO/Trp-labelled peptides of different chain lengths (N, taken as number of peptide units), expectation values for the steady-state fluorescence intensities (S_N) from the relative lifetimes, and theoretical initial contact probability (ρ_N) obtained for different polymer chain models

N	Experiment[a]		IC model[b]		SALF model[b,c]	
	τ_N, ns	τ_N/τ_0[d]	ρ_N[e]	S_N[f]	ρ_N[e]	S_N[f]
4	14.3	0.0286	0.0304	0.0257	0.0081	0.0278
6	19.5	0.0390	0.0171	0.0364	0.0056	0.0380
10	30.5	0.0610	0.0090	0.0575	0.0024	0.0591
14	45.6	0.0912	0.0057	0.0874	0.0013	0.0890
22	74.4	0.149	0.0028	0.150	0.0018	0.152
∞	500[g] (=τ_0)	1.00	0.00	≡1.00	0.00	≡1.00

[a] From [6], single-photon counting values. [b] Calculated by numerical simulation of fluorescence decays according to Eqs. (5)–(9) with b = 5 Å and a/b = 0.6; the diffusion coefficient was varied to fit the apparent lifetime of the simulated trace (monoexponential function) to the experimental result. [c] Values of r_0/b = 0.1 and c/b = 1.15 were assumed in the simulation. [d] This value corresponds to the expectation value of the relative steady-state fluorescence intensity derived from the experimental lifetimes if static quenching was absent and if the decay was strictly monoexponential; this corresponds to the approximate solution in Eq. (12), i.e., $S_N \approx C\tau_N$ with $C = 1/\tau_0$. [e] Expectation value for the fraction of static quenching. [f] Theoretical value of the relative steady-state fluorescence intensity (normalized to unity in the absence of intramolecular fluorescence quenching, i.e., $N \longrightarrow 8$) taking into account both the fraction of static quenching and the deviations from monoexponentiality; this corresponds to the precise theoretical solution of Eq. (12), i.e., $S_N = \int_0^\infty I_N(t)dt$. [g] Taken as the fluorescence lifetime in the absence of quenching [6].

a decrease in the slope α from –1.44, –1.49 to –1.57, again very close to the theoretical values. The same collision rate calculations according to the SALF model are shown in Fig. 4b for a representative simulation with r_0/b = 0.1 and c/b = 1.15, corresponding to a minimum angle between connected segments of 70°. It is seen that, in the whole length range, the log–log plots are no longer linear. The slight negative curvature reproduced by the SALF model reflects the introduction of practically relevant parameters such as chain stiffness. However, the negative curvature is still much less pronounced than the negative curvature observed in experimental studies [3, 6]. As for the other investigated models (Gaussian and IC), the slope α obtained according to the SALF model becomes more negative with increasing reaction radius, but the absolute values remain close to –1.5.

The constancy of the slope for the different chain models is quite surprising in view of the large deviations among the distribution functions (Fig. 1). Deviations of the conformational distribution of short chains from the ideal Gaussian one are therefore unlikely to be responsible for the disagreement of the length dependence plots with theoretical predictions. The deviations could be related to the shortcomings of the chain models presently employed. Alternatively, the assumption of a constant diffusion coefficient for chains of different lengths may be inappropriate.

When the end-to-end diffusion coefficient D in the modified diffusion equation (5) was varied in order to fit the numerically calculated traces to the experimental ones for the DBO–Trp pair in polypeptides [6], the intramolecular diffusion constants in Table 3 were obtained (b was taken as 5 Å and a/b as 0.6). Compared with the diffusion of free amino acid molecules in H_2O, which have diffusion coefficients of ca. 10^{-5} cm^2/s [44], the end-to-end diffusion of polypeptides with 4–22 amino acids are at least one order of magnitude smaller. For example, at room temperature in D_2O, for N = 6 the diffusion coefficient is 7.2×10^{-7} cm^2/s (IC) and 2.3×10^{-6} cm^2/s (SALF). These values are in the same range as those suggested by Lapidus *et al.* for related peptides with 3–19 amino acids (4×10^{-7} cm^2/s) [3]. Buckler *et al.* also applied FRET to study the struc-

Table 3. End-to-end diffusion coefficients calculated from the experimental lifetimes (cf. Table 2) of DBO/T rp-labelled polypeptide chains of different chain lengths (N, taken as number of peptide units)

N	$D \times 10^7$, cm^2 s^{-1}	
	IC model[a]	SALF model[a,b]
4	5.4	22
6	7.2	23
10	9.6	29
14	10.2	31
22	11.1	33

[a] The diffusion coefficients were calculated as described in the text. A segment length b = 5 Å and a reaction radius a/b = 0.6 were used in the calculation. [b] Values of r_0/b = 0.1 and c/b = 1.15 were applied in the simulation.

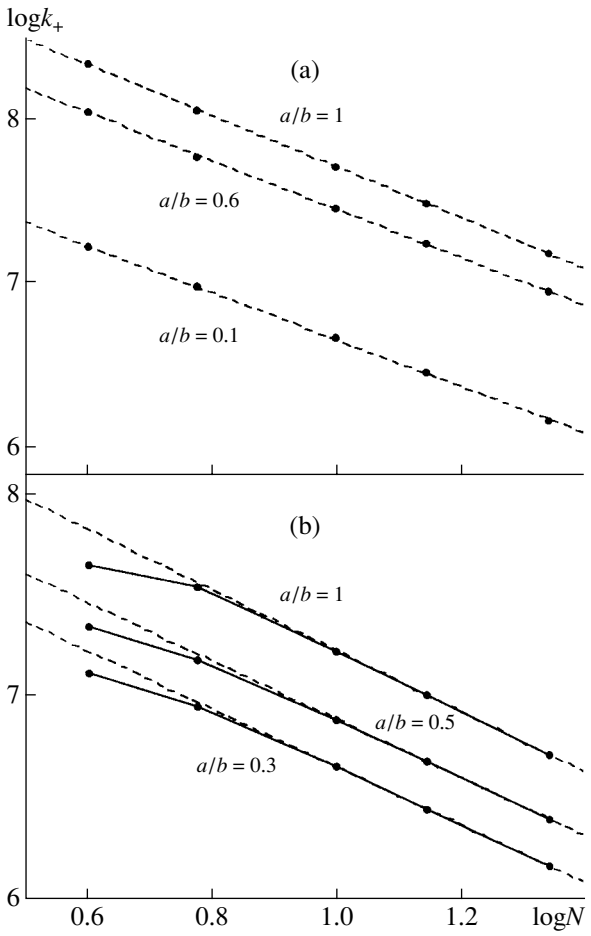

Fig. 4. Dependence of end-to-end collision rate, k_+ on the chain length (N = 4 to 22). k_+ was calculated for different reaction radii with the distribution functions obtained from a) the IC model and b) the SALF model. (a) Linear fits are shown for N = 4 to 22 with slopes of –1.44 (a/b = 0.1), –1.49 (a/b = 0.6), and –1.57 (a/b = 1.0). (b) Linear fits are shown for N = 10 to 22 with slopes of –1.44 (a/b = 0.3), –1.45 (a/b = 0.5), and –1.49 (a/b = 1.0); note the deviation from the linear fit at small N.

ture of denatured ribonuclease A [19]. For the 21-residue segment, the end-to-end diffusion constant was determined to range from $(1.5–8)\times10^{-7}$ cm^2/s. In a recent study on the CAGQW peptide by Yeh *et al.* [39], diffusion coefficients of 3.25×10^{-6} and 8.9×10^{-6} cm^2/s were computed for the AMBER and CHARMM force fields, respectively. These are consistent with our values obtained for the SALF model. (In a FRET study involving oligopeptides with 4–9 repeating units of *N*5-(2-hydroxyethyl)-(2-hydroxyethyl)-L-glutamine in a mixture of glycerol and trifluoroethanol, Haas *et al.* obtained considerably lower diffusion coefficients of $(3–8.5)\times10^{-8}$ cm^2/s [15]. This must be primarily due to the high viscosity of this solvent mixture.)

The choice of the chain model and the related distribution function has a pronounced effect on the calculated diffusion coefficients. From Table 3, it can be seen that the intramolecular diffusion constants based on the SALF model are systematically larger than those based on the IC model at the same length. This is expected, since both volume interaction and the angular restraints tend to keep the chain ends further apart (cf. the maximum of $4\pi r^2 g_N(r)$ in Fig. 1), so that, on average, longer distances must be passed to achieve contact and quenching. In other words, the two chain ends are further apart in the SALF model and must travel a longer way during the same time to conform to the experimental results. This manifests itself in a larger calculated diffusion coefficient.

One also observes a decrease in the diffusion constants for smaller values of N (Table 3). This trend is presumably the underlying reason for the negative curvature observed experimentally [3, 6, 15, 21]. It appears that shorter chains limit flexibility and hinder end-to-end collisions more than longer ones do; i.e., shorter chains may exhibit a larger "internal friction" [15]. Consequently, end-to-end collision becomes increasingly difficult for shorter chains. These results lead us to suggest that steric hindrance of the (bio)polymer side chains and the potential barriers of bond rotation lead to the peculiarities of the experimental length dependence, i.e., the deviation of the slope, as well as the negative curvature, in the $\log(k_+)–\log(N)$ plots. The internal friction dominant in short chains is not considered in the present MC calculations, but can be included into MC simulations through the use of appropriate force fields (to obtain more realistic distribution functions) in combination with molecular dynamics simulation and solvation effects (to reproduce the kinetics). Some initial work in this direction has recently been reported [40, 45].

CONCLUSIONS

We used the Monte Carlo technique to simulate the equilibrium conformational distribution of short polymer chains and the related kinetics of end-to-end collision. Different chain models of the rigid-segment type were employed. We showed that the distribution functions for short polymer chains vary substantially from the Gaussian distribution expected for long chains. Simulations of the chain dynamics for a representative experimental system (DBO–Trp) demonstrate that the kinetics of end-to-end collision becomes monoexponential on time scales above 2 ns. This is in agreement with the most recent experimental findings for probe–quencher systems and suggests that a local equilibrium is maintained in the related experimental systems, i.e., conformational fluctuations are sufficiently fast to maintain a constant shape of the distribution function during the quenching process. Moreover, the integrated steady-state fluorescence intensity is expected to be proportional to the fluorescence lifetimes, since deviations from monoexponentiality are small and since the fraction of static quenching is too small to be experi-

mentally relevant (<1%). With respect to the characteristic plots of the end-to-end collision rates of the polymer chains versus the chain length in $\log(k_+) - \log(N)$ format, the experimentally observed slope and pronounced curvature cannot be reproduced with a constant diffusion coefficient. Presumably, this curvature is due to an "internal friction" in short biopolymers, which results in a reduced diffusion coefficient of the chain ends and, therefore, slower end-to-end contact rates in short chains.

ACKNOWLEDGMENTS

This work was supported by the Swiss National Science Foundation and by National Research Programme 47, "Supramolecular Functional Materials."

APPENDIX

COMPARISON OF COLLISION-INDUCED QUENCHING VERSUS FRET TO ANALYZE CHAIN DYNAMICS

Another popular experimental technique for probing conformational dynamics in polymer and biopolymer chains is based on fluorescence resonance energy transfer (FRET) [12–20]. In this technique, an energy donor *D* and an energy acceptor *A* are attached at opposite ends of the polymer chain. The energy donor is excited by a short light pulse and then decays spontaneously as well as via FRET, which proceeds according to the Förster equation [46]

$$w(r) = \frac{1}{\tau_0}\left(\frac{R_0}{r}\right)^6. \qquad (13)$$

Here, R_0 is the Förster radius and r is the distance between the donor and the acceptor. In this case, the distribution of end-to-end distances results in a continuum of transfer rates, which is in contrast to the collision-induced quenching mechanism in the DBO–Trp and related probe–quencher systems. Note that FRET occurs over different distances with different rates, while collision-induced quenching occurs exclusively upon contact and thereby reflects an elementary reaction. The polymer chain undergoes conformational changes during the excited state lifetime, which renders the analysis of quenching by the FRET mechanism more complex. (The relative orientational motion of the two chromophores (alignment of electric transition dipole moments) also influences the energy transfer rate [35]. This additional complication in the interpretation of FRET data will not be further discussed here.) The distance-dependent energy transfer decay must be added to Eq. (5) and results in the equation [15, 17, 32, 33]

$$\frac{\partial}{\partial t}g_N^*(r,t) = -\frac{1}{\tau_0}\left(1+\left(\frac{R_0}{r}\right)^6\right)g_N^*(r,t) + D\frac{1}{r^2}\frac{\partial}{\partial r}r^2\frac{\partial}{\partial r}g_N^*(r,t) + D\frac{1}{r^2}\frac{\partial}{\partial r}\left(r^2 g_N^*(r,t)\frac{\partial}{\partial r}\beta U(r)\right), \qquad (14)$$

which is subject to a boundary condition:

$$\frac{\partial}{\partial r}g_N^*(r,t) + g_N^*(r,t)\frac{\partial}{\partial r}\beta U(r)\Big|_{r=r_0} = 0. \qquad (15)$$

FRET experiments can, in principle, yield both the end-to-end distance distribution and the intrachain diffusion coefficient. However, since these parameters are tightly correlated, the recovery of both the distribution and the diffusion coefficient from the donor fluorescence decay becomes very difficult [16]. (Beechem and Haas suggested that the equilibrium distance distribution and the intramolecular diffusion coefficient can be recovered by global analysis of both donor and acceptor fluorescence decay and growth curves [16]. However, direct excitation of the acceptor is difficult to avoid in experimental systems, which generally complicates this type of analysis (14].) In practice, the analysis of FRET data depends either on the knowledge of the diffusion coefficient or on the knowledge of the distribution function. Normally, the end-to-end distance distribution has to be built first by a suitable chain model or by a second set of experiments under different experimental conditions, e.g., in a solvent of high, in which where *D* is negligible.

The advantage of using collision-induced quenching systems such as the DBO–Trp pair to analyze chain dynamics lies in the fact that the rate of end-to-end collision can be directly extracted from the experimental (monoexponential) decay traces. Monoexponential decays suggest that the local equilibrium condition is satisfied, which is expected for a small contact radius and slow decay rates. Information on the chain dynamics can therefore be obtained without the assumption of a theoretical model for polymer dynamics and without the related numerical calculations according to diffusion equations; these operations are only necessary when absolute diffusion coefficients are warranted (see the related section in the main text).

FRET decay traces are inherently nonmonoexponential due to the continuum of transfer rates [15, 17, 18]. A bi- or even triexponential function is required for adequate fitting, but the related rate constants obtained from the fits have no readily apparent meaning. (We suggest that the nonmonoexponentiality of the decays (picosecond time regime) observed in the case of fast intramolecular electron transfer in peptides [10] may also be the result of distance-dependent electron transfer rates. Electron transfer, unlike hydrogen atom transfer or exciplex formation, does not strictly occur upon contact but may occur over sizable distances through

space or through the solvent (ca. 5–8 Å) and over larger distances through bonds. Electron transfer probe–quencher systems appear less suitable than FRET systems for investigating polymer chain dynamics, since the distance dependence of quenching by electron transfer is not simple to predict.) Srinivas *et al.* recently carried out a Brownian dynamics simulation for FRET between the two ends of a Rouse chain and reported that the survival probability becomes monoexponential only under very special conditions, namely if (i) the Förster radius is very small and (ii) the solvent is nonviscous [35]. While these are exactly the conditions of a local equilibrium [18, 33, 35–37], these are also conditions under which an exchange mechanism is favored over FRET [47, 48]. In other words, if one intends to measure end-to-end collision rates by means of energy transfer or to apply the WF and SSS theories to intrachain energy transfer, it is recommended that a probe–quencher pair with an exchange mechanism of energy transfer be employed. Unfortunately, such donor–acceptor pairs, which should also display monoexponential decay and growth kinetics, have apparently not yet been employed in intramolecular quenching [35, 36].

REFERENCES

1. S. J. Hagen, J. Hofrichter, A. Szabo, and W. A. Eaton, Proc. Natl. Acad. Sci. USA **93**, 11615 (1996).
2. M. I. Wallace, L. Ying, S. Balasubramanian, and D. Klenerman, Proc. Natl. Acad. Sci. USA **98**, 5584 (2001).
3. L. J. Lapidus, W. A. Eaton, and J. Hofrichter, Proc. Natl. Acad. Sci. USA **97**, 7220 (2000).
4. W. G. McGimpsey, L. Chen, R. Carraway, and W. N. Samaniego, J. Phys. Chem. A **103**, 6082 (1999).
5. O. Bieri, J. Wirz, B. Hellrung, *et al.*, Proc. Natl. Acad. Sci. USA **96**, 9597 (1999).
6. R. R. Hudgins, F. Huang, G. Gramlich, and W. M. Nau, J. Am. Chem. Soc. **124**, 556 (2002).
7. N. L. Goddard, G. Bonnet, O. Krichevsky, and A. Libchaber, Phys. Rev. Lett. **85**, 2400 (2000).
8. Y. Shen, S. V. Kuznetsov, and A. Ansari, J. Phys. Chem. B **105**, 12202 (2001).
9. A. Ansari, S. V. Kuznetsov, and Y. Shen, Proc. Natl. Acad. Sci. USA **98**, 7771 (2001).
10. G. Jones II, L. N. Lu, H. Fu, *et al.*, J. Phys. Chem. B **103**, 572 (1999).
11. W. M. Nau and X. Wang, Chem. Phys. Chem. **3**, 393 (2002).
12. E. Haas, C. A. McWherter, and H. A. Scheraga, Biopolymers **27**, 1 (1988).
13. E. Haas and I. Z. Steinberg, Biophys. J. **46**, 429 (1984).
14. J. R. Lakowicz, J. Kusba, W. Wiczk, *et al.*, Biophys. Chem. **39**, 79 (1991).
15. E. Haas, E. Katchalski-Katzir, and I. Z. Steinberg, Biopolymers **17**, 11 (1978).
16. J. M. Beechem and E. Haas, Biophys. J. **55**, 1225 (1989).
17. J. R. Lakowicz, J. Kusba, I. Gryczynski, *et al.*, J. Phys. Chem. **95**, 9654 (1991).
18. J. R. Lakowicz, J. Kusba, W. Wiczk, *et al.*, Chem. Phys. Lett. **173**, 319 (1990).
19. D. R. Buckler, E. Haas, and H. Scheraga, Biochemistry **34**, 15965 (1995).
20. G. Liu, J. E. Guillet, E. T. B. Al-Takrity, *et al.*, Macromolecules **23**, 4164 (1990).
21. K. A. Zachariasse, A. L. Macanita, and W. Kühnle, J. Phys. Chem. B **103**, 9356 (1999).
22. G. Wilemski and M. Fixman, J. Chem. Phys. **60**, 866 (1974).
23. G. Wilemski and M. Fixman, J. Chem. Phys. **60**, 878 (1974).
24. A. Szabo, K. Schulten, and Z. Schulten, J. Chem. Phys. **72**, 4350 (1980).
25. M. A. Winnik, Acc. Chem. Res. **18**, 73 (1985).
26. M. Doi, Chem. Phys. **9**, 455 (1975).
27. P. E. Rouse, Jr., J. Chem. Phys. **21**, 1272 (1953).
28. B. H. Zimm, J. Chem. Phys. **24**, 269 (1956).
29. A. Y. Grosberg and A. R. Khokhlov, *Statistical Physics of Macromolecules* (Nauka, Moscow, 1989; Am. Inst. Phys., New York, 1994).
30. P. J. Flory, *Statistical Mechanics of Chain Molecules* (Wiley, New York, 1969; Mir, Moscow, 1971).
31. G. Liu and J. E. Guillet, Macromolecules **23**, 2969 (1990).
32. E. N. Bodunov, M. N. Berberan-Santos, and J. M. G. Martinho, J. Lumin. **96**, 269 (2002).
33. E. N. Bodunov, M. N. Berberan-Santos, and J. M. G. Martinho, High Energy Chem. **36**, 245 (2002).
34. R. W. Pastor, R. Zwanzig, and A. Szabo, J. Chem. Phys. **105**, 3878 (1996).
35. G. Srinivas, A. Yethiraj, and B. Bagchi, J. Chem. Phys. **114**, 9170 (2001).
36. A. V. Barzykin, K. Seki, and M. Tachiya, J. Chem. Phys. **117**, 1377 (2002).
37. T. Bandyopadhyay and S. K. Ghosh, J. Chem. Phys. **116**, 4366 (2002).
38. R. Zwanzig, Phys. Rev. **124**, 983 (1961).
39. I.-C. Yeh and G. Hummer, J. Am. Chem. Soc. **124**, 6563 (2002).
40. U. Pischel, X. Zhang, B. Hellrung, *et al.*, J. Am. Chem. Soc. **122**, 2027 (2000).
41. W. M. Nau, G. Greiner, H. Rau, *et al.*, J. Phys. Chem. A **103**, 1579 (1999).
42. F. C. Collins and G. E. Kimball, J. Colloid Sci. **4**, 425 (1949).
43. W. R. Ware and T. L. Nemzek, Chem. Phys. Lett. **23**, 557 (1973).
44. S. J. Hagen, J. Hofrichter, and W. A. Eaton, J. Phys. Chem. B **101**, 2352 (1997).
45. W. F. van Gunsteren, R. Bürgi, C. Peter, and X. Daura, Angew. Chem. Int. Ed. Engl. **40**, 352 (2001).
46. T. Förster, Ann. Phys. (Leipzig) **2**, 55 (1948).
47. J. P. MacManus, C. W. Hogue, B. J. Marsden, *et al.*, J. Biol. Chem. **265**, 10358 (1990).
48. E. Toledano, M. B. Rubin, and S. Speiser, J. Photochem. Photobiol. A **94**, 93 (1996).

Chimia 57 (2003) 161–167

ISSN 0009–4293

Exploiting Long-Lived Molecular Fluorescence

Werner M. Nau*, Fang Huang, Xiaojuan Wang, Huseyin Bakirci, Gabriela Gramlich, and Cesar Marquez
*Werner Prize Winner 2002

Abstract: Fluorophores based on the azo chromophore 2,3-diazabicyclo[2.2.2]oct-2-ene, referred to as fluorazophores, display an exceedingly long fluorescence lifetime. Besides the use in time-resolved screening assays, where the long-lived fluorescence can be time-gated, thereby improving the signal to background ratio, a distinct application of fluorazophores lies in the area of biopolymer dynamics. For this purpose, one chain end is labeled with a fluorazophore and the other one with an efficient fluorescence quencher. The fluorescence lifetime of the probe/quencher-labeled peptide then reflects the kinetics of intramolecular end-to-end collision. Applications to polypeptides are described and control experiments which establish the nature of the quenching mechanism as a diffusive process requiring intimate probe/quencher contact are described.

Keywords: Azoalkanes · Fluorescence · Kinetics · Photochemistry · Peptides

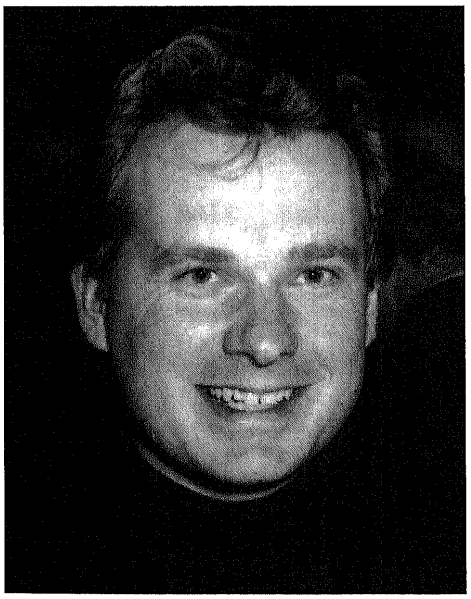

*Correspondence: Prof. Dr. W.M. Nau
School of Engineering and Science
International University Bremen
Campus Ring 1
D–28759 Bremen
Tel.: +49 421 200 3233
Fax: +49 421 200 3229
E.Mail: w.nau@iu-bremen.de
and
Department of Chemistry
University of Basel
Klingelbergstrasse 80
CH–4056 Basel

Werner Nau graduated with a M.Sc. in Chemistry 1992 from St. Francis Xavier University, Canada. His thesis was supervised by D. Klapstein and dealt with molecular spectroscopy (UV, IR, photoelectron) of acyl iso(thio)cyanates. He got his Ph.D. together with W. Adam in 1994 from the University of Würzburg on the EPR and transient absorption spectroscopy of 1,3-cyclopentanediyl diradicals. Thereafter, Werner Nau spent his postdoctoral studies with J.C. Scaiano at the University of Ottawa, where he worked on the mechanistic photochemistry of n,π*-excited states. In 1996, he joined J. Wirz at the University of Basel, where he has started up with an independent research group and became a SNF assistant professor in 2000. In the same year he finished his habilitation. Since the fall semester 2002 he has been appointed as a professor of chemistry at the newly founded International University Bremen.

His research interests lie in the general area of physical organic chemistry and focus on photochemistry, radical chemistry, supramolecular chemistry, and biomolecular chemistry, including both synthetic-preparative, mechanistic, kinetic, and spectroscopic aspects. He has recently introduced a novel class of fluorescent probes, referred to as fluorazophores, which are based on the azo chromophore of 2,3-diazabicyclo[2.2.2]oct-2-ene. Fluorazophores are applied as sensors for antioxidants, versatile guest molecules in supramolecular chemistry, kinetic probes for biopolymer folding, and fluorophores for time-resolved screening assays.

Werner Nau has held numerous fellowships, among others a Kekulé and Liebig fellowship of the Fonds of the Chemical Industry, a NATO fellowship, a NSERC International fellowship, and a SNF Profil fellowship. His work has led to the award of several prizes, including the 1999 International Grammaticakis-Neumann prize for photochemistry, awarded by the Swiss Group for Photochemistry and Photobiology, and the 2000 ADUC-Prize, awarded for his habilitation thesis.

Fluorescent probes and sensors are well-established tools in analytical and biological chemistry, spanning such diverse applications as calcium ion detection, cell staining, and polarity sensing [1]. An interesting sub-class of fluorescent probes comprises chromophores with a particularly long fluorescence lifetime, *e.g.* more than 50 ns [2]. Perhaps the simplest yet very important application based on long-lived fluorescence (or generally luminescence) relies on the reliable differentiation of long fluorescence lifetimes from any shorter-lived luminescence components. This is of interest, in particular, for screening assays where fluorescent probes are employed to signal molecular events such as the inhibition of an enzyme by a library of potential drugs. Short-lived emission is ubiquitous and may stem from other additives, sample impurities, biological components, scattered light, the solvent, or sample container materials of cuvettes and microplates.

The shorter-lived components can be eliminated from detection through a time-gate, such that the emission from the long-lived fluorescent label (which serves as the signaling unit) can be selectively detected. This reduces the background during the measurement dramatically. An instructive example is depicted in Fig. 1, which compares the fluorescence decay of a long-lived fluorescent probe (τ = 500 ns) with that of a shorter-lived fluorescing component (τ = 10 ns), with the latter one, however, being much more intense (10^6 times larger preexponential factor). If as usual the integrated fluorescence intensity would be compared through steady-state methods, a 'signal-to-background' of 0.00005:1 would result, which would prevent any useful information to be obtained. If one carries out the experiment in lifetime mode with a time-gate between 200–1000 ns and integrates the areas under the curves, the 'signal-to-background' ratio becomes better than 10000:1, an impressive improvement by more than eight orders of magnitude, which has its underlying reason in the exponential decay kinetics of the fluorescence. This improvement renders the selective detection of long-lived fluorophores in so-called 'time-resolved' screening assays generally an entirely instrumental problem. In particular, the real background may be dominated by detector noise rather than contributions from short-lived emission.

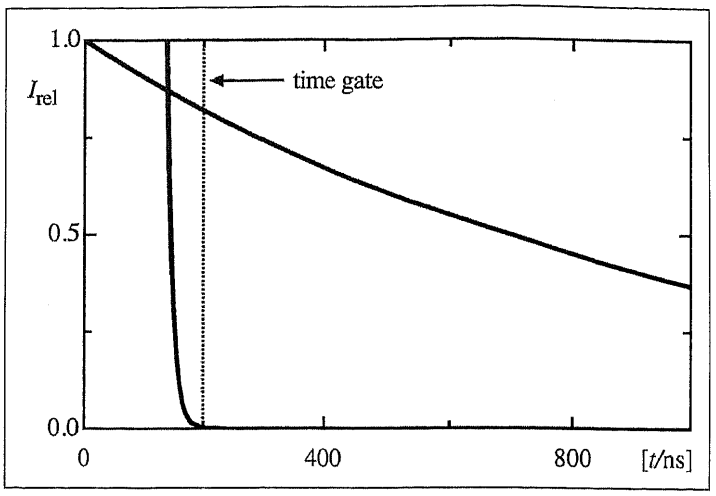

Fig. 1. Comparison of the fluorescence decay of a long-lived fluorescent probe (τ = 500 ns) with that of a shorter-lived component (τ = 10 ns); the shorter-lived component is 10^6 times more intense (relative preexponential factors). A suitable time gate for use in a time-resolved assay is shown at 200 ns.

Relatively few organic molecules display lifetimes in this long time regime, with azoalkanes derived from 2,3-diazabicyclo[2.2.2]oct-2-ene (DBO) displaying the longest fluorescence lifetime in solution [3]. The record for the longest fluorescence lifetime of an organic chromophore in solution lies currently at 1.03 µs (in aerated H_2O!) [4] and is held by the supramolecular complex (CB7•DBO) between the parent azoalkane and cucurbit[7]uril (CB7), a barrel-like organic host molecule [5]. Over the past six years, we have investigated this interesting chromophore in great detail and have prepared several DBO derivatives, which we refer to as fluorazophores ('fluorescent azo chromophores'). Some of the investigated derivatives are shown in Scheme 1.

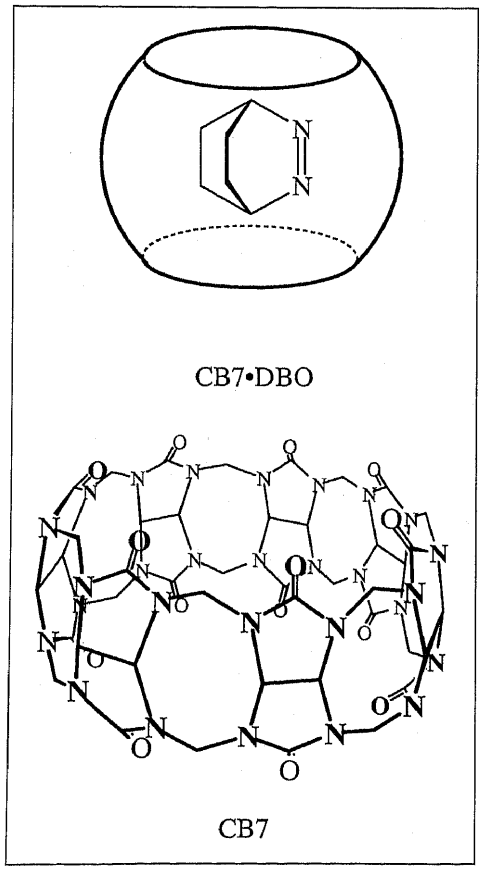

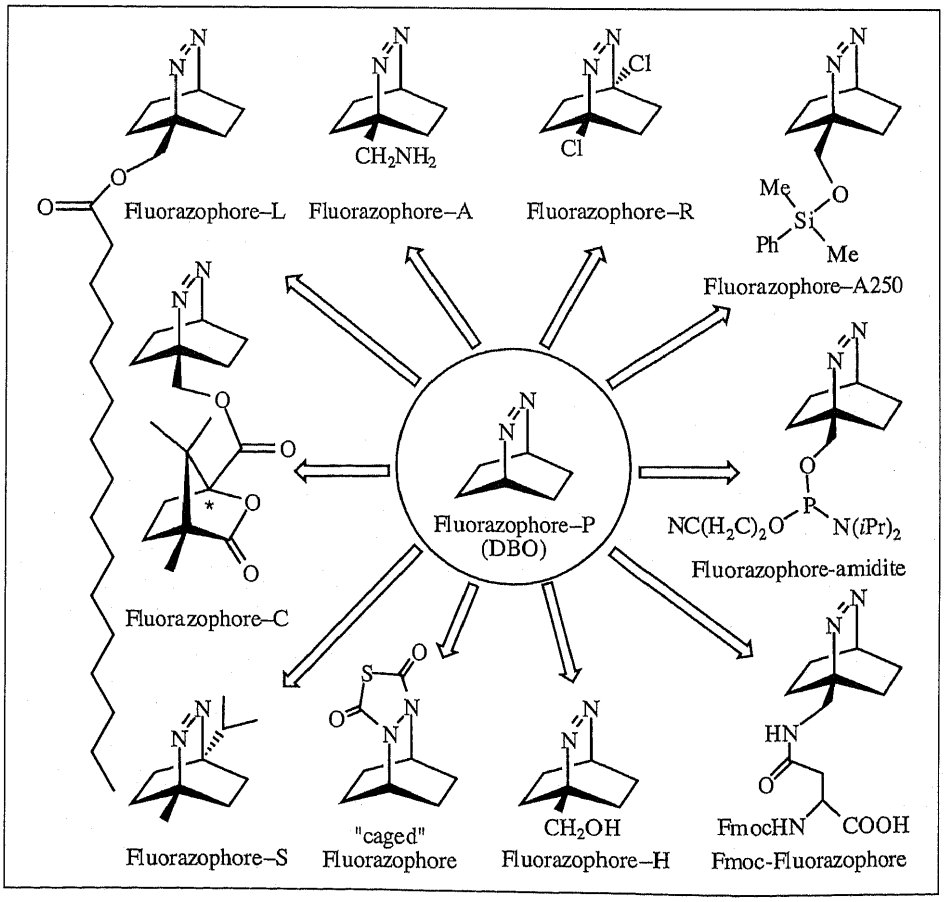

Scheme 1

A representative synthetic sequence to obtain Fmoc-Fluorazophore is shown in Scheme 2, which has been scaled up to afford typically 3 g of Fmoc-DBO in an overall yield of 10%, sufficient for the commercial synthesis of up to 30 polypeptides (10 mg scale).

The intriguing photophysics of fluorazophores has been worked out in great detail [6–11] and the fascinating quenching pathways have been investigated through a combination of experimental and theoretical methods [12–14]. On the more applied side, fluorazophores have proven to be useful as sensors for antioxidant activity, both in solution [15][16] as well as in membrane-mimetic systems [17], as probes for measuring the kinetics of association with supramolecular systems [18][19], as tools to investigate the geometries of cyclodextrin inclusion complexes by means of circular dichroism [20][21], and as probes for the polarizability inside molecular container molecules [22].

Most recently, we have employed fluorazophores to measure the kinetics of end-to-end collision in biopolymers (k_{coll} in Scheme 3), including peptides [23][24], and oligonucleotides [25]. For this purpose, the fluorazophore (P) is attached to one end of the biopolymer and an efficient (nearly diffusion-controlled) fluorescence quencher (Q) is attached to the other side; in peptides this quencher moiety is usually tryptophane and in oligonucleotides guanine. The kinetics of fluorescence quenching can then be equated to the rate of end-to-end collision, which has proven difficult to obtain accurately by alternative techniques.

Keeping in mind that alternative methods have other advantages [26][27], the fluorazophore approach presents, arguably, the most sensitive and most accurate tool for measuring end-to-end contact in biopolymers known to date. Note that this application is made possible by the exceedingly long fluorescence lifetime, which allows the fluorazophore to 'wait' sufficiently long until it is being approached (and immediately quenched) by the other end; this diffusive approach of the chain ends takes 10 ns to 1 μs in aqueous solution. The lifetime of fluorazophores (*ca.* 505 ns in D_2O under air) is therefore ideally suited for investigations in this time regime.

Being able to measure the absolute rates for the motions within biopolymers or at least knowing the time scale for these processes is of fundamental importance for understanding the mechanism of protein folding [28], for predicting the kinetics of intramolecular reactions in biopolymers (formation of hydrogen bonds, cystine bridges, proton transfer, electron transfer)

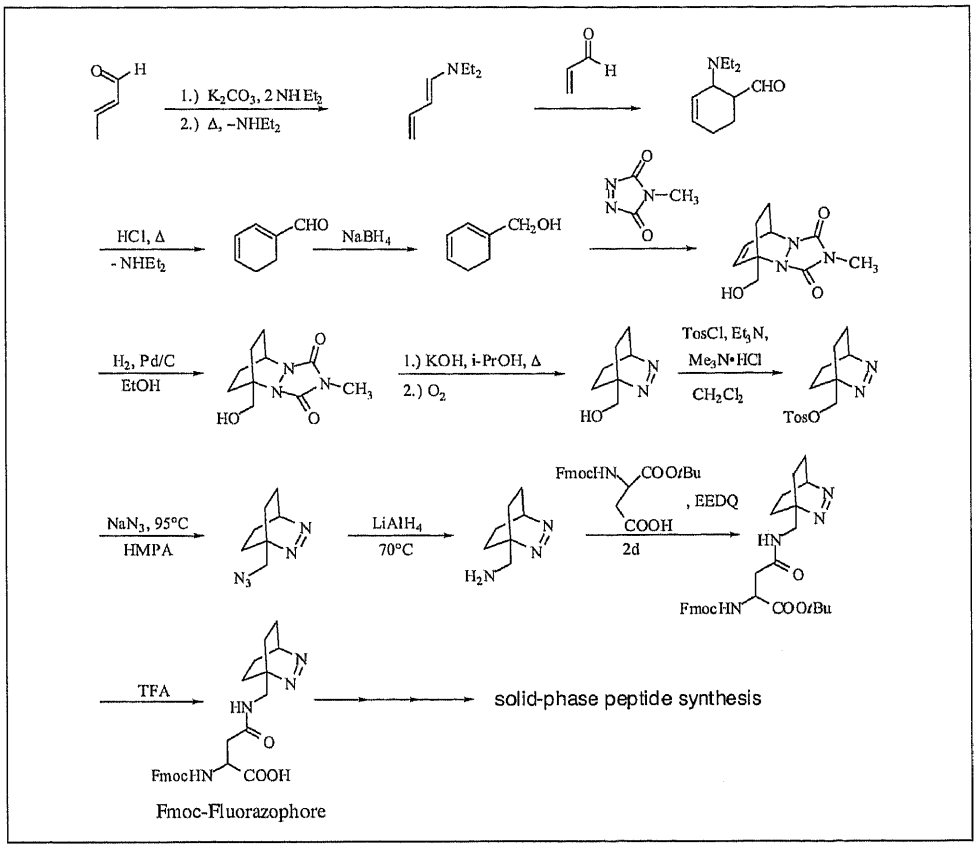

Scheme 2

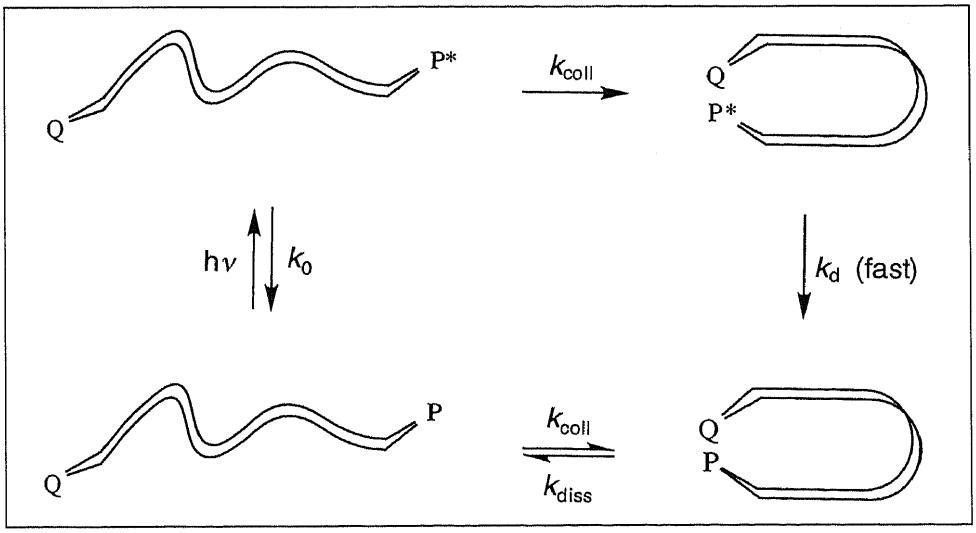

Scheme 3

[29], and for understanding protein domain motions [30]. The size of biopolymers and the effects of solvation, including salt effects, still present a major challenge to computational chemistry, which demands experimental data. The latter, in turn, may provide invaluable benchmark values for the calibration of theoretical models [31].

A simple problem already arises if one attempts to predict the time scale of diffusion-controlled end-to-end collision in (bio)polymers from the available rates for diffusion-controlled intermolecular reactions. To allow a comparison, it is useful to compare the probability for intramolecular and intermolecular encounter complex formation between two fragments.

Consider Scheme 4a, the intermolecular case. We assume an ideal solution with no enthalpic interactions between the probe (P) and the quencher (Q) molecules. The concentration of the encounter complex, C_{PQ}, can be obtained according to Eqn. (1) with V_e being the volume of the encounter complex with radius a (spherical approximation). C_P^0 and C_Q^0 are the total concentrations of P and Q. The 'equilibrium constant' for encounter complex formation is then given by Eqn. (2), assuming that the concentration of molecules in contact is

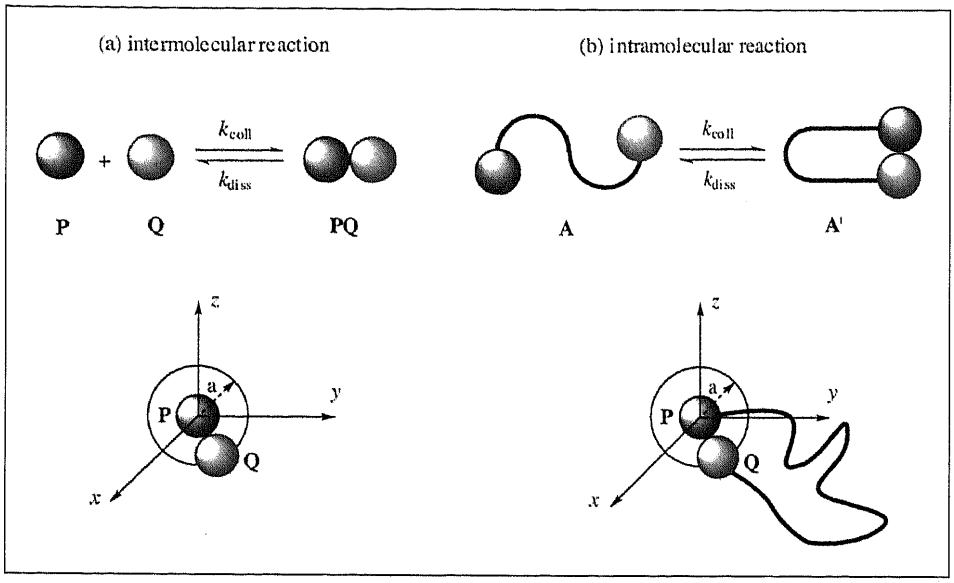

Scheme 4

small (dilute solution, *i.e.* $C_P \approx C_P{}^0$ and $C_Q \approx C_Q{}^0$). It follows that the equilibrium constant for encounter complex formation (in units of m^3mol^{-1}) equals the volume of the encounter complex multiplied with the Avogadro constant (N_a). This in turn corresponds, due to the absence of enthalpic effects, to the loss of entropy associated with the formation of the encounter complex, *i.e.* $\Delta_{coll}S^0 = R\ln(1000K_{inter}C^0)$, where the factors 1000 and C^0, the standard concentration in M, are added to give a dimensionless equilibrium constant.

$$C_{PQ} = C_P{}^0 N_a V_e C_Q{}^0 = C_P{}^0 C_Q{}^0 N_a \frac{4}{3}\pi a^3 \quad (1)$$

$$K_{inter} = \frac{C_{PQ}}{C_P C_Q} \approx \frac{C_{PQ}}{C_P{}^0 C_Q{}^0} = \frac{4}{3}\pi a^3 N_a \quad (2)$$

The intramolecular case, Scheme 4b, describes the pertinent situation for encounter complex formation within a biopolymer chain labeled with a probe (P) and a quencher (Q) at opposite ends. For simplicity, we assume that the chain does not introduce additional interactions between probe and quencher except to restrict the distance by which they can diffuse apart (ideal chain, Gaussian chain). Like for the intermolecular case, we assume no enthalpic interactions between the probe and the quencher residues. The fraction of chains with the two ends in contact, ($C_{A'}$), can be obtained in this case from the distribution function (g) in Eqn. (3), which has analytical solutions for a very long chain ($N >> 1$, with N the number of chain segments) and for the shortest chain ($N = 2$). r is taken as the distance between the chain ends and b equals the length of an individual chain segment. The 'equilibrium constant' for end-to-end encounters is then given by Eqn. (4), which assumes for the case of a very long chain ($N >> 1$) that the concentration of molecules in contact is small ($C_A \approx C_A + C_{A'}$). Again, this relates directly to the loss of entropy associated with the formation of an end-to-end encounter complex within an ideal chain, *i.e.* $\Delta_{coll}S^0 = R\ln K_{intra}$.

$$g(r) = \left(\frac{3}{2\pi\langle r^2\rangle}\right)^{3/2} \exp\left(-\frac{3r^2}{2\langle r^2\rangle}\right) \text{ with } \langle r^2\rangle = Nb^2 \text{ for } N >> 1$$
$$g(r) = \frac{1}{8\pi r b^2} \text{ for } N = 2 \quad (3)$$

$$K_{intra} = \frac{C_{A'}}{C_A} \approx \frac{C_{A'}}{C_A + C_{A'}} = \int_0^a g(r)4\pi r^2 dr \approx \frac{4}{3}\pi a^3 \left(\frac{3}{2\pi\langle r^2\rangle}\right)^{3/2} = \frac{4}{3}\pi a^3 \left(\frac{3}{2\pi N b^2}\right)^{3/2} \text{ for } N >> 1$$
$$K_{intra} = \frac{C_{A'}}{C_A} = \frac{\int_0^a g(r)4\pi r^2 dr}{1 - \int_0^a g(r)4\pi r^2 dr} = \frac{(a/b)^2}{4 - (a/b)^2} \text{ for } N = 2 \quad (4)$$

The kinetics of end-to-end contact formation for the intramolecular reaction can be related to that of the intermolecular reaction (Eqn. (5)) if one reduces the equilibrium constants to ratios of microscopic rate constants and considers further that the elementary rate of dissociation of the encounter complex must be identical for both species within the approximations made ($k_{diss}^{intra} = k_{diss}^{inter}$). Recall, in particular that the only function of the chain for the intramolecular case is to limit the distance between probe and quencher.

$$\frac{K_{intra}}{K_{inter}} = \frac{k_{coll}^{intra}/k_{diss}^{intra}}{k_{coll}^{inter}/k_{diss}^{inter}} = \frac{k_{coll}^{intra}}{k_{coll}^{inter}} \quad (5)$$

Use of the respective expressions for the equilibrium constants for intermolecular and intramolecular encounter complex formation then affords Eqn. (6). If one further expresses the intermolecular collision rate constant through the relationship between the intermolecular diffusion rate constant and the diffusion coefficient ($k_{coll}^{inter} = 4D\pi a N_a$), one obtains Eqn. (7), with D being the mutual intermolecular diffusion coefficient.

Eqn. (7) provides the ideal relationship between the unknown rate constant for intramolecular end-to-end collision and the known (diffusion-controlled) rate constant for an intermolecular probe-quencher pair. Accordingly, the rate of end-to-end collision in a biopolymer increases linearly with the diffusion coefficient and size of the encounter complex (radius a), it depends inversely on the cubed chain segment length (b), and it decreases with increasing chain length (N) with the characteristic exponent of –3/2. Eqn. (7) has been derived in a different context by Szabo, Schulten, and Schulten through an analysis of the first passage time of end-attached groups based on a modified Smoluchowski equation [32][33].

$$\frac{k_{coll}^{intra}}{k_{coll}^{inter}} = \frac{\frac{4}{3}\pi a^3 \left(\frac{3}{2\pi N b^2}\right)^{3/2}}{\frac{4}{3}\pi a^3 N_a} = \frac{1}{N_a}\left(\frac{3}{2\pi N b^2}\right)^{3/2} \text{ for } N >> 1 \quad (6)$$

$$k_{coll}^{intra} = k_{coll}^{inter} \frac{1}{N_a b^3}\left(\frac{3}{2\pi}\right)^{3/2} N^{-3/2} = \frac{4D\pi a N_a}{N_a b^3}\left(\frac{3}{2\pi}\right)^{3/2} N^{-3/2} = \sqrt{\frac{54}{\pi}}\frac{Da}{b^3} N^{-3/2} \text{ for } N >> 1 \quad (7)$$

To apply Eqn. (7), one may use commonly accepted intermolecular diffusion coefficients of 10^{-5} cm^2s^{-1} in water (the mutual diffusion coefficient in Eqn. (7) corresponds to twice this value), a van-der-Waals reaction radius of 5 Å, and a chain segment length of 5 Å (typical for one peptide unit). The resulting estimates for the intramolecular collision times ($1/k_{coll}$) are 0.2 ns for $N = 4$ and 2.7 ns for $N = 20$. This means that end-to-end contact formation in biopolymers in solution may occur as fast as several ns according to the simplest theoretical framework. These theoretical rates can now be compared with the experimental results obtained from the fluorazophore probe/quencher technique in synthetic polypeptides.

Our initial experimental study focused on the length dependence of the end-to-end collision rates in peptides with the general structure Trp-(Gly-Ser)$_n$-DBO-NH_2 (structure below); these peptides are water soluble and presumed to be 'structureless' according to a previous study [26]. This is an important requirement to apply theories based on Gaussian chain behavior [34][35].

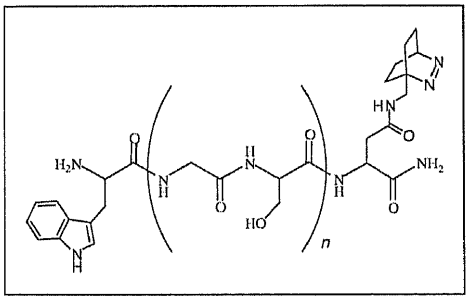

The fluorescence decays of all peptides as recorded with the time-correlated single photon counting technique were strictly monoexponential (Fig. 2). The resulting fluorescence lifetimes (τ) for the peptides with different length are listed in the Table and range from 10–75 ns. Subject to the assumption of diffusion-controlled quenching, the collision rates can be directly obtained through a correction for the inherent fluorescence lifetime (τ_0) according to Eqn. (8). The data for the collision rate constants demonstrate that end-to-end contact formation in short polypeptides may occur as fast as 10 ns in water, significantly faster than previous estimates of rates for peptides with the same length, but also substantially smaller than expected from the ideal-chain behavior according to Eqn. (7) (see above). Presumably, the diffusion coefficients of the peptide chain ends are much smaller than those of the free probe and quencher; the use of smaller diffusion coefficients in Eqn. (7) than the intermolecular ones would bring the theoretical data much closer to the experimental ones [36].

$$k_{coll} = 1/\tau - 1/\tau_0 \qquad (8)$$

Table. Fluorescence lifetimes and end-to-end collision rate constants for Trp–(Gly–Ser)$_n$–DBO–NH_2 polypeptides

n	N[a]	τ / ns[b]	k_{coll} / 10^7 s^{-1}[c]
0	2	23.3	4.1
1	4	14.3	6.8
2	6	19.5	4.9
4	10	30.5	3.1
6	14	45.6	2.0
10	22	74.4	1.1

[a]Number of peptide units between probe and quencher. [b]Fluorescence lifetime in aerated D_2O at 23 °C measured by time-correlated single photon counting. [c]Obtained from Eqn. 8 with τ_0 = 500 ns.

The dependence of the collision rates on the chain length as derived in Eqn. (7) predicts a linear increase of the logarithmic collision rates with the logarithm of the number of chain segments (N). The corresponding plot (Fig. 3) for the experimental data shows that this linear relationship is not observed. Instead, one obtains a plot with a strong negative curvature. Moreover, the theoretical slope [34][35] of –3/2 is only reached for the longer chains. These variances indicate deviations from the ideal behavior, which are presumably related to effects of chain stiffness, which impose an increased internal friction for end-to-end collision in the short chains [36].

The interpretation of the fluorescence lifetimes in terms of end-to-end collision rate constants requires a collision-induced fluorescence quenching, *i.e.* probe and quencher must come into van-der-Waals contact (2–3 Å distance) for quenching to occur. This is naturally fulfilled for quenching by hydrogen atom transfer or exciplex-induced quenching, which are the two prototypal quenching mechanisms of the DBO chromophore [3][6][8][13][14][37–39]. However, quenching by electron transfer, which presents an alternative quenching mechanism, could operate through bond (superexchange mechanism); it could also occur over a considerable distance through space or through the solvent (up to 5–8 Å) and must therefore be excluded [40]. The same applies for Dexter-type triplet energy transfer, which has been employed in other intramolecular probe/quencher pairs to assess end-to-end contact formation [26][41][42]. Quenching over larger distances than van-der-Waals contact would result in a continuum of distance-dependent rate constants, which could not be analyzed in terms of a diffusion-controlled collision

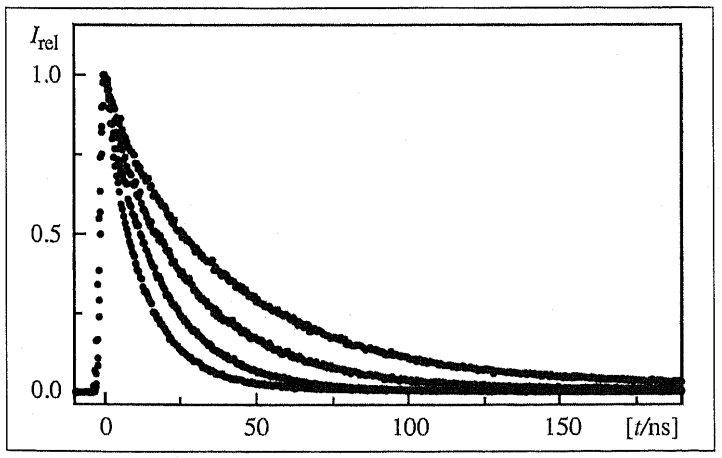

Fig. 2. Fluorescence decays (time-correlated single photon counting, normalized intensity) of Trp–(Gly–Ser)$_n$–DBO–NH_2 polypeptides (n = 1, 2, 4, and 6). The lowest trace corresponds to n = 1, the uppermost one to n = 6.

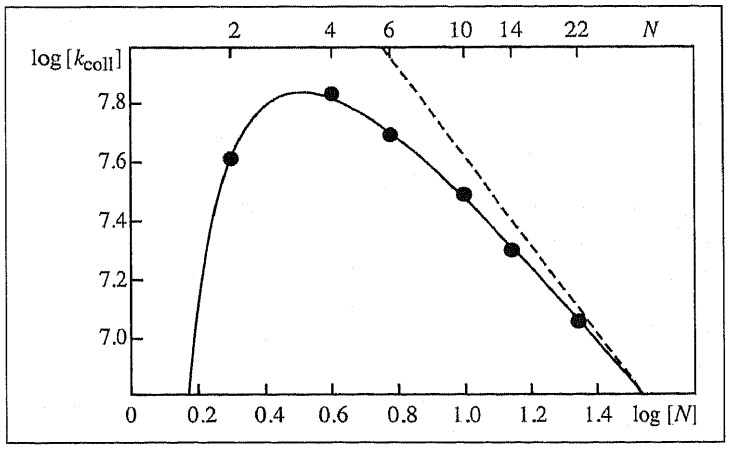

Fig. 3. Double-logarithmic plot of the end-to-end collision rate constants (k_{coll}) of Trp–(Gly–Ser)$_n$–DBO–NH_2 polypeptides *versus* the peptide length, taken as the number of intervening peptide units (N). The dashed line has a slope of –3/2 and is shown to illustrate the deviation from the theoretical behavior (Eqn. 7).

process. In this case, quenching presents no longer an elementary reaction to which a single rate constant can be assigned. In fact, fluorescence resonance energy transfer, which operates over even larger distances, has proven inapplicable to obtain the pertinent elementary rate constants [26][43].

In view of the possible complications due to distance-dependent quenching rates, it appeared compulsory to establish experimentally that quenching through bond or through the solvent do in fact not apply for the DBO/Trp probe/quencher pair. We have therefore performed a series of carefully designed control experiments (Schemes 5–7). Control experiments of this type are strongly recommended to establish alternative methods for assessing end-to-end contact formation, in particular if triplet energy transfer or electron transfer (both of which are candidates for distance-dependent quenching rates) are the postulated quenching mechanisms.

In the first experiment (Scheme 5), we have compared the fluorescence lifetime of the shortest peptide, in which probe and quencher are directly attached, with the longer ones. The lifetime of the shortest peptide is in fact longer than for the next longer one (Table), which speaks strongly against a through-bond quenching mechanism, but can be understood in terms of internal friction (steric hindrance effects) [36]. We encounter this effect in daily life: It is more difficult to make a knot in a very short rope than in a longer one.

In the second experiment (Scheme 6), we have exchanged the presumably flexible amino acids glycine and serine in the backbone of the peptide by rigid cyclic proline spacers. The proline peptide has a much longer lifetime than the glycine-serine one, close to the lifetime in the absence of quencher (505 ns in D_2O). This suggests that quenching through bond is unlikely since the number of bonds remains identical in both species. The effect of rigidifying the backbone provides also strong evidence that it is the diffusion between the chain ends which is decisive for the quenching process. Incidentally, it should also be mentioned that any increase in the solvent viscosity, as it can be achieved, for example, through the addition of denaturants like urea (5 M) or guanidinium chloride (6 M) also decreases the end-to-end collision rates of flexible DBO/Trp polypeptides, consistent with a diffusive process.

In the third experiment (Scheme 7), we have left the peptide backbone unchanged, but have added cucurbit[7]uril (CB7) to the aqueous solution of the peptide. As demonstrated by NMR experiments, CB7 complexes selectively and quantitatively the

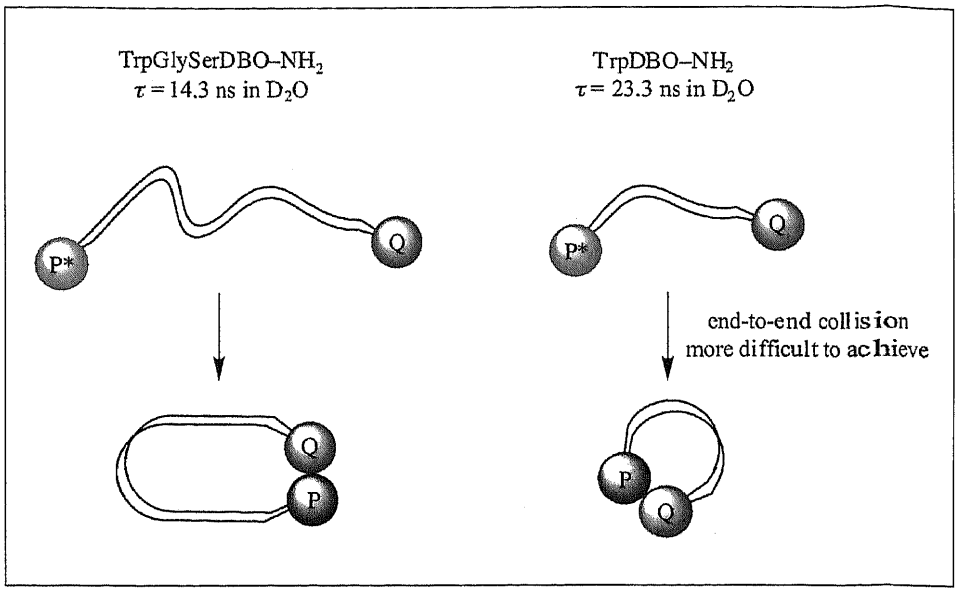

Scheme 5

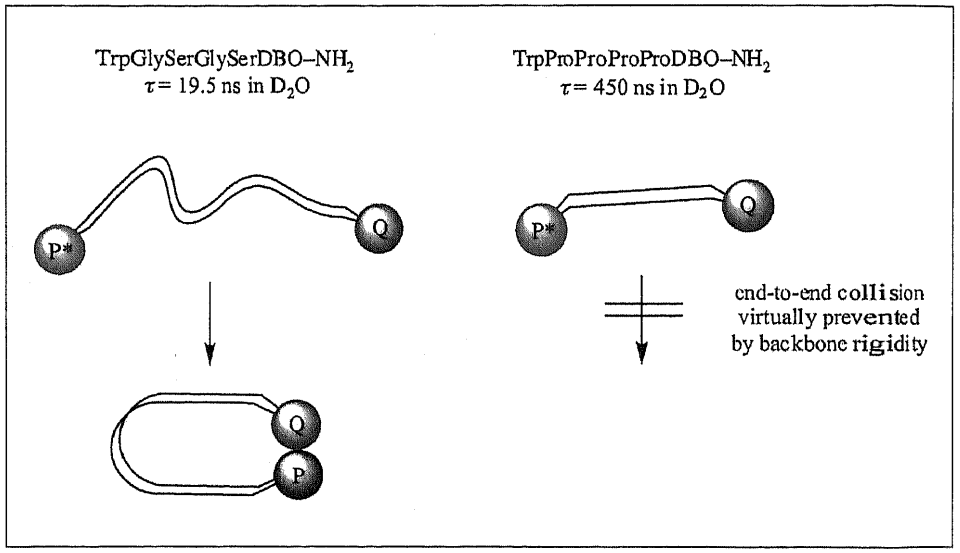

Scheme 6

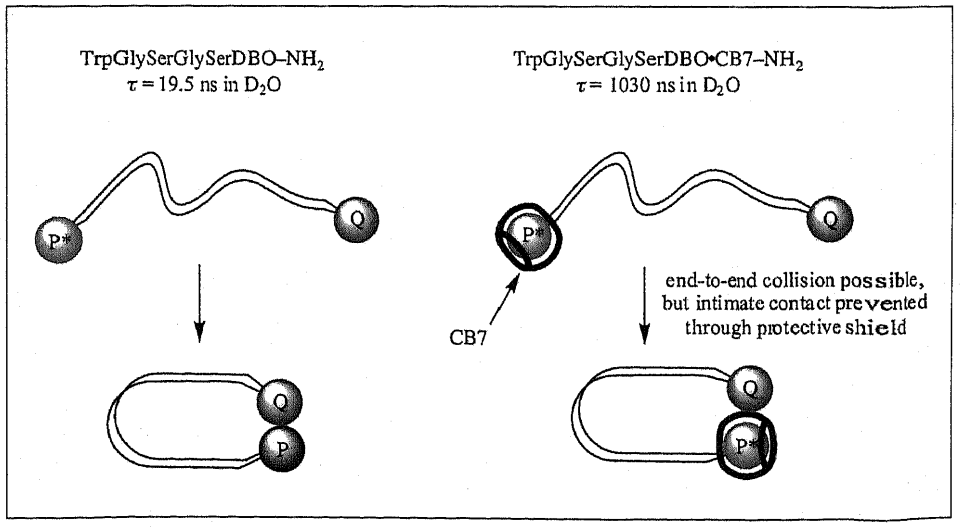

Scheme 7

DBO chromophore ($K = 4 \times 10^5\ M^{-1}$) and thereby provides a 'protective shield' around the chromophore.[22] This shield prevents van-der-Waals contact with the quencher, which is still free to diffuse since solvent and peptide backbone have remained unchanged. The resulting lifetime of the complexed peptide was found to be 1.03 µs, suggesting that the quencher is not able to quench the excited probe at all (the longer lifetime than in D_2O results from the exclusion of oxygen and the solvent from the cavity). This result provides strong evidence for the view that quenching requires intimate contact. If quenching would occur through space or through the solvent it should have also been mediated through the supramolecular wall.

It follows from the control experiment in Scheme 6, that the fluorescence lifetimes of DBO/Trp end-labeled peptides are a quantitative measure of the flexibility or rigidity of the peptide backbone. We have therefore most recently synthesized a series of random-coil peptides, in which Trp and DBO are separated by a sequence of identical amino acids (see structure below) [24]. Each peptide has a characteristic fluorescence lifetime, which can be interpreted in terms of the conformational flexibility, which a particular amino acid imposes on the backbone. This allows one to define *a conformational flexibility scale for amino acids in peptides*. The following order of flexibility applies, where glycine gives rise to the most flexible peptide and proline produces the most rigid one:

Gly > Ser > Asp, Asn, Ala > Thr, Leu > Phe, Glu, Gln > His, Arg > Lys > Val > Ile > Pro

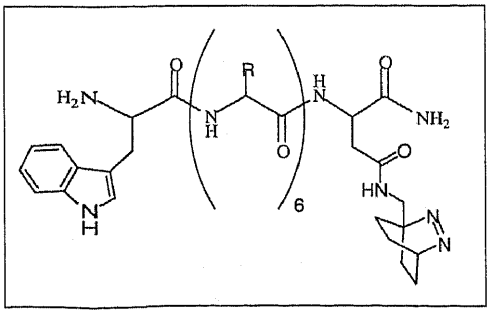

In summary, the intramolecular fluorescence quenching of fluorazophores provides a distinct tool for investigations in the area of biopolymer dynamics. Future studies will involve oligonucleotides, larger, structured peptides, mutation effects, the determination of activation energies, and the transfer of the kinetic results to applications in high-throughput screening technology, where the long fluorescence lifetime provides the additional advantage of suppressing background fluorescence through time-resolved detection (see Fig. 1).

Acknowledgements

This work was generously supported through the Swiss National Science Foundation (grant No. 620–58000). The studies were also performed within the Swiss National Research Program "Supramolecular Functional Materials" NFP 47 (grant No. 4047–057552).

Received: February 25, 2003

[1] B. Valeur, 'Molecular Fluorescence', Wiley-VCH, Weinheim, **2002**.
[2] W.M. Nau, X. Wang, *ChemPhysChem* **2002**, *3*, 393–398.
[3] W.M. Nau, *EPA Newsl.* **2000**, *70*, 6–29.
[4] C. Marquez, W.M. Nau. Unpublished result.
[5] a) W.L. Mock, in 'Comprehensive Supramolecular Chemistry', vol. 2, Ed.: F. Vögtle, Elsevier, Oxford, **1996**, pp. 477–493; b) J. Kim, I.S. Jung, S.Y. Kim, E. Lee, J.K. Kang, S. Sakamoto, K. Yamaguchi, K. Kim, *J. Am. Chem. Soc.* **2000**, *122*, 540–541.
[6] U. Pischel, X. Zhang, B. Hellrung, E. Haselbach, P.-A. Muller, W.M. Nau, *J. Am. Chem. Soc.* **2000**, *122*, 2027–2034.
[7] U. Pischel, W.M. Nau, *J. Phys. Org. Chem.* **2000**, *13*, 640–647.
[8] U. Pischel, X. Allonas, W.M. Nau, *J. Inf. Recording* **2000**, *25*, 311–321.
[9] U. Pischel, W.M. Nau, *J. Am. Chem. Soc.* **2001**, *123*, 9727–9737.
[10] U. Pischel, W.M. Nau, *Photochem. Photobiol. Sci.* **2002**, *1*, 141–147.
[11] D. Klapstein, U. Pischel, W.M. Nau, *J. Am. Chem. Soc.* **2002**, *124*, 11349–11357.
[12] W.M. Nau, G. Greiner, J. Wall, H. Rau, M. Olivucci, M.A. Robb, *Angew. Chem. Int. Ed.* **1998**, *37*, 98–101.
[13] A. Sinicropi, U. Pischel, R. Basosi, W.M. Nau, M. Olivucci, *Angew. Chem. Int. Ed.* **2000**, *39*, 4582–4586.
[14] A. Sinicropi, R. Pogni, R. Basosi, M.A. Robb, G. Gramlich, W.M. Nau, M. Olivucci, *Angew. Chem. Int. Ed.* **2001**, *40*, 4185–4189.
[15] W.M. Nau, *J. Am. Chem. Soc.* **1998**, *120*, 12614–12618.
[16] X. Zhang, C. Erb, J. Flammer, W.M. Nau, *Photochem. Photobiol.* **2000**, *71*, 524–533.
[17] G. Gramlich, J. Zhang, W.M. Nau, *J. Am. Chem. Soc.* **2002**, *124*, 11252–11253.
[18] W.M. Nau, X. Zhang, *J. Am. Chem. Soc.* **1999**, *121*, 8022–8032.
[19] X. Zhang, G. Gramlich, X. Wang, W.M. Nau, *J. Am. Chem. Soc.* **2002**, *124*, 254–263.
[20] X. Zhang, W.M. Nau, *Angew. Chem. Int. Ed.* **2000**, *39*, 544–547.
[21] B. Mayer, X. Zhang, W.M. Nau, G. Marconi, *J. Am. Chem. Soc.* **2001**, *123*, 5240–5248.
[22] C. Marquez, W.M. Nau, *Angew. Chem. Int. Ed.* **2001**, *40*, 4387–4390.
[23] R.R. Hudgins, F. Huang, G. Gramlich, W.M. Nau, *J. Am. Chem. Soc.* **2002**, *124*, 556–564.
[24] F. Huang, W.M. Nau, *Angew. Chem. Int. Ed.* **2003**, *42*, in press.
[25] X. Wang, W.M. Nau. Unpublished results.
[26] O. Bieri, J. Wirz, B. Hellrung, M. Schutkowski, M. Drewello, T. Kiefhaber, *Proc. Natl. Acad. Sci. USA* **1999**, *96*, 9597–9601.
[27] L.J. Lapidus, W.A. Eaton, J. Hofrichter, *Proc. Natl. Acad. Sci. USA* **2000**, *97*, 7220–7225.
[28] A.R. Fersht, *Curr. Opin. Struct. Biol.* **1997**, *7*, 3–9.
[29] D. Pogocki, E. Ghezzo-Schöneich, C. Schöneich, *J. Phys. Chem. B* **2001**, *105*, 1250–1259.
[30] S. Hayward, *Proteins* **1999**, *36*, 425–435.
[31] I.-C. Yeh, G. Hummer, *J. Am. Chem. Soc.* **2002**, *124*, 6563–6568.
[32] A. Szabo, K. Schulten, Z. Schulten, *J. Chem. Phys.* **1980**, *72*, 4350–4357.
[33] R.W. Pastor, R. Zwanzig, A. Szabo, *J. Chem. Phys.* **1996**, *105*, 3878–3882.
[34] U.W. Suter, M. Mutter, P.J. Flory, *J. Am. Chem. Soc.* **1976**, *98*, 5740–5745.
[35] M. Mutter, U.W. Suter, P.J. Flory, *J. Am. Chem. Soc.* **1976**, *98*, 5745–5748.
[36] X. Wang, E.N. Bodunov, W.M. Nau, submitted for publication.
[37] W.M. Nau, U. Pischel, *Angew. Chem. Int. Ed.* **1999**, *38*, 2885–2888.
[38] W.M. Nau, G. Greiner, H. Rau, M. Olivucci, M.A. Robb, *Ber. Bunsen-Ges. Phys. Chem.* **1998**, *102*, 486–492.
[39] W.M. Nau, G. Greiner, H. Rau, J. Wall, M. Olivucci, J.C. Scaiano, *J. Phys. Chem. A* **1999**, *103*, 1579–1584.
[40] A.K. Mishra, R. Chandrasekar, M. Faraggi, M.H. Klapper, *J. Am. Chem. Soc.* **1994**, *116*, 1414–1422.
[41] W.G. McGimpsey, L. Chen, R. Carraway, W.N. Samaniego, *J. Phys. Chem. A* **1999**, *103*, 6082–6090.
[42] P.J. Wagner, P. Klán, *J. Am. Chem. Soc.* **1998**, *121*, 9626–9635.
[43] E. Haas, E. Katchalski-Katzir, I.Z. Steinberg, *Biopolymers* **1978**, *17*, 11–31.

J|A|C|S
ARTICLES
Published on Web 12/30/2003

Kinetics of End-to-End Collision in Short Single-Stranded Nucleic Acids

Xiaojuan Wang[†] and Werner M. Nau*[,†,‡]

Contribution from the Departement Chemie, Universität Basel, Klingelbergstrasse 80, CH-4056 Basel, Switzerland, and the School of Engineering and Science, International University Bremen, Campus Ring 1, D-28759 Bremen, Germany

Received September 1, 2003; E-mail: w.nau@iu-bremen.de.

Abstract: A novel fluorescence-based method, which entails contact quenching of the long-lived fluorescent state of 2,3-diazabicyclo[2.2.2]-oct-2-ene (DBO), was employed to measure the kinetics of end-to-end collision in short single-stranded oligodeoxyribonucleotides of the type 5′-DBO−$(X)_n$-dG with X = dA, dC, dT, or dU and $n = 2$ or 4. The fluorophore was covalently attached to the 5′ end and dG was introduced as an efficient intrinsic quencher at the 3′ terminus. The end-to-end collision rates, which can be directly related to the efficiency of intramolecular fluorescence quenching, ranged from 0.1 to 9.0 × 10^6 s^{-1}. They were strongly dependent on the strand length, the base sequence, as well as the temperature. Oligonucleotides containing dA in the backbone displayed much slower collision rates and significantly higher positive activation energies than strands composed of pyrimidine bases, suggesting a higher intrinsic rigidity of oligoadenylate. Comparison of the measured collision rates in short single-stranded oligodeoxyribonucleotides with the previously reported kinetics of hairpin formation indicates that the intramolecular collision is significantly faster than the nucleation step of hairpin closing. This is consistent with the configurational diffusion model suggested by Ansari et al. (Ansari, A.; Kuznetsov, S. V.; Shen, Y. *Proc. Natl. Acad. Sci. USA* **2001**, *98*, 7771−7776), in which the formation of misfolded loops is thought to slow hairpin formation.

Introduction

Recent work on nucleic acid dynamics has focused on the formation of single-stranded DNA (ssDNA) hairpins,[1−8] which are believed to play a key role in many biological functions, including gene expression and regulation,[9−11] DNA transcription,[12,13] as well as DNA transposition.[14] Hairpin formation includes not only the collision of the two arms but also the fast zipping of the stem part. To describe the hairpin-to-coil transition, a two-state model of an all-or-none transition between open and closed states was introduced by Libchaber and coworkers.[1,2] However, the kinetics of hairpin formation displayed a non-Arrhenius temperature dependence in some cases which points to a more complex mechanism.[5,6] Ansari and coworkers[6,7] suggested a configurational diffusion model, in which the ssDNA can be transiently trapped in misfolded states prior to the nucleation step. The test of this model requires experimental end-to-end collision rates in ssDNA, which we are now providing for the first time. To allow a direct comparison, we have studied ssDNA fragments which correspond in their size to the loop segments of the previously studied entire hairpins.

We employed a novel method which uses 2,3-diazabicyclo-[2.2.2]-oct-2-ene (DBO) as a fluorescent probe. The extremely long fluorescence lifetime of DBO (325 ns in aerated water and 420 ns in deaerated water) and its quenching mechanism, which requires a close probe-quencher contact, offer the possibility to monitor intramolecular collisions in the submicrosecond scale which has proven difficult to realize by alternative techniques. A phosphoramidite DBO derivative (**2**) was synthesized and directly applied in automated solid-phase synthesis to obtain 5′-DBO-labeled oligonucleotides (see below). The end-to-end collision rates were measured through the intramolecular fluorescence quenching of DBO by a guanine base as quencher

[†] Departement Chemie, Universität Basel, Klingelbergstrasse 80, CH-4056 Basel, Switzerland.

[‡] School of Engineering and Science, International University Bremen, Campus Ring 1, D-28759 Bremen, Germany.

(1) Bonnet, G.; Krichevsky, O.; Libchaber, A. *Proc. Natl. Acad. Sci. U.S.A.* **1998**, *95*, 8602−8606.
(2) Goddard, N. L.; Bonnet, G.; Krichevsky, O.; Libchaber, A. *Phys. Rev. Lett.* **2000**, *85*, 2400−2403.
(3) Ying, L.; Wallace, M. I.; Klenerman, D. *Chem. Phys. Lett.* **2001**, *334*, 145−150.
(4) Wallace, M. I.; Ying, L.; Balasubramanian, S.; Klenerman, D. *J. Phys. Chem. B* **2000**, *104*, 11 551−11 555.
(5) Wallace, M. I.; Ying, L.; Balasubramanian, S.; Klenerman, D. *Proc. Natl. Acad. Sci. U.S.A.* **2001**, *98*, 5584−5589.
(6) Ansari, A.; Kuznetsov, S. V.; Shen, Y. *Proc. Natl. Acad. Sci. U.S.A.* **2001**, *98*, 7771−7776.
(7) Shen, Y.; Kuznetsov, S. V.; Ansari, A. *J. Phys. Chem. B* **2001**, *105*, 12 202−12 211.
(8) Kuznetsov, S. V.; Shen, Y.; Benight, A. S.; Ansari, A. *Biophys. J.* **2001**, *81*, 2864−2875.
(9) Zazopoulos, E.; Lalli, E.; Stocco, D. M.; Sassone-Corsi, P. *Nature* **1997**, *390*, 311−315.
(10) Goodfellow, P. N.; Camerino, G. *Cell. Mol. Life Sci.* **1999**, *55*, 857−863.
(11) McCaffrey, A. P.; Meuse, L.; Pham, T.-T. T.; Conklin, D. S.; Hannon, G. J.; Kay, M. A. *Nature* **2002**, *418*, 38−39.
(12) Catasti, P.; Chen, X.; Moyzis, R. K.; Bradbury, E. M.; Gupta, G. *J. Mol. Biol.* **1996**, *264*, 534−545.
(13) Soldatenkov, V. A.; Chasovskikh, S.; Potaman, V. N.; Trofimova, I.; Smulson, M. E.; Dritschilo, A. *J. Biol. Chem.* **2002**, *277*, 665−670.
(14) Lee, G. S.; Neiditch, M. B.; Sinden, R. R.; Roth, D. B. *Mol. Cell. Biol.* **2002**, *22*, 2068−2077.

10.1021/ja038263r CCC: $27.50

Scheme 1

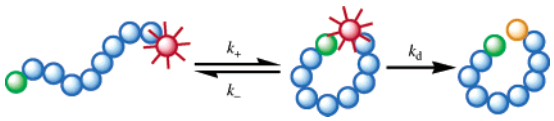

at the 3′ terminus (Scheme 1). The efficient quenching of DBO by guanine ensures that the end-to-end collision in a random-coiled oligonucleotide (k_+ in Scheme 1) is followed by rapid deactivation of the excited state (k_d) before the chain ends dissociate (k_-). In this limiting kinetic scenario, the quenching rate constant (k_q) equals the pertinent rate constant for end-to-end collision (k_+). The k_q values provide therefore a direct measure of the flexibility of the oligonucleotide backbone.

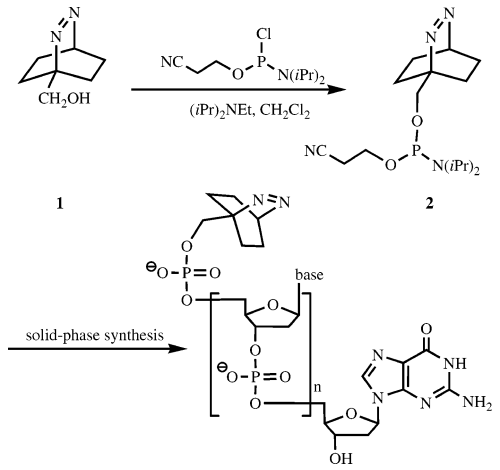

Experimental Section

Materials. Commercial materials were from Fluka or Aldrich. 1-Hydroxymethyl-2,3-diazabicyclo[2.2.2]-oct-2-ene (**1**) was synthesized according to a literature procedure.[15] The primary hydroxyl group was converted to 2-cyanoethyl *N*,*N*-diisopropylphosphoramidite by using the phosphitylating reagent $ClP(OCH_2CH_2CN)N(iPr)_2$. The DBO-labeled oligonucleotides were synthesized by Amplimmun AG (Madulaina, Switzerland) in 1.0 μmol scale in >95% purity; the DBO phosphoramidite (**2**) was coupled to the 5′-terminus of synthetic oligonucleotides during the last stage of the automated solid-phase synthesis. RP-HPLC (5−70% acetonitrile in 0.1 M triethylamine acetate (TEAA)) was used for desalting and removal of failure sequences. The remaining TEAA from the eluant was removed by lyophilization.

Synthesis of DBO-Phosphoramidite (2). A solution of dry 1-hydroxymethyl-2,3-diazabicyclo[2.2.2]-oct-2-ene (**1**, 337 mg, 2.4 mmol) and anhydrous diisopropylethylamine (0.7 mL, 4 mmol) in 16 mL of dichloromethane was stirred under argon. 2-Cyanoethyl *N*,*N*-diisopropylphosphoramidochloridite (0.6 mL, 2.8 mmol) was added dropwise, the mixture was then stirred for 2 h, transferred to a separatory funnel along with 50 mL of ethyl acetate and washed with saturated sodium chloride solution (2 × 40 mL). The organic phase was dried over anhydrous sodium sulfate, filtered, and then rotary-evaporated to yield a yellowish oil. Purification by flash column chromatography (SiO_2, ethyl acetate/dichloromethane/triethylamine 5:5:1) yielded a colorless oil (580 mg, 71%). It was dissolved in ethyl acetate, precipitated from *n*-hexane at −20 °C, filtered off quickly and evaporated to dryness to give **2** as a colorless solid which melts at room temperature (490 mg, 60%). ^{31}P NMR ($CDCl_3$, 400 MHz): δ 145.89 ppm;^{1}H NMR ($CDCl_3$, 400 MHz): δ 1.12−1.20 (m, 2H, CH_2), 1.21 (d, J = 6.8 Hz, 12H, CH_3), 1.31−1.37 (m, 2H, CH_2), 1.57−1.68 (m, 4H, CH_2), 2.65 (dt, J = 6.6, 2.5 Hz, 2H, CH_2CN), 3.60−3.70 (m, 2H, CHN), 3.81−3.94, (m, 2H, CH_2O), 4.12−4.16 (m, 1H, CH_2O), 4.25−4.30 (m, 1H, CH_2O), 5.15 (t, J = 3.5 Hz, 1H, CH) ppm; ^{13}C NMR ($CDCl_3$, 400 MHz): δ 20.8 (CH_2), 21.9 (2C, CH_2), 23.9 (2C, CH_2), 25.0 (4C, CH_3), 43.6 (2C, CHN), 58.9 (CH_2O), 62.3 (CHN), 67.4 (C_q), 69.4 (CH_2O), 118.0 (CN) ppm. FAB−MS (NBA) 340; Calcd 340.4.

Sample Preparation. Concentrations of labeled synthetic oligonucleotides in water were calculated from the absorbance at 260 nm (A_{260}).[16] The fluorescent probe displays a weak absorbance in the near UV (λ_{max} ca. 365 nm, ϵ ca. 50 cm^{-1} M^{-1}) but is transparent at 260 nm,[17] such that no correction for the probe absorption is necessary in the calculation of the oligonucleotide concentration. The strand concentrations in all measurements were adjusted to 60−80 μM, sufficiently low to exclude intermolecular fluorescence quenching.

Fluorescence Measurements. All measurements were performed in aerated water at 25 °C except for the temperature-dependent experiments. Fluorescence decays were recorded on a laser-flash photolysis setup (LP900, Edinburgh Instruments, Edinburgh, Scotland) with 7-mJ, 355-nm pulses of 4 ns width from a Nd:YAG laser (Minilite II, Continuum, Santa Clara, CA), or on a time-correlated single-photon counting (TCSPC) fluorometer (FLS920, Edinburgh Instruments) by using a 1.5-ns pulse-width H_2 flash lamp at 370 nm. Fluorescence was monitored at 440 nm. The resulting data were analyzed by mono-exponential fitting to afford the respective fluorescence lifetimes with typical errors of ±3%.

Results

Selection of Intrinsic Quencher. The quenching methodology in Scheme 1 requires the selection of an efficient fluorescence quencher, which should ideally be an intrinsic component of the respective biopolymer. While in the case of peptides this role can be taken over by the amino acids tryptophan or tyrosine,[18,19] guanine presents the best choice when applying this method to oligonucleotides. In fact, when comparing the bimolecular quenching rate constants of free DBO by different mono-nucleotides[20] the order GMP (dGMP) > dTMP > UMP ≈ CMP (dCMP) ≫ AMP (dAMP) results, with GMP (dGMP) yielding a high rate constant of 5.0×10^8 $M^{-1}s^{-1}$ in aerated water, 40 times faster than the quenching rate of AMP (dAMP), but less than the diffusion-controlled limit.

Diffusion coefficients of probe and quencher when covalently linked to a biopolymer should fall at least 1 order of magnitude below the values for intermolecular diffusion of free molecules.[21−23] This is due to the movement restriction and the internal friction imposed by the chain backbone. As a result, intramolecular reactions between a probe and a quencher may be controlled by intrachain diffusion even if the rate of the corresponding intermolecular reaction falls up to 1 order of magnitude below the diffusion-controlled limit like for the dGMP/DBO pair. Consequently, it is reasonable to assume that the *intramolecular* quenching process between DBO and guanine is collision-controlled,[24] i.e., quenching occurs before

(15) Zhang, X.; Gramlich, G.; Wang, X.; Nau, W. M. *J. Am. Chem. Soc.* **2002**, *124*, 254−263.
(16) Borer, P. N. *Handbook of Biochemistry and Molecular Biology*, 3rd ed.; CRC Press: Cleveland, 1975.
(17) Nau, W. M.; Wang, X. *ChemPhysChem* **2002**, *3*, 393−398.
(18) Hudgins, R. R.; Huang, F.; Gramlich, G.; Nau, W. M. *J. Am. Chem. Soc.* **2002**, *124*, 556−564.
(19) Huang, F.; Nau, W. M. *Angew. Chem., Int. Ed. Engl.* **2003**, *42*, 2269−2272.
(20) Marquez, C.; Pischel, U.; Nau, W. M. *Org. Lett.* **2003**, *5*, 3911−3914.
(21) Lapidus, L. J.; Eaton, W. A.; Hofrichter, J. *Proc. Natl. Acad. Sci. U.S.A.* **2000**, *97*, 7220−7225.
(22) Hagen, S. J.; Hofrichter, J.; Eaton, W. A. *J. Phys. Chem. B* **1997**, *101*, 2352−2365.
(23) Liu, G.; Guillet, J. E.; Al-Takrity, E. T. B.; Jenkins, A. D.; Walton, D. R. M. *Macromolecules* **1990**, *23*, 4164−4167.

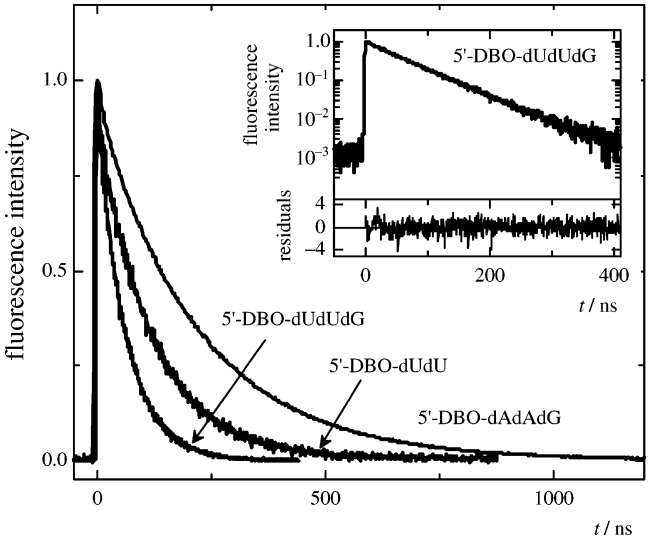

Figure 1. Fluorescence decays of DBO-labeled ssDNA (normalized intensity, recorded by TCSPC). Shown in the inset is a fluorescence decay on a semilogarithmic scale.

the probe/quencher pair dissociates ($k_d \gg k_-$). The deactivation mechanism of DBO by guanine is presumed to be direct or exciplex-mediated quenching by N−H hydrogen abstraction[17,25−27] as evidenced by the significant solvent deuterium isotope effect of 1.4.[20] This quenching by hydrogen atom transfer requires a close probe/quencher contact, another important requirement for applying the methodology in Scheme 1.

Fluorescence Quenching by End-to-End Collisions. Sequences of single-stranded oligonucleotides were designed as 5′-DBO−$(X)_n$-dG, where X = dC, dT, dU, or dA and $n = 2$ or 4. At room temperature, these oligonucleotides do not possess a stable secondary structure (random coil, cf. Scheme 1) although base-stacking interactions are partly maintained between purine bases.[28,29] Solutions of the oligonucleotides displayed monoexponential fluorescence decays (Figure 1), i.e., each oligonucleotide has a specific "fluorescence lifetime", τ_{obs}, similar to the situation for DBO-labeled polypeptides[18,19] and consistent with recent numerical simulations.[30]

The excited DBO decays through three channels: (*i*) quenching upon contact with guanine at the other end through mutual diffusion of the chain ends, (*ii*) quenching upon contact with bases in the backbone (mainly the nearest neighboring nucleotide), and (*iii*) the inherent decay through fluorescence and nonradiative processes. To extract the first component, i.e., the kinetics of end-to-end collision, reference strands with identical sequence but without the 3′ terminal quencher (5′-DBO−$(X)_n$) were measured in all cases; the fluorescence lifetime of these reference strands (τ_0) reflects only the last two kinetic components (*ii*) and (*iii*), since the nature of the backbone is retained. The quenching rate constants related to quenching by guanine (k_q) can then be obtained according to eq 1, which corresponds, subject to the assumption of nearly-quantitative quenching upon contact ($k_d \gg k_-$), to the rate of end-to-end collision (k_+ in eq 2)

$$k_q = \frac{1}{\tau_{obs}} - \frac{1}{\tau_0} \quad (1)$$

$$k_q = \frac{k_+ k_d}{k_d + k_-} \approx k_+, \text{ for } k_d \gg k_- \quad (2)$$

In the actual experiments, there is a significant decrease of the fluorescence lifetime when guanine is attached, i.e., $\tau_{obs} < \tau_0$. In the case of 5′-DBO-$(dU)_2$-dG and 5′-DBO−$(dU)_2$ (Figure 1), for example, the lifetimes are 58 ns (τ_{obs}) and 120 ns (τ_0), respectively, corresponding to $k_q = 9.0 \times 10^6\ s^{-1}$.[31] The lifetime shortening is due to the efficient quenching by dG and the conformational fluctuation of the flexible backbone which allows the chain ends to reach conformations where end-to-end contact is possible (cf. Discussion).

Table 1. Rate Constants and Activation Energies for End-to-End Collision in Single-Stranded Oligonucleotides

oligonucleotide	τ_{obs}/ns	τ_0/ns[a]	$k_+/(10^6\ s^{-1})$[b]	E_a/(kJ/mol)[c]	log$A$[d]
5′-DBO-dAdA-dG	215	243	0.54	43	13.3
5′-DBO-dTdT-dG	60	94	6.0	14	9.2
5′-DBO-dCdC-dG	67	123	6.7	14	9.3
5′-DBO-dUdU-dG	58	120	9.0	12	9.0
5′-DBO-dAdC-dG	106	162	3.2	20	10.0
5′-DBO-dAdAdAdA-dG	247	255	0.12	33	10.9
5′-DBO-dTdTdTdT-dG	72	87	2.4	14	9.0
5′-DBO-dCdCdCdC-dG	96	115	1.8	16	9.0
5′-DBO-dUdUdUdU-dG	83	118	3.6	10	8.3
5′-DBO-dAdCdAdC-dG	131	164	1.5	15	8.7

[a] τ_0 is the lifetime of the reference strand with identical sequence but without the 3′ terminal dG as quencher, 5′-DBO-$(X)_n$. [b] At 25 °C, error in data is 10%. [c] Temperature range 25−40 °C; error in data is ±3 kJ/mol. [d] Temperature range 25−40 °C; error in data is 20%.

Rate Constants and Activation Energies for End-to-End Collision in ssDNA. The intramolecular quenching rate constants for ssDNA containing a backbone of different length composed of different types of nucleotides were determined in a temperature range between 25 and 40 °C (Table 1). It was found that the longer strands ($n = 4$) show slower end-to-end collision rates than the shorter strands ($n = 2$), with a typical factor of 2−4 difference. This length dependence is in line with expectations for end-to-end collision processes in (bio)polymers,[30] and was previously observed for polypeptides.[18] In contrast to the polypeptides, however, we did not observe slower rates for the shortest derivative, i.e., the end-to-end collision rate constant for the shortest homologue in which probe and quencher are directly attached to each other ($n = 0$, 5′-DBO-dG) is the fastest ($\tau_{obs} = 29$ ns, $k_q = 33 \times 10^6\ s^{-1}$). Moreover, the end-to-end collision rates are strongly dependent on the kind of nucleotide in the backbone with the order dU > dT ≈ dC ≫ dA. Again, this is similar to the situation for polypeptides, where

(24) If intramolecular fluorescence quenching of DBO by guanine in oligonulceotides were not fully controlled by intrachain diffusion, the extrapolated end-to-end collision rates could be somewhat larger, which would, in fact, further strengthen our principal conclusion with respect to the mechanism of ssDNA hairpin formation.

(25) Nau, W. M.; Greiner, G.; Rau, H.; Wall, J.; Olivucci, M.; Scaiano, J. C. *J. Phys. Chem. A* **1999**, *103*, 1579−1584.
(26) Pischel, U.; Zhang, X.; Hellrung, B.; Haselbach, E.; Muller, P.-A.; Nau, W. M. *J. Am. Chem. Soc.* **2000**, *122*, 2027−2034.
(27) Pischel, U.; Nau, W. M. *J. Am. Chem. Soc.* **2001**, *123*, 9727−9737.
(28) Mills, J. B.; Vacano, E.; Hagerman, P. J. *J. Mol. Biol.* **1999**, *285*, 245−257.
(29) Saenger, W. *Principles of Nucleic Acid Structure*; Springer-Verlag: New York, 1984.
(30) Wang, X.; Bodunov, E. N.; Nau, W. M. *Opt. Spectrosc.* **2003**, *95*, 560−570.

(31) The question arises whether the lifetime of 5′-DBO-$(dU)_3$ is a more suitable reference for 5′-DBO-$(dU)_2$-dG than 5′-DBO-$(dU)_2$. However, since the lifetimes of 5′-DBO-$(dU)_2$ (120 ns) and 5′-DBO−$(dU)_4$ (118 ns) are virtually the same (Table 1), the length of the reference oligonucleotide appears to be no critical parameter.

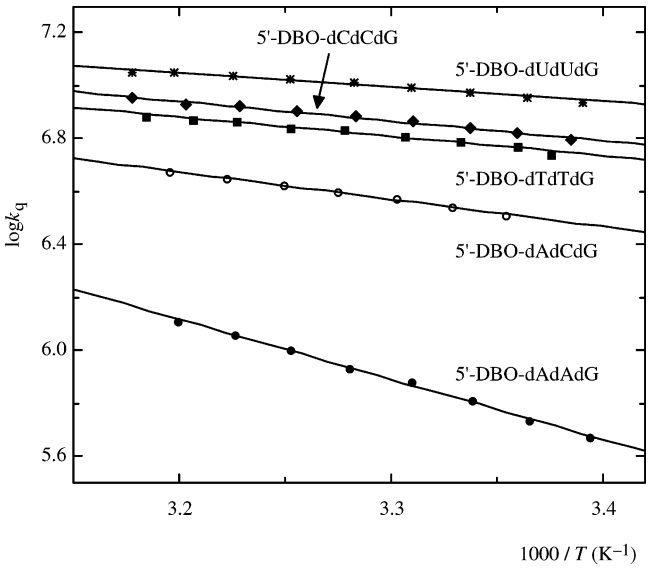

Figure 2. Arrhenius plots of the quenching rate constants in DBO-labeled ssDNA.

the type of amino acid in the backbone is also a crucial parameter in determining the flexibility.

The rate data in Table 1 reveal that about 10^6 collisions occur per second between the chain ends of short ssDNA fragments. Electron transport through DNA, which has attracted significant attention due to its importance for DNA damage and repair, has been reported to occur in ssDNA at a rate of ca. 10^6 s^{-1} with two intervening dT between electron donor and acceptor.[32] This is quite similar to the rate constants for end-to-end collision determined herein, which supports the suggestion that electron transport in ssDNA may proceed through intrachain contact.[32,33]

The intramolecular collision rate constants measured for pyrimidine-derived oligonucleotides ($1.8-9.0 \times 10^6$ s^{-1}) fall up to 1 order of magnitude below those for flexible polypeptides with the same number of monomer units (e.g., 3.3 and 2.5×10^7 s^{-1} for Trp-(Ser)$_4$-DBO and Trp-(Ala)$_4$-DBO in D_2O). The end-to-end collision rate for tetraadenylate (1.2×10^5 s^{-1}) is also 1 order of magnitude slower than those for relatively rigid peptides (e.g., 3.7 and 2.6×10^6 s^{-1} for Trp-(Val)$_4$-DBO and Trp-(Ile)$_4$-DBO in D_2O).[19,34] Oligonucleotides are apparently more rigid than polypeptides. This result may not be further surprising but because the experimental data for intramolecular contact formation in oligonucleotides were previously unavailable, the end-to-end collision rates of ssDNA have been presumed to be similar to those of flexible polypeptides.[7] The present experimental data demonstrate that these biopolymers differ substantially with respect to their flexibility as assessed through the relative mobility of the chain ends.

Arrhenius plots (Figure 2) afforded the activation energy for intramolecular fluorescence quenching of DBO by guanine (E_a, Table 1), which should reflect the energy required for those conformational changes which bring the two chain ends in a short oligonucleotide into contact. All measured activation energies were positive. This is a nontrivial result, because apparent negative activation energies have been reported for ssDNA hairpin formation.[5,6] The activation energies for dU, dT, and dC strands were all close to 16 kJ/mol, the activation energy for solvent viscous flow in H_2O.[35] This suggests immediately that end-to-end collision is limited by solvent friction and only modulated through a probability factor which differentiates the types of nucleotides. The latter could derive from variations in the conformational freedom for bond rotations as imposed by the different steric demand of the bases.

In contrast, end-to-end collision in oligoadenylates displayed significantly higher activation energies, 43 kJ/mol for 5′-DBO-(dA)$_2$-dG and 33 kJ/mol for 5′-DBO−(dA)$_4$-dG, which point to a higher intrinsic 'rigidity' of oligoadenylates. Clearly, end-to-end collision in oligoadenylate is limited by internal friction (not by solvent friction as for the pyrimidine strands), which provides also strong support for the assumption that the intramolecular quenching of DBO by guanine in oligonucleotides is determined by intrachain diffusion (k_+ in Scheme 1), not by an intrinsic activation barrier for excited-state deactivation (k_d).

Because it is known that adjacent adenines can undergo base-stacking interactions,[28,29] two additional ssDNA were investigated, in which the adenine bases in the strands were replaced by cytosine in an alternating manner (see data for 5′-DBO-dAdC-dG and 5′-DBO-dAdCdAdC-dG in Table 1). End-to-end collision in these strands became significantly faster and the rate constants were on the same order of magnitude as those for oligopyrimidines. In addition, the activation energies of end-to-end collision in these oligonucleotides were much smaller than those of oligoadenylates and close to the activation energy of solvent viscous flow.

Discussion

Although experimental data for end-to-end collision rates have recently been reported for polypeptides,[18,19,21,36] the characteristic time scale for intrachain collision in single-stranded nucleic acids has remained elusive. We have now transferred to oligonucleotides the methodology of using intramolecular fluorescence quenching of DBO to obtain the kinetics of intrachain diffusion. The principle of measuring end-to-end collision rates by fluorescence quenching is shown in Scheme 1. This method requires not only a long-lived fluorescent probe to allow quenching through the relatively slow (ns−μs time scale) intrachain diffusion to compete with spontaneous deactivation but requires also a contact quenching mechanism to relate the kinetics of quenching directly to the kinetics of end-to-end collision. Both requirements are fulfilled for the DBO chromophore.[17] In the case of polypeptides, tryptophan was selected as quencher.[18,19] In single-stranded oligonucleotides, guanine can take over this role. Both are the most efficient intrinsic fluorescence quenchers of DBO among natural amino acids and nucleobases, respectively. In view of the comprehensive mechanistic information established in the course of the polypeptide

(32) Meggers, E.; Dussy, A.; Schafer, T.; Giese, B. *Chem. Eur. J.* **2000**, *6*, 485−492.
(33) Kan, Y.; Schuster, G. B. *J. Am. Chem. Soc.* **1999**, *121*, 10 857−10 864.
(34) The fact that Trp is a better intermolecular quencher of DBO fluorescence ($k_q = 21 \times 10^8$ M^{-1}s^{-1}) than guanine ($k_q = 5.0 \times 10^8$ M^{-1}s^{-1}) cannot be responsible for the observed large difference in intramolecular quenching rate constants between peptides and oligonucleotides. When Tyr is used as quencher in peptides, which is similarly efficient ($k_q = 5.6 \times 10^8$ M^{-1}s^{-1}) as guanine, the difference remains, with the rates in peptides being reduced by a factor of 2−3.
(35) The activation energy of solvent viscous flow in H_2O in the relevant temperature range (298−313 K) was obtained by plotting lnη versus 1/T with the viscosities taken from Cho, C. H.; Urquidi, J.; Singh, S.; Robinson, G. W. *J. Phys. Chem. B* **1999**, *103*, 1991−1994.
(36) Bieri, O.; Wirz, J.; Hellrung, B.; Schutkowski, M.; Drewello, M.; Kiefhaber, T. *Proc. Natl. Acad. Sci. U.S.A.* **1999**, *96*, 9597−9601.

studies[37] and in view of additional control experiments performed for ssDNA (cf. Supporting Information), we interpret the intramolecular quenching rate constants (k_q) of the DBO/guanine probe/quencher pair in oligonucleotides in terms of end-to-end collision rate constants (k_+ in Scheme 1) according to eq 2.

The quenching rate data in Table 1 provide the first direct experimental measure of the collision rates between the chain ends in single-stranded oligonucleotides. The slow collision rates for the oligoadenylates stand out and the related strands show also significantly higher activation energies than the oligopyrimidine strands. Because the DNA strands presently employed cannot form intramolecular hydrogen bonds or stable secondary structures, the energy barrier for the quenching process is a measure of the energy required for the conformational changes of the oligonucleotide backbone which bring the probe and quencher into contact. This energy barrier is a composite of the apparent activation energy for solvent viscous flow and the energy barrier of internal friction, i.e., the bond rotations required for end-to-end collision.

It is appropriate to argue, akin to the situation for peptides,[19] that strands whose ends collide with the slowest rates are the most rigid ones. This means that the kinetics of end-to-end collision in ssDNA provides also a direct measure of their intrinsic flexibility. The 10 times slower end-to-end collision rates and the substantial activation energies signal therefore a higher 'rigidity' of oligoadenylates, which is qualitatively consistent with the trend observed by Hagerman and co-workers through persistence length measurements.[28] This increased rigidity is presumably due to two reasons. On one hand, purine bases are larger than pyrimidines, which decreases the intrachain diffusion coefficient and imposes higher steric restrictions toward bond rotation. On the other hand, adjacent purine bases undergo sizable base-stacking interactions,[28,29] which impose a barrier toward free bond rotation.

To evaluate the relative importance of these two factors (steric hindrance versus base-stacking interaction) control experiments were performed with 5′-DBO-dAdC-dG and 5′-DBO-dAdCdAdC-dG strands, in which the purine base stacking is destroyed by the alternating cytosine bases.[2,38] These strands show much faster rate constants and also smaller activation energies for end-to-end collision than the homogeneous dA strands (Table 1), which suggests that the major contributor to the rigidity of the oligoadenylates strands is due to base stacking. However, the rate constants and activation energies do not quite reach the values for the pyrimidine strands, which indicates that the larger size of adenine and the related steric hindrance involved during conformational changes has an effect as well. The control experiments with the mixed purine/pyrimidine strands immediately demonstrate that the flexibility of DNA fragments cannot be predicted in an incremental fashion from the flexibility of strands containing only identical bases, but that synergetic effects, in particular base-stacking interactions between neighboring purine bases, operate.

The measured activation energy for end-to-end collision in 5′-DBO-$(dA)_2$-dG suggests that the destruction of base-stacking interaction in an AAG unit may require as much as 30−40 kJ/mol, which compares well with the stabilization energy of a single AA base stack obtained by molecular modeling (34 kJ/mol).[38] Interestingly, the activation energy for the longer adenine strand, 5′-DBO-$(dA)_4$-dG, is *smaller* than that of the shorter one. Presumably, the conformation for end-to-end contact formation in 5′-DBO-$(dA)_4$-dG has a larger circle radius, which renders steric hindrance effects less important and which may even allow the base-stacking interaction to be partially retained during the collision process. This trend is consistent with the analysis of Ansari and co-workers which implies that the energetic cost of bending a molecular chain to a loop should decrease with increasing length.[7]

The flexibility of DNA is deemed important in additional key events, including electron transfer[32,33,39] as well as nucleic acid−protein selective binding.[40−42] In fact, the higher intrinsic rigidity of single-stranded oligoadenylates observed in the present study may provide a possible explanation for the reduced binding of the SSB protein with poly(dA), compare binding enthalpies of −14 kcal/mol for poly(dA), −75 kcal/mol for poly(dT), and −85 kcal/mol for poly(dC).[43] The binding to the protein requires a substantial conformational change of the ssDNA, the energetic cost of which is highest in poly(dA) due to the required unstacking, cf. activation energies in Table 1.

Oligopyrimidines do not show substantial base-stacking interactions at room temperature.[28,44] Our observations that the end-to-end collision rates of strands composed of dT, dU, and dC differed weakly and the activation energies were all close to 16 kJ/mol, the activation energy of the solvent viscous flow in water,[35] indicated that the friction with solvent molecules during conformational changes is the main contributor to the energy barrier. This applies both for the shorter ($n = 2$) as well as the longer ($n = 4$) oligonucleotides studied. The differences between the absolute rate constants for dT and dU strands are small, but nevertheless consistent with their molecular structure. The faster quenching of dU relative to dT strands can be related to the lack of the extra methyl group which will exhibit increased steric hindrance effects in the course of the required bond rotations in dT strands. A general relationship between the size of the residue in the chain segments and the rate of end-to-end collision has already been recognized in polypeptides, where larger residues also tend to slow this process.[19]

The absolute rate constants for end-to-end collision in ssDNA are essential for the understanding of the mechanism of ssDNA hairpin formation.[1−8] In particular, these elementary rate data can provide information on whether it is the kinetics of end-to-end contact formation that is rate-determining for hairpin formation. An ssDNA hairpin is composed of a single-stranded loop part and a double-stranded stem part with several base pairs. Ansari and co-workers have suggested that the rate-determining step in hairpin formation is the formation of a loop with a 'correct' base pair.[6,7] They argued that only a 'correct' nucleating loop can result in rapid zipping of the hairpin, but that intrachain collisions in ssDNA can also form misfolded loops which do not lead to subsequent zipping of the stem part and thereby

(37) Nau, W. M.; Huang, F.; Wang, X.; Bakirci, H.; Gramlich, G.; Marquez, C. *Chimia* **2003**, *57*, 161−167.
(38) Aalberts, D. P.; Parman, J. M.; Goddard, N. L. *Biophys. J.* **2003**, *84*, 3212−3217.
(39) O'Neill, M. A.; Barton, J. K. *J. Am. Chem. Soc.* **2002**, *124*, 13 053−13 066.
(40) Hogan, M. E.; Roberson, M. W.; Austin, R. H. *Proc. Natl. Acad. Sci. U.S.A.* **1989**, *86*, 9273−9277.
(41) Hogan, M. E.; Austin, R. H. *Nature* **1987**, *329*, 263−266.
(42) Suck, D. *Biopolymers* **1997**, *44*, 405−421.
(43) Kozlov, A. G.; Lohman, T. M. *Biochemistry* **1999**, *38*, 7388−7397.
(44) Camerman, N.; Fawcett, J. K.; Camerman, A. *J. Mol. Biol.* **1976**, *107*, 601−621.

reduce the hairpin formation rate. Their results showed that the closing rate for a DNA hairpin with 4 dT in the loop is ca. 0.8×10^5 s^{-1} (25 °C).[6] Our experiments afforded an end-to-end collision rate of 2.4×10^6 s^{-1} for 5′-DBO-$(dT)_4$-dG, which is much faster and suggests that the time for hairpin formation is 'longer' than expected from the time of forming a loop. This result is consistent with the idea that not all end-to-end or other intrachain contacts induce hairpin formation, i.e., there are mismatches and inefficient contacts, which require the ssDNA to explore several local minima conformations until the 'correct' nucleating loop is reached. The absolute rate constants for end-to-end collision in oligonucleotides provide therefore strong support for the configurational diffusion model by Ansari and co-workers.

Moreover, previous work on the formation of DNA hairpins[5,6] have afforded *negative* activation energies for the folding rates, which are in contrast to the positive activation energy of end-to-end collision rates reported herein. This contrast provides further support that hairpin formation, unlike end-to-end collision of random-coiled oligonucleotides, involves a transition state with lower enthalpy than the initial state.[6,45] In terms of the model by Ansari and co-workers, the initial state corresponds to the random-coiled ssDNA and the apparent transition state is the loop in which a single correct base pair is formed; the hydrogen bonds in this base pair stabilize the transition state, which provides the underlying reason for the measured negative activation energy. The oligonucleotides in our systems cannot form stable base pairs during end-to-end collision, such that a positive activation energy results, which is characteristic for the temperature dependence of the solvent viscosity and the energy required for conformational changes, including the unstacking of purine bases.

Finally, it is noteworthy that the absolute rates for end-to-end collision in oligonucleotides as well as peptides are also manifested in the kinetics of secondary structure formation. For example, the presently reported rates for oligonucleotides are 1 order of magnitude slower than those for polypeptides with the same number of residues,[18,19] suggesting a relatively higher 'rigidity' of oligonucleotides. This is in fact reflected also in the rates for hairpin formation in oligonucleotides as well as in peptides, with the latter (as β-hairpins) being formed 1 order of magnitude faster.[1,5,46]

Conclusions

We have shown that the end-to-end collision rates of short ssDNA can be experimentally measured by employing a fluorescence-based method, in which the end-attached chromophore DBO is efficiently quenched upon contact with dG at the other end. These elementary kinetic data are essential to predict the time scale and determine the mechanism of secondary structure formation, e.g., for hairpins, to evaluate the rigidity of different base sequences, and they provide benchmark values for the development of computational methods for ssDNA dynamics. The present experiments in dependence on temperature and base sequence show that oligoadenylate is much more rigid than the oligonucleotides composed of pyrimidines, which is mainly due to the base-stacking interactions in oligoadenylate. Compared to the kinetics of DNA hairpin formation, which has been previously studied, the end-to-end collision rate of the oligonucleotide corresponding to the hairpin loop part is 1 order of magnitude faster. This contrast indicates that the effective intrachain diffusion is strongly slowed during hairpin formation, which supports the configurational diffusion model, where misfolded loops are presumed to slow hairpin formation.

Acknowledgment. This study was performed within the Swiss National Research Program "Supramolecular Functional Materials" (NRP 47, Grant No. 4047-057552) and supported by the Schweizerischer Nationalfonds (Grant No. 620-58000).

Supporting Information Available: Control experiments to establish methodology. This material is available free of charge via the Internet at http://pubs.acs.org.

JA038263R

(45) Eaton, W. A.; Munoz, V.; Hagen, S. J.; Jas, G. S.; Lapidus, L. J.; Henry, E. R.; Hofrichter, J. *Annu. Rev. Biophys. Biomol. Struct.* **2000**, *29*, 327−359.

(46) Munoz, V.; Henry, E. R.; Hofrichter, J.; Eaton, W. A. *Proc. Natl. Acad. Sci. U.S.A.* **1998**, *95*, 5872−5879.

Supporting Information

Kinetics of End-to-End Collision in Short Single-Stranded Nucleic Acids

Xiaojuan Wang[†] and Werner M. Nau[*, †, ‡]

Contribution from the Departement Chemie, Universität Basel, Klingelbergstrasse 80, CH-4056 Basel, Switzerland, and the School of Engineering and Science, International University Bremen, Campus Ring 1, D-28759 Bremen, Germany

Control experiments to establish methodology. Control experiments were performed to establish the validity of the interpretation of the experimental data in terms of intrachain contact formation. To exclude a through-bond mechanism of fluorescence quenching (e.g., superexchange electron transfer), different oligonucleotides with identical separation between probe and quencher were studied: 5'-DBO-dCdCdG, 5'-DBO-dCdCdGdA, and 5'-DBO-dCdCdGdAdAdA. If a through-bond quenching mechanism would operate, the lifetimes should remain the same due to the identical probe/quencher separation. Instead, the fluorescence lifetime increased from 67 to 86 to 93 ns, which can be reconciled in terms of two effects related to intrachain diffusion: The adenosine attached to the 3' terminus (*i*) shields the quencher from the approach of the probe through steric hindrance and base stacking and (*ii*) decreases the effective diffusion coefficient of the chain end. Both factors reduce quenching and lengthen the lifetime. The more pronounced increase in lifetime upon attachment of the first adenosine further demonstrates that the steric hindrance effect is the more important contributor. Incidentally, this

experiment demonstrates that the fluorescence-based method is not restricted to measurement of end-to-end collision processes, but can also be used to measure contact formation between one end and any position within an oligonucleotide (i.e., quenching by an internal guanosine).

To demonstrate that neighboring guanine bases contribute independently to quenching, we have compared the quenching efficiency in nucleotides with a guanine doublet, 5'-DBO-dCdCdGdG, with those containing single guanines, 5'-DBO-dCdCdGdA and 5'-DBO-dCdCdAdG. 5'-DBO-dCdCdAdA was used as a reference, since adenine is also a purine base, but does not serve as an efficient quencher of DBO fluorescence. The resulting rate constants are listed in the supporting Table 2. Note first that the quenching rate of 5'-DBO-dCdCdGdA is larger than that of 5'-DBO-dCdCdAdG, because the quenching efficiency decreases as the distance between probe and quencher increases. More striking, the quenching rate of 5'-DBO-dCdCdGdG is as large as the combined quenching rate constants of 5'-DBO-dCdCdGdA and 5'-DBO-dCdCdAdG, but not larger; the two adjacent guanines contribute independently to the quenching. This result is in line with exciplex-induced quenching following collision between the probe and an individual guanine, but speaks against an electron transfer quenching mechanism since a guanine doublet should serve as a better (more than additive) electron donor site due to a decreased oxidation potential.[1,2]

Table 2. Intramolecular fluorescence quenching in DBO-labeled oligonucleotides

oligonucleotide	τ_{obs}/ ns	k_q / (10^6 s^{-1}) [a]
5'-DBO-dCdCdAdA	128	reference
5'-DBO-dCdCdGdA	86	3.8
5'-DBO-dCdCdAdG	99	2.3
5'-DBO-dCdCdGdG	73	5.9

[a] At 25°C, error in data is 10%.

References

(1) Saito, I.; Takayama, M.; Sugiyama, H.; Nakatani, K.; Tsuchida, A.; Yamamoto, M. *J. Am. Chem. Soc.* **1995**, *117*, 6406-6407.

(2) Lewis, F. D.; Wu, T.; Liu, X.; Letsinger, R. L.; Greenfield, S. R.; Miller, S. E.; Wasielewski, M. R. *J. Am. Chem. Soc.* **2000**, *122*, 2889-2902.

Corresponding author:

Prof. Dr. Werner M. Nau

School of Engineering and Science

International University Bremen

Campus Ring 1

D-28759 Bremen

Germany

Application of FRET donor/acceptor pairs with small critical radius to recover structural and dynamic properties of short flexible peptides

Fang Huang,[a] Xiaojuan Wang,[a] Elisha Haas,[b] and Werner M. Nau[*, a, c]

[a] Departement Chemie, Universität Basel, Klingelbergstrasse 80, CH-4056 Basel, Switzerland

[b] Department of Life Sciences, Bar-Ilan University, Ramat-Gan 52900, Israel

[c] School of Engineering and Science, International University Bremen, Campus Ring 1, D-28759 Bremen, Germany

w.nau@iu-bremen.de

Abstract

Intramolecular fluorescence resonance energy transfer (FRET) has been measured to recover detailed structural and dynamic properties in flexible Gly-Ser peptides. Two fluorescence energy donor/acceptor pairs with very small Förster critical radius (< 10Å) are introduced, where either naphthalene or tryptophan serves as energy donor and 2,3-diazabicyclo[2.2.2]oct-2-ene (DBO) as acceptor. The fluorescence decays of the donor (naphthalene) and acceptor (DBO) in the presence and absence of FRET have been measured and subjected to global data analysis. The recovered intramolecular diffusion coefficients ($0.78 - 20 \times 10^{-7}$ cm^2/s) were found to be much smaller than those of free amino acids (10^{-5} cm^2/s), which provides experimental evidence that the diffusion of the chain ends of these biopolymers is considerably slowed down. The slowest diffusion coefficients were obtained for the shortest peptides, which is consistent with expectations from theoretical studies. Shorter chains are proposed to exhibit a larger internal friction, which limits chain flexibility. Additionally, the intramolecular energy transfer efficiency has been measured for both donor/acceptor pairs and the effective average end-to-end distances were calculated, which are compared with independently determined end-to-end collision rates in the same set of peptides.

Introduction

How proteins fold and how proteins function remain to be two of the most important and fundamental questions in protein science. The kinetics and dynamics of peptide chain motions presents an indispensable element in this context. The sequence and rate of the formation of the individual secondary structures will be critical for the correct folding to the functional native conformation of a protein,[1] while the rates of hinge or shear domain motions in a protein will be decisive for substrate binding.[2,3] Peptide motion, as an essential step for conformational changes of peptides and proteins, is therefore indispensable in protein folding and protein functions.

To explore the mechanism, predict the rate limit in protein folding, and to disclose the relationship between the function and flexibility of different regions in a protein, several photophysical methods for monitoring intramolecular collisions in peptides have been established. For this purpose, a probe and quencher are introduced at the two ends or in two positions of a peptide,[4-6] and the intramolecular collision rates are then extracted from the kinetics of quenching of the excited probe, either a triplet state monitored by transient absorption, or a fluorescent singlet state. All of these methods are based on an assumption that the excited probe is quenched by the quencher through contact, which has been experimentally established for the fluorescence-based method.[7] Any quenching that can occur over a longer distance, including super electron transfer and fluorescence resonance energy transfer (FRET), should therefore be avoided.[6] While the use of FRET as spectroscopic ruler[8] to estimate average distances in static, large proteins is well-established, its application to short flexible peptides as more dynamic systems has been less frequently explored.[9,10] The latter can be used to recover the end-to-end distribution function and diffusion coefficients of the chain ends as additional key parameters.[9]

The short peptides, for which the end-to-end collision rates have been determined in previous studies, have typical lengths between 2–20 amino acid residues, suggesting average

end-to-end distance on the order of 10 Å. In order to investigate such short peptides by FRET, and thereby obtain complementary information on the dynamics, it is essential to design FRET donor/acceptor pairs with Förster critical radii (R_0) on the same order of magnitude, i.e., 10 Å.[11,12] This is because the determination of distances by FRET is most accurate when the donor/acceptor distance lies within a range of $0.5R_0$–$2.0R_0$. This limitation restricts the choice of donor/acceptor pairs dramatically, since in addition to a very low oscillator strength of the acceptor, both donor and acceptor must ideally be small organic chromophores and in addition, the acceptor should have no absorption at the excitation wavelength of the donor.

The previously investigated peptides were of the type Trp–backbone–DBO, where the backbone represents the characteristic amino acid sequence and where DBO presents 2,3-diazabicyclo[2.2.2]oct-2-ene, a fluorescent azo chromophore with an exceedingly long lifetime, which is efficiently quenched intramolecularly by forming an intimate contact with Trp to allow the accurate determination of the end-to-end collision rate constants between the chain ends represented by the *C*-terminal probe (DBO) and the *N*-terminal quencher.[6,13,14]

We reckoned that the identical peptides, i.e., Trp–backbone–DBO could be employed as FRET systems, by exciting Trp as donor and monitoring the singlet energy transfer to DBO as acceptor. Luckily, it turned out further that the Förster critical radius for this pair is exactly the 10 Å required to apply FRET for reliable distance measurements in the identical set of peptides, and therefore to allow an excellent and self-consistent comparison of experimental data, namely the previously determined end-to-end collision rates. In a second step, it turned out that substitution of Trp by the very closely related naphthylalanine (Nal) provides an additional insight and some advantages due to the longer donor lifetime while preserving the very short Förster critical radius at the same value.

The results of this FRET study are described in this paper for peptides of different chain length, Nal-(Gly-Ser)$_n$-DBO and Trp-(Gly-Ser)$_n$-DBO[6] (n = 0, 1, 2, 4, 6 and 10, cf. Scheme

1), for which we expected substantial variations in the end-to-end distribution functions and diffusion coefficients.[15]

Experimental Section

Materials. All commercial materials were from Fluka or Aldrich. The DBO-labeled peptides were commercially synthesized in > 95% purity (Affina, Berlin). Details on the synthesis of the probe and its suitability in solid-phase peptide synthesis can be obtained from our previous study.[6]

Fluorescence measurements. Fluorescence decays were recorded on a time-correlated single photon counting (TCSPC) fluorometer (FLS920, Edinburgh Instruments, Edinburgh, Scotland) by using a 1.5-ns pulse-width H_2 flash lamp or a Picoquant picosecond pulsed diode laser (λ_{ex} = 373 nm, ca. 50 ps pulse width) for excitation. The peptide concentrations were adjusted to 10-100 μM, sufficiently low to exclude intermolecular interactions. Experiments were carried out in D_2O under air to keep the experimental conditions consistent with previous study, where the end-to-end collision rates for peptides with the same backbone have been measured.[6] For each peptide, Nal-(Gly-Ser)$_n$-DBO, three independent fluorescence decay traces were collected. Upon excitation of the naphthalene chromophore (λ_{ex} = 285 nm), the temporal evolution of the fluorescence of both the donor (naphthalene λ_{em} = 335 nm) and the acceptor (DBO λ_{em} = 450 nm) were monitored. In an independent set of experiments the fluorescence decay of acceptor (DBO) was also measured for direct excitation (λ_{ex} = 373nm). To obtain the donor decay in the absence of FRET, a reference peptide, Nal-(Gly-Ser)$_6$, was synthesized, in which only the donor moiety, naphthalene, is present, i.e., without acceptor.

Solid-phase fluorescence experiments were carried out in trehalose glass with 1 mM naphthylalanine and 77 mM DBO. Trehalose glass was prepared by heating 5 g trehalose with ca. 0.5 mL water to ~130 °C to obtain a viscous solution with dissolved naphthylalanine and DBO, which was then quickly poured into a 1 cm cuvette and allowed to cool down to get a transparent glassy matrix.

Absorption spectra were recorded on a Cary 4000 UV-Vis spectrometer (Varian) and stead-state fluorescence spectra on a Cary Eclipse fluorometer (Varian)

Data analysis. There are two factors which affect the efficiency of FRET: (1) the end-to-end distance distribution, i.e., the donor/acceptor distance, which is dependent on the sequence and the length of the peptides, and (2) the conformational flexibility, since the peptide chains undergo conformational changes during the excited state lifetime. The latter leads to diffusional fluctuations of donor acceptor distance during the probe lifetime, which enhances the FRET efficiency by a varying degree. In principle, the time-resolved decay of the surviving excited donor sites is described by the following distribution function:[10,15,16]

$$\frac{\partial}{\partial t} g_{\mathrm{N}}^{*}(r,t) = -\frac{1}{\tau_0}\left(1+\left(\frac{R_0}{r}\right)^6\right) g_{\mathrm{N}}^{*}(r,t) + D\frac{1}{r^2}\frac{\partial}{\partial r} r^2 \frac{\partial}{\partial r} g_{\mathrm{N}}^{*}(r,t) + D\frac{1}{r^2}\frac{\partial}{\partial r}\left(r^2 g_{\mathrm{N}}^{*}(r,t)\frac{\partial}{\partial r}\beta U(r)\right) \quad (1)$$

D is the mutual intramolecular end-to-end diffusion constant, which is the sum of the individual diffusion coefficients of the two chain ends. β^{-1} is the product of the Boltzman constant and temperature ($\beta = 1/k_{\mathrm{B}}T$), and $U(r)$ is the potential energy of the chain possessing an end-to-end distance r. If the ground-state equilibrium distribution $g_{\mathrm{N}}(r)$ is known, the potential energy can be obtained according to Equation 2, assuming no perturbation of the distribution function upon excitation of the donor.[10,17]

$$\beta U(r) = -\ln g_{\mathrm{N}}(r) \quad (2)$$

Equation 1 can be used to calculate the survival probability density of an excited state at distance r subject to the boundary condition

$$\frac{\partial}{\partial r} g_N^{*}(r,t) + g_N^{*}(r,t)\frac{\partial}{\partial r}\beta U(r)\Big|_{r=a} = 0 \quad (3)$$

FRET experiments can in principle yield both, the end-to-end distance distribution and the intrachain diffusion coefficient. However, since these parameters are tightly correlated, the recovery of both distribution and diffusion coefficient from the donor fluorescence decay becomes very difficult. According to Haas and coworkers this problem is overcome by global

analysis of both the donor and acceptor fluorescence decays and growth curves.[9] This approach of "over-determination" has been adapted in this paper.

Results

Intramolecular energy transfer from naphthalene to DBO. In a pervious work, efficient singlet-singlet energy transfer from naphthalene to DBO has been observed,[18] where naphthalene and DBO were directly connected through a short dimethylsiloxy tether. The experimental results (for *n*-hexane as solvent) suggested that the effective average end-to-end distance between naphthalene and DBO is as short as 5.2 Å, which means that naphthalene and DBO come essentially in contact (orbital overlap) such that exchange energy transfer mechanism was expected to be dominant. In the present set of experiments with peptides, FRET was expected to become dominant due to the longer and more rigid tether and due to the more viscous aqueous solution which both favor FRET over exchange- energy transfer due to (1) a larger average end-to-end distances and (2) slower diffusion.

In order to corroborate the participation of FRET in the case of the Nal/DBO doubly labeled peptides, a control experiment was performed, in which a host molecule, cucurbit[7]uril (CB7), was added to solutions of Nal-(Gly-Ser)$_6$-DBO and Nal-(Gly-Ser)$_6$, respectively. It has been demonstrated that DBO can be included into the cavity of CB7 to form a supramolecular host-guest complex, where CB7 can serve as a protective shield to exclude the contact between DBO and naphthalene.[7,19] Independent control experiment revealed that naphthalene is also included into CB7. At the selected concentrations of peptide (3.8×10^{-5} M) and CB7 (7.5×10^{-4} M) less than 1% of peptide is uncomplexed, owing to the high binding constants, $(5 \pm 1) \times 10^4$ M^{-1} for Nal•CB7 and $(4 \pm 1) \times 10^5$ M^{-1} for DBO•CB7. The salient feature of this control experiment is that the complexed chromophores cannot undergo exchange energy transfer due to the separation imposed by the supramolecular host, but only FRET, which is free to operate through space. Indeed, under such conditions the resonance energy transfer between naphthalene and DBO is still observed in both steady-state

and time-resolved measurements. The emission spectrum of the doubly labeled peptide Nal-(Gly-Ser)$_6$-DBO in the presence of CB7 is shown in Figure 4, where the emission of DBO above 400 nm was observed with excitation of naphthalene at 285 nm. When time-resolved measurements were performed, the fluorescence decay of the naphthalene residue in both Nal-(Gly-Ser)$_6$ and Nal-(Gly-Ser)$_6$-DBO could be roughly fitted with a monoexponential decay function, lifetimes of 73 ns and 62 ns were observed. The significantly longer lifetime than that of free naphthalene under the same condition without CB7 (37 ns) was also an evidence that the naphthalene residue in both peptides has been efficiently protected by CB7 from the quenching of oxygen. However, the obviously shorter naphthalene lifetime in the doubly labeled peptide Nal-(Gly-Ser)$_6$-DBO suggested that the excited naphthalene can still be quenched by DBO even in the cavity of CB7. Recall that the inclusion of DBO by CB7 in peptide Trp-(Gly-Ser)$_2$-DBO excludes completely the quenching by tryptophan (increasing the lifetime of DBO from 20 ns to 1030 ns), where a contact quenching mechanism applies.[7] This control experiment suggests that a close contact is not necessary for the quenching of naphthalene by DBO and that a through-space electron or energy transfer process, which can occur through the walls of the supramolecular cages, dominates at long distances. The possibility of an electron transfer mechanism, however, has been excluded in a previous work on the basis of the endergonic thermodynamics.[18] The energy transfer efficiency for peptide Nal-(Gly-Ser)$_6$-DBO in the presence of CB7, calculated from fluorescence lifetime, is 15.1%, suggesting an effective distance of energy transfer of 13.1 Å, which corresponds to the average end-to-end distance of this peptide. This average end-to-end distance is a little longer than the corresponding one in the absence of the CB7 (See Table 2 and 3), because that the donor and acceptor are prevented to approach closer than the cucurbituril diameter when they are included by CB7 (Scheme 2). Admittedly, this experiment does not provide compulsory evidence that FRET dominates in the uncomplexed peptide as well, but it is an appealing experiment to address the question by means of supramolecular technology.

The quenching rate constants of naphthalene by DBO in the intermolecular case were also measured in D_2O (η = 1.1 cP), H_2O (η = 0.89 cP) and acetonitrile (η = 0.345 cP), which are 5.7×10^9 $M^{-1}s^{-1}$, 6.3×10^9 $M^{-1}s^{-1}$, and 9.5×10^9 $M^{-1}s^{-1}$ at 25°C, respectively, demonstrating diffusion-controlled quenching.

Characterization of FRET donor/acceptor pair. The critical Förster radius (R_0) for resonance energy transfer from naphthalene to DBO in D_2O was calculated according to Förster theory from the overlap (J) of the absorption spectrum of DBO and the fluorescence emission spectrum of naphthalene. The R_0 value of the Nal/DBO energy donor/acceptor pair in D_2O is 9.8 ± 0.2 Å ($J = 3.05 \times 10^{11}$ $M^{-1}cm^{-1}nm^4$). Note that the critical radius in H_2O is the same as in D_2O within error due to the very similar spectra, quantum yield (this work) and refractive index.[20] Naphthalene has a fluorescence lifetime of 37 ns in both H_2O and D_2O. Peptide-attached naphthalene and DBO, Nal-$(Gly\text{-}Ser)_6$ and $(Gly\text{-}Ser)_6$-DBO, were also applied to measure R_0. Results show that the attachment to peptides does not affect J and R_0 values.

Alternatively, R_0 was obtained by measuring the fluorescence decay in the absence of diffusion and energy migration among donor molecules, which can be described by Equations 4 and 5.[21]

$$I = I_0 \exp\left[-t/\tau - 2\left(C_A/C_{0A}\right)\left(t/\tau\right)^{1/2}\right] \quad (4)$$

$$C_{0A} = 3000/2\pi^{3/2}NR_0^3 \quad (5)$$

Here, τ is the lifetime in the absence of quencher, C_A is the concentration of the acceptor and C_{0A} is the critical acceptor concentration for energy transfer.

The pertinent measurements were done in solid trehalose, where diffusion could be neglected.[22] Additionally, the concentration of the acceptor DBO (77 mM) was controlled to be much higher than that of the naphthylalanine donor (1 mM) such that the energy migration between donor molecules (homo-FRET) could be neglected. Note that naphthylalanine was

used instead of naphthalene in the solid phase experiments because the preparation of the solid sample needs enhanced temperatures, where naphthalene itself sublimes. The fluorescence decay was recorded and then applied to Equations 4 and 5 to calculate R_0. The result is 9.4 ± 0.4 Å, consistent within error with the value calculated from the spectral overlap. The slightly smaller value may come from the difference of the medium, e.g., a larger refractive index in trehalose than in water.

Time-resolved fluorescence measurements. The time-resolved fluorescence decay of naphthalene residue (λ_{em} = 335 nm) was recorded in the donor-only-labeled peptide and the donor/acceptor doubly-labeled peptides by donor excitation (λ_{ex} = 285 nm) (representative decay traces are shown in Figure 1). The decay trace of the donor-only-labeled peptide can be fitted with a mono-exponential function with a lifetime of 36 ns, similar to the decay of free naphthalene. However, a multi-exponential function is required in the case of the doubly-labeled peptides due to the continuum of energy transfer rates. The fitting results are summarized in Table 1; for simplicity and ease of comparison, "average" fluorescence lifetimes are provided also for the multiexponential decays by a weighing procedure. Expectedly, the average fluorescence lifetimes of the naphthalene donor residue are consistently shorter than that of free naphthalene as a result of energy transfer. The lifetimes increase with increasing peptide length, indicating a reduced FRET efficiency in the longer peptides.

The time-resolved fluorescence decay traces of the DBO acceptor residue (λ_{em} = 450 nm) was measured by exciting the naphthalene donor residue (λ_{ex} = 285 nm, Figure 2) as well as by directly exciting DBO (λ_{ex} = 373 nm). The direct excitation of the DBO acceptor residue resulted in a monoexponential decay, with the lifetimes increase with peptide chain length as well, from 135 ns for Nal–DBO to 270 ns for Nal-$(Gly\text{-}Ser)_{10}$-DBO. These lifetimes fall shorter than the fluorescence lifetimes of the DBO-only-labeled peptide (e.g., 403 ns for $(Gly\text{-}Ser)_6$-DBO) as a consequence of some intramolecular exciplex-induced quenching of the

excited DBO by the ground-state naphthalene residue; this quenching channel becomes less efficient as the distance between probe and quencher increases. The fluorescence response of the DBO acceptor residue upon excitation of naphthalene as donor is characterized by a rapid growth and slower decay, which can be understood in terms of the initial population of the excited DBO by FRET and its subsequent deactivation. The time constant characterizing the decay component found for DBO populated by FRET was identical, within error, to the time constant measured upon direct excitation. This is not necessarily expected since the FRET experiment populates a subpopulation of peptide conformations in which the DBO and naphthalene chromophores are within distances and geometries suitable for FRET, while the direct excitation samples the conformational ensemble average.

End-to-end distance distribution and intramolecular diffusion coefficient. The time-resolved fluorescence data for each peptide were analyzed according to Equation 1 by employing the Globals software package (Experimental section).[9] The mean end-to-end distance and the intramolecular diffusion coefficient were calculated for all peptides. The results are summarized in Table 2.

Firstly, the fluorescence data were directly employed in fitting. The representative end-to-end distance distributions recovered from direct global analysis are shown in Figure 3. From the parameters in Table 2 we can see that the mean end-to-end distance is significantly shorter than the contour length (sum of length of the individual segments), and increases only slowly with increasing backbone length. For example, while the contour length increases from 22.8 Å for Nal-(Gly-Ser)$_2$-DBO to 53.2 Å for Nal-(Gly-Ser)$_6$-DBO the extracted mean end-to-end distances increase merely from 7.96 Å to 10.91 Å. This suggests that the Gly-Ser peptide chains are highly flexible and form more random-coil-type than extended conformations. On the other hand, the obtained intramolecular diffusion coefficients are all on the order of 10^{-7} cm^2/s and increase with chain length for the shorter peptides ($N \leq 10$) to reach an upper limit for the longer ones ($N \geq 10$).

Due to the high correlation of the parameters the errors remained large even in the over-determined global analysis, which required a model-assisted data analysis to better expose the salient features of the trends of the diffusion coefficients. For this purpose, we calculated a set of approximate root mean square end-to-end distances as $\langle R^2 \rangle = Ll$, where L is the contour length and l is the Kuhn length of Gly-Ser peptides, both obtained by assuming a length of one peptide unit as 3.8 Å.[23] It was found that the calculated means (R_{mean}) are close to the fitted ones but change in a more systematic way. Re-analysis of the kinetic data by constraining the R_{mean} values provided an improved set of distributions and diffusion coefficients. The recovered intramolecular diffusion coefficients were also found to lie in the range of 10^{-7}cm^2/s to 10^{-6}cm^2/s, which are in the same order of magnitude as values for similar peptides obtained experimentally[5,24] and theoretically,[25] and one to two orders of magnitude slower than those of free amino acids.[26] For the available values (N ≤ 10), the coefficients increase with contour length.

Energy transfer efficiency. Average energy transfer efficiency in the system can be calculated through time-resolved or steady–state fluorescence measurements according to the following equations:

$$\Phi_{ET} = 1 - \frac{I}{I_0} \tag{6a}$$

$$\Phi_{ET} = 1 - \frac{\tau}{\tau_0} \tag{6b}$$

I and I_0 as well as τ and τ_0 are the fluorescence intensity and average lifetime of the donor residue in the presence and absence of the acceptor residue, respectively. Equation 6b is only valid if the fluorescence decay can be fitted monoexponentially. This is not the case for the present FRET systems, such that the fluorescence intensity was preferred in the calculation of the energy transfer efficiency.

Figure 4 shows the fluorescence emission spectra (donor excitation) of the doubly-labeled peptides with different contour lengths and the naphthalene donor-only-labeled peptide. In the absence of the DBO acceptor, a strong emission of the naphthalene donor was observed from 300–400 nm. In the Nal/DBO doubly-labeled peptides, the emission of naphthalene was significantly reduced and the typical emission of DBO appeared at longer wavelength as a consequence of singlet-singlet energy transfer. With increasing peptide length, the intensity of naphthalene fluorescence recovers again partially as a result of a reduced energy transfer efficiency. As a peculiarity, it has to be noted that the DBO fluorescence intensity remains surprisingly constant regardless of the large variations in donor fluorescence; this is due to the delicate balance of two factors since the shorter peptides show more efficient energy transfer, but also shorter DBO fluorescence lifetimes due to more efficient intramolecular quenching of the excited acceptor by the ground state donor.

The steady-state fluorescence results are summarized in Table 3. The average energy transfer efficiency calculated according to the changes of naphthalene emission is strongly dependent on the contour length of the peptides. It decreases from 94% for the shortest Nal-DBO peptide to 60% of the longest one, Nal-(Gly-Ser)$_{10}$-DBO. There are two parameters that can principally reduce the energy transfer efficiency: longer average distances or slower conformational fluctuation rates. The recovered intramolecular diffusion coefficients actually increase for the longer peptides, which demonstrates that the reduced energy transfer efficiency derives from a larger end-to-end distance in the longer peptides.

The effective average end-to-end distance at which energy transfer occurs, R'_{mean}, can be calculated from the energy transfer efficiency according to Equation 7.

$$\Phi_{ET} = \frac{R_0^{\,6}}{R_0^{\,6} + R'^{\,6}_{mean}} \qquad (7)$$

In case that the conformations of the peptides are fixed, i.e, no fluctuations occur during the lifetime of excited donor, R'_{mean} will be equal to the equilibrium average end-to-end distances

(R_{mean}), returned from the global analysis. However, in the case of Gly-Ser peptides, the high flexibility of the backbone facilitates rapid conformational changes, such that the R'_{mean} values reflects the average distances at which energy transfer occurs, which will be naturally shorter than the equilibrium average end-to-end distance, R_{mean}, as a consequence of the vastly more efficient transfer rates at shorter distance (R^6 dependence). Additionally, the difference between R'_{mean} and R_{mean} should be larger for the longer peptides because the reduced energy transfer efficiency in the longer peptides results in a longer lifetime of the donor residue, which makes it possible that even peptides with remote donor/acceptor separation have sufficient time for diffusion to explore conformations with suitable energy transfer distanced.

The R'_{mean} values obtained from steady-state measurements in Table 3 with the R_{mean} values recovered by global analysis in Table 2 are generally consistent with the above expectations: for the shorter peptides, the R'_{mean} value are quite similar to R_{mean} due to the high energy transfer efficiency, but with increasing contour length, the R_{mean} values become significantly larger than the corresponding R'_{mean} values. However it is also noticed that the assumed R_{mean} value for the shortest Nal-DBO peptide, 5.4 Å, is shorter than the calculated R'_{mean} value, 6.2 Å. This suggested that the model used for predicting the root mean square end-to-end distance has some shortcoming for the very short chain with only two peptide bonds. In fact, both numerical simulations,[15] molecular dynamics simulations,[27] as well as end-to-end collision rate measurements[6] have demonstrated that the very short peptide is an outlier due to its apparently higher rigidity, which is now also borne out by a higher-than-expected effective average distance of energy transfer, again suggesting a more extended conformation.

FRET from tryptophan donor to DBO acceptor residue. The fluorescence and triplet-triplet absorption of tryptophan has been intensively employed to study the structural and dynamic properties of protein and peptides.[28-30] The emission of tryptophan in water is very broad with a maximum at 350 nm. The large overlap with the absorption of DBO makes FRET possible. The critical radius, R_0, for the Trp/DBO energy donor/acceptor pair was also

calculated from the spectra overlap ($J = 3.97 \times 10^{11}$ $M^{-1}cm^{-1}nm^4$, being the same for peptide-linked tryptophan and DBO, Trp-$(GlySer)_6$ and $(GlySer)_6$-DBO), and a value of 9.9 ± 0.2 Å, virtually the same as for the Nal/DBO pair, which allows one to conduct closely related experiment.

In this paper, we also employed the steady-state fluorescence intensity of tryptophan (donor) to calculate the energy transfer efficiency and the effective average end-to-end distance. The chemical structure of Nal and Trp is very similar (Scheme 1); it is therefore a very good approximation that the structural and dynamic properties of these two series of peptides such as the equilibrium end-to-end distance distribution and the intramolecular diffusion coefficient are very similar. There is, however, an important photophysical difference between the two probes, which should have a direct and predictable effect on the energy transfer efficiencies. Namely, the fluorescence lifetime of Trp is shorter than that of Nal by one full order of magnitude, which limits the probability that FRET is induced through diffusional fluctuation and conformational changes, but favor a static energy transfer. In other words, the contribution of the diffusion-enhanced FRET, and therefore the overall FRET efficiency is reduced in the Trp-based peptides (Table 3). An additional manifestation of this notion is that the Trp peptides should give rise to systematically larger R'_{mean} value (closer to the equilibrium R_{mean}), which is supported by the experimental data in Table 3.

Participation of intermolecular energy transfer. It should be noted that the global analysis is based on the assumption that the FRET process only occurs between naphthalene and DBO attached in the same peptide, i.e., that the change of the fluorescent property of the naphthalene residue is only caused by an *intramolecular* energy transfer process. To exclude *intermolecular* energy transfer or other quenching processes, control experiments were performed. For this purpose, the donor–only labeled peptide, 100 μM Nal-(Gly-Ser)$_6$ D_2O solution was excited at 285 nm. The emission spectrum between 290-550 nm showed a typical naphthalene fluorescent peak at 335 nm. After the addition of the acceptor-only

labeled peptide, 100 μM (Gly-Ser)$_6$-DBO, 285-nm excitation did not lead to DBO emission. Additionally, time-resolved measurement demonstrated that before and after addition of acceptor-only labeled peptide, the lifetime of naphthalene in the donor-only peptide remained unchanged, indicating the absence of quenching. These control experiments suggested that at 100 μM, the upper limit of peptide concentration applied in the fluorescence measurements in this paper, no intermolecular energy transfer happens, i.e., any FRET observed in the doubly-labeled peptides must occur intramolecularly.

In addition, this experiment provides conclusive evidence that association between the peptides does not occur at typical experimental concentrations, since aggregation would situate probe and quencher in sufficiently close proximity to allow FRET. In addition, aggregation should be further disfavored by the lower concentration employed in most experiments.

Discussion

FRET is widely employed, besides its application in supramolecular photonic devices,[31] to measure molecular conformational changes and probe-quencher distances, mostly intramolecularly in biopolymers.[9,10,32,33] One of the key problems in the application of FRET is the selection of suitable donor/acceptor pairs with the appropriate Förster critical radii, which is due to the very strong distance dependence of the energy transfer rate and therefore transfer efficiency (Figure 5).

Note that most conventional FRET probe/quencher pairs have critical radii ranging from 20–100 Å.[34] The resonance energy donor/acceptor pairs employed in this paper, Trp/DBO and Nal/DBO, have similar, very small critical radii of 9.9 Å and 9.8 Å respectively, and should therefore be suitable to probe chromophore separations at such short distances. Since FRET measurements are most sensitive in the range where the distance between probe and quencher lies between 0.5 R_0 and 2 R_0, the present probe/quencher pairs should excel when probe/quencher separation between 5–20 Å are to be investigated. For average energy transfer

distance below 5 Å energy transfer would be too fast and efficient (> 98%, $k_{ET} > 64k_0$), while above 20 Å it is too inefficient (< 2%, $k_{ET} > 1/64k_0$), compare Figure 5. The average end-to-end distances in the short flexible Gly-Ser peptides studied in this work range from a few angstrom to less than 20 Å, and are are therefore ideally suited for the present FRET pairs.

An additional motivation for using donors and acceptors with small molecular size as well as small Förster critical radii comes from theoretical work and molecular dynamic simulations. These have shown that the survival probability of energy donor/acceptor pairs in doubly-labeled polymer chains can be most accurately recovered from the approximate theories, such as WF theory or the SSS model, if the Förster critical radius and chormophore sizes are smaller or similar to the chain length.[11,12] Evidently, this theoretical condition cannot be fulfilled by most established FRET donor/acceptor pairs when the end-to-end distances become very short. In comparison, the energy donors used in the present work (tryptophan or naphthalene) and in particular the acceptor (DBO) are very small compared with conventional fluorescent probes.[35] This specific advantage together with the small Förster critical radius around 10 Å make it possible to recover the structural and dynamic properties of short peptides from the fluorescence decays, based on the modified Smoluchowski equation and global analysis.[36]

Singlet-singlet energy transfer may occur through an exchange (Dexter) or a resonance (FRET) mechanism, or both.[18,34,37] Transfer due to exchange interaction become more important at very small donor/acceptor separation, while FRET dominates at longer distance. In our previous work, where naphthalene and DBO were separated by a dimethylsiloxy tether and measured in *n*-hexane, energy transfer from naphthalene to DBO was considered to occur mainly through Dexter mechanism due to the very short and flexible tether and very lower solvent viscosity.[18] In the current work on a more rigid peptide chain and more viscous solvent, we expect FRET to become dominant. Actually, the ratio of energy transfer through

Dexter and FRET can be estimated roughly. At the rapid-diffusion limit of fluorescence resonance energy transfer, the upper limit of energy transfer rate can be estimated by eq. 8.[34,38]

$$k_{\mathrm{FRET}} = \frac{2.523R_0^6}{\tau_D r^3} \tag{8}$$

τ_D is the lifetime (in s) of the donor in the absence of the energy transfer and r is the distance of closest approach of the donor and acceptor (in nm), which is taken as 0.4 from the reaction distance for Trp/DBO.[27] The calculated FRET rate constant is found to be 1.1×10^9 $M^{-1}s^{-1}$, much smaller than the experimental intermolecular quenching rate constant of naphthalene by DBO (ca. 6×10^9 $M^{-1}s^{-1}$ in water, see Results), indicating that a Dexter mechanism dominates in the intermolecular case with less than 20% of energy transfer through FRET. However, this does not mean that Dexter is also dominant in the case of intramolecular energy transfer, which is due to a slower intramolecular diffusion, which puts the exchange mechanism at a disadvantage since it requires a close donor/acceptor approach. Both current work and previous work have shown that intramolecular diffusion coefficients fall at least one order of magnitude below the respective intermolecular ones,[5,24-26] which suggests the energy transfer rate by Dexter will decrease by at least 10 times in the intramolecular case. On the other hand, the intrinsic distance dependence of the energy transfer rates by FRET remains almost unchanged. It is therefore reasonable to assume that FRET becomes dominant in the peptides investigated.

Experimentally, time-resolved fluorescence decay traces of donor and acceptor were recorded for each peptide in the presence and absence of FRET. The fluorescence decay traces of naphthalene in the presence of FRET cannot be satisfactorily fitted monoexponentially. Nevertheless, a biexponential fit is sufficient to describe the decay traces and even in this case the contribution of the longer-lived component is small (< 10%). It is possible to define an “average” lifetime (Table 1) and employ it to calculated an apparent intramolecular quenching rate constant by energy transfer, which can be compared with the

end-to-end collision rate constants previously determined for the same Gly-Ser peptide backbone (k_q values in Table 1).[6] The results entered in Table 1 as k_{qET} values and plotted in Figure 6 as the logarithmic rate constants versus log$N$, with N taken as number of peptide units. Such plots are common in polymer and biopolymer kinetics[4-6] in order to evaluate deviations from ideal-chain behavior. As can be seen, the apparent quenching rate constants from FRET fall far above the end-to-end collision rates, which suggests that the quenching of the donor by the acceptor does not occur through a well-defined and intimate contact, but through a longer-range interaction characteristic for FRET. In addition, the inversion at very short donor/acceptor, which is found for the end-to-end collision rates disappears, although a negative curvature remains, which reflects steric hindrance effects prominent in very short chain. This discriminating feature also points to a quenching mechanism with looser geometrical constraints, namely FRET, which depends primarily on the distance.

The fluorescence decay traces were accordingly subjected to global analysis according to the pertinent FRET model (eq. 1). This analysis yielded the equilibrium end-to-end distance distributions (for example see Figure 3) and the intrachain diffusion coefficient (Table 2). The recovered intramolecular diffusion coefficients lie in the reasonable range of 10^{-7}cm^2/s, at least one order of magnitude smaller than the diffusion of free amino acid molecules (ca. 10^{-5}cm^2/s in H_2O).[23] Most importantly, a decrease of the diffusion constants for the shorter peptides is observed. In a previous study,[15] we have numerically simulated the dynamics of the short Gly-Ser peptides and suggested that a slower diffusion coefficient of shorter peptides would be the underlying reason for the negative curvature and the weaker length-dependent end-to-end collision rates (Figure 6) compared with theoretical prediction for the ideal chain model. The results in the present paper now verify this suggestion experimentally. The lower diffusion coefficients in the shorter peptides can be most intuitively in terms of steric hindrance effects, since a short backbone restricts motion of the chain ends more than a longer one does. In addition, the lower diffusion coefficients can be interpreted in terms of a

higher “internal friction”, which is yet another conceptual approach to chain stiffness in polymers and biopolymers.[14,39]

The time-resolved fluorescence measurements in the Trp/DBO doubly-labeled peptides, which are exactly those for which the end-to-end collision rates have been measured, were less conclusive and not amenable for more detailed global analysis. This is because the time-resolved fluorescence decay of tryptophan is complex and non-monoexponential even in the absence of acceptors.[34] Even free tryptophan shows a bi-exponential trace in neutral aqueous solution. In Trp/DBO-labeled peptides, the decay pattern becomes more complex. As a second complication, the very broad emission of tryptophan overlaps with that of DBO, which would require a ratiometeric method to discriminate the fluorescence of the DBO acceptor upon excitation of tryptophan as donor. Nevertheless, the integrated energy transfer efficiency can be determined from steady-state fluorescence measurements, which allows at least estimates of the effective average end-to-end distances.

The directly observable properties of fluorescent labeled biopolymer chain, such as the end-to-end collision rates and the intramolecular energy transfer efficiency in peptides and oligonucleotides, are dependent on two factors: the equilibrium end-to-end distance distribution and the flexibility of the backbone. The Trp/DBO probe/quencher pair has been proven to provide a measure of the end-to-end collision rates in peptides, where DBO serves as a long-lived probe and Trp as a selectively collision-induced quencher.[6,7,13] By changing the role of tryptophan from the contact quencher to that of an energy donor with DBO acting as acceptor, or by exchanging tryptophan by the closely related naphthalene as donor, it is now possible to obtain approximate distributions. The results are shown for naphthalene in Figure 3, obtained by global analysis. The data for tryptophan allow a more direct estimate on the average end-to-end distances and therefore distributions because the singletlifetime of tryptophan is very short (< 3 ns), such that the Brownian motion during its excited state lifetime cannot result in a large displacement, especially because of the relatively small

diffusion coefficients of the chain ends. The effective average energy transfer distance, R'_{mean}, recovered from the Trp/DBO FRET system should therefore fall only slightly below the actual average distance under equilibrium conditions, R_{mean}. In a first approximation, the average energy transfer distances obtained from (steady-state) FRET in Trp/DBO peptides can be taken as measure of the average end-to-end distance. This approximation should hold particularly well for rigid peptides or in very viscous media where the motion of the chain on a 3-ns time scale can be neglected.[14] Even in the case of the presently investigated flexible Gly-Ser peptides, the agreement between the energy transfer distance obtained from Trp/DBO FRET (Table 3) are in satisfactory agreement with the experimental values by global fitting of the Nal/DBO FRET data, as well as the theoretical values for an ideal chain model (Table 2).

Conclusions

Two energy donor/acceptor pairs (naphthalene/DBO and tryptophan/DBO) with very small Förster radius (R_0 ~10 Å) have been applied to recover structural and dynamic properties of short flexible peptides through intramolecular FRET. These donor/acceptor pairs with very small critical radius have proven very suitable for investigating these very short biopolymers. In addition, FRET efficiencies in the tryptophan/DBO donor/acceptor pair allowed direct estimates the average end-to-end distance of peptides, which is made possible by the short fluorescence lifetime of tryptophan. Global analysis of the time-resolved fluorescence decay traces and end-to-end distances obtained from the ideal chain model were also employed to improve the accuracy of the results. The results confirmed that the intramolecular diffusion coefficients are one to two orders of magnitude smaller than the intermolecular diffusion coefficients. The smallest diffusion coefficients were observed in the shorter peptides, in line with previous numerical simulations result.

Acknowledgement

This work was supported by the Swiss National Science Foundation and by the NRP 47 "Supramolecular Functional Materials". We would like to acknowledge the experimental help of R. Meyer in this project.

References:

1 C. M. Dobson, Protein folding and misfolding, *Nature*, 2003, **426**, 884-890.

2 G. E. Schulz, Domain motions in proteins, *Curr. Opin. Struct. Biol.*, 1991, **1**, 883-888.

3 F. G. Parak, Proteins in action: the physics of structural fluctuations and conformational changes, *Curr. Opin. Struct. Biol.*, 2003, **13**, 552-557.

4 O. Bieri, J. Wirz, B. Hellrung, M. Schutkowski, M. Drewello and T. Kiefhaber, The speed limit for protein folding measured by triplet-triplet energy transfer, *Proc. Natl. Acad. Sci. USA*, 1999, **96**, 9597-9601.

5 L. J. Lapidus, W. A. Eaton and J. Hofrichter, Measuring the rate of intramolecular contact formation in polypeptides, *Proc. Natl. Acad. Sci. USA*, 2000, **97**, 7220-7225.

6 R. R. Hudgins, F. Huang, G. Gramlich and W. M. Nau, A fluorescence-based method for direct measurement of submicrosecond intramolecular contact formation in biopolymers: An exploratory study with polypeptides, *J. Am. Chem. Soc.*, 2002, **124**, 556-564.

7 W. M. Nau, F. Huang, X. Wang, H. Bakirci, G. Gramlich and C. Marquez, Exploiting long-lived molecular fluorescence, *Chimia*, 2003, **57**, 161-167.

8 L. Stryer and R. P. Haugland, Energy transfer: A spectroscopic ruler, *Proc. Natl. Acad. Sci. USA*, 1967, **58**, 719-726.

9 J. M. Beechem and E. Haas, Simultaneous determination of intramolecular distance distributions and conformational dynamics by global analysis of energy transfer measurements, *Biophys. J.*, 1989, **55**, 1225-1236.

10 E. Haas, E. Katchalski-Katzir and I. Z. Steinberg, Brownian motion of the ends of oligopeptide chains in solution as estimated by energy transfer between the chain ends, *Biopolymers*, 1978, **17**, 11-31.

11 G. Srinivas, A. Yethiraj and B. Bagchi, Nonexponentiality of time dependent survival probability and the fractional viscosity dependence of the rate in diffusion controlled reactions in a polymer chain, *J. Chem. Phys.*, 2001, **114**, 9170-9178.

12 G. Srinivas, A. Yethiraj and B. Bagchi, FRET by FET and dynamics of polymer folding, *J. Phys. Chem. B*, 2001, **105**, 2475-2478.

13 F. Huang and W. M. Nau, A conformational flexibility scale for amino acids in peptides, *Angew. Chem. Int. Ed. Engl.*, 2003, **42**, 2269-2272.

14 F. Huang, R. R. Hudgins and W. M. Nau, Primary and secondary structure dependence of peptide flexibility assessed by fluorescence-based measurement of end-to-end collision rates, 2004, submitted for publication.

15 X. Wang, E. N. Bodunov and W. M. Nau, Fluorescence quenching kinetics in short polymer chains: Dependence on chain length, *Opt. Spectrosc.*, 2003, **95**, 560-570.

16 J. R. Lakowicz, J. Kusba, I. Gryczynski, W. Wiczk, H. Szmacinski and M. L. Johnson, End-to-end diffusion and distance distributions of flexible donor-acceptor systems obseved by energy transfer and frequency-domain fluorometry; Enhanced fesolution by global analysis of externally quenched and nonquenched samples, *J. Phys. Chem.*, 1991, **95**, 9654-9660.

17 A. Szabo, K. Schulten and Z. Schulten, First passage time approach to diffusion controlled reactions, *J. Chem. Phys.*, 1980, **72**, 4350-4357.

18 U. Pischel, F. Huang and W. M. Nau, Intramolecular singlet-singlet energy transfer in antenna-substituted azoalkanes, *Photochem. Photobiol. Sci.*, 2004, **3**, 305-310.

19 C. Marquez, U. Pischel and W. M. Nau, Selective fluorescence quenching of 2,3-diazabicyclo[2.2.2]oct-2-ene by nucleotides, *Org. Lett.*, 2003, **5**, 3911-3914.

20 H. A. H. Billiet, J. P. J. Van Dalen, P. J. Schoenmaker and L. De Galan, Measurement of deuterium oxide elution data in reversed-phase liquid chromatography with a microwave induced plasma detection, *Anal. Chem.*, 1983, **55**, 847-851.

21 K. K. Pandey, H. C. Joshi and T. C. Pant, Migration effects on excitation energy transfer by decay analysis using a nanosecond fluorimeter, *Chem. Phys. Lett.*, 1988, **148**, 472-478.

22 L. J. Lapidus, W. A. Eaton and J. Hofrichter, Dynamics of intramolecular contact formation in polypeptides: Distance dependence of quenching rates in a room-temperature glass, *Phys. Rev. Lett.*, 2001, **87**, 258101/258101-258101/258104.

23 S. J. Hagen, J. Hofrichter and W. A. Eaton, Rate of intrachain diffusion of unfolded cytochrome c, *J. Phys. Chem. B*, 1997, **101**, 2352-2365.

24 D. R. Buckler, E. Haas and H. A. Scheraga, Analysis of the structure of ribonuclease A in native and partially denatured states by time-resolved nonradiative dynamic excitation energy transfer between site-specific extrinsic probes, *Biochemistry*, 1995, **34**, 15965-15978.

25 I.-C. Yeh and G. Hummer, Peptide loop-closure kinetics from microsecond molecular dynamics simulations in explicit solvent, *J. Am. Chem. Soc.*, 2002, **124**, 6563-6568.

26 T. E. Creighton, *Proteins: Structures and Molecular Properties*. 2nd ed. New York, W. H. Freeman and Company, 1993.

27 M. Zacharias, D. Roccatano, unpublished results.

28 Dynamics of intramolecular contact formation in polypeptides: Distance dependence of quenching rates in a room-temperature glass. Phys. Rev. Lett., 2001:258101/258101-258101/258104.

29 V. Gopalan, R. Golbik, G. Scheriber, A. R. Fersht and S. Altman, Fluorescence properties of a tryptophan residue in an aromatic core of the protein subunit of ribonuclease P from Escherichia coli, *J. Mol. Biol.*, 1997, **267**, 765-769.

30 D. P. Millar, Time-resolved fluorescence spectroscopy, *Curr. Opin. Struct. Biol.*, 1996, **6**, 637-642.

31 M. A. Hossain, H. Mihara and A. Ueno, Novel peptides bearing pyrene and coumarin units with or without β-cyclodextrin in their side chains exhibit intramolecular fluorescence resonance energy transfer, *J. Am. Chem. Soc.*, 2003, **125**, 11178-11179.

32 A. A. Deniz, et al., Single-molecule protein folding: Diffusion fluorescence resonance energy transfer studies of the denaturation of chymotrypsin inhibitor 2, *Proc. Natl. Acad. Sci. U. S. A.*, 2000, **97**, 5179-5184.

33 B. Schuler, E. A. Lipman and W. A. Eaton, Probing the free-energy surface for protein folding with single-molecule fluorescence spectroscopy, *Nature*, 2002, **419**, 743-747.

34 J. R. Lakowicz, *Principles of Fluorescence Spectroscopy*. 2nd ed. New York, Kluwer Academic/Plenum Publishers, 1999.

35 W. M. Nau and X. Wang, Biomolecular and supramolecular kinetics in the submicrosecond time range: The fluorazophore approach, *ChemPhysChem*, 2002, **3**, 393-398.

36 T. Bandyopadhyay and S. K. Ghosh, Diffusion influenced end-to-end reaction of a flexible polymer chain: the memory effect, *J. Chem. Phys.*, 2002, **116**, 4366-4369.

37 S. Faure, C. Stern, R. Guilard and P. D. Harvey, Role of the spacer in the singlet-singlet energy transfer mechanism (Forster vs Dexter) in cofacial bisporphyrins, *J. Am. Chem. Soc.*, 2004, **126**, 1253-1261.

38 C. F. Meares, S. M. Yeh and L. Stryer, Exchange interaction contribution to energy-transfer between ions in the rapid-diffusion limit, *J. Am. Chem. Soc.*, 1981, **103**, 1607-1609.

39 X. Wang and W. M. Nau, Kinetics of end-to-end collision in short single-stranded nucleic acids, *J. Am. Chem. Soc.*, 2004, **126**, 808-813.

Captions for schemes and figures

Scheme 1. Structure of doubly labeled peptides: a) Nal/DBO labeled peptides, Nal-(Gly-Ser)$_n$-DBO and b) Trp/DBO labeled peptides, Trp-(Gly-Ser)$_n$-DBO.

Scheme 2. Structure of CB7 combined peptides Nal-(Gly-Ser)$_6$-DBO.

Figure 1. Time-resolved fluorescence decay of naphthalene donor in doubly labeled peptides a) Nal-DBO, b) Nal-(Gly-Ser)$_2$-DBO, c) Nal-(Gly-Ser)$_6$-DBO, d) Nal-(Gly-Ser)$_{10}$-DBO, and in the donor-only peptide e) Nal-(Gly-Ser)$_6$. λ_{ex} = 285nm, λ_{em} = 335nm.

Figure 2. Time-resolved fluorescence decay of DBO acceptor in doubly labeled peptides a) Nal-DBO, b) Nal-(Gly-Ser)$_2$-DBO, c) Nal-(Gly-Ser)$_6$-DBO, and d) Nal-(Gly-Ser)$_{10}$-DBO. λ_{ex} = 285nm, λ_{em} = 450nm.

Figure 3. Representative end-to-end distance distribution in Nal/DBO doubly labeled peptides recovered from direct global analysis: Nal-DBO (——), Nal-(Gly-Ser)$_2$-DBO (----), and Nal-(Gly-Ser)$_6$-DBO (— - — - —).

Figure 4. Fluorescence emission spectra of doubly labeled peptides Nal-(Gly-Ser)$_n$-DBO (solid line, from lower to the upper ones, n = 0, 1, 2, 4, 6, and 10, respectively) and naphthalene donor-only peptide (dashed line, Nal-(Gly-Ser)$_6$), as well as the emission spectrum of peptide Nal-(Gly-Ser)$_6$-DBO (3.8×10^{-5} M) in the presence of CB7 (7.5×10^{-4} M) (dotted line). λ_{ex} = 285 nm.

Figure 5. FRET efficiency dependent on the donor/acceptor distance.

Figure 6. Double logarithmic plot of $k_{q,ET}$ (open cycle) and k_q (solid cycle) versus peptide length (data taken from Table 1). A function of the type y = a –1.5x – b/x was fitted to the experimental data (a = 9.37, b = 0.392 for data obtained from collision-based experiments,[6] and a = 9.57, b = 0.229 for data obtained from experiments based on singlet-singlet energy transfer from current work). The dash-dot-dash line has a slope of –1.5 and is shown to illustrate the deviation from the theoretical behavior.

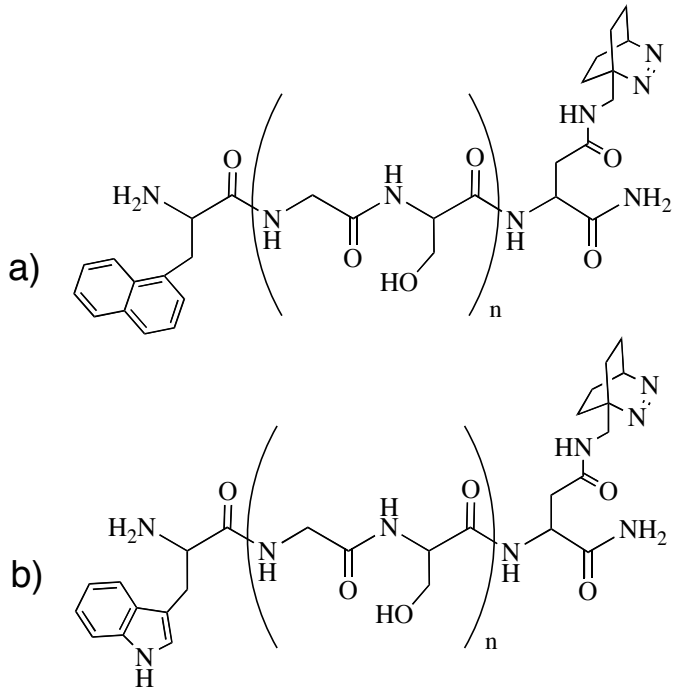

Scheme 1

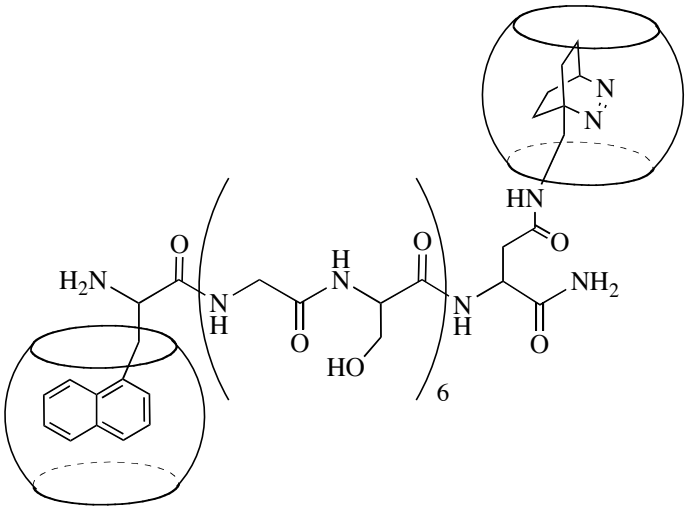

Scheme 2

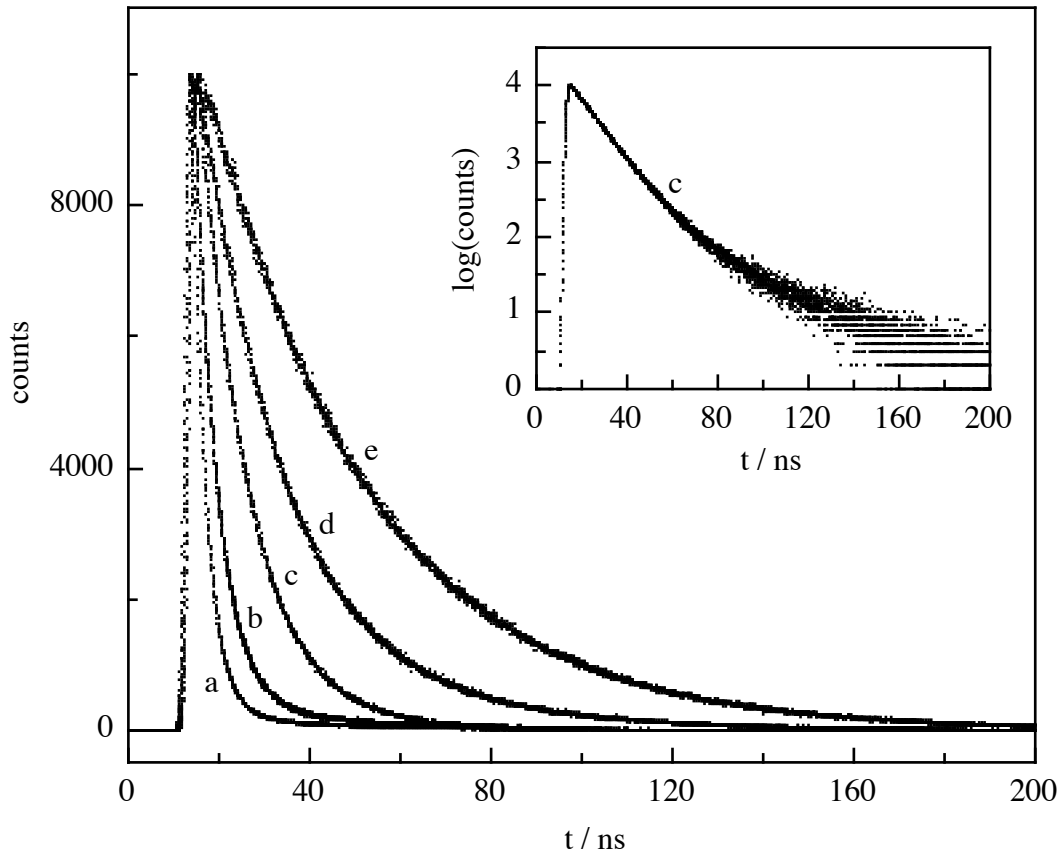
counts
8000
4000
0
0
40
80
120
160
200
t / ns
a
b
c
d
e
log(counts)
4
3
2
1
0
0
40
80
120
160
200
t / ns
c

Figure 1

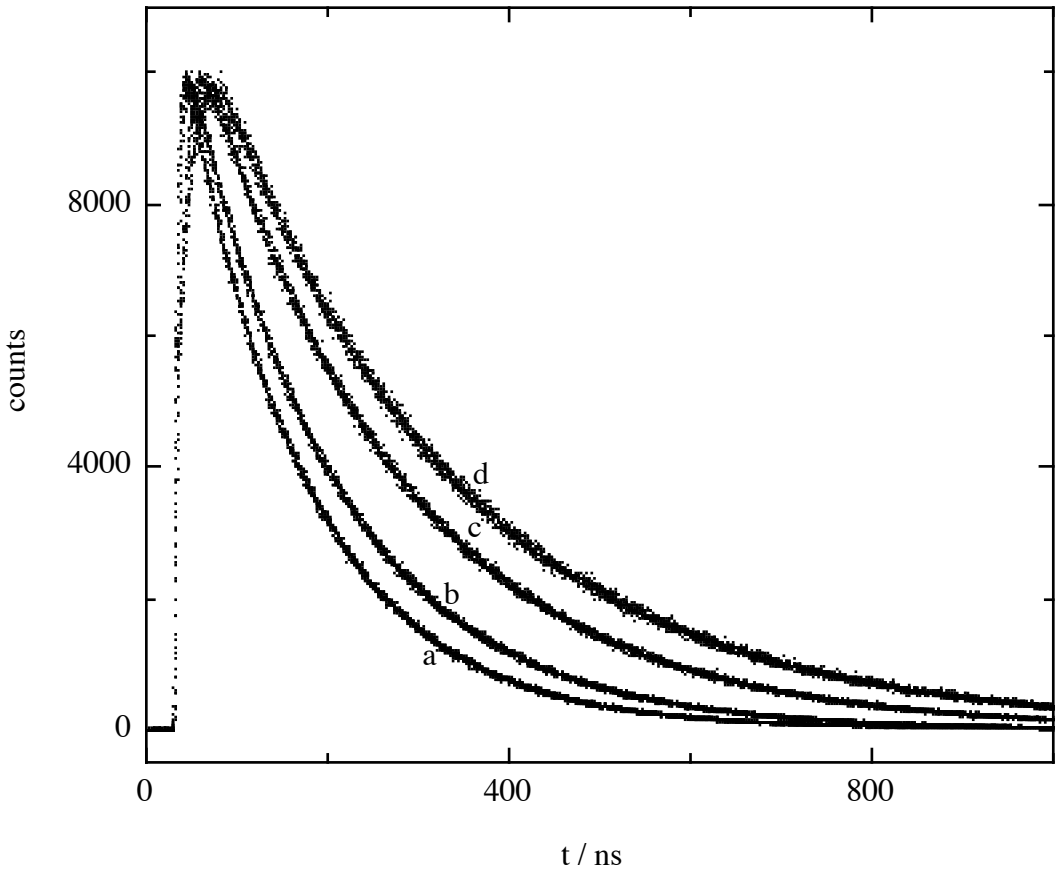

Figure 2

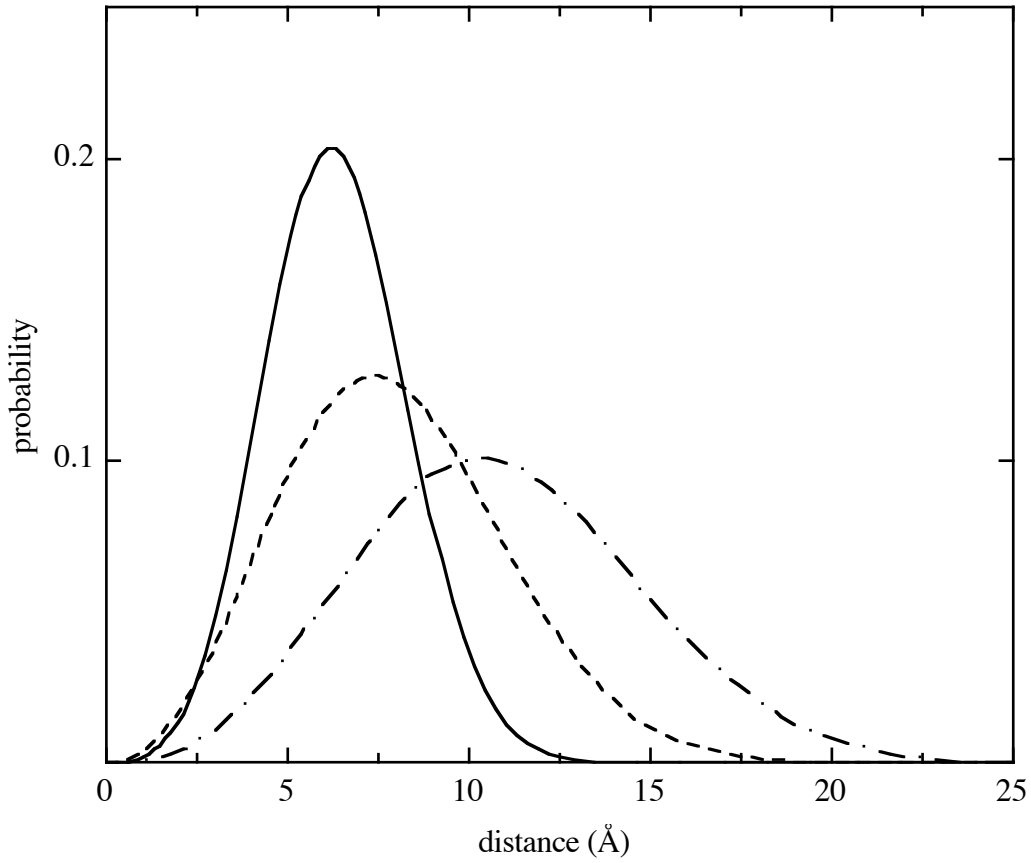

Figure 3

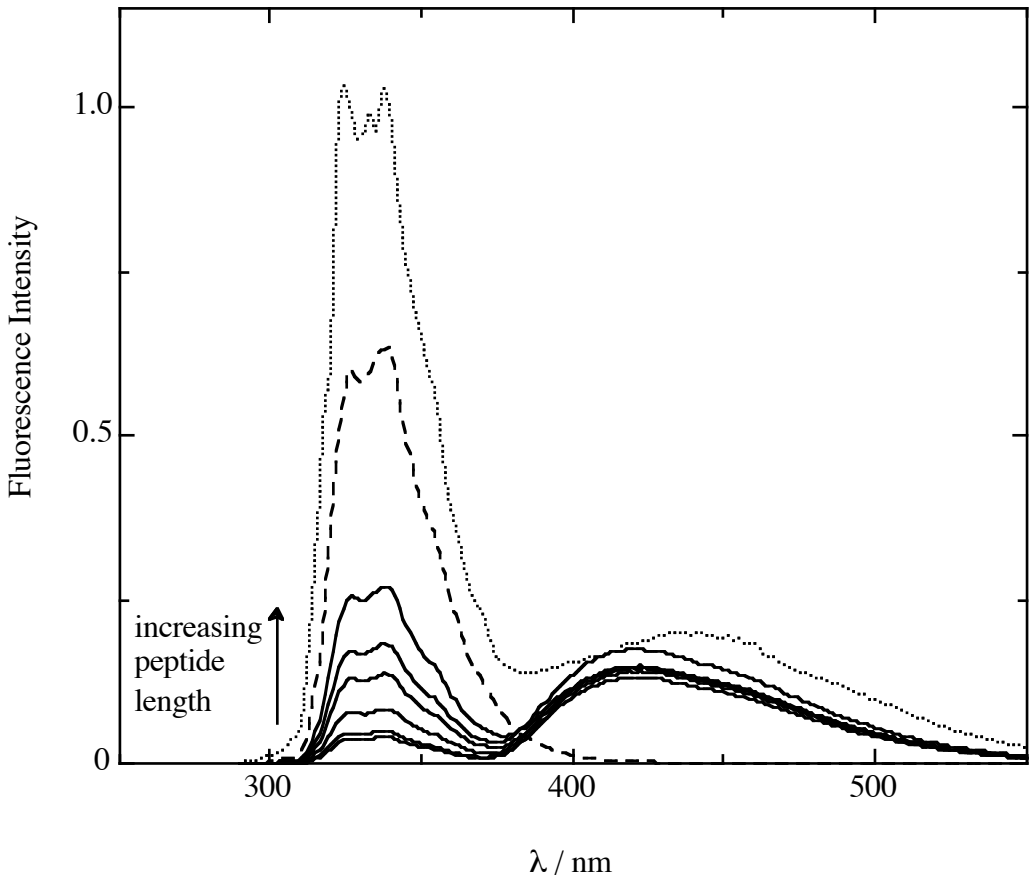
Fluorescence Intensity
1.0
0.5
0
increasing
peptide
length
300
400
500
λ / nm

Figure 4

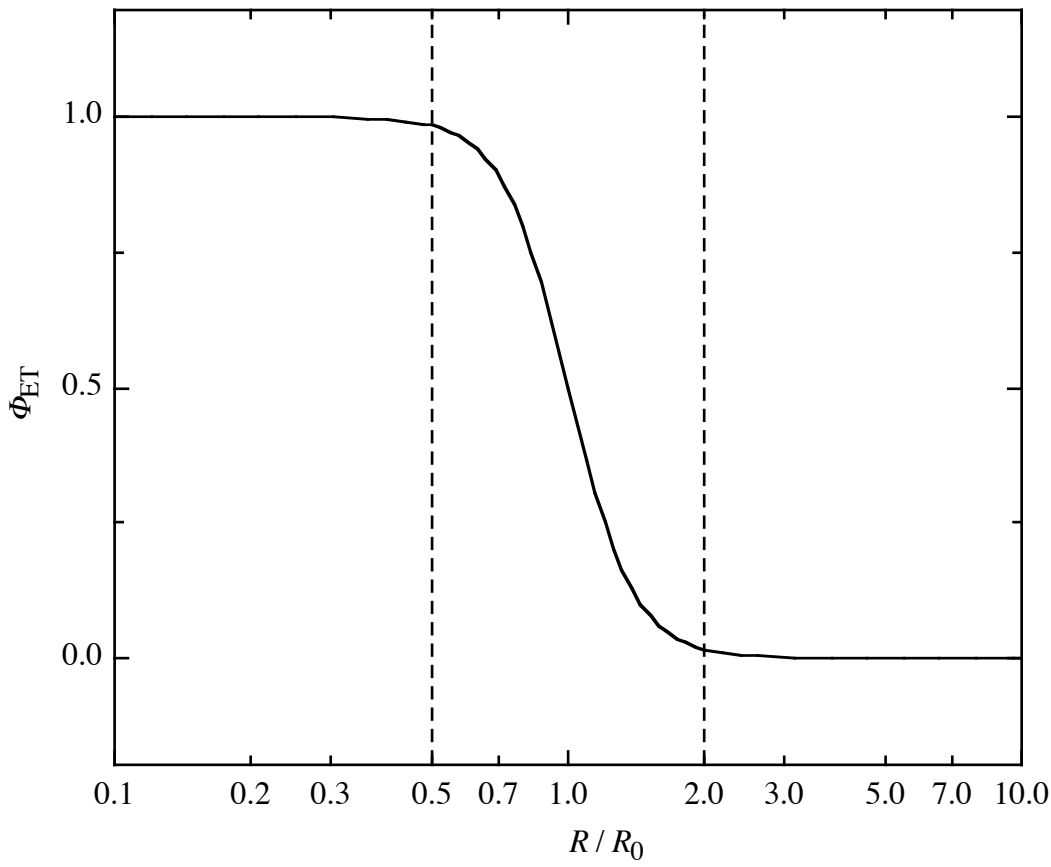

Figure 5

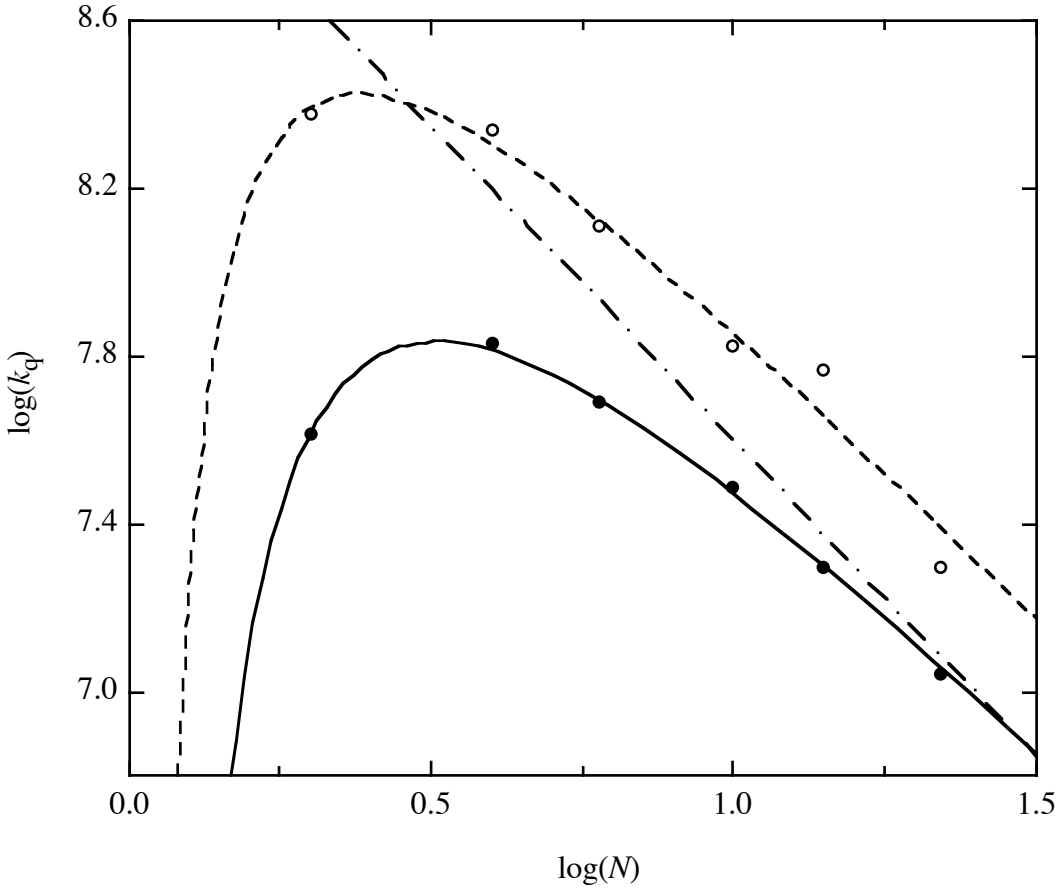

Figure 6

Table 1. Parameters of naphthalene fluorescence lifetimes in donor-only-labeled and donor/acceptor doubly-labeled peptides[a]

peptide	N	$\tau_i(\alpha_i)$ (ns)[b]	χ^2	$\langle\tau\rangle$ (ns)[c]	k_{qET} ($10^7 s^{-1}$)[d]	k_q ($10^7 s^{-1}$)[e]
Nal-(G-S)$_6$		35.5(1.000)	1.01	35.5		
Nal-DBO	2	3.1(0.975), 25.8(0.025)	1.28	3.7	24	4.1
Nal-G-S-DBO	4	3.5(0.966), 22.6(0.034)	1.36	4.1	22	6.8
Nal-(G-S)$_2$-DBO	6	5.0(0.961), 35.4(0.039)	1.09	6.2	13	4.9
Nal-(G-S)$_4$-DBO	10	8.3(0.920), 36.0(0.080)	1.09	10.5	6.7	3.1
Nal-(G-S)$_6$-DBO	14	10.8(0.978), 36.4(0.022)	1.11	11.4	5.9	2.0
Nal-(G-S)$_{10}$-DBO	22	18.2(0.904), 45.0(0.095)	1.12	20.7	2.0	1.1

[a] λ_{ex} = 285 nm and λ_{em} = 335 nm.

[b] Recovered lifetimes (τ_i) and preexponential factors (α_i, normalized) of single or double exponential fits to time-resolved fluorescence decay of naphthalene residue in different peptides.

[c] Lifetime averages ($\sum \alpha_i \tau_i$) for multi-exponential fits.[24]

[d] Apparent quenching rate constants of naphthalene by DBO, calculated from the average lifetime of naphthalene in Nal-(Gly-Ser)$_n$-DBO peptides.

[e] Collision-controlled intrachian quenching rate constants of DBO by tryptophan, taken from Ref. 6.

Table 2. Distance distribution and diffusion coefficient recovered from global analysis for Nal-(GlySer)$_n$-DBO peptides.

			direct global analysis			model-assistant analysis		
n	N	L (Å)[a]	R_{mean} (Å)[b]	D (10^{-7}cm^2/s)	χ^2	R_{mean} (Å)[c]	D (10^{-7}cm^2/s)	χ^2
0	2	7.6	6.14	2.67	1.12	5.4	0.78	1.42
1	4	15.2	6.26	2.76	1.09	7.6	5.44	1.10
2	6	22.8	7.96	4.03	1.13	9.3	11.69	1.14
4	10	38.0	10.39	5.66	1.11	12.0	14.73	1.12
6	14	53.2	10.91	4.91	1.08	14.2	79.0	1.10
10	22	83.6	14.76	4.47	1.16	17.8	4.2	1.16

[a] Contour length, $L = N\,l$, where N is the number of intervening peptide units and l is the length per unit (Kuhn length), taken as 3.8 Å.

[b] Experimental average end-to-end distance obtained by FRET measurements and direct global analysis.

[c] Root mean square end-to-end distance of each peptide calculated from the relationship $R_{mean} = l\sqrt{N}$.

Table 3. Energy transfer efficiency and effective end-to-end distance in peptides Donor-(Gly-Ser)$_n$-DBO with naphthalene and tryptophan serve as energy donor.

		Donor = naphthalene		Donor = tryptophan	
n	N	Φ_{ET}	R'_{mean} (Å)	Φ_{ET}	R'_{mean} (Å)
0	2	0.94	6.2	0.94	6.4
1	4	0.92	6.5	0.86	8.6
2	6	0.87	7.1	0.79	9.5
4	10	0.73	8.3	0.68	10.7
6	14	0.70	8.5	0.65	11.3
10	22	0.61	9.1	0.58	11.0